Neurotransmitters and receptors in the motion vision pathway of *Drosophila*

Sandra Fendl

Graduate School of
Systemic Neurosciences
LMU Munich

Dissertation der
Graduate School of Systemic Neurosciences
der Ludwig-Maximilians-Universität
München

3rd of November 2020

Supervisor
Prof. Dr. Alexander Borst
Max-Planck-Institute of Neurobiology, Martinsried, Germany

First Reviewer: Prof. Dr. Alexander Borst
Second Reviewer: Dr. Frank Schnorrer

Date of Submission: 3rd of November 2020
Date of Defense: 24th of February 2021

SUMMARY

The fruit fly *Drosophila melanogaster* is one of the most popular model organisms being used in the life sciences. Due to its small number of neurons compared to other vertebrate species and its genetic access, it has also proven itself to be an optimal model organism for neuroscience. Especially, the field of systems neuroscience has made quick advances in its study of neural circuits of the fly brain underlying sensory perception such as olfaction and vision, as well as complex behaviors such as mating, learning, and memory.

The motion vision pathway in the optic lobe of the fruit fly is a prominent example of a computation-performing neural circuit that researchers have been trying to understand for decades. While the wiring of the main circuit elements has been described via EM-reconstructions and their response properties have been characterized comprehensively, the molecular mechanisms of direction-selectivity still remain elusive. However, subcellular components such as neurotransmitter receptors and ion channels are important since they define the sign and the temporal dynamics of synaptic connections within a circuit. Hence, the main focus of my thesis was the investigation of neurotransmitter receptors in the primary motion sensing T4/T5 neurons of the fly brain, including the development of required genetic tools.

First, we developed a protocol for super-resolution STED imaging in *Drosophila* brain slices which allowed us to resolve fine dendritic structures of individual T4/T5 neurons deep inside the brain (**Manuscript 1**). Second, we used the glutamate sensor iGluSnFR to characterize the temporal dynamics of the three glutamatergic cell types of the motion vision pathway L1, Mi9 and LPi (**Manuscript 2**). We validated the usability of iGluSnFR for measuring glutamate signaling in adult *Drosophila* brains and found that responses recorded with iGluSnFR are faster than GCaMP signals of the same cells. In **Manuscript 3**, we developed new genetic strategies for conditional protein labeling. Specifically, we introduced FlpTag, a tool for endogenous, conditional labeling of proteins by means of a flippase-dependent, invertible GFP cassette integrated in the endogenous gene locus. Using these methods, we explored the subcellular localizations of neurotransmitter receptors for glutamate, GABA, acetylcholine and voltage-gated ion channels in T4/T5 neurons in *Drosophila melanogaster*. Within the dendrite, receptor subunits localize to different regions and in a spatial order that exactly matches the EM-reconstructed synapse numbers and

distributions of the different input neurons described in previous studies. Further, we discovered a strictly segregated subcellular distribution of two voltage-gated ion channels in dendrite vs. axonal fibers in T4/T5 neurons. These findings lay the foundation for future functional investigations of receptors and ion channels in T4/T5 neurons and will be used by biophysically realistic model simulations of the motion-detecting circuit.

In summary, we employed new methods to investigate neurotransmitters, their corresponding receptors, and voltage-gated ion channels in the motion vision pathway of the fruit fly. This work advanced our understanding of the biophysical mechanisms of motion-vision. Future studies can build on it to investigate the full molecular repertoire of T4/T5 neurons. Potentially, the strategies presented in this thesis can be expanded to different circuits or even different species in the future.

CONTENT

LIST OF FIGURES

1. INTRODUCTION

1.1 The model organism *Drosophila melanogaster*

1.1.1 History of fruit fly research

The fruit fly *Drosophila melanogaster* is one of the most commonly used model organisms across all life sciences. It has been studied since the early 20th century when Nettie Stevens brought fruit flies into Thomas Hunt Morgan's laboratory at the Bryn Mawr College. She studied spermatogenesis in mealworms and different dipteran fly species and discovered the sex chromosomes (Stevens, 1905; 1908). Later, Morgan did his first experiments with these tiny flies describing the inheritance of their eye color and the underlying *white* gene on the X-chromosome (Morgan & Cattell, 1912). In 1933 the Nobel Prize in Physiology or Medicine was awarded to Morgan "for his discoveries concerning the role played by the chromosome heredity".

The influence *Drosophila* has had on basic research over the past century can be showcased by the Nobel Prizes awarded for findings made with the fruit fly (overview in Fig. 1). In 1946, H. J. Müller won the Nobel Prize "for defining the effects of X-rays on mutation rates". Almost 50 years later, in 1995, the Nobel Prize was awarded to E. B. Lewis, C. Nüsslein-Vollhard and E. Wieschaus for their discoveries of genes involved in embryo development. After these findings the field of *Drosophila* developmental biology took off and more and more researchers used the potential of flies for their research up until today. R. Axel and L. B. Buck were awarded the Nobel Prize in 2004 "for their discoveries of odorant receptors and the organization of the olfactory system" in both mice and flies. In 2011, J. A. Hoffmann won the Nobel Prize for his discovery of the *Toll*-gene which is crucial for the immune system of the fly. The last Nobel Prize thus far for research done with *Drosophila* was awarded to J. C. Hall, M. Rosbash and M. W. Young in 2017 "for their discoveries of molecular mechanisms controlling the circadian rhythm".

Figure 1. Photographs of Nobel prize winners for *Drosophila* research.
Image taken with permission from Prokop A., 2018.
(https://www.openaccessgovernment.org/fruit-fly-research/52396/).

Drosophila melanogaster continues to be a widely used model organism ever since due to an ever-evolving array of traits. First, rearing fruit flies in the lab is inexpensive and easy. It mainly requires plastic tubes with food paste and temperature-controlled incubators. Second, their generation time is rather short (approximately 10 days at 25° C) which makes it possible to study many generations in relatively short time and in general more test animals can be sacrificed. Third, even though *Drosophila* is an invertebrate, 60% of its genome is homologous to that of humans and 75% of human disease genes have homologs in flies (Ugur et al., 2016; Mirzoyan et al., 2019). This makes *Drosophila* an attractive model organism not only for basic cell and developmental biology, but also for studies of diseases and medical research.

1.1.2 *Drosophila melanogaster*'s toolbox for systems neuroscience

The fruit fly is not only a great model organism for cell and developmental biology, but also for neuroscience including systems neuroscience. The common goal in systems neuroscience is to understand how the brain integrates sensory inputs and transforms them into behavioral output. In order to understand these mechanisms, researchers are focusing on a behavior of interest, investigating underlying neural circuits and the way these neurons perform certain computations. *Drosophila* constitutes an ideal model organism to study all the above-mentioned aspects. On the one hand, fruit flies possess a brain with a relatively small number of only 100.000 neurons compared to the 70 million neurons in the mouse brain or 86 billion in a human brain. This relatively small number indicates a less complex brain and increases the chances of understanding it. On the other hand, flies are capable of rather complex behaviors stemming from sensory modalities such as olfaction and vision, as well as higher order behaviors such as learning. The small number of neurons makes it possible to dissect whole circuits and discover all cell types involved in a specific behavior.

Furthermore, *Drosophila* comes with an enormous genetic toolbox that has been developed over decades and is still growing continuously. Amongst the most powerful inventions is the binary **UAS-Gal4** expression system which allows for cell-type-specific expression of any gene of interest (Brand & Perrimon, 1993). Derived from yeast, the transcription factor Gal4 binds to the Upstream Activation Sequence (UAS) to activate transcription of any gene downstream of the UAS sequence. Only when the so-called Gal4 driver fly line and the UAS effector fly line are crossed, the offspring will show cell-type-specific UAS-Gal4 driven expression

of gene *X* (Fig. 2). In the early days of this new technique, Gal4 lines were generated by randomly inserting Gal4 with P-element transposons into the fly genome. Nowadays, DNA fragments with presumed enhancer activity are directly cloned from the genomic DNA to generate thousands of Gal4 driver lines and intersectional split-Gal4 lines addressing most of the fly's cell types (Pfeiffer et al., 2008, 2010; Jenett et al., 2012).

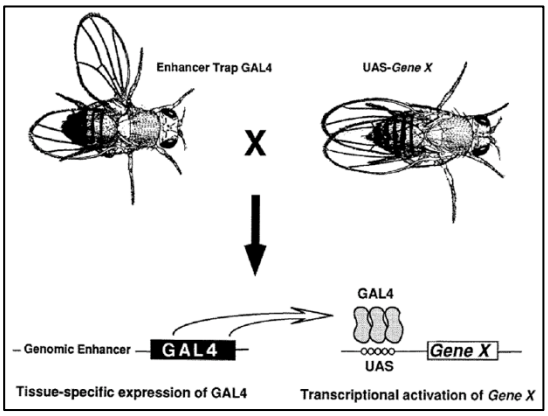

Figure 2. The UAS-Gal4 system in *Drosophila*.
Two flies, the enhancer trap Gal4- line and the UAS-Gene X line, are crossed for directed gene expression. The enhancer trap line consists of a genomic enhancer fused to the Gal4 sequence, while the UAS-reporter-line consists of a UAS sequence followed by the Gene X (Brand & Perrimon, 1993). Tissue-specific Gal4 will bind to the UAS sequence to elicit expression of gene *X* in a cell-type-specific manner. Image taken with permission from Brand & Perrimon, 1993.

One of the simplest applications of the UAS-Gal4 system is expression of a structural marker which is a cytosolic or membrane-tethered fluorescent protein such as GFP or mCherry, in the cells of interest to study their morphology using light microscopy. Furthermore, the MultiColor FlpOut (MCFO) tool can be used to stochastically label individual neurons in different colors for high-throughput neuroanatomical investigations. For this method, the expression of multiple membrane-targeted and distinct epitope-tagged proteins is controlled both by a transcriptional driver and by stochastic, recombinase-mediated excision of transcription-terminating cassettes. (Nern et al., 2015).

Especially in circuit neuroscience, the UAS-Gal4 system is frequently used to manipulate neural activity by cell-type-specific expression of activators or inhibitors. For activation of neurons, the ionotropic purinoceptor P2X2 can be expressed cell-type-specifically and application of ATP will lead to depolarization of the cells. It was demonstrated that the P2X2-based activation of the giant fiber neuron leads to typical escape behaviors in flies (Lima & Miesenböck, 2005). For heat-inducible neural activation, the thermosensitive cation channel TrpA1 is used

especially in behavioral paradigms in *Drosophila* (Hamada et al., 2008). More recently, optogenetic, light-sensitive ion channels like the cation channel Channelrhodopsin-2, ReaCHR, and Chrimson allow to excite neurons with precise temporal resolution (Nagel et al., 2003; Lin et al., 2013; Klapoetke et al., 2014). Alternately, potent inhibitors of neural activity such as tetanus toxin (TNT) are used in order to abolish neurotransmitter release, and the inwardly rectifying potassium channel Kir2.1 which hyperpolarizes neurons (Sweeney et al., 1995; Baines et al., 2001). For heat-inducible blocking of synaptic transmission UAS-shibire^{ts1} enables reversible inactivation of neurons (Kitamoto, 2001). Recently, optogenetic inhibition of neural activity via light-sensitive channels has been introduced to flies. The light-gated anion channel GtACR allows for effective silencing of neurons in the visual system of *Drosophila* (Mauss et al., 2017).

On the molecular side, there are numerous tools available to study the role of specific genes in *Drosophila*. The most prominent method for conditional loss-of-function studies is the knockdown of genes with RNA interference (RNAi), a method that degrades mRNA, eventually preventing translation of the protein. Large scale libraries contain thousands of UAS-RNAi lines that enable the cell-type-specific inactivation of any gene of interest (Dietzl et al., 2007; Perkins et al., 2015). However, RNAi knockdowns are rarely complete and off-target effects can occur (Ma et al., 2006; Perkins et al., 2015). Recently, the rise of CRISPR/Cas9 genome editing has expanded the toolkit for conditional loss of function studies in *Drosophila* (Port et al., 2014; 2020; Heidenreich & Zhang, 2016).

1.2 Neurotransmitters, receptors, and voltage-gated ion channels in *Drosophila*

In the late 19th century, the Spanish neuroscientist Santiago Ramón y Cajal laid the foundation for what is known as the ‘neuron doctrine’. His Golgi stainings of brain samples from different species led him to the conclusion that nerve cells were discrete individual units, contrasting Camillo Golgi’s ‘reticular theory’ which states that the brain is a single, continuous network. Later, Golgi’s hypothesis was discarded and Cajal’s neuron doctrine was shown to be indeed the correct description of the nervous system as we know it today: Nerve cells are discrete individual cells. They form networks via synapses, i.e. the cellular structures where two neurons connect to each other. Two types of synapses exist: chemical synapses on the postsynaptic side, and electrical synapses. In the electrical synapse, gap junction

proteins form paired channels in both the pre- and postsynaptic membrane, constituting a pore through which ions can flow bidirectionally (Purves et al., 2001). In the chemical synapse, the presynaptic neuron releases a neurotransmitter which binds to transmitter receptors in the membrane of the postsynaptic neuron initiating an electrical response which can either excite or inhibit the postsynaptic neuron (detailed steps of signal transduction in Fig. 3).

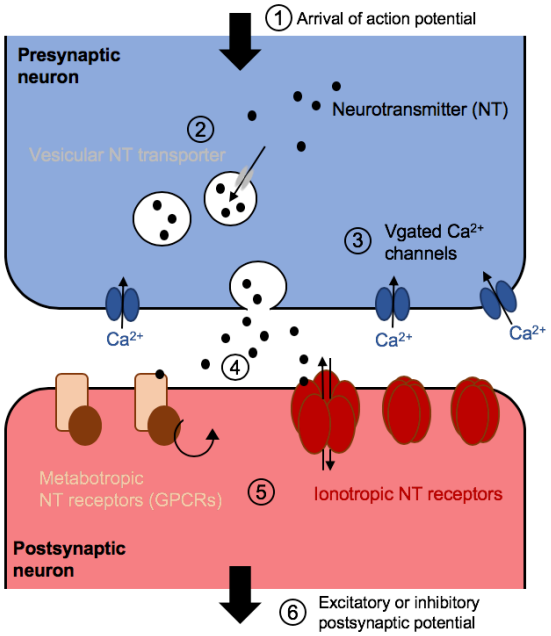

Figure 3. Schematic overview of a chemical synapse.
The action potential arrives at the presynaptic terminal **(1)**, where neurotransmitter (NT) is packed into vesicles via vesicular NT transporters **(2)**. Depolarization of the presynaptic terminal leads to influx of Ca^{2+} via voltage-gated (Vgated) Ca^{2+}-channels **(3)**. Ca^{2+} causes the fusion of the NT-filled vesicles with the presynaptic membrane and release of NT into the synaptic cleft. NT binds to either metabotropic NT receptors or ionotropic NT receptors in the postsynaptic membrane **(4)**. In the case of the metabotropic receptor (G-protein coupled receptor, GPCR) a second messenger cascade is initiated which can lead to excitation or inhibition of the postsynaptic neuron **(5, 6)**. Ionotropic NT receptors are ligand-gated ion channels that allow the flux of ions in or out of the postsynaptic neuron **(5)**, causing direct excitatory or inhibitory potentials **(6)**. Figure adapted from Fig. 7.19 from 'Introductory Animal Physiology', Sanja Hinic-Frlog, 2019.

Neurotransmitter receptors are membrane proteins which can be divided into ionotropic and metabotropic receptors. Ionotropic receptors are ligand-gated ion channels composed of a transmembrane domain including the ion conduction pore and an extracellular domain including the ligand-binding domain. Ions like Na^+, Cl^-, Ca^{2+}, or K^+ flow in and out of cells via the ion pore in ionotropic receptors. Usually, several subunits form one ionotropic receptor, which can be for instance a tetramer or a pentamer (Cascio, 2004).

Metabotropic receptors are coupled with G-proteins and act indirectly on ion channels via signal transduction mechanisms. They are also called seven-transmembrane helix proteins as they possess seven membrane-spanning helices. The G proteins are typically composed of a α-, β- and γ-subunits, whereby the type of α-subunit defines the cellular response cascade (Rosenbaum et al., 2009). For instance, a G-protein coupled receptor with the $G_{i/0}$ α-subunit inhibits the enzyme adenyl cyclase which in turn leads to closed Ca^{2+}-channels and inhibition of neural activity (Sprang et al., 2007). The G_S-subunit, in contrast, activates adenylyl cyclase, causing increased cAMP levels and neural activation.

For my doctoral thesis, I studied neurotransmitters and receptors in the visual system of the fruit fly in the context of the motion-sensing T4/T5 neurons. In the following chapter I will give a general introduction to the most important neurotransmitters and their corresponding receptors in *Drosophila*.

1.2.1 Glutamate

Glutamate is the main excitatory transmitter in the mammalian central nervous system and at the *Drosophila* neuromuscular junction. It is the most abundant amino acid in the human and fly brain and present in every cell. The vesicular glutamate transporter VGlut is responsible for glutamate uptake and storage into vesicles (Daniels et al., 2004). Immunohistochemical signal of VGlut in axonal terminals or somata is considered the standard marker for glutamatergic neurons (Mahr & Aberle, 2006; Daniels et al., 2008). Numerous glutamatergic neurons exist throughout the *Drosophila* brain (Daniels et al., 2008 and Raghu et al., 2011) and several studies demonstrated the excitatory action of glutamate (Das et al., 2011a; 2011b; Wu et al., 2007; Xia et al., 2005).

There are 15 putative ionotropic glutamate receptor subunits and one metabotropic glutamate receptor described in *Drosophila* (Fig. 4). The ionotropic glutamate receptors (iGluRs) can be divided into NMDA and non-NMDA glutamate receptors. Two NMDA receptors, Nmdar-1 and Nmdar-2, have previously been described. They are involved in sleep behavior (Tomita et al., 2015), and olfactory learning and memory (Xia et al., 2005) in *Drosophila*. The best described non-NMDA iGluRs are GluRIIA, GluRIIB and GluRIIC which are found at the neuromuscular junction (NMJ) in the fruit fly. In total, there are around 12 iGluR subunits. Interestingly, it was shown in 2013 that glutamate can also act as an inhibitory neurotransmitter when it binds to the glutamate-gated ion channel GluClα (Liu & Wilson, 2013). The

inhibitory effects of GluClα are crucial for olfactory processing in the antennal lobe (Liu & Wilson, 2013) and were shown to play an important role in motion opponency in the visual system of the fly (Mauss et al., 2015). Furthermore, glutamate can also act on a slower G-protein coupled receptor (GPCR), the metabotropic glutamate receptor mGluR which is expressed presynaptically in the fly NMJ (Bogdanik et al., 2004). At the presynaptic site mGluRs modulate presynaptic excitability and synaptic architecture. It was also shown that mGluRs have an inhibitory effects on clock neurons (Hamasaka et al., 2007).

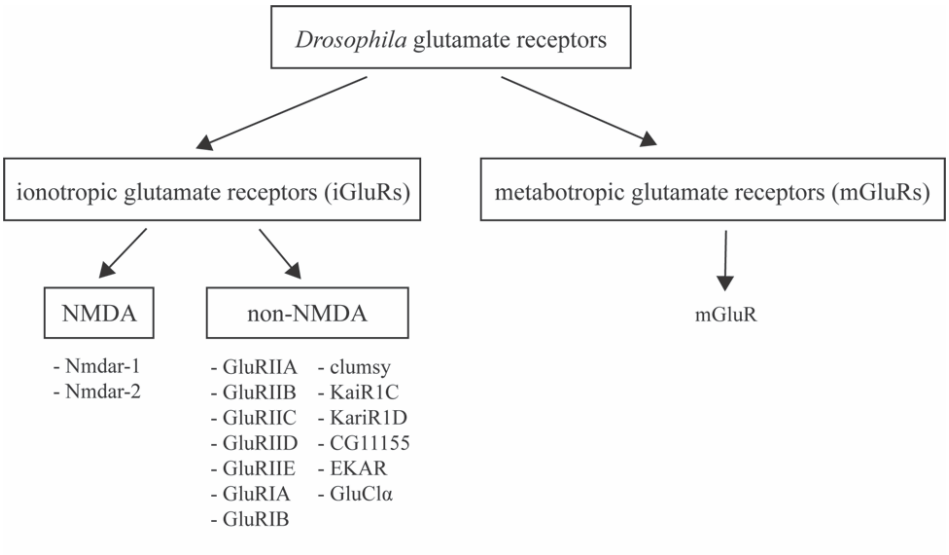

Figure 4. Overview of glutamate receptor subunits in *Drosophila*.
There are ionotropic and metabotropic glutamate receptors. Only one metabotropic Glu receptor has been described. Ionotropic Glu receptors can be divided into NMDA- and non-NMDA-receptors.

1.2.2 GABA

γ-aminobutyric acid or short 'GABA' is the main inhibitory neurotransmitter in both mammals and invertebrates. GABA is synthesized from glutamate by the enzyme glutamic acid decarboxylase (GAD), which is also considered the standard marker for GABAergic neurons (Jackson et al., 1990; Featherstone et al., 2000). GABA is packed and stored in vesicles via VGAT which is the vesicular GABA transporter. VGAT can also be used as a marker for terminals of GABAergic neurons (Kolodziejczyk et al., 2008; Fei et al., 2010). It was shown that in VGAT mutants GABA release is decreased which in turn impairs object tracking in flies but not the optomotor response (Fei et al., 2010). These findings hint towards distinct roles of GABAergic signaling in the visual system of *Drosophila*.

In *Drosophila*, three genes are described to encode GABA-gated chloride channel subunits: the so-called ionotropic $GABA_A$ receptors Rdl, Lcch3 and Grd (Fig. 5). Rdl, the best studied GABA receptor A-type subunit, stands for 'resistant-to-dieldrin' since it was first characterized in a mutant that is resistant to the cyclodiene insecticide dieldrin due to a single amino acid replacement (Ffrench-Constant et al., 1993; 1991b; Ffrench-Constant and Rocheleau, 1992; Ffrench-Constant and Roush, 1991a). Rdl is highly expressed in the antennal lobes and the mushroom body (Harrison et al., 1996; Davis, 2004); in the latter it negatively regulates associative olfactory memory (Liu et al., 2007). Furthermore, Rdl is also found on the dendrites of lobula plate tangential cells in the visual system of the fly (Raghu et al., 2007). Recently it was demonstrated that its inhibitory effects are important for creating ON-selectivity in the visual pathway (Molina-Obandoet al., 2019). Less is known about the two other ionotropic GABA receptor subunits, Lcch3 and Grd. Rdl is known to form homomers in the heterologous expression system of *Xenopus laevis* oocytes (Hosie & Sattelle, 1996). When co-expressed in cell culture, Lcch3 and Rdl can also form functioning GABA heteromers that respond to GABA application (Zhang et al., 1995). However, *in vivo* they are not expected to form this type of heteromeric GABA channel since the two subunits are differentially distributed in the fly brain as shown by immunohistochemistry (Hosie et al., 1997). Interestingly, it was reported that Lcch3 and Grd form heteromeric cation-channels when expressed in *Xenopus* oocytes, leading to excitatory currents (Gisselmann et al., 2004). Davis et al., also found in their RNAseq study that Lcch3 is expressed in optic lobe neurons either together with Grd or Rdl, indicating a possible role of Lcch3/Grd heteromers *in vivo* (Davis et al., 2020). However, it is still unknown, if this subunit combination also leads to excitatory currents *in vivo*.

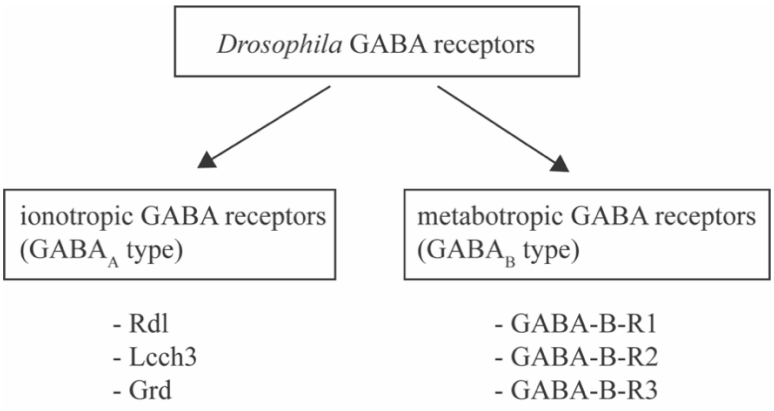

Figure 5. Overview of GABA receptor subunits in *Drosophila*.
There are three ionotropic $GABA_A$ type receptors and three metabotropic $GABA_B$ type receptors described.

GABA can also act as a slow inhibitory transmitter when it binds to metabotropic GABA B-type receptors. There are three metabotropic subunits described in *Drosophila*: Gaba-b-r1, Gaba-b-r2 and Gaba-b-r3 (Fig. 5). This type of inhibition via $GABA_B$ receptors was found to take place in projection neurons in the antennal lobe allowing for subtractive gain control (Suzuki et al., 2020). Furthermore, Gaba-b-r2 receptors mediate the regulation of olfactory information via presynaptic inhibition of olfactory receptor neurons (Olsen & Wilson, 2008). $GABA_B$ receptors are also involved in sleep drive and behavioral responses to alcohol (Ki & Lim, 2019; Ranson et al., 2020). It is thought that Gaba-b-r1 and Gaba-b-r2 are co-expressed together *in vivo* since *in situ* hybridization showed their localization in similar regions, whereas Gaba-b-r3 is differentially distributed (Mezler et al., 2001). Recently, Gaba-b-r1 was found to be expressed in the antennal lobe, the visual system, the mushroom body and the ellipsoid body, whereas Gaba-b-r3 was only expressed in the ellipsoid body, but not in the mushroom body (Deng et al., 2019). Taken together, several studies described the distribution and functional relevance of the metabotropic GABA receptor subunits in *Drosophila*. However, a comprehensive picture of $GABA_B$ receptors, how they are combined in differentially tuned oligomers *in vivo* and their specific functional roles stills remain elusive.

1.2.3 Acetylcholine

Acetylcholine (ACh) is the oldest and best studied neurotransmitter in both vertebrates and invertebrates. The synthesizing enzyme for ACh is the choline acetyltransferase (ChAT) (Greenspan, 1980; Salvaterra & McCaman, 1985) and the vesicular ACh transporter VAChT loads the transmitter into vesicles (Kitamoto et al., 1998). Hence, both ChAT and VAChT are markers for cholinergic neurons, whereby VAChT can be found predominantly in ACh release sites in the axon terminals.

There are 13 ACh receptor subunits described in the *Drosophila* genome (Fig. 6); from those 10 are ionotropic, so-called nicotinic ACh receptors, named after their agonist nicotine; Dα1-Dα7 and Dß1-Dß3. Furthermore, there are 3 metabotropic subunits, so-called muscarinic ACh receptors named after their agonist muscarine; mAChR-A, mAChR-B and mAChR-C. The nicotinic ACh receptors are ligand-gated cation channels permeable to mainly Na^+ and K^+, but also to Ca^{2+}. On the other hand, muscarinic ACh receptors are G-protein coupled and act via second messenger cascades (Shapiro et al., 1989; Brody & Cravchik, 2000).

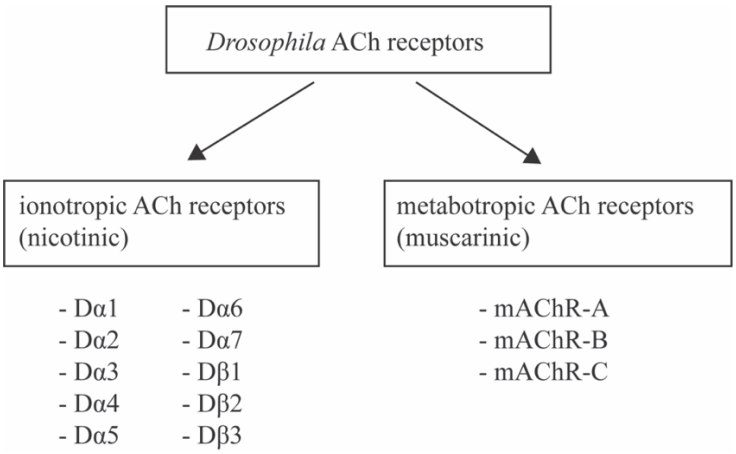

Figure 6. Overview of acetylcholine (ACh) receptor subunits in *Drosophila*.
There are ten ionotropic, nicotinic ACh receptors and three metabotropic, muscarinic ACh receptors described.

The most explored ACh receptor subunit in *Drosophila* is Dα7 (or nAChRα7), which forms a homomeric pentamer ACh receptor with excitatory effects (Fayyazuddin et al., 2006). Mutant analyses showed that Dα7 is important in the giant fiber where it mediates jump escape behavior in flies (Fayyazuddin et al., 2006). It has also been found that the ACh subunit Dα7 is localized to the dendrites of lobula plate tangential cells (LPTCs), the widefield optic flow sensors of the fly motion vision pathway (Raghu et al., 2009). Back then, this mainly demonstrated cholinergic, excitatory inputs to LPTCs. Only a few years later it was shown that this cholinergic input comes from the first-order direction-selective T4/T5 neurons (Mauss et al., 2014). Less is known about the other nicotinic ACh receptor subunits. Studies mainly done in heterologous expression systems showed that the subunits Dα5, Dα6 and Dα7 can form functioning heteromers *in vitro* (Lansdell & Millar, 2004; Lansdell et al., 2012). However, it still remains unknown, if these heteromers are also formed *in vivo*.

Experiments with stable *Drosophila* cell culture demonstrated the excitatory effects of mAChR-A via the $G_{q/11}$-mediated second messenger cascade leading to increased intracellular Ca^{2+} levels (Millar et al., 1995). Surprisingly, a recent study showed that mAChR-A has inhibitory effects on Kenyon cells in the olfactory system of the fly. This cholinergic inhibition acts on Kenyon cell dendrites where it facilitates synaptic plasticity in odor-associated learning (Bielopolski et al., 2019). mAChR-B is coupled to $G_{i/o}$ which inhibits the enzyme adenylyl cyclase leading to decreased Ca^{2+} levels and hence inhibitory effects on the neuron (Ren et al., 2015). Recently, inhibitory mAChR-B was shown to produce the sign-inversion for establishing the OFF-channel in the larval *Drosophila* visual pathway (Qin et al., 2019). To date,

nothing is known about the functional roles or distribution of the third metabotropic ACh receptor subunit, mAchR-C (Xia et al., 2016).

1.2.4 Monoamines (neuromodulators)

Besides the main neurotransmitters glutamate, GABA, and acetylcholine there exist several other transmitters, which belong to the class of monoamines: dopamine, serotonin, octopamine, tyramine and histamine. In the following chapter, I will introduce dopamine, serotonin and octopamine as well as their corresponding receptors.

In *Drosophila*, around 128 dopaminergic neurons can be found exclusively in the central brain and are organized in 8 clusters (Kasture et al., 2018). **Dopamine** is one of the so-called 'neuromodulators' since it acts on many neurons and circuits simultaneously to modulate sleep, rest and activity, aggression, memory formation, courtship, feeding and learning (Nitz et al., 2002; Schwaerzel et al., 2003; Riemensperger et al., 2011; Alekseyenko et al., 2013; Waddell, 2013; Yamagata et al., 2015; Berry et al., 2015; Aso & Rubin, 2016). Four GPCR dopamine receptors have been characterized in the fruit fly: Dop1R1, Dop1R2, D2R and DopEcR. The first two, Dop1R1 and Dop1R2 belong to the G_s protein family whereas D2R is G_i-coupled. Upon dopamine binding to the GPCRs Dop1R1 or Dop1R2 the enzyme adenylyl cyclase is activated which in turn leads to increased cAMP levels and a second messenger cascade that induces EPSCs. Conversely, D2R is G_i-coupled which inhibits the enzyme adenylyl cyclase, eventually causing inhibition of the neuron (Hearn et al., 2002). Furthermore, the fly genome includes the non-canonical receptor DopEcR which is a steroid hormone receptor with affinity for both ecdysone and dopamine. It plays a role in courtship memory in mushroom body circuits (Ishimoto et al., 2013).

Serotonin is another important state-dependent neuromodulator that regulates a long list of behaviors in the fruit fly, such as sleep, place memory, circadian rhythm, feeding, aggression and memory formation (Yuan et al., 2005; Sitaraman et al., 2008; Alekseyenko et al., 2010; Majeed et al., 2016; Kaneko et al., 2017; Scheunemann et al., 2018; Kasture et al., 2018). There are around 80 serotonergic neurons in the central brain of *Drosophila*, arranged in discrete clusters (Sitaraman et al., 2008; Kasture et al., 2018). Five G protein-coupled serotonin receptors have been described in *Drosophila*, which are 5HT-R1A, 5HT-R1B, 5HT-R2A, 5HT-R2B and 5HT-R7. The serotonin receptor 5HT-R1A is $G_{i/o}$- coupled and was shown

to have inhibitory effects in vivo (Yuan et al., 2006; Blenau & Thamm, 2011; Luo et al., 2012). 5HT-R2A and -2B are Gq-coupled, but their physiological properties in vivo have not been described yet. The Gs-coupled serotonin receptor 5HT-R7 is thought to cause neural excitation via increasing cAMP-levels and is essential for courtship and mating (Becnel et al., 2011). A recent study demonstrated that some neurons involved in early visual processing in the fly optic lobe are regulated by serotonin (Gschweng et al., 2020).

Octopamine, the invertebrate counterpart to the mammalian hormone epinephrine, is associated with the initiation of movement, flight, aggression, learning, memory and sleep (Sombati & Hoyle, 1984; Brembs et al., 2007; Zhou et al., 2008; El-Kholy et al., 2015). Furthermore, sensory systems like vision are modulated by octopamine in a state-dependent manner in *Drosophila* (Suver et al., 2012). For more active states of the fly such as walking or flying, octopamine shifts the temporal-frequency tuning of several neurons of the visual pathway to higher frequencies (Longden & Krapp, 2010; Jung et al., 2011; Suver et al., 2012; Arenz et al., 2017; Strother et al., 2018). There are 6 octopamine receptors described in *Drosophila*: Oamb, Octα2R, Octß1R, Octß2R, Octß3R and Oct-TyR.

Histamine is an important neurotransmitter in the visual system of many arthropods including *Drosophila* as it is released by photoreceptors, the first layer of light-sensitive cells in the optic lobe (Hardie, 1989). Two genes are known to encode histamine receptors in *Drosophila*: *ora transientless* (*ort*) and *Histamine-gated chloride channel subunit 1* (*HisCl1*) (Gisselmann et al., 2002; Zheng et al., 2002; Gengs et al., 2002). Both receptors are histamine-gated chloride channels, hence, they hyperpolarize cells.

1.2.5 Voltage-gated ion channels

Voltage-gated ion channels are sensitive to changes in membrane potential which lead to conformational changes and gating of ions. They are selectively permeable to the major physiological ions Na^+, Ca^{2+}, and K^+. Hence, they can be subdivided into voltage-gated sodium, calcium, and potassium channels (Fig. 7). Voltage-gated ion channels are essential for cell excitability and influence the electrical signaling within and between cells. Most of our knowledge about voltage-gated ion channels and their physiological dynamics stems from the pioneering work of Hodgkin and Huxley. Between 1939 and 1952 they developed a method for intracellular recordings of the squid giant axon, recorded the first action potential, and analyzed

ion channel kinetics (Hodgkin & Huxley, 1939, 1945; Schwiening, 2012). Later, their work culminated in their famous mathematical model of the action potential in 1952 (Hodgkin & Huxley, 1952).

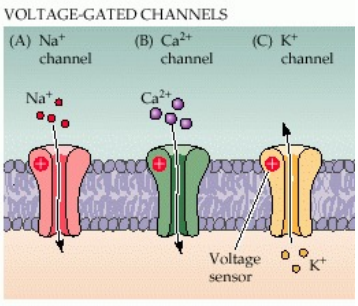

Figure 7. Overview of voltage-gated ion channels.
The three most important classes of voltage-gated ion channels are Na^+ channels (A), Ca^{2+} channels (B), and K^+ channels (C). Na^+ channels are permeable to Na^+ ions which flow into the cell. Ca^{2+} channels are permeable to Ca^{2+} ions which flow into the cell. K^+ channels, on the other hand, are permeable to K^+ ions which are gated out of the cell. Image taken with permission from Purves et al., 2001.

Voltage-gated sodium channels are critical for rapid depolarization due to the influx of sodium ions into the neuron (Warmke et al., 1997). The only voltage-gated sodium channel gene described in *Drosophila* is *paralytic* (*para*). It is required for the generation of action potentials mediated by sodium. Furthermore, para also plays a role during development by regulating the proliferation of neuroblast lineages, the progenitors of *Drosophila* neurons (Piggott et al., 2019).

Voltage-gated calcium channels mediate the influx of Ca^{2+} ions in response to arriving action potentials. Calcium channels are composed of the primary structural subunit, the so-called alpha1 subunit, together with beta, alpha2/delta or gamma subunits (Catterall, 1998). The alpha subunit of the voltage-gated calcium channel in *Drosophila* is cacophpy (cac) which induces neurotransmitter release at presynaptic active zones (Iniguez et al., 2013).

Voltage-gated potassium channels play an important role in repolarizing the depolarized cell to its resting potential. The first identified voltage-gated potassium channel in *Drosophila* is Shaker (Kamb et al., 1987). Later, several other voltage-gated potassium channels were discovered, such as Shab, Shaw, Shal, Eag, Sei, Elk, and Slo (Frolov et al., 2012).

1.3 Methods for studying neurotransmitters and receptors

In order to fully understand neural circuits, it is essential to define neurotransmitter phenotypes of presynaptic cell types and the transmitter receptors used by the postsynaptic partners. Neurotransmitters can act on a range of different receptors composed of exchangeable subunit combinations, leading to either excitation or inhibition, or modulation with differential temporal dynamics. Hence, neurotransmitter receptors define the sign as well as the time course of any chemical synaptic connection. Several approaches have been established in *Drosophila* for studying neurotransmitters and receptors. For defining the neurotransmitters used by specific neural cell types, markers such as transmitter-synthesizing enzymes or vesicular transporters are used. For instance, the vesicular transporter for glutamate VGlut is a well-established marker for glutamatergic neurons and GAD, the synthesizing enzyme of GABA, is a marker for GABAergic neurons (Mahr & Aberle, 2006; Daniels et al., 2008; Kolodziejczyk et al., 2008). On the postsynaptic site, the question is not only which receptors are expressed, but also where they are localized.

To investigate both the transmitter phenotype and the receptors with molecular approaches one can either look at RNA or protein levels. Methods focusing on RNA levels can answer, if a neurotransmitter or receptor is expressed in the cell of interest. Investigations at the protein level provide information on expression levels and localization of transmitter release sites or receptors. In the following paragraphs, I will highlight the most important methods for investigation of neurotransmitters and receptors at the RNA and at the protein level.

1.3.1 RNA level

When a gene is expressed in a cell of interest, the first detectable product is the mRNA molecule. Hence, mRNA levels of a given gene are used as readout of expression levels. There are several methods to measure RNA levels of a certain gene in the cell type of interest. Those can be sub-divided into methods which retain spatial information and those that only look at expression levels without the context of spatial localization.

One of the earliest techniques for quantification of gene expression is the **qRT-PCR** (quantitative real-time PCR) or qPCR (quantitative PCR). Here, the neurons of interest (usually GFP-labeled) are extracted from the brain by either picking single

cells (Takemura et al., 2011; Mauss et al., 2015) or by FACS sorting (Porter et al., 2017). The mRNA is isolated from the collected cells and reverse-transcribed into complementary DNA (cDNA) which can be analyzed on the qPCR machine. In the qPCR reaction, the amplified DNA is quantified via incorporated fluorescent dyes and the expression of the target gene is quantified as fold-changes in comparison to an internal reference gene.

A quickly evolving method for transcriptome analysis is **RNA sequencing (RNAseq)** which measures presence and quantity of mRNA in the cells of interest. RNAseq emerged about 15 years ago while next-generation sequencing was on the rise (Weber, 2015). Initially, it was applied to sequence the transcriptome of plants like *Zea mays* or *Arabidopsis thaliana* (Emrich et al., 2007; Weber et al., 2007). Afterwards it quickly revolutionized many research areas across the life sciences, including neurobiology (Ecker et al., 2017). The typical workflow of an RNAseq experiment looks as follows: The mRNA is extracted from the cells/ neurons of interest (usually via FACS cell sorting), fragmented and reverse-transcribed into more stable cDNA. The cDNA is sequenced using high-throughput, next-generation sequencing methods and the reads are aligned to a reference genome. Eventually, the relative expression levels of the annotated genes can be extracted. In the past years, besides bulk RNAseq of only one cell type at a time, single cell RNAseq (scRNAseq) has been developed and improved. scRNAseq allows for RNAseq of individual cells, enabling sequencing of many cell types at the same time extracted from one organism or tissue. For this method, microfluidic devices are used to encapsulate individual cells in droplets which carry a unique "barcode" (Kimmerling et al., 2016). In the subsequent sequencing step, the barcoded cells can be mixed together and individual cells can be identified by their barcodes. The obtained reads for every cell are analyzed with hierarchical cluster analysis and cell types are inferred from cluster similarity. While not all RNAs can be annotated due to low RNA material availability, this method for example allows to track transcriptomic changes of several cell types during development (Kurmangaliyev et al., 2019; Hoermann et al., 2020). Recently, several studies investigated neurotransmitter and receptor expression in numerous cell types of the *Drosophila* brain using RNAseq and scRNAseq (Pankova & Borst, 2016; Konstantinides et al., 2018; Davie et al., 2018; Davis et al., 2020).

Since RNA is collected from the soma, it does not provide spatial information about where in the tissue or the cell the specific mRNA was localized. To circumvent this

issue, researchers have developed powerful fluorescent *in situ* hybridization (FISH) methods to analyze endogenous mRNA sequences in intact tissues (Long et al., 2017; Meissner et al., 2019). FISH uses fluorescent probes specific to the mRNA of interest which can be detected under a conventional confocal microscope. Thereby, the presence and localization of mRNA molecules can be examined using FISH. A recent study expanded existing FISH probes to all important neurotransmitters and defined their expression pattern in the whole fruit fly brain (Meissner et al., 2019). A new innovative approach builds on RNAseq while maintaining spatial information: Spatial transcriptomics. In 2016, Ståhl and colleagues developed spatial RNAseq, for which they analyzed histological sections of mouse brain and human breast cancer on an array of primers with positional barcodes. They received high-quality RNAseq data with preserved two-dimensional spatial information (Ståhl et al., 2016). Additionally, Slide-seq, a spatial RNAseq approach which uses a surface covered with DNA-barcoded beads revealed spatial gene expression patterns in the mouse cerebellum (Rodriques et al., 2019). These methods seem to be promising for identifying the bigger picture of brain-wide expression patterns in many species.

1.3.2 Protein level

Detecting the localization of a protein of interest in its cellular environment is pivotal across all life sciences. Proteins can be detected either by immunohistochemical staining with fluorescently-tagged antibodies or by introducing tags directly into the genetic locus. Furthermore, the techniques can be divided into pan-neuronal labeling of the protein of interest and conditional, cell-type-specific labeling.

Pan-neuronal protein labeling

Immunohistochemical staining first appeared in 1941 to detect the bacterium *pneumococcus* with a fluorescent antibody (Coons et al., 1941) and has ever since undergone a tremendous improvement and expansion of techniques. The oldest system for protein detection in intact tissue is immunohistochemical staining with antibodies which bind to the protein in fixed tissue. Using fluorescent or confocal microscopy, images are acquired and the distribution of the protein can be analyzed. However, antibodies for every protein of interest do not exist and epitope recognition might be influenced by tissue fixation (Fritschy, 2008). Furthermore, the specificity of antibodies needs to be tested carefully since some antibodies can bind to several proteins with similar epitopes leading to false-positive results. When it comes to neurotransmitters and receptors, the available antibodies are limited (overview in Kolodziejczyk et al., 2008). Anti-VGlut, anti-GAD1 and anti-GABA antibodies

have been used successfully to characterize glutamatergic or GABAergic neurons, respectively (Jackson et al., 1990; Hamasaka et al., 2005; Mahr & Aberle, 2006; Daniels et al., 2008).

An alternative approach is to directly introduce a fluorescent tag into the endogenous locus of the gene. Large-scale approaches like MiMIC and FlyFos generated large fly line libraries with GFP-tagged genes (Venken et al., 2011; Nagarkar-Jaiswal et al., 2015; Sarov et al., 2016). The **MiMIC** (Minos Mediated Integration Cassette) library used the transposon Minos to generate more than 7000 fly lines with random insertions of the MiMIC cassette (Venken et al., 2011). Those can be either used as gene traps or further transformed to protein traps via recombinase-mediated cassette exchange (RMCE). To date, according to the GDP database, there exist 15.736 RMCE MiMIC lines with GFSTF or TG4 insertions. The GFSTF MiMIC lines contain a GFP cassette in a coding-intron of the gene flanked by splice acceptor and donor which eventually generates an endogenously GFP-tagged protein (Nagarkar-Jaiswal et al., 2015). The tagged **FlyFos TransgeneOme (fTRG)** library comprises around 900 fly lines, each containing an extra copy of a gene with a GFP-knock in coding for one GFP-tagged protein. 207 lines were analyzed by stainings and live imaging of ovaries, embryos, pupae or adults. Importantly, the GFP-tagged proteins could be visualized at endogenous expression levels, localizing to subcellular compartments. While there are some MiMIC GFSTF lines available for neurotransmitter markers (VGlut, Gad1), the fTRG library does not cover any of the transmitter synthesizing enzymes or vesicular transporters. Both libraries contain lines with GFP-tagged transmitter receptors, readily available for immunostainings. Additionally, Kondo et al. created 75 lines with C-terminal tagged neurotransmitter receptor genes which can be exchanged with a Venus-tag (Kondo et al., 2020).

Cell-type-specific protein labeling

The genetic toolbox of *Drosophila* including the UAS-Gal4 system makes it possible to express effector genes only in specific cell types. **Gal4 enhancer trap lines** are generated by either randomly inserting the Gal4 coding sequence into the genome with transposons or directly fusing it to a promoter sequence and subsequently integrating into the genomic DNA. For the analysis of neurotransmitter types and receptors, Gal4 lines with insertions upstream of the relevant genes or direct fusions can be exploited. When crossed to e.g. a UAS-tdTomato or UAS-GFP line, these Gal4 lines label cells which express the gene of interest (e.g. neurotransmitter marker or transmitter receptor). For instance, the Gal4 enhancer trap line OK371 was

initially described to label motoneurons and glutamatergic neurons in general, with the enhancer fragment OK371 9 kb upstream of the VGlut gene (Mahr & Aberle, 2006). Later, a new Gal4 enhancer trap line was generated by fusing Gal4 with a "5.5 kb piece of DNA immediately upstream of the *dvglut* translation start" (Daniels et al., 2008). The authors of the study used it to visualize glutamatergic cells in the larval and adult *Drosophila* CNS. Another study identified glutamatergic neurons in the visual system of the fly using this *dvglut* -Gal4 line (Raghu & Borst, 2011).

Transposon-based or manually cloned enhancer trap lines are labor intensive and often not precise. Hence, several new methods have been developed in order to achieve a more accurate cell type specific expression. The "Trojan plug-and-play" toolbox introduced the so-called **Trojan Gal4 (TG4)** cassette that can be inserted into coding intron MiMIC sites in the endogenous locus of the gene of interest (Diao et al., 2015). Here, the T2A peptide promotes the translation of the Gal4 protein independent of the endogenous protein it has been inserted into. TG4 lines are available for some glutamate and ACh receptors for which they can act as expression reporters. This study was complemented by the T2A-Gal4 library that included around 1000 lines with T2A-Gal4 insertion in the endogenous gene locus (Lee et al., 2018). The authors also developed CRIMIC (CRISPR-Mediated Integration Cassette) a vector and protocol for CRISPR-based insertion of T2A-Gal4 in desired coding introns of genes lacking a MiMIC insertion. Recently, another study provided T2A-Gal4 lines specifically for 75 C-terminally tagged neurotransmitter receptor genes (Kondo et al., 2020).

Preferably, one would not only like to know which cells express the gene of interest, but also where in the cell the protein is localized. Specifically, when studying neurotransmitter receptors, the subcellular distribution plays an important role. To this end, researchers use **UAS-lines** to express the coding sequence of a receptor of interest with a GFP- or tag-insertion (e.g. HA or FLAG). Sanchez-Soriano and colleagues generated a UAS-Rdl::HA line to study dendrites in motoneurons using the GABA receptor Rdl as a marker for postsynaptic sites (Sánchez-Soriano et al., 2005). The same line was used in a second study to investigate the distribution of inhibitory synapses in lobula plate tangential cells in the fly optic lobe (Raghu et al., 2009). Kuehn and Duch combined the UAS-Rdl::HA line with a UAS-Da7::GFP line to show that inhibitory, GABAergic and excitatory, cholinergic synapses are differentially distributed in the flight motor neuron MN5 (Kuehn & Duch, 2013).

The most elegant and reliable protein-labeling technique would combine both **cell-type-specificity and endogenous targeting**. To date, however, this has only rarely been achieved. In 2014, synaptic tagging with recombination (STaR) was developed- "a method for labeling endogenous presynaptic and postsynaptic proteins in a cell-type-specific fashion" (Chen et al., 2014). In this study, the authors modified the presynaptic protein *Brp* and the postsynaptic protein *ort* (histamine receptor) such that these proteins were labeled with the small tags V5 or OLLAS in a conditional way only in the cell types of interest (Fig. 8A). These modified genetic sequences were introduced via BACs in different lading sites of the fly genome. They found that both number and localization of synapses correlate with the findings from earlier EM studies (Chen et al., 2014). Similarly, Pankova and Borst developed an recombinase-dependent, inducible HA-tagged VAChT-allele for identifying the cholinergic phenotype of Mi1 and Tm3 neurons in the motion vision pathway of the fly (Pankova & Borst, 2017) (Fig. 8B).

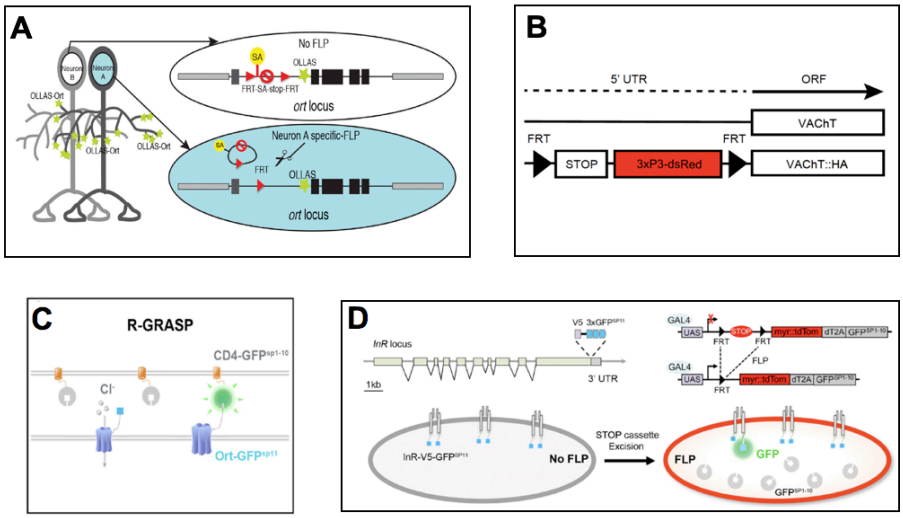

Figure 8. Overview of existing tools for conditional, endogenous labeling of neurotransmitter-related proteins and receptors.
A) Scheme of the STaR (Synaptic Tagging with Recombination) method applied to the histamine receptor ort (Chen et al., 2014). Image taken with permission from Chen et al., 2014. **B)** FRT-STOP-FRT-VAChT::HA allele which allows for conditional HA-tagging of the VAChT protein only upon cell-type-specific expression of FLP (Pankova & Borst, 2017). Image taken with permission from Pankova & Borst, 2017. **C)** Scheme of Receptor-GRASP (R-GRASP) for histamine receptor ort; reconstitution of the two GFP halfs GFP^{sp1-10} and GFP^{sp11} fused to the presumed pre- and postsynaptic cell types generates full GFP, indicating synaptic contacts via the ort channel (Luo et al., 2020). **D)** Scheme of the split-GFP tagging strategy to visualize the endogenous insulin receptor (InR) in single cells (Luo et al., 2020). Images in C and D taken with permission from Luo et al., 2020.

A recent study exploits the principle idea of GRASP (GFP reconstitution across synaptic partners) to develop two new methods for receptor tagging (Luo et al., 2012). The first one, Receptor-GRASP showed neuronal contact sites via the

histamine receptor Ort between photoreceptors R7 and Dm8 neurons. Here, one half of the GFP (spGFP1-10) is membrane-tethered and expressed in the presynaptic neuron while the other half (Ort-GFPsp11) is extracellularly fused to the ort receptor (Fig. 8C). Furthermore, the authors applied "split-GFP tagging" to reveal the endogenous expression pattern of the insulin receptor InR in the optic lobe and in Dm8 dendrites. A combination of introducing a split-GFP half and V5 tag into the endogenous locus of InR and a flippase-dependent expression of myr::tdTomato and the other GFP half leads to endogenous, cell-type-specific tagging of the receptor (Fig. 8D). Kondo et al. used a similar approach with the split-GFP system to endogenously tag dopamine receptors (Kondo et al., 2020).

1.3.3 Functional tools

The standard techniques for measuring neural activity are electrophysiological recordings as well as genetically encoded calcium indicators (GECIs). Since the concentration of calcium in a neuron is increased drastically upon depolarization, it can be used as a proxy for the cell's activity. Genetically encoded calcium indicators, such as GCaMP sensors are designed by fusing the calcium binding protein calmodulin to the circularly permutated green fluorescent protein (cpGFP) (Nakai et al., 2001). Upon calcium-binding to the calmodulin unit, the GCaMP protein undergoes a conformational change and the cpGFP absorbs the excitation light resulting in emitted fluorescence. Since the early 2000s, GECis are constantly improved in their sensitivity, affinity, signal-to-noise ratio, rise and decay kinetics, and dynamic range (Chen et al., 2013; Dana et al., 2019). Recently, the GCaMP suite was expanded with the newest jGCaMP7 version which provides improved detection of spikes and allows tracking of larger populations of neurons (Dana et al., 2019). Since many *Drosophila* neurons are too small for electrophysiological recordings, calcium imaging with GCaMP sensors still remains the method of choice for recording neural activity in the majority of cases. However, due to the slow dynamics of the GCaMP sensors, the temporal resolution is worse than the resolution obtained with electrophysiological recordings of membrane voltage.

Furthermore, changes in intracellular calcium concentrations are only one characteristic of neural activity which can be measured. After the increase of calcium concentration, the presynaptic terminals release neurotransmitter. Several sensors for neurotransmitter have been developed for imaging the functional properties of transmitter release. The **glutamate sensor iGluSnFR,** for instance, was constructed from the *E. coli* glutamate binding protein GltI and circularly permutated GFP

(Marvin et al., 2013). It is displayed on the extracellular side of the neuronal membrane, where it responds to glutamate in a sensitive and fast manner. Using this glutamate sensor, it was shown that Y-type retinal ganglion cells in the inner plexiform layer of the mouse retina release glutamate in a transient fashion at the central levels and in a sustained manner near the borders (Borghuis et al., 2013). Further, iGluSnFR allowed for imaging of glutamate-release from more than 13000 bipolar cell axon terminals in the mouse retina, demonstrating that the interplay of dendritic excitatory inputs and axonal inhibitory inputs generates the functional diversity of bipolar cells (Franke et al., 2017). We used iGluSnFR to characterize the glutamate transmission of three glutamatergic neurons in the motion vision pathway of the fruit fly and compared it with the GCaMP responses (**Manuscript 2**; Richter et al., 2018). A recent study used iGluSnFR to characterize the neurotransmission between a glutamatergic lamina neuron and its postsynaptic partners which underlies the mediation of ON selectivity in the fly visual system (Molina-Obando et al., 2019).

Furthermore, the genetically encoded acetylcholine sensor GACh, based on a muscarinic ACh receptor and cpGFP was developed. It was shown to have suitable sensitivity, signal-to-noise ratio, and kinetics to monitor ACh signals in cultured cells, and in vivo in mice and flies (Jing et al., 2018). Recently, this GACh sensor was used to demonstrate multi-directed ACh transmission in the mouse retina (Sethuramanujam et al., 2020). A similar ACh sensor, called iAChSnFR, was introduced by Borden et al. (Borden et al., 2020). Using the design principles for creating iGluSnFR, the GABA sensor iGABASnFR was constructed from *Pseudomonas fluorescens* periplasmic GABA binding protein and cpGFP (Marvin et al., 2019). The authors applied iGABASnFR to record GABA transmission in the zebrafish cerebellum during swimming and in awake mice. Lately, a genetically encoded sensor for the neuromodulator dopamine became available (Patriarchi et al., 2018).

1.4 *Drosophila* motion vision

The detection of the direction in which a visual signal is moving is called motion vision. Every day, when we open our eyes, we can recognize objects in our visual field and we can easily tell in which direction they move. Since our brain constantly performs this task seemingly effortless while we are walking through the world, it might come as a surprise that this requires an intricate computation. The

photoreceptors in the retina detect the visual environment like a simple pixel-array camera: a sequence of two-dimensional luminance distributions. It is only by the computation of subsequent circuits, that information about the direction of movement can be extracted (Borst & Helmstaedter, 2015).

While the fruit fly is navigating through the air in order to find food or a mating partner, neural circuits in its brain use an enormous computational power to extract this information from the visual scenery. Due to self-motion during walking or flying, the visual input is dominated by the so-called optic flow, panoramic image shifts, which are extracted from the visual environment by local motion detectors (Mauss & Borst, 2020). Optic flow provides information for course control and estimation of travel speed. However, from a computational point of view, the neural processing underlying motion vision is still not fully understood despite decades of research. In the following chapter I will introduce the anatomy of the motion vision circuit, the most important algorithmic models for motion detectors as well as underlying neurotransmitters and receptors.

1.4.1 Motion vision circuit

In the fly, visual information is processed in the optic lobes, the region of the brain behind the facette eyes which occupy almost two thirds of the whole brain. The optic lobe comprises four neuropils: the lamina, the medulla, the lobula and the lobula plate. The first two neuropils, the lamina and the medulla are organized in around 700-800 columns which allow for retinotopic sampling of the visual space (Zeleny, 1922) (Fig. 9A).

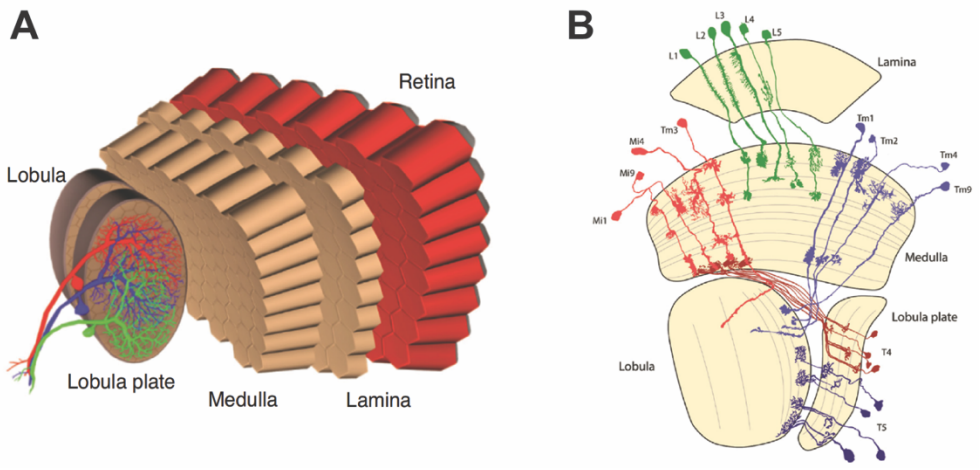

Figure 9. Schematic overview of the fly optic lobe.
A) Schematic cross-section of the optic lobe with the retina, and the four neuropils, lamina, medulla, lobula and lobula plate. In the lobula plate, three lobula plate tangential cells are depicted in green, blue and red. **B)** Most important cell types in the motion vision pathway

in the horizontal cross-section of the optic lobe: L1-L5 in the lamina (green), (trans-) medulla neurons in the medulla (bright red and purple), and T4 (dark red) and T5 neurons (dark purple). Images in A and B taken with permission from Borst et al., 2020.

The first cells in the eye that receive light are the **photoreceptors** which project from the retina to the lamina. They convert the energy from the light to cellular, electric signals by a phototransduction cascade. In response to light photoreceptors depolarize and transmit histamine to their downstream partners, the lamina cells. There are eight types of photoreceptors in *Drosophila*, six of those devoted to motion vision (R1-6) and the other two mainly to color vision (R7 and R8) (Heisenberg & Buchner, 1977; Yamaguchi et al., 2008, 2010). Photoreceptors hyperpolarize lamina cells via a histamine-gated chloride channel (Hardie, 1989), called HisCl encoded by the ort gene (Gisselmann et al., 2002).

There are five **lamina** monopolar cells (L1-L5) that project from the lamina to the medulla, connecting photoreceptors and medulla/ transmedulla neurons (overview of the most important cell types in Fig. 9B). Similar to the mammalian retina, the detection of light increments and light decrements is processed in two parallel circuits, the ON pathway with the glutamatergic L1 neurons as the main input and the OFF pathway with the cholinergic L2 neurons as the main input (Joesch et al., 2010). Both L1 and L2 respond to light stimulation with a hyperpolarization elicited by photoreceptors via histamine-gated chloride channels. When the light is turned off, L1 and L2 respond with a rebound excitation (Yang et al., 2016). It has been speculated that the sign inversion between L1 and their postsynaptic neurons in the ON pathway is achieved by the inhibitory glutamate receptor GluClα. Recently it has been shown that this ON-OFF transition is a multi-synaptic process that indeed involves GluClα (Molina-Obando et al., 2019). Although blocking of L1 and L2 impairs any behavioral response to motion stimuli (Rister et al., 2007), they are not the exclusive inputs to the motion vision pathway. Cholinergic L3 neurons respond to moving dark edges and provide input to the OFF pathway via Tm9 neurons (Silies et al., 2013; Fisher et al., 2015a), as well as to the ON pathway via Mi1 and Mi9 (Takemura et al., 2017). L4 neurons which depolarize in response to light decrements receive input mainly from photoreceptors R6 and L2 and project onto Tm2 (Rister et al., 2007; Meier et al., 2014). Overall, neurons in the motion vision pathway already form a complex microcircuit in the first processing stage in the lamina (Rister et al., 2007).

In the next neuropil, the **medulla**, the wiring complexity is increasing with an increased number of cell types. Here, the medulla and transmedulla (crossing from the medulla to the lobula complex) neurons relay information from the lamina monopolar neurons to the T4 and T5 neurons, the first stage of direction-selectivity in the motion vision circuit, which will be described in the next paragraph. Several electron microscopy (EM) studies revealed the presynaptic partners of T4/T5 neurons (Takemura et al., 2013; Shinomiya et al., 2014; 2019; Takemura et al., 2017) T5 neurons in the OFF-pathway receive input from Tm1, Tm2, Tm4, Tm9, TmY15 and CT1, while T4 neurons in the ON pathway receive input from Mi1, Tm3, Mi4, Mi9, TmY15, C3 and CT1 (Takemura et al., 2017; Shinomiya et al., 2019). Furthermore, numerous functional studies described the physiological response properties of T4/T5's presynaptic partners (Behnia et al., 2014; Meier et al., 2014; Strother et al., 2014; Ammer et al., 2015; Fisher et al., 2015a; Serbe et al., 2016; Yang et al., 2016; Arenz et al., 2017; Drews et al., 2020). Those cover a range of different temporal and spatial receptive fields with low-pass or band-pass characteristics, all showing non-direction-selective responses.

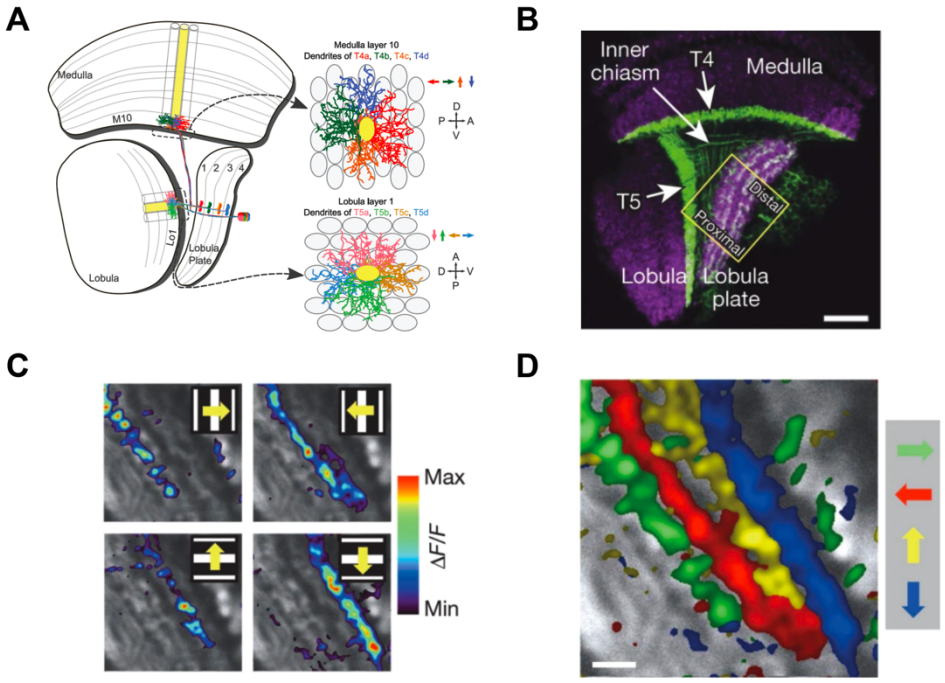

Figure 10. Anatomy and functional response properties of motion-detecting T4/T5 neurons as recorded with Ca^{2+}-Imaging.
A) Scheme of optic lobe in horizontal view with four representative T4 and T5 neurons (subtypes a, b, c, d). T4 neurons have dendrites in layer 10 of the medulla (M10) and T5 neurons have dendrites in layer 1 of the lobula (Lo1). Both T4 and T5 neurons project into the lobula plate with each subtype only targeting one layer. On the right side the four subtypes of T4/T5 dendrites are depicted (frontal view). The four subtypes' dendrites point in one of the four cardinal directions against their preferred directions (indicated by arrows). A, P, D, V: Anterior, Posterior, Dorsal, Ventral. Image taken with permission from Hoermann et al., 2020. **B)** Confocal image of the optic lobe with anti-Dlg background staining (magenta) and

GFP-labeled T4/T5 neurons (green); scale bar 20 μm (Maisak et al., 2013) **C)** Relative fluorescent changes (DF/F) in the lobula plate obtained by two photon imaging of T4/T5 axon terminals expressing GCaMP5 during presentation of moving gratings in four cardinal directions (Maisak et al., 2013). **D)** The results from C combined into one image with DF/F color-coded for each of the four cardinal directions of motion which lead to activity in only one of the four layers at a time. Scale bar 5 μm (Maisak et al., 2013). Images from B, C, and D taken with permission from Maisak et al., 2013.

T4 and T5 neurons are the elementary motion detectors of the fly, representing the first stage of direction-selective responses along the circuit. T4 and T5 neurons come in four subtypes, each sending their axons into one of the four layers in the lobula plate. Each T4/T5 dendrite collects information from approximately 8 columns, with every subtype pointing into one of the four cardinal directions (Fig. 10A and 10B). T4 dendrites of the ON pathway reside in layer 10 of the medulla and respond only to light increments, while T5 dendrites of the OFF pathway reside in layer 1 of the lobula, responsive to light decrements (Maisak et al., 2013). Upon stimulation with moving gratings, each subtype of T4/T5 neurons responds only to movement in one of the four cardinal directions (Fig. 10C and D). Further downstream in the lobula plate, T4/T5 neurons provide cholinergic input to lobula plate tangential cells (LPTCs) (Mauss et al., 2014; Shinomiya et al., 2014). Blocking the synaptic output of T4/T5 cells leads to unresponsive LPTCs and diminished behavioral responses to moving visual stimuli (Schnell et al., 2012; Maisak et al., 2013; Bahl et al., 2013; Schilling & Borst, 2015).

Lobula plate tangential cells (LPTCs) are the first direction-selective neurons which were described in the blowfly (Dvorak et al., 1975). LPTCs are motion-sensitive neurons that integrate ON and OFF signals in large, wide-field receptive fields (Joesch et al., 2010; Schnell et al., 2012) (Fig. 11A). Their response to moving stimuli is direction-selective and motion-opponent with a depolarization to stimuli in preferred direction and a hyperpolarization in response to stimuli in null direction (Schnell et al., 2012) (Fig. 11B). The source of this motion-opponent inhibition was discovered a few years later: Lobula plate-intrinsic (**LPi** neurons) receive excitatory input from e.g. T4/T5 neurons in layer 3 and project onto LPTCs in the neighboring layer 4, providing inhibition via glutamate and the glutamate-gated chloride channel GluClα (Mauss et al., 2015). Thereby, LPTCs receive null direction inhibition via LPis which renders LPTCs motion-opponent and increases flow-field selectivity during flight.

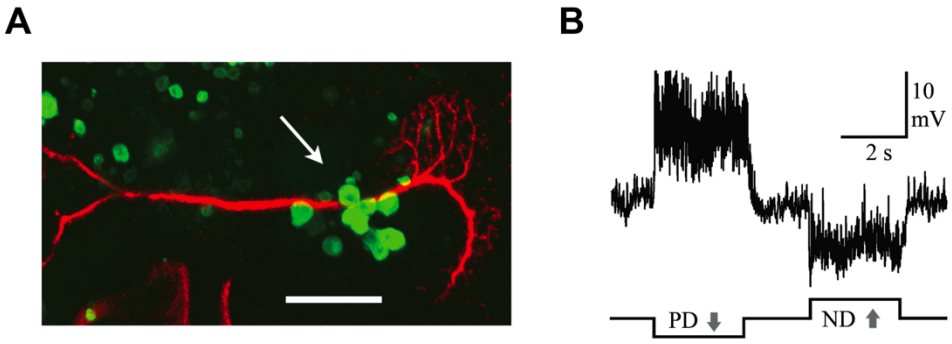

Figure 11. Anatomy and response profile of a lobula plate tangential cell (LPTC).
A) Anatomy of a lobula plate tangential cell (VS) as seen after an electrophysiological recording. Cell bodies of LPTCs are labeled in green with GFP. The recorded cell was injected with Alexa-568 (red) to highlight the anatomy of the whole cell (dendrite on the right). Scale bar 25 µm (Joesch et al., 2008). **B)** Changes in membrane potential of the VS cell seen in A: direction-selective response with a depolarization upon stimulation with a moving grating in preferred direction (PD) and a hyperpolarization in null direction (ND) (Joesch et al., 2008). Images in A and B taken with permission from Joesch et al., 2008.

1.4.2 Algorithmic models

In the late 1950s, scientists for the first time recorded from direction-selective units in the cerebral cortex of cats, the optic tectum of frogs and pigeons and the retinae of rabbits (Lettvin et al., 1959; Hubel & Wiesel, 1959; Barlow et al., 1964). At the same time several studies posit mathematical models to explain how neurons compute the direction of motion. The two most prominent algorithmic models for motion detection were coined by Hassenstein and Reichardt and later by Barlow and Levick (Hassenstein and Reichardt, 1956; Barlow and Levick, 1965).

The common motif of both models is the comparison of signals originating from two adjacent points in visual space via a delay-and-compare mechanism. In the Hassenstein-Reichardt-detector, the input arm on the null side is delayed and a multiplicative non-linearity leads to preferred direction (PD) enhancement for signals moving in the preferred direction (Fig. 12A). In the Barlow-Levick detector the input arm on the preferred side is delayed, the non-linearity is inhibitory, causing null direction (ND) suppression for signals moving along the null direction (Fig. 12B). For the longest time, these algorithmic models seemed to be the two competing options. However, a new proposed model combines the two of them. This so-called three-arm detector model incorporates motifs of both the Hassenstein-Reichardt-detector and the Barlow-Levick-detector: PD enhancement and ND suppression combined in one model with three arms (Leong et al., 2016; Haag et al., 2016) (Fig. 12C).

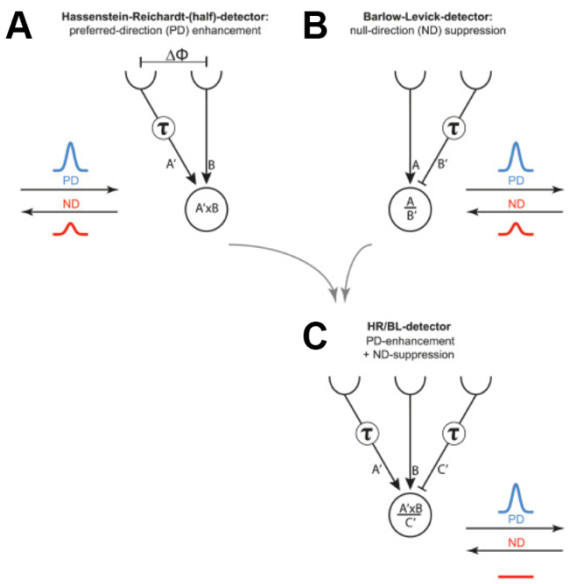

Figure 12. Overview of different algorithmic models for motion detection.
A) In the Hassenstein-Reichardt detector (half-detector is shown here), a delay (t) on arm A' activated by motion in the preferred direction (PD) causes coincidence of the two signals from neighboring photoreceptors (separated by an angle, Df). A multiplicative non-linearity results in an enhanced response for PD (PD enhancement). (Arenz et al., 2017) **B)** In the Barlow-Levick detector, the delay is located on the opposite arm B', and the non-linearity is suppressive/inhibitory, causing a null-direction (ND) suppression. (Arenz et al., 2017) **C)** The three-arm detector combines both PD enhancement and ND suppression. Images taken with permission from Arenz et al., 2017.

How does this algorithmic three-arm-detector model map onto the anatomy and cell types of the circuit described above? The first stage of direction-selective cells are the T4/T5 neurons which sample visual input from around 8 columns. Their presynaptic partners have been identified in EM studies, including synapse numbers and synapse distributions (Shinomiya et al., 2019) (Fig. 13). For every T4/T5 subtype, the input synapses are distributed in a specific spatial order along the dendrite from the most proximal site close to the entry point of the axon to the most distal tips, pointing against its preferred direction (Fig. 13C and 13D). T4 neurons receive glutamatergic input from Mi9 on their distal tips, GABAergic input on the proximal side from Mi4, C3 and CT1 and cholinergic input from Mi1 and Tm3 in the central area of the dendrite. Moreover, TmY15 provides GABAergic input all over the T4 dendrite with the highest synapse numbers on the proximal side. In addition, T4 dendrites from the same subtype are interconnected on the distal dendritic tips (Shinomiya et al., 2019). Conversely, T5 neuron receive no glutamatergic input at all. GABAergic CT1 and TmY15 provide input to the proximal side of the T5 dendrite, while cholinergic Tm1, Tm2, Tm4, Tm9 and T5 from the same subtype synapse onto the central and distal dendritic area (Shinomiya et al., 2019).

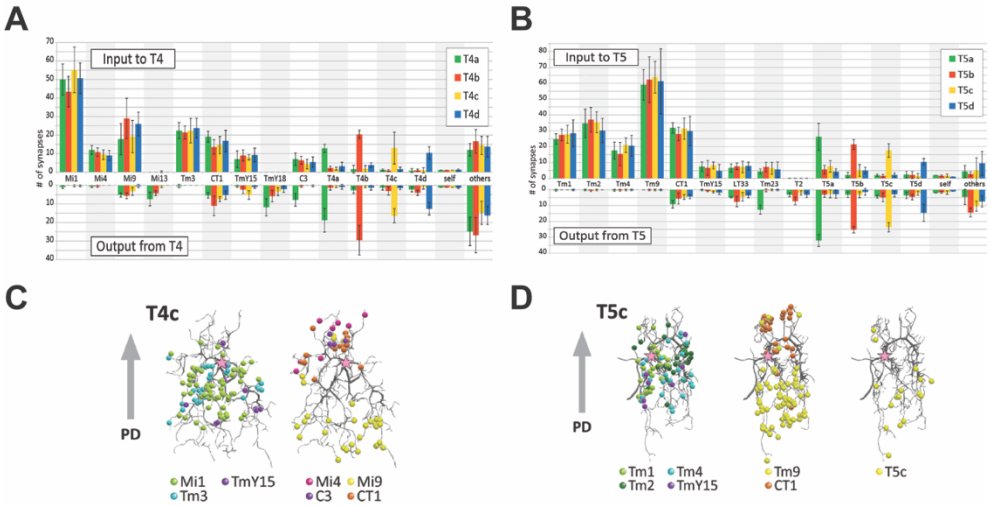

Figure 13. Input synapses to T4/T5 neurons, their numbers and distribution on dendrites. Number of input and output synapses of T4 dendrites in the medulla **(A)** and T5 dendrites in the lobula **(B)** obtained by EM reconstruction. Indicated are average numbers of synapses per connection for a single T4/T5 cell, mean (+SD) for five representative cells for each subtype**. C) and D)** Distribution of synaptic sites of the different input neurons to T4 **(C)** and T5 **(D)** dendrites. Shown here are T4c/T5c neurons which detect upward motion (indicated by arrow: PD, preferred direction). Pink stars indicate the first branch point of the dendrite. Images taken with permission from Shinomiya et al., 2019.

By integrating their columnar inputs in a specific spatio-temporal manner during visual stimulation, T4/T5 neurons perform the computation of motion direction. The functional properties of their presynaptic partners have been described in great detail with temporal dynamics covering both fast and transient, as well as slow and sustained cells (Behnia et al., 2014; Ammer et al., 2015; Fisher et al., 2015b; Fisher et al., 2015a; Serbe et al., 2016; Arenz et al., 2017; Strother et al., 2017, 2018; Drews et al., 2020). Several studies assigned different input neurons to the arms of the algorithmic model, based on their spatial arrangement on the T4/T5 dendrite and their temporal dynamics with respect to the proposed delay (Arenz et al., 2017; Strother et al., 2017; Shinomiya et al., 2019). In the ON pathway, Mi9 is supposedly constituting the arm on the preferred side, while the GABAergic neurons Mi4, C3 and CT1 are responsible for ND suppression. In the central area of the T4 dendrite, Mi1 and Tm3 constitute the central arm of the algorithmic three-arm detector (Fig. 14A). In the OFF-pathway, Tm9 is supposed to be the outer arm on the preferred side, performing PD enhancement, while the only GABAergic cell CT1 on the null side is responsible for ND suppression. In the central T5 dendrite area, Tm1, Tm2 and Tm4 act as the central direct arm of the detector (Fig. 14B).

However, the functional *in vivo* examination of the contribution of the different input neurons to T4/T5's computation by blocking experiments has been difficult (Strother

et al., 2017). Furthermore, the sign of the glutamatergic, GABAergic and cholinergic input neurons can only be defined by investigating the corresponding transmitter receptors on the postsynaptic sites which have been elusive in the past. The question remains: Which receptors receive this repertoire of different neurotransmitters at the level of T4/T5 dendrites?

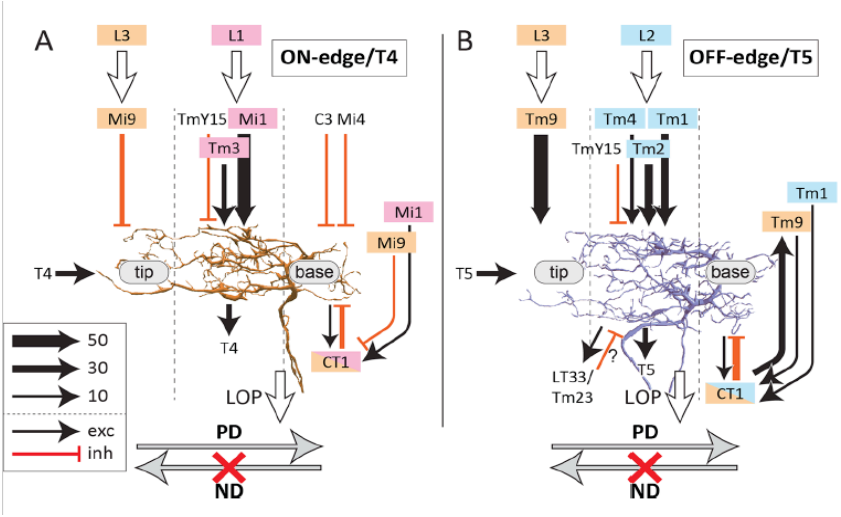

Figure 14. Scheme of inputs and outputs from T4 and T5 dendrites.
Scheme of T4 **(A)** and T5 **(B)** dendrites with their corresponding input neurons and distribution of synaptic inputs from tip to base. The input strength for every input neuron as defined by the synapse number is indicated by stroke strength (s. legend in the lower left corner); dotted lines mark the boundaries of the corresponding medulla/ lobula columns. Images taken with permission from Shinomiya et al., 2019.

1.5 Conclusion and aims

In my dissertation, I sought to investigate the subcellular, molecular basis of motion detection in the fruit fly. Over the years the research field has moved from deciphering the big picture including wiring diagram and physiological characterization of the circuit elements to more subcellular, biophysical questions: How are neurons performing a multiplication? Why are so many different neurotransmitters impinging on the motion-detecting neurons? Which receptors and channels are present on the T4/T5 dendrites and how are they distributed? Are the transmitter receptors acting on inhibitory or excitatory conductances in T4/T5 neurons? The first necessary step to answer these questions is describing which receptors are present and how they are distributed in T4/T5 neurons.

In my first publication, we developed a protocol for super-resolution STED microscopy in *Drosophila* brain slices (**Manuscript 1**). This approach led to

improved resolution compared to conventional confocal microscopy allowing to resolve fine dendritic structures of T4/T5 neurons.

Further, I co-authored a study about glutamate signaling in the fly visual system (**Manuscript 2**). In this work we demonstrated the usability of the glutamate sensor iGluSnFR in glutamatergic neurons of the *Drosophila* brain and showed that it is significantly faster than the Ca^{2+}-sensor GCaMP6f. Using immunohistochemical stainings against VGluT, we confirmed the glutamatergic phenotype of L1, Mi9 and LPi neurons.

Finally, we developed tools for labeling neurotransmitter receptors and voltage-gated ion channels in a cell-type-specific manner and explored their distribution in motion-sensing T4/T5 neurons (**Manuscript 3**). We found that the glutamate receptor GluClα, the GABA receptor Rdl and the ACh receptor Dα7 are asymmetrically arranged on T4/T5 dendrites. Further, we characterized the localization of the voltage-gated ion channels para and Ih in T4/T5 neurons.

2. PUBLICATIONS

2.1 Manuscript 1: STED imaging in *Drosophila* brain slices

Abstract

Super-resolution microscopy is a very powerful tool to investigate fine cellular structures and molecular arrangements in biological systems. For instance, stimulated emission depletion (STED) microscopy has been successfully used in recent years to investigate the arrangement and colocalization of different protein species in cells in culture and on the surface of specimens. However, because of its extreme sensitivity to light scattering, super-resolution imaging deep inside tissues remains a challenge. Here, we describe the preparation of thin slices from the fruit fly (*Drosophila melanogaster*) brain, subsequent immunolabeling and imaging with STED microscopy. This protocol allowed us to image small dendritic branches from neurons located deep in the fly brain with improved resolution compared with conventional light microscopy.

Authors

Sandra Fendl*, Jesus Pujol-Marti*, Joel Ryan, Alexander Borst, and Robert Kasper

* equal contribution

Contributions

S.F., J.P.M., and A.B. conceived the study and designed the experiments. S.F. developed the protocol and performed all experiments. J.P.M. wrote the manuscript with the help of all authors. R.K. and. J.R. provided technical support.

Chapter 10

STED Imaging in *Drosophila* Brain Slices

Sandra Fendl*, Jesús Pujol-Martí*, Joel Ryan, Alexander Borst, and Robert Kasper

Abstract

Super-resolution microscopy is a very powerful tool to investigate fine cellular structures and molecular arrangements in biological systems. For instance, stimulated emission depletion (STED) microscopy has been successfully used in recent years to investigate the arrangement and colocalization of different protein species in cells in culture and on the surface of specimens. However, because of its extreme sensitivity to light scattering, super-resolution imaging deep inside tissues remains a challenge. Here, we describe the preparation of thin slices from the fruit fly (*Drosophila melanogaster*) brain, subsequent immunolabeling and imaging with STED microscopy. This protocol allowed us to image small dendritic branches from neurons located deep in the fly brain with improved resolution compared with conventional light microscopy.

Key words STED, *Drosophila melanogaster*, Immunofluorescence, Cryostat sectioning, Brain slice

1 Introduction

When imaging biological samples with conventional light microscopy many ultrastructural details kept hidden due to the diffraction barrier. The diffraction barrier was first described by Ernst Abbe in 1873 and is known as the Abbe criterion $d = \lambda / 2\,NA$ with the wavelength of light λ and the numerical aperture of the lens NA [1]. The Abbe criterion results in a resolution for standard confocal microscopy of ~250 nm in both the X and Y axes. Fine structures of cells and intracellular compartments are usually much smaller, often occurring very close to each other in the range of tenth of nm, and thus cannot be resolved with conventional light microscopy. Therefore, many efforts have been made to overcome this fundamental limit resulting in super-resolution microscopy methods namely stimulated emission depletion microscopy (STED) and stochastic optical reconstruction microscopy

*Author contributed equally with other authors.

Yolanda Markaki and Hartmann Harz (eds.), *Light Microscopy: Methods and Protocols*, Methods in Molecular Biology, vol. 1563, DOI 10.1007/978-1-4939-6810-7_10,

(STORM) or photo-activated localization microscopy (PALM) [2–5]. STORM and PALM rely on repetitive nanometer precise localization of single fluorophores which is achieved either by blinking or photo-activation of fluorophores. STED microscopy utilizes the physical concept of stimulated depletion by precise overlay of the excitation beam with the so called STED beam. The donut shape of the STED beam results in fluorescence only from the very center of the two beams.

Even though STED microscopy is a well-established and widely used tool in today's molecular and cell biology research, STED imaging in deep tissue remains challenging. This is mostly due to the fact that light gets scattered in tissue. Consequently, STED microscopy has been mostly used in cells in culture and in the most outer layers of living tissues [6, 7]. Researchers, especially in the molecular, cellular, and circuit neurosciences, have tried to overcome this limitation in recent years. In this direction, optical clearing methods that reduce light scattering while preserving cell morphology and fluorophore brightness have been developed [8]. Such methodology allows for super-resolution imaging of relatively large brain volumes, opening the possibility of large-scale connectome studies based on light-microscopy. Alternatively, super-resolution microscopy applied to thin brain sections has been successfully used to map synaptic inputs onto individual dendrites [9] and to investigate the molecular architecture of synapses in the mouse brain [10]. This methodology, however, has been little explored for imaging in the adult brain of *Drosophila melanogaster* [11].

Here, we present a protocol for super-resolution imaging of subcellular structures of individual neurons located deep in the adult *Drosophila* brain. First, we took advantage of the *Drosophila* genetic toolbox to generate flies with brains expressing a membrane-bound fluorescent protein in a few genetically defined neurons [12–15] (Fig. 1a). Second, we prepared twelve micrometers thin sections from these brains to assure that neurons of interest are closest to coverslip and thus reduce light scattering. We next performed immunostaining and imaged the dendrites of the labeled neurons with STED microscopy (Fig. 1b). After imaging and analysis we found that the overall neuronal morphology seems to be preserved when compared with our results from confocal light-microscopy of whole-mount *Drosophila* brains (compare Fig. 1a, b). Moreover, the

Fig. 1 (continued) the two T4 neurons shown in *top panel*. Thin dendritic branches cannot be resolved. Scale bars = 5 μm. (**b**) Detailed views of individual T4/T5 dendritic arbors labeled after immunostaining and confocal/STED imaging on brain slices. Thin brain slices were prepared as described in this protocol from optic lobes with a few T4/T5 neurons labeled, like the one shown in (**a**). Secondary antibodies used to label the neurons shown here were conjugated with either Atto 647N or Abberior STAR 635P dyes. In both cases, a resolution enhancement from confocal to STED microscopy can be observed, allowing the visualization of small dendritic branches. Scaler bars = 2.5 μm. All images are shown as RAW data and are maximal projections from several confocal planes. Brightness was adjusted for display purposes

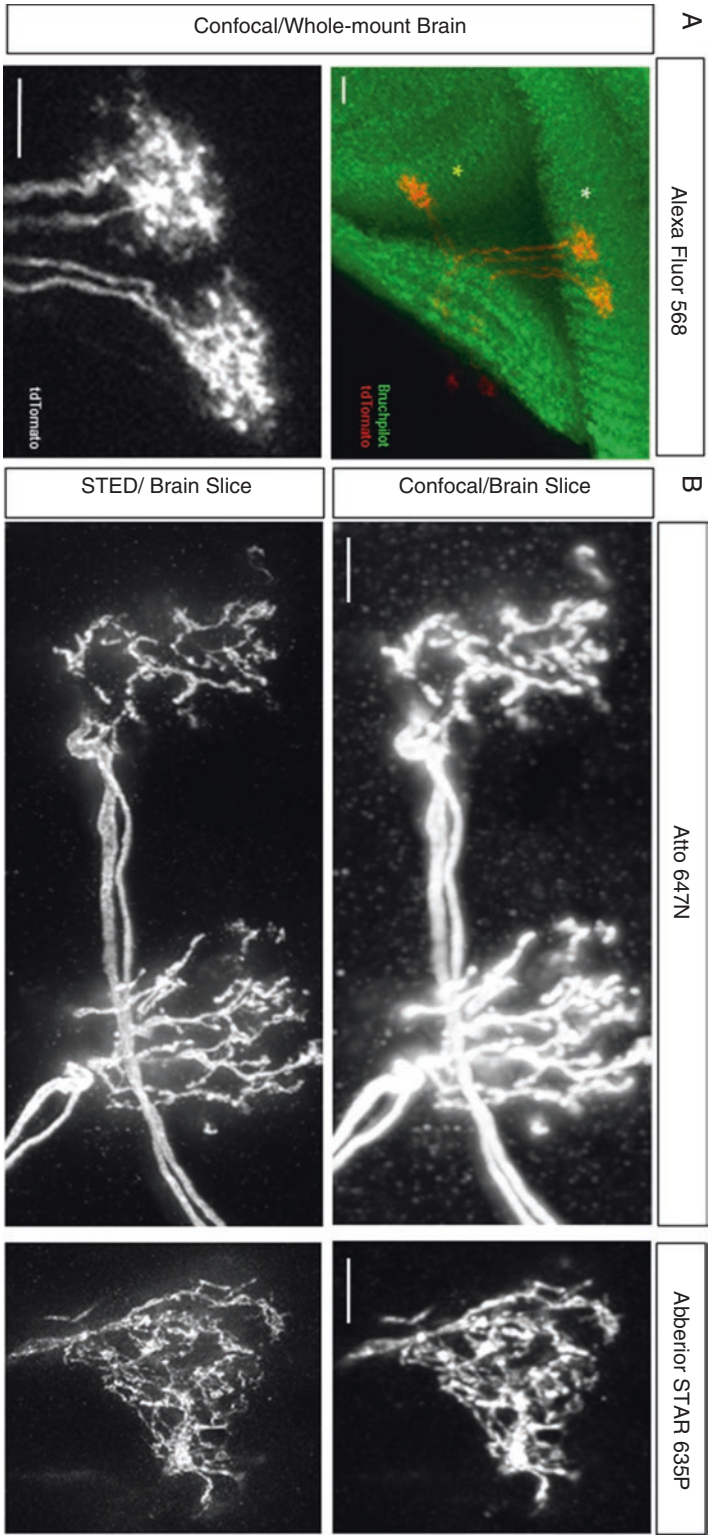

Fig. 1 (**a**) *Top*: Region of a *Drosophila* optic lobe with two T4 neurons (*white asterisk*) and one T5 neuron (*yellow asterisk*) labeled after immunostaining and confocal imaging of the whole mount adult brain [18]. The optic lobe neuropil was immunolabeled with anti-bruchpilot [19]. The T4/T5 neurons shown express a membrane-bound tdTomato fluorescent protein and were immunolabeled with anti-DsRed. Secondary antibody used to label the neurons was conjugated with Alexa Fluor 568 dye. *Bottom*: Detailed view of the dendritic arbors from

resolution of the STED images improved when compared to conventional light microscopy in brain sections (Fig. 1b). We tested two different secondary antibodies conjugated to either Atto 647N or Abberior STAR 635P dyes. In both cases, a resolution enhancement from confocal to STED microscopy could be observed, allowing a better visualization of small dendritic branches (Fig. 1b). This protocol, when combined with genetic and immunohistochemistry tools, provides a promising starting point to examine the presence and distribution of proteins at the nanoscale level in neurons of *Drosophila*, an extensively used model in current neuroscience research [16, 17].

2 Materials

2.1 Reagents

1. PBS: Phosphate-buffered Saline (pH 7.2).
2. PBST: Phosphate-buffered Saline (pH 7.2) with 0.3 % Triton X-100.
3. Sucrose Buffer: 30 % sucrose in PBST (store at 4 °C).
4. Blocking Buffer: 4 % Bovine Serum Albumin (BSA, Sigma-Aldrich), 5 % Normal Goat Serum (NGS, Sigma-Aldrich) in PBST.
5. Fixation Buffer: 4 % paraformaldehyde (PFA, Electron Microscopy Sciences) in PBST (store at 4 °C).
6. Primary antibody: DsRed Polyclonal Antibody (Source: Rabbit, Clonetech).
7. Secondary antibodies: Anti-Rabbit Atto647N (Source: Goat, Sigma-Aldrich) or Anti-Rabbit Abberior® STAR 635P (Source: Goat, Abberior).
8. TDE mounting medium O (Abberior).
9. Cryostat mounting medium (Richard-Allan Scientific™ Neg-50™ Gefrierschnittmedium, Thermo Fisher Scientific).
10. Adult *Drosophila* of the desired genotype (*see* **Note 1**).

2.2 General Laboratory Equipment

1. 0.2 mL tubes (Thermo Fisher Scientific).
2. Microscope Slides: Superfrost Ultra Plus Adhesion Slides (Thermo Fisher Scientific).
3. Cover glasses: 22 × 40 mm, #1.5 (Thermo Fisher Scientific).
4. Dissecting Microscope.
5. Forceps (#55, Dumont).
6. Dissecting dishes.
7. Kimwipes tissues (Kimberly-Clark).

8. Razor Blades (VWR).
9. Nail Polish (transparent).
10. Lab Rocker (Custom-built).
11. Shandon Coverplate Holder (Thermo Fisher Scientific).
12. Cryostat Leica CM3050 S.

2.3 STED Microscope

Abberior Instruments STED system equipped with a 775 nm pulsed STED laser, 594 nm and 640 nm pulsed excitation laser, UPlan APO 100× 1.4 oil objective (Olympus), 2 APD detectors (Excelitas) for gated detection and a spatial light modulator (Hamamatsu) for generating the donut shape.

Typical gating time was 234 ps between excitation pulse and start of the fluorescence detection.

3 Methods

3.1 Dissection and Fixation of Fly Heads

1. Collect adult flies of the desired genotype and anesthetize them on ice. Transfer them to dissecting dish filled with PBST, use forceps to detach fly heads from body, pull out proboscis, and remove trachea with forceps (*see* **Note 2**).
2. Fix fly heads for 30 min in Fixation Buffer in a 0.2 mL tube at room temperature on a lab rocker (*see* **Note 3**).
3. Remove fixative and wash heads three times for 15 min in PBST.
4. Infiltrate heads with Sucrose Buffer for at least 3 h (up to 24 h) at 4 °C (*see* **Note 4**).

3.2 Cryosectioning of Fly Heads

1. Settings Cryostat: Set chamber temperature to −21 °C and object temperature to −18 °C. Set section thickness to 12–16 μm.
2. Add Cryostat mounting medium to the sample holder and freeze it inside the cryostat until hardened.
3. Trim the block in a square form with a conventional razor blade.
4. Under the dissection microscope transfer the heads to the sample holder with frozen mounting medium block and cover the brains with cryostat mounting medium.
5. Let the block freeze at least 10 min inside the cryostat until hardened.
6. Pick up sections with microscope slides and let them dry at room temperature for at least 10 min. Keep the slides at 4 °C for storage or continue with immunolabeling.

3.3 Immunolabeling of Sections in "Shandon Coverplate Holder"

1. Assemble the microscope slides with head sections in the Shandon Coverplate Holder.
2. Block the slices for 1 h in Blocking Buffer at room temperature.
3. Add primary antibody diluted in PBST (1:300) and incubate the samples overnight at 4 °C.
4. Wash three times with PBST for 15 min each.
5. Add secondary antibody diluted in PBST (1:200 for anti-Rabbit Atto 647 N and 1:500 for anti-Rabbit Abberior ®STAR 635P (*see* **Note 9**)) and incubate the samples overnight at 4 °C (*see* **Note 8**).
6. Wash three times in PBST for 15 min each.

3.4 Mounting

1. Keep microscope slides with head sections in the Shandon Coverplate Holder.
2. Mount slides in TDE Mounting Medium O (for use with oil immersion objectives) (*see* **Note 5**).
3. Add three to five drops TDE Solution A to the slides in the holder. Incubate for 20 min.
4. Repeat **step 7** with TDE Solution B, C, and D.
5. Remove the slides from the Shandon Coverplate Holder. Clean the area around the brain sections with Kimwipes tissues (*see* **Note 6**).
6. Add one drop of TDE Solution D to the brain sections and cover it with a clean cover glass (22 × 40 mm).
7. Seal the edges of the cover glass with clear nail polish and store the samples at 4 °C in the dark (*see* **Note 7**).

3.5 Imaging

1. Find area of interest with 10x objective then switch to 100× oil objective (apply immersion oil).
2. Check quality of labeling and colors in confocal mode (*see* **Note 10**).
3. Apply STED laser and check for best STED power to achieve sufficient depletion. STED power depends on the label and can vary from sample to sample. Gating settings should be adjusted as well.
4. As a general rule we increased excitation power from confocal to STED imaging 3-fold and accumulated 3-5 frames per image.
5. For 3D STED add second donut and adjust STED power accordingly.

4 Notes

1. For sparse labeling of neurons [14, 15], we combined in single flies the following transgenes: R57C10-Flp2::PEST, VT50384-lexA, and LexAop-frt-stop-frt-CD4::tdTomato. The weak flippase FLP2::PEST is expressed pan-neurally and stochastically removes the FRT-flanked stop cassette, allowing LexA-driven expression of a membrane-tagged red fluorescent protein (CD4::tdTomato).
2. The dissection procedure should take ~10–25 min per experiment. It is critical to minimize dissection time to avoid tissue degradation.
3. Add up to ten heads into one tube for proper fixation.
4. Leave heads in Sucrose Buffer until they sink to the bottom. Thereby, the tissue is cryo-protected.
5. TDE Mounting Medium is matching the refractive index of the embedding medium to that of the oil immersion by subsequent steps of incubation in different TDE solutions. Thus, optical aberrations and scattering are minimized. As a result, light penetrates more deeply into the specimen and the imaging contrast is enhanced.
6. It is essential to remove all excess mounting medium around the sections to enable a proper sealing of the cover glass with nail polish.
7. The cover glass should be as clean as possible for STED microscopy. Clean the glass with ethanol if necessary.
8. We tested several dye combinations for simultaneous dual-color STED imaging experiments. We found that Anti-Rabbit Atto594 (Sigma-Aldrich) can be used together with either Atto 647N or Abberior® STAR 635P. In terms of brightness and photo stability all three dyes could be used in our experiments.
9. For dual-color STED imaging, the expression levels of the two proteins to be immunolabeled are critical to avoid bleed-through in the emission channels if not matched properly.
10. This protocol can be used to apply STORM with *Drosophila* brain slices as well. We did some preliminary tests and used Alexa647 and Atto532 as two color dye combinations. For STROM the results would greatly benefit from even thinner brain slices and the structure of interest as close to the cover slide as possible. In addition the mounting medium needs to be changed to a switching buffer containing glucose oxidase and mercaptoethanol or other thiol containing reagents.

Acknowledgments

We are indebted to H. Leonhardt and the BioImaging Network Munich for generous support. We thank Marianne Braun and Ursula Weber for excellent help with technical procedures, and Aljoscha Nern, Gerald M. Rubin, and Barry Dickson for providing transgenic flies.

References

1. Abbe E (1973) Beiträge zur Theorie des Mikroskops und der mikroskopischenWahrnehmung. Archiv für mikroskopische Anatomie 9:413–418
2. Klar TA, Jacobs S, Dyba M, Egner A, Hell SW (2000) Fluorescence microscopy with diffraction resolution barrier broken by stimulated emission. Proc Natl Acad Sci U S A 97: 8206–8210
3. Betzig E, Patterson GH, Sougrat R, Lindwasser OW, Olenych S, Bonifacino JS, Davidson MW, Lippincott-Schwartz J, Hess HF (2006) Imaging intracellular fluorescent proteins at nanometer resolution. Science 313(5793):1642–1645
4. Rust MJ, Bates M, Zhuang X (2006) Sub-diffraction-limit imaging by stochastic optical reconstruction microscopy (STORM). Nat Methods 3(10):793–795
5. Hess ST, Girirajan TP, Mason MD (2006) Ultra-high resolution imaging by fluorescence photoactivation localization microscopy. Biophys J 91(11):4258–4272
6. Lau L, Lee YL, Matis M, Axelrod J, Stearns T, Moerner WE (2011) STED super-resolution microscopy inDrosophilatissue and in mammalian cells. Proc SPIE Int Soc Opt Eng 7910:79101N
7. Berning S, Willig KI, Steffens H, Dibaj P, Hell SW (2012) Nanoscopy in a living mouse brain. Science 335(6068):551
8. Ke MT, Nakai Y, Fujimoto S, Takayama R, Yoshida S, Kitajima TS, Sato M, Imai T (2016) Super-resolution mapping of neuronal circuitry with an index-optimized clearing agent. Cell Reports 14(11):2718–2732
9. Sigal YM, Speer CM, Babcock HP, Zhuang X (2015) Mapping synaptic input fields of neurons with super-resolution imaging. Cell 163(2):493–505
10. Dani A, Huang B, Bergan J, Dulac C, Zhuang X (2010) Superresolution imaging of chemical synapses in the brain. Neuron 68:843–856
11. Spühler IA, Conley GM, Scheffold F, Sprecher SG (2016) Super resolution imaging of genetically labelled synapses in Drosophila brain tissue. Front Cell Neurosci 10:142
12. Rodríguez AdV, Didiano D, Desplan, C (2011) Power tools for gene expression and clonal analysis in Drosophila. NatureMethods 9(1): 47–55
13. Venken KJT, Simpson JH, Bellen HJ (2011) Genetic manipulation of genes and cells in the nervous system of the fruit fly. Neuron 72: 202–230
14. Nern A, Pfeiffer BD, Svoboda K, Rubin GM (2011) Multiple new site-specific recombinases for use in manipulating animal genomes. Proceedings of the National Academy of Sciences of the United States of America 108(34):14198–14203
15. Nern A, Pfeiffer BD, Rubin GM (2015) Optimized tools for multicolor stochastic labeling reveal diverse stereotyped cell arrangements in the fly visual system. Proceedings of the National Academy of Sciences of the United States of America 112(22):E2967–E2976
16. Bellen HJ, Tong C, Tsuda H (2010) 100 years of Drosophila research and its impact on vertebrate neuroscience: a history lesson for the future. Nat. Rev. Neurosci. 11:514–522
17. Kazama H (2015) Systems neuroscience in Drosophila: conceptual and technical advantages. Neuroscience 296:3–14
18. Maisak MS, Haag J, Ammer G, Serbe E, Meier M, Leonhardt M, Schilling T, Bahl A, Rubin GM, Nern A, Dickson BJ, Reiff DF, Hopp E, Borst A (2013) A directional tuning map of Drosophila elementary motion detectors. Nature 500:212–216
19. Wagh DA, Rasse TM, Asan E, Hofbauer A, Schwenkert I, Duerrbeck H, Bucher S, Dabauvalle MC, Schmidt M, Qin G, Wichmann C, Kittel R, Sigrist SJ, Bucher E (2006) Bruchpilot, a Protein with Homology to ELKS/CAST, Is Required for Structural Integrity and Function of Synaptic Active Zones in Drosophila. Neuron 49(6):833–844

2.2 Manuscript 2: Glutamate signaling in the fly visual system

Abstract

For a proper understanding of neural circuit function, it is important to know which signals neurons relay to their downstream partners. Calcium imaging with genetically encoded calcium sensors like GCaMP has become the default approach for mapping these responses. How well such measurements represent the true neurotransmitter output of any given cell, however, remains unclear. Here, we demonstrate the viability of the glutamate sensor iGluSnFR for 2-photon in vivo imaging in *Drosophila melanogaster* and prove its usefulness for estimating spatiotemporal receptive fields in the visual system. We compare the results obtained with iGluSnFR with the ones obtained with GCaMP6f and find that the spatial aspects of the receptive fields are preserved between indicators. In the temporal domain, however, measurements obtained with iGluSnFR reveal the underlying response properties to be much faster than those acquired with GCaMP6f. Our approach thus offers a more accurate description of glutamatergic neurons in the fruit fly.

Authors

Florian G. Richter*, **Sandra Fendl***, Jürgen Haag, Michael S. Drews, and Alexander Borst

* equal contribution

Contributions

F.G.R., S.F., and A.B. conceived the study and designed the experiments. F.G.R. conducted and analyzed the imaging experiments for Mi9 and L1. S.F. performed and analyzed all stainings. J.H. performed and analyzed the LPi experiments. M.S.D. performed data analysis and model fitting of the receptive fields. F.G.R. wrote the manuscript with the help of all authors.

Article

Glutamate Signaling in the Fly Visual System

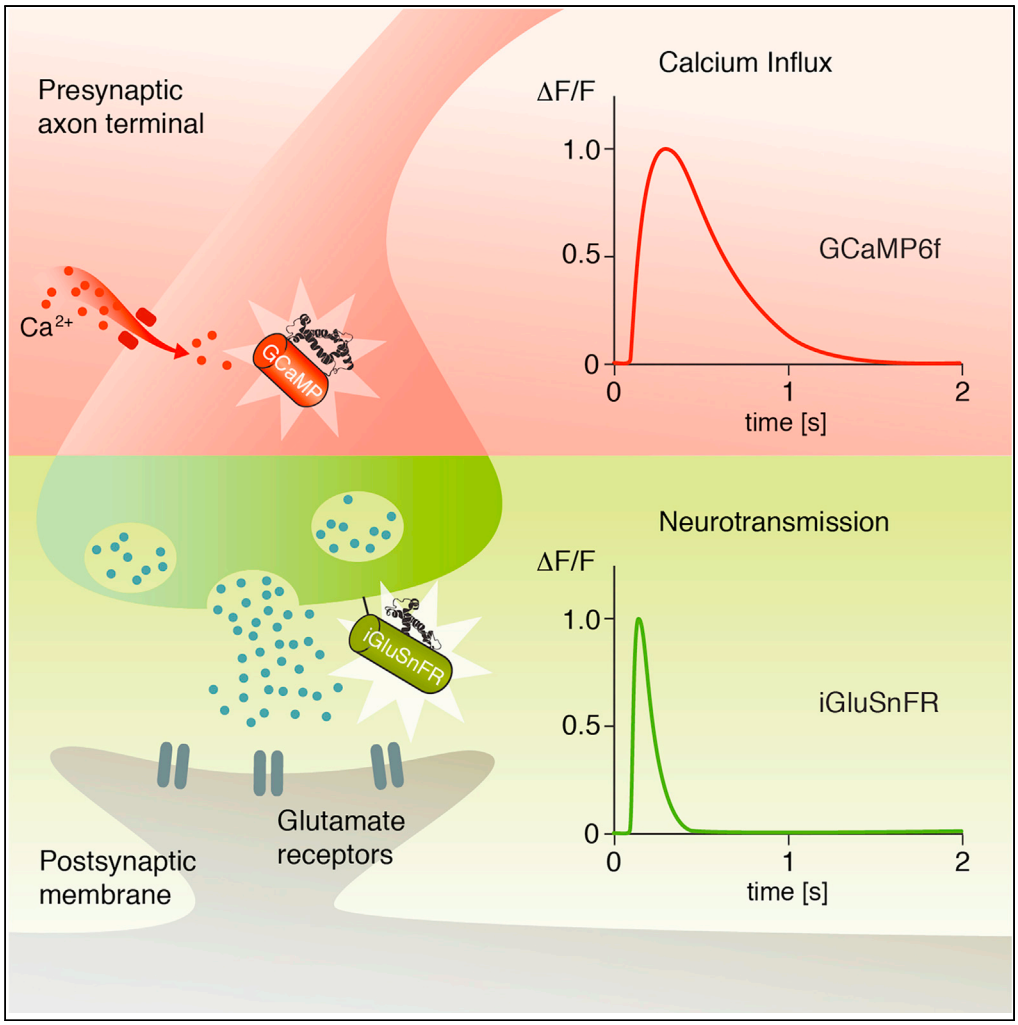

Florian G. Richter, Sandra Fendl, Jürgen Haag, Michael S. Drews, Alexander Borst

frichter@neuro.mpg.de (F.G.R.)
aborst@neuro.mpg.de (A.B.)

HIGHLIGHTS

The glutamate sensor iGluSnFR is suitable for 2-photon imaging in the fruit fly

Response properties obtained with iGluSnFR are much faster than those with GCaMP6f

Spatial aspects of receptive fields are preserved between indicators

Richter et al., iScience 7, 85–95
September 28, 2018
https://doi.org/10.1016/j.isci.2018.08.019

iScience

CellPress

Article

Glutamate Signaling in the Fly Visual System

Florian G. Richter,[1,2,*] Sandra Fendl,[1,2] Jürgen Haag,[1] Michael S. Drews,[1] and Alexander Borst[1,3,*]

SUMMARY

For a proper understanding of neural circuit function, it is important to know which signals neurons relay to their downstream partners. Calcium imaging with genetically encoded calcium sensors like GCaMP has become the default approach for mapping these responses. How well such measurements represent the true neurotransmitter output of any given cell, however, remains unclear. Here, we demonstrate the viability of the glutamate sensor iGluSnFR for 2-photon *in vivo* imaging in *Drosophila melanogaster* and prove its usefulness for estimating spatiotemporal receptive fields in the visual system. We compare the results obtained with iGluSnFR with the ones obtained with GCaMP6f and find that the spatial aspects of the receptive fields are preserved between indicators. In the temporal domain, however, measurements obtained with iGluSnFR reveal the underlying response properties to be much faster than those acquired with GCaMP6f. Our approach thus offers a more accurate description of glutamatergic neurons in the fruit fly.

INTRODUCTION

To understand how neural circuits operate and carry out certain computations, it is essential to observe the signals that are transmitted from cell to cell. Synaptic transmission via chemical synapses proceeds in four major stages: (1) Depolarization in the presynapse opens voltage-gated calcium channels. (2) The resulting calcium influx leads to the fusion of transmitter-filled vesicles and the presynaptic membrane. (3) Transmitter molecules are released into the synaptic cleft where they diffuse and bind receptors in the postsynaptic membrane. (4) The subsequent activation of these receptors leads to opening or closing of ion channels, either directly or indirectly, with the resulting ion flux ultimately changing the postsynaptic membrane conductance and potential (reviewed in [Di Maio, 2008]). This fundamental signaling cascade, from electric potential to calcium to transmitter release to postsynaptic electric potential, orchestrates computation within any neuronal circuit.

For monitoring voltage changes, electrophysiology is the default approach. Here, direct observations of both de- and hyperpolarization in pre- or postsynaptic cells are possible. Due to the position or size of many neurons, however, direct single-cell recordings are often not feasible and have to be replaced by indirect extracellular recordings or optical imaging. Only recently genetically encoded voltage indicators (GEVIs) have emerged as powerful tools for recording neuronal activity (Cao et al., 2013; Jin et al., 2012; St-Pierre et al., 2014; Tsutsui et al., 2013; Yang et al., 2016). Experiments with optical voltage indicators such as ASAP2f that are compatible with 2-photon imaging, however, remain challenging due to weak signal-to-noise ratio (Yang et al., 2016). The fluorescence level of genetically encoded calcium indicators (GECIs) is thought to correlate with transmitter release and is therefore suitable for identifying the crucial signal to the postsynaptic cell (Zucker, 1993). Although GECIs are being improved continuously and some variants were designed to have especially fast kinetics (e.g., GCaMP6f [Chen et al., 2013]), temporal resolution is still limited due to calcium buffering (Borst and Abarbanel, 2007). This usually leads to decay constants in the order of several hundreds of milliseconds that vary depending on the system under observation (Arenz et al., 2017; Chen et al., 2013). For glutamatergic neurons, a tool to potentially overcome these limitations is the recently developed fast glutamate sensor iGluSnFR (Marvin et al., 2013).

Visual motion detection is a canonical example for computation in neural microcircuits. Prevalent models posit that, in both mammalian retina and fly visual system, local direction selectivity emerges from the nonlinear interaction between precisely tuned spatiotemporal filters (Barlow and Levick, 1965; Von Hassenstein and Reichardt, 1956). Recent work in connectomics on the visual system of *Drosophila melanogaster* has revealed this computation to be implemented by a circuit that consists of only a few dozen individual cells (Takemura et al., 2017). The optic lobe is the largest neuropil in the fruit fly's brain and consists of the

[1]Max-Planck-Institute of Neurobiology, 82152 Martinsried, Germany

[2]These authors contributed equally

[3]Lead Contact

*Correspondence: frichter@neuro.mpg.de (F.G.R.), aborst@neuro.mpg.de (A.B.)

https://doi.org/10.1016/j.isci.2018.08.019

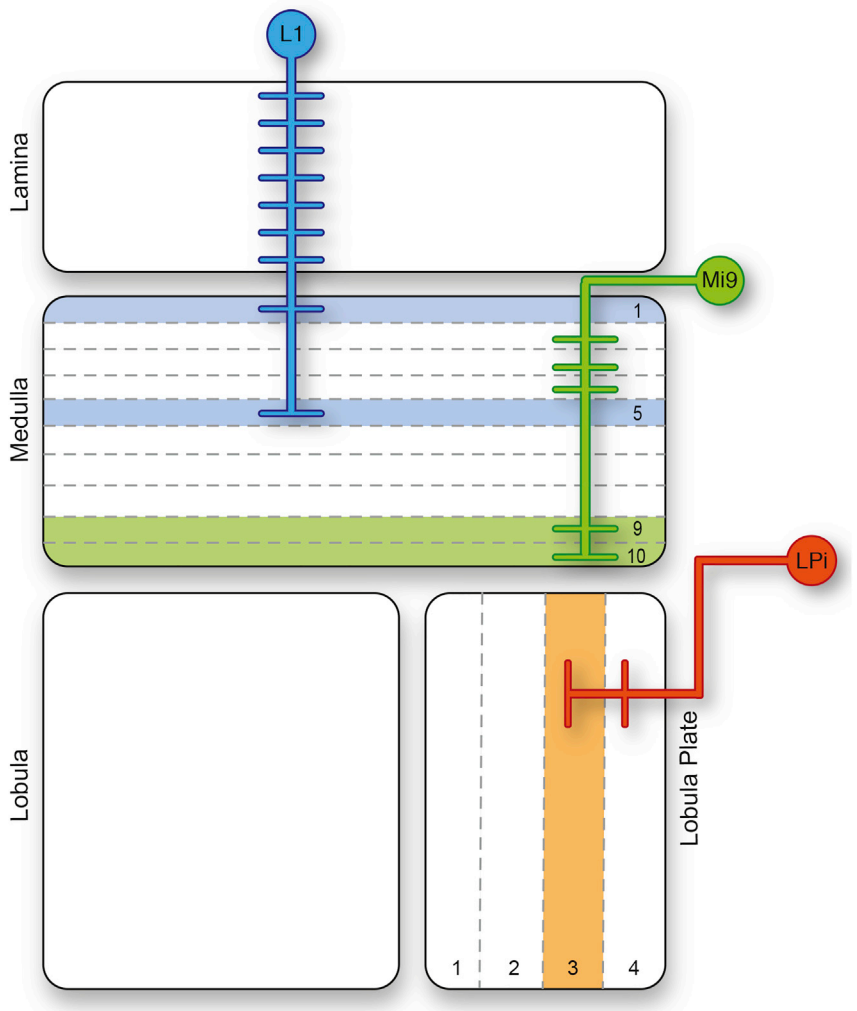

Figure 1. Schematic of the *Drosophila* Optic Lobe

Schematic of the *Drosophila* optic lobe with glutamatergic cell types in the motion vision pathway. The three cell types are not directly connected to each other but play an import role in the circuit. For the sake of simplicity, postsynaptic partners of the glutamatergic neurons are not displayed but can be reviewed in Mauss et al. (2015) and Takemura et al. (2011, 2017). Colored layers indicate area where we imaged glutamate release of the respective cell type.

four consecutive neuropils: lamina, medulla, lobula, and lobula plate (Figure 1). Lamina monopolar cells L1 and L2, among others, receive direct photoreceptor input and feed into two parallel pathways (Bausenwein et al., 1992; Bausenwein and Fischbach, 1992; Borst, 2014; Clark et al., 2011; Joesch et al., 2010; Rister et al., 2007; Shinomiya et al., 2014; Silies et al., 2013; Takemura et al., 2017; Tuthill et al., 2013). The ON pathway processes the motion of light increments, whereas the OFF pathway processes the motion of light decrements only (Eichner et al., 2011; Joesch et al., 2013, 2010). Among the medulla interneurons that connect the lamina cells to direction-selective T4 and T5 neurons (Maisak et al., 2013; Takemura et al., 2017), we find the glutamatergic cell Mi9 that has been characterized with a receptive field responsive to OFF in the center and an antagonistic ON surround (Arenz et al., 2017; Strother et al., 2017). T4 and T5 neurons each come in four subtypes, tuned to one of the four cardinal directions, and project, according to their preferred direction, to one of the four layers in the lobula plate. Here, T4 and T5 cells make excitatory cholinergic connections onto the dendrites of large tangential cells as well as onto inhibitory lobula plate interneurons (LPis). These neurons in turn inhibit large field tangential cells in the adjacent layer during null direction motion and thus increase their flow-field selectivity (Hausen et al., 1980; Hopp et al., 2014; Schnell et al., 2010; Scott et al., 2002; Wasserman et al., 2015). To provide this inhibition, LPis release glutamate onto the glutamate

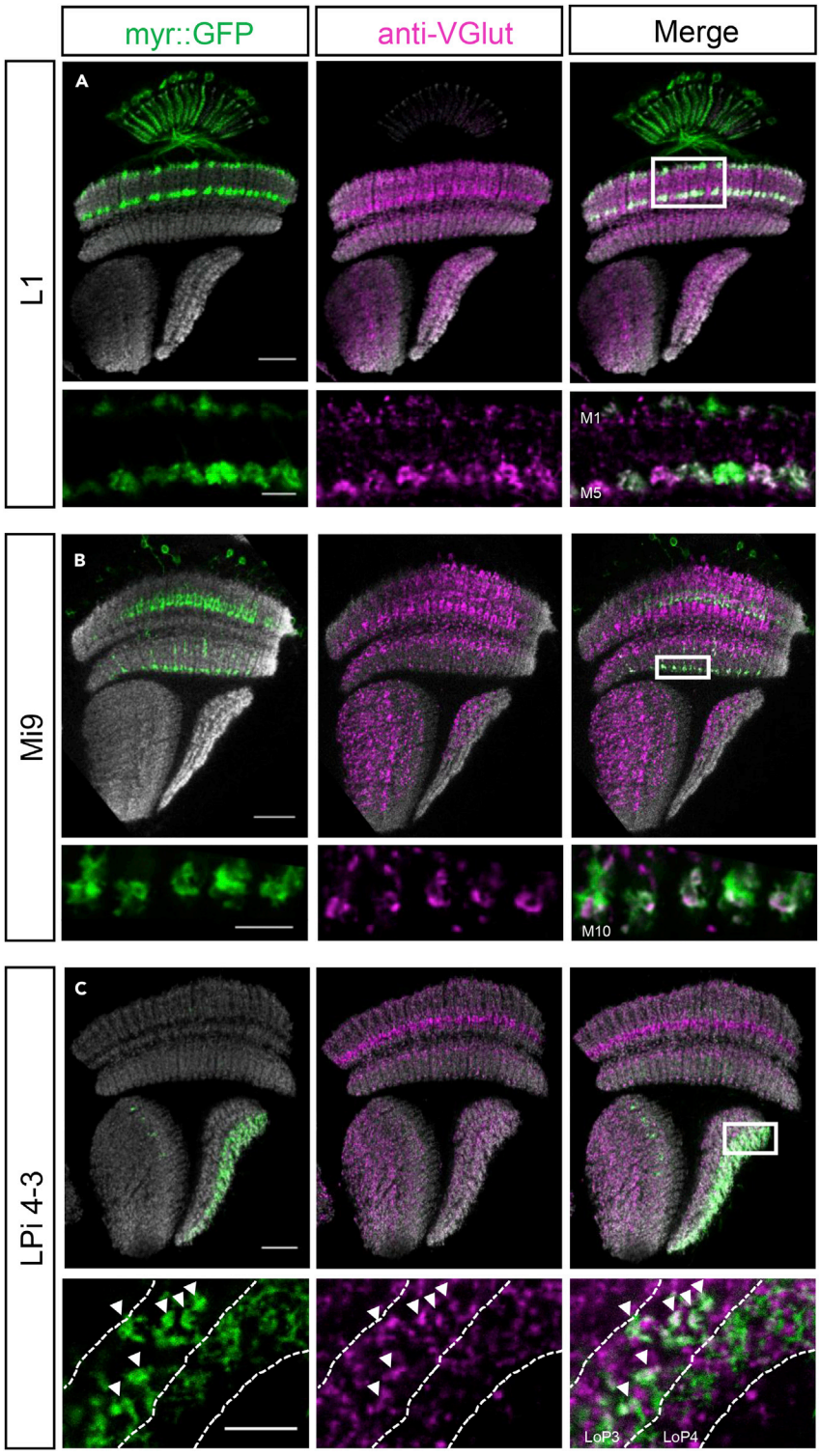

Figure 2. Vesicular Glutamate Transporter VGlut Localizes to Axon Terminals of L1, Mi9, and LPi4-3 Neurons Indicating their Glutamatergic Phenotype

(A–C) Upper rows show overviews of optic lobes with L1 (A), Mi9 (B), and LPi4-3 (C) labeled with myr::GFP (green), background staining against bruchpilot brp (gray), and anti-VGlut staining (magenta). In the lower rows higher magnifications of axon terminals of L1, Mi9, and LPi4-3 neurons are depicted (sections marked with white boxes in overview images).

Figure 2. *Continued*

(A) L1 axon terminals in medulla layers 1 and 5 show overlapping signal with anti-VGlut staining.

(B) VGlut protein co-localizes with Mi9 axons in layer 10 of the medulla.

(C) Lobula plate intrinsic neurons LPi4-3 have their dendrites in layer 4 and project their terminals to layer 3. Labeled with arrowheads are LPi boutons in layer 3 showing overlapping signal with anti-VGlut staining. Shown here are single planes of confocal stacks. Scale bar for overview of optic lobes is 20 μm. For higher magnification close-ups the scale is 5 μm. White dashed lines in the lower panel are manually drawn and indicate layers of the lobula plate.

receptor GluClα, which is an inhibitory glutamate receptor only found in invertebrates (Liu and Wilson, 2013; Mauss et al., 2015, 2014).

The exact biophysical mechanisms by which T4 and T5 become direction selective remain unclear. To understand on a cell-by-cell level how direction selectivity is achieved, precise measurements of the signals transmitted between neurons are crucial. In this study, we focus on the final stage of the synaptic signaling cascade, i.e., transmitter release. First, we confirm the neurotransmitter phenotype of all known glutamatergic cell types (L1, Mi9, LPi) in the *Drosophila* motion vision pathway. Second, using the recently developed fast glutamate sensor iGluSnFR (Marvin et al., 2013), we comprehensively characterize their spatiotemporal response profiles and compare them with the ones obtained expressing the genetically encoded calcium indicator GCaMP6f (Chen et al., 2013).

RESULTS

The Vesicular Glutamate Transporter VGlut Localizes to Axon Terminals of L1, Mi9, and LPi4-3 Neurons

VGlut or DVGLUT (CG9887) is the only vesicular glutamate transporter known in *Drosophila*. VGlut is located in the vesicle membrane of glutamatergic neurons where it fills the synaptic vesicles with glutamate. The protein localizes to presynaptic terminals of all known glutamatergic neuromuscular junctions (NMJs) as well as to synapses throughout the CNS neuropil in *Drosophila* (Daniels, 2004). Hence, VGlut is the most commonly used marker for glutamatergic neurons. Several antibodies have been raised against VGlut to identify glutamatergic neurons in the nervous system of the fruit fly (Daniels, 2004; Mahr and Aberle, 2006).

Recent studies revealed the glutamatergic phenotype of L1, Mi9, and LPi neurons—each of them a crucial element of the motion vision pathway of the fruit fly (Joesch et al., 2010; Kolodziejczyk et al., 2008; Mauss et al., 2015; Takemura et al., 2017, 2011). The somata of these cell types showed positive immunoreactivity against the VGlut antibody, which was raised against a C-terminal peptide—CQMPSYDPQGYQQQ (Daniels, 2004). Interestingly, this antibody labeled mainly cell bodies of designated neurons. Since it is known that the vesicular glutamate transporter VGlut is localized to axon terminals, we investigated the glutamatergic transmitter phenotype of L1, Mi9, and LPi4-3 in more detail. We used a different anti-VGlut antibody (Mahr and Aberle, 2006), which only labels neuronal arborizations in the optic lobe neuropil and no somata. In general, the VGlut protein is highly abundant throughout all four neuropils of the optic lobe (Figure 2).

The axon terminals of L1 neurons show clear overlap with the anti-VGlut signal in layer M1 and M5 of the medulla (Figure 2A). The vesicular glutamate transporter VGlut resides at the presynaptic sites of L1 neurons, which indicates their glutamatergic phenotype. In layer M10 of the medulla, the same is found for Mi9 neurons: VGlut staining in this layer is co-localized with GFP-labeled Mi9 axon terminals (Figure 2B). This suggests that Mi9 neurons are glutamatergic and that they are the only source of glutamate in layer M10 of the medulla. Furthermore, we found an overlapping signal of LPi4-3 terminals in layer 3 of the lobula plate and anti-VGlut staining (Figure 2C). This confirms recent findings (Mauss et al., 2015) that described LPi neurons as glutamatergic, being presynaptic only in one of the two layers where it arborizes.

In summary, we could show that the protein VGlut localizes to axon terminals of the glutamatergic neurons L1, Mi9, and LPi4-3.

Faster Sensor Kinetics Enable More Precise Characterization of Visual Interneurons

One commonly used approach to characterize a sensory neuron is to find its preferred stimulus. This can be achieved by using a white noise input and cross-correlating the resulting output with the input (Dayan and

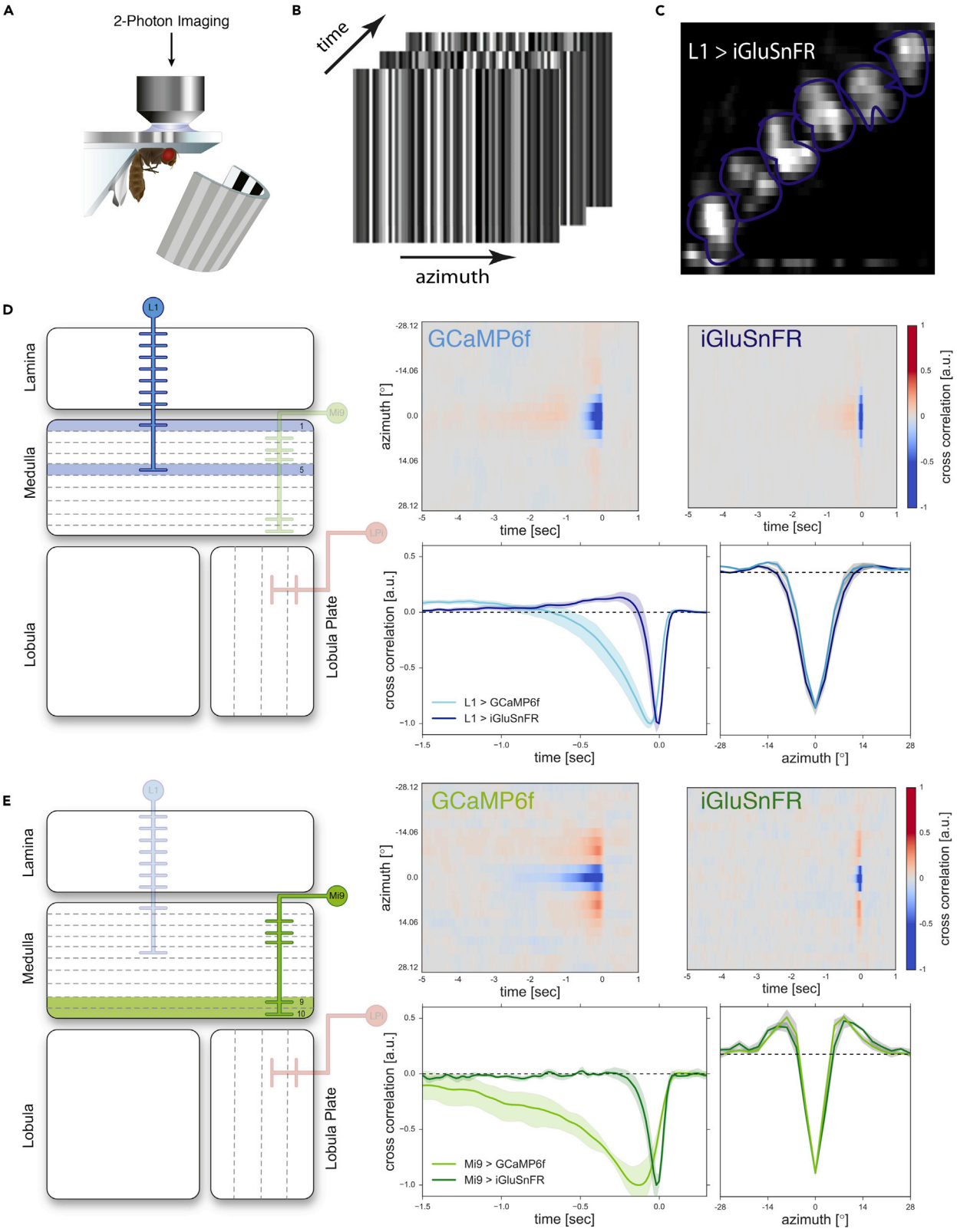
A
2-Photon Imaging
B
time
azimuth
C
L1 > iGluSnFR
D
L1
Lamina
Medulla
Lobula
Mi9
LPi
Lobula Plate
GCaMP6f
iGluSnFR
azimuth [°]
time [sec]
cross correlation [a.u.]
L1 > GCaMP6f
L1 > iGluSnFR
azimuth [°]
E
Mi9
Mi9 > GCaMP6f
Mi9 > iGluSnFR

Figure 3. Response Properties of the ON Pathway Columnar Elements L1 and Mi9

(A) Experimental setup: Fly tethered to a plastic holder under the 2-photon microscope looking onto the stimulus arena (see also Transparent Methods).

(B) Schematic of three frames of the white noise stimulus consisting of 64 horizontal bars.

(C) Example of 2-photon image of L1 expressing iGluSnFR. In purple are manually drawn region of interest ROIs.

(D) Left: Schematic of the *Drosophila* optic lobe. The cell type related to the right panel is highlighted. Right upper panel: Averaged aligned spatiotemporal receptive fields after reverse correlation of L1 expressing either the glutamate indicator iGluSnFR (5 flies and 66 cells) or GCaMP6f (5 flies and 60 cells). Cross sections along space and time axes result in receptive fields in right lower panel. Spatial receptive fields do not differ significantly for both indicators. Temporal kernels differ substantially. Impulse responses are shorter for iGluSnFR than for GCaMP6f. Shaded areas indicate a confidence interval of 95%.

(E) Same as (D) only for Mi9 (with iGluSnFR: 5 flies, 26 cells; with GCaMP6f: 5 flies, 50 cells).

Abbott, 2013; French, 1976; Ringach and Shapley, 2004), which yields the linear spatiotemporal receptive field as a result (e.g., Figures 3D and 3E, upper panel). The receptive field of a neuron is defined as the location of a stimulus in space and the time relative to its occurrence in which the neuron's response is modulated by the stimulus. The receptive field also describes the specific filtering properties of a system, in space as well as in time. Here, we use simple first-order low-pass, high-pass, or band-pass filters to quantify these filtering properties using the measured receptive fields. A low-pass filter only allows low frequencies to pass and attenuates high frequencies. Conversely, a high-pass filter attenuates low frequencies and allows high frequencies to pass. A band-pass filter is a combination of a high-pass and a low-pass filter in series, allowing signals within a certain frequency band to pass and attenuating all others (Cruse, 1996). In a linear system, the filters characterized this way are equivalent to the neurons' impulse responses. The temporal impulse response reveals critical aspects of the cellular response kinetics (Dayan and Abbott, 2013; Ringach and Shapley, 2004).

For this reason, we characterized the spatial extent of the receptive fields as well as the response dynamics of all known glutamatergic cells in the motion vision circuit of *Drosophila* L1, Mi9, and LPi4-3. Expressing either the fast version of the genetically encoded calcium indicator GCaMP6f (Chen et al., 2013) or the fast glutamate-sensing reporter iGluSnFR (Marvin et al., 2013) with cell-type-specific Gal4 driver lines, we imaged glutamate and calcium signals in single axon terminals (Figure 3C). To precisely map the receptive fields of these cells, we used a one-dimensional white noise stimulus consisting of 2.8° wide vertical bars covering the full extent of the arena (180°, Figure 3B, see also Methods). The spatiotemporal receptive fields were then determined from the neuron's calcium or glutamate response by reverse correlation. Cross sections through the peak of the spatiotemporal receptive fields along the space axis therefore yield the one-dimensional spatial receptive fields depicted in Figures 3D and 3E. Cross sections along the time axis yield the temporal filtering properties of the neuron (Chichilnisky, 2001; Dayan and Abbott, 2013; French, 1976; Ringach, 2004).

To calculate the spatial extent of the cells' receptive field, we fitted a Mexican hat function (also called difference of Gaussians) that best resembled the center-surround structure of the estimated spatial receptive fields. Both neurons show a small confined center of ~7° for Mi9 and 9–11° for L1. The full width at half maximum of the surround is about 40–50° for L1 and 20–30° for Mi9. Considering the uncertainty of the fitted model parameters, these values are similar and lie in the same order of magnitude when comparing results from imaging with both sensors. In addition, testing the raw data of both conditions against each other we find no significant difference (see Figures S2A and S2B, p value > 0.5, Welch's t test) of spatial receptive fields neither for L1 nor for Mi9. Both neurons show a small confined center of ~7° for Mi9 and 9–11° for L1. The size of the surround has the same order of magnitude for both sensors, 40–50° for L1 and 20–30° for Mi9. This is within the range of uncertainty that the fit is subject to. Testing the raw data of both conditions against each other for the two cell types, however, does not yield a significant difference (see Figures S2A and S2B, right panel).

For a reliable estimation of the time constants of the temporal responses, we transferred the impulse responses of L1 and Mi9 into frequency space and fitted either a first-order low-pass or a first-order band-pass filter to the neurons' responses (see Figures S1C and S1D). For L1, we find that the data are best represented by a band-pass filter. The filter derived from the iGluSnFR signal has a low-pass time constant of 70 ms and a high-pass time constant of about 400 ms (see Figure S1A). The time constants derived from the GCaMP6f signal are significantly larger with low-pass and high-pass time constants of 350 and about 1,180 ms, respectively. For Mi9, we find that the temporal properties are best described by a low-pass filter. The estimated time constant of the Mi9 temporal kernel (Figure 3D, lower

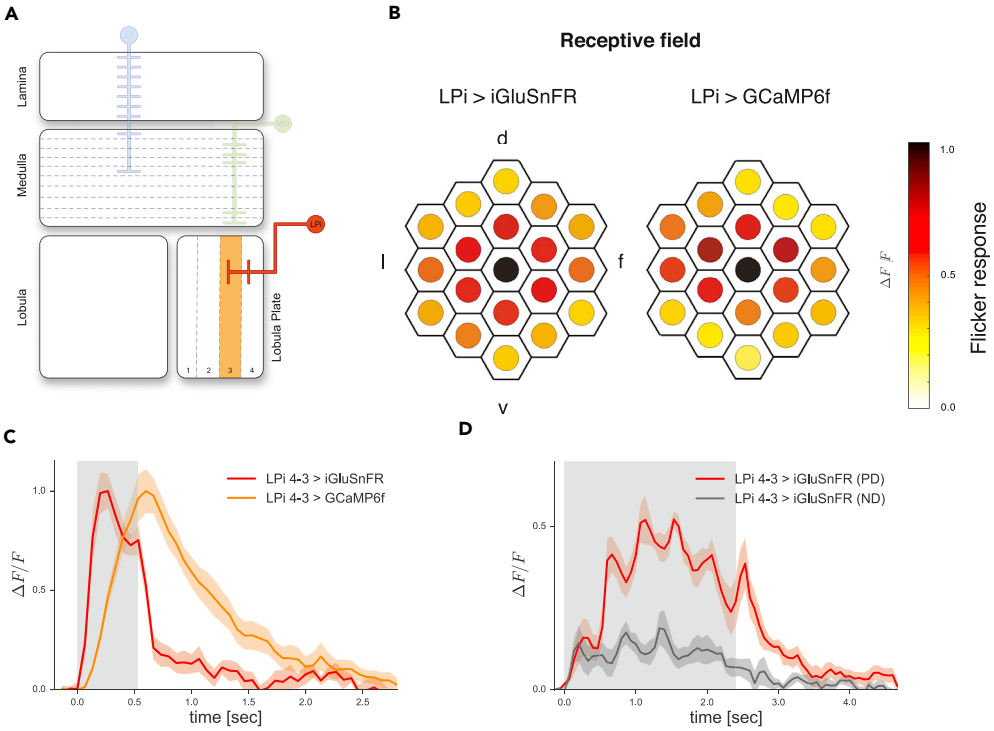

Figure 4. Response Properties of the Direction Selective Lobula Plate Interneuron LPi4-3

(A) Schematic of the *Drosophila* optic lobe with LPi4-3 highlighted.

(B) Comparison of spatial receptive field size of LPi4-3 cells recorded with iGluSnFR (left, n = 24 cells from 7 flies) or GCaMP6f (right, n = 14 cells from 5 flies). The responses of individual cells to flicker stimuli presented at 19 different columnar positions were averaged after alignment to the maximum (in black) and normalization. d, Dorsal; v, ventral; l, lateral; f, frontal.

(C) Time course of LPi4-3 response upon local flicker stimulation. The decay of the signal is faster for iGluSnFR response.

(D) LPi4-3 expressing iGluSnFR show glutamatergic direction selective responses (n = 8 cells from 5 flies). Five consecutive flicker stimuli were shown along the preferred (downward) or null (upward) direction of the neuron, acting as apparent motion. Shaded areas indicate mean ± SEM.

left) is 75 ms when measured with iGluSnFR compared with about 610 ms when measured with GCaMP6f (see Figure S1B).

For both cell types, the temporal kernel of the calcium response can be derived by low-pass filtering the faster glutamate signal. This is because the kinetics of the calcium sensor can be approximated by a low-pass filter when the intracellular calcium concentration is small compared to the KD value of the indicator (Borst and Abarbanel, 2007). For both cells, i.e., L1 and Mi9, we can fit the glutamatergic signal to the calcium signal by filtering it with a low-pass filter with a time constant of 360 ms (see Figures S2A and S2B, left panel). LPis, as motion-selective neurons, are not suitable for white noise analysis. To characterize the response properties of the LPi4-3 (Figure 4A), we first stimulated single ommatidia with local flicker stimuli that were placed precisely onto the lattice of the fly's eye via a custom-built telescopic device (see Transparent Methods and [Haag et al., 2017, 2016]). LPi4-3 cells responded to the individual pulses with different amplitudes, depending on the position of the stimulus (Figure 4C). The maximum response (Figure 4B, black center) of a recorded neuron was then set as the receptive field's center. All other responses to adjacent stimulation are normalized accordingly. Single flicker stimulations in the center of the receptive field show different time courses (Figure 4C) when using the two different indicators. The onset of the calcium response is much slower when compared with the glutamate response. In fact, whereas the glutamate signal shows a short transient peak response and then plateaus after ~500ms, the calcium signal does not resolve any similar details in the time course of the response. The calcium signal decays back to zero in approximately 2 s after stimulus offset, whereas the glutamatergic signals are back at the baseline level in less than 200 ms. This loss-of-response features can be explained by the characteristics of the

calcium indicator, which acts as a low-pass filter (Borst and Abarbanel, 2007). Low-pass filtering the glutamate response (τ = 446 ms, Figure S2C) results in a similar slope and decay as the calcium response. We also asked if the glutamatergic signal of the LPis is indeed direction selective as expected from Mauss et al. (2015). To asses this question we tested LPi4-3 cells with five light pulses of 472 ms duration positioned along the dorsoventral axis of the eye. When stimulated sequentially from dorsal to ventral (Figure 4D), the cell responded more strongly (PD, red line) than when we showed the same stimulus in the opposite direction (ND, black line, paired sample t test, p value < 0.01). We therefore conclude that the sensor is indeed also suitable for resolving glutamatergic direction-selective signals.

DISCUSSION

In this study we showed that all three investigated cell types (L1, Mi9, LPi4-3) express the vesicular transporter for glutamate, VGlut, in their axon terminals (Figure 2). To our knowledge, L1, Mi9, and LPi are the only glutamatergic cells in the *Drosophila* motion vision circuit. Two studies using either antibody stainings (Kolodziejczyk et al., 2008) a Flp-out analysis of the dvGlutCNSIII-Gal4 driver line (heat-shock inducible flipase excises stop-cassette upstream of mCD8-GFP to label only a few cells) (Raghu and Borst, 2011) found L2 cells to be glutamatergic. However, a recent RNA sequencing study that characterized gene expression patterns of more than 60 different cell types of the optic lobe could not confirm the expression of VGlut in L2 (Davis et al., 2018). Although they could identify other cell types like Dm cells, Lai, PB_1, Tm29, and TmY5a as glutamatergic due to their expression of VGlut, none of the other cells in the motion vision circuit (besides L1, Mi9, and LPi) seem to express VGlut. The role of Dm, Lai, PB, Tm29, and TmY5a cells in general and their potential contribution to motion vision in the fly brain are not known to date.

We also demonstrated that the spatial receptive fields measured with the glutamate sensor iGluSnFR are almost identical to the ones measured with the calcium sensor GCaMP6f (Figures 3 and 4). Both neurons possess a local OFF center receptive field with a differently strong antagonistic ON surround. Surround inhibition is a phenomenon frequently found in the early processing stages in visual systems: Bipolar and ganglion cells of the mammalian retina possess receptive fields with an antagonistic center-surround structure (reviewed in Shapley and Lennie, 1985), and first-order interneurons of the insect compound eye share this feature as well (Srinivasan et al., 1982). Functionally, a neuron with a center-surround antagonism acts as a spatial band-pass filter, enhancing the neuron's responses to edges over full field illuminations. Such band-pass filtering reduces redundancy in natural images (Srinivasan et al., 1982). We find such spatial band-pass characteristics for both cell types, L1 and Mi9. Based on their spatial receptive fields, we predict, for instance, no response of Mi9 to wide field dark flashes since the integral of the spatial receptive field is close to zero.

In the time domain, however, the glutamate signal turned out to be much faster than the calcium signal derived from the same cells. Due to their small size, many visual interneurons in the fly brain are inaccessible to electrophysiological recordings, so only a few direct recordings have been reported (Behnia et al., 2014; Gruntman et al., 2018; Juusola et al., 2016). Since data from voltage recordings from L1, Mi9, and LPi are not available so far, a direct comparison with the time constant estimated here is not possible. Simulation studies predicted time constants between 50 and 100 ms for the delayed input to the fly motion-detecting neurons (Eichner et al., 2011; Leonhardt et al., 2016). Since Mi9 is thought to provide this signal to T4 cells, the elementary motion-sensing neurons in the ON pathway, the low-pass time constant of 75 ms estimated here matches this prediction well. In addition, a previous study determined the low-pass time constant for Mi9 to be around 550 ms from calcium imaging experiments. A deconvolution of the filter with an estimated GCaMP kernel led to a resulting time constant of 63 ms (Arenz et al., 2017). This result again is in line with the time constants of the Mi9-iGluSnFR of 75 ms reported here.

In the mammalian CNS, glutamate is the most abundant and major excitatory transmitter (Meldrum, 2000; Traynelis et al., 2010). Glutamate binds to two types of receptors: metabotropic (mGluRs) and ionotropic glutamate receptors (iGluRs). iGluRs can be divided into N-methyl-D-aspartate (NMDA) and non-NMDA receptors (α-amino-3-hydroxy-5-methyl-4-isoxazolepropionic acid [AMPA] and kainate receptors) according to their response to agonist molecules NMDA and AMPA (Mosbacher et al., 1994). Analysis of the *Drosophila* genome annotated 14 iGluRs genes, which show sequence similarities with vertebrate AMPA, kainite, and NMDA receptors (Littleton and Ganetzky, 2000). However, the kainite receptor DKaiR1D and the AMPA receptor DGluR1A have different agonist/antagonist selectivity from the vertebrate's pharmacology-based classification (Li et al., 2016). Furthermore, invertebrates like *Drosophila melanogaster* possess a third type of iGluR, the so-called glutamate-gated chloride channel GluClα, which

is inhibitory (Cully et al., 1996; Liu and Wilson, 2013). Glutamate can also act on metabotropic glutamate receptors, which signal via slower G-protein-coupled pathways. In mammals, eight mGluRs have been described (Conn and Pin, 1997). In contrast, the *Drosophila* genome encodes only one functional mGluR (DmGluRA), which is expressed at the glutamatergic NMJ localized in the presynaptic boutons (Bogdanik et al., 2004). Regarding the broad range of glutamate receptors in *Drosophila*, glutamate can act as a fast, slow, excitatory, or inhibitory transmitter (Li et al., 2016; Liu and Wilson, 2013; Mauss et al., 2015).

This gives rise to interesting speculations about the respective role of glutamate for each of the cell types investigated. In the case of the LPis, glutamate binds to the inhibitory glutamate receptor GluClα on the dendrites of large-field tangential cells, inhibiting them during null direction motion and, thus, enhancing their flow-field selectivity (Mauss et al., 2015). In the case of L1, the glutamatergic output signal seems to be key for the sign inversion of L1's OFF response in the ON pathway. This is because all *Drosophila* photoreceptors (R1-R8) depolarize upon illumination and release histamine onto lamina neurons, which results in the opening of chloride channels (Hardie, 1989; Hardie and Raghu, 2001). Therefore, lamina monopolar cells transiently hyperpolarize upon illumination onset and respond with a rebound excitation at illumination offset (Laughlin et al., 1987). L1 and L2 neurons respond in an identical way (Joesch et al., 2010). L1 possess an OFF receptive field center (Figure 3D) and therefore depolarizes to OFF stimuli, in contrast to its described downstream synaptic partners, which depolarize to ON stimuli (Arenz et al., 2017; Behnia et al., 2014; Strother et al., 2017; Yang et al., 2016). Hence, an inversion of the sign must occur at the synapse of L1 and its downstream partners. Since L1 is glutamatergic and GluClα is the only inhibitory receptor described in *Drosophila*, the glutamatergic signal is likely to be responsible for this sign inversion. Whether the downstream partners of L1 indeed express GluClα, however, is beyond the scope of this study and awaits further investigation. The hypothesis outlined above suggests that the mechanism by which a common photoreceptor input signal is split into an ON and an OFF pathway in invertebrates is different from the one in the mammalian retina where glutamatergic photoreceptors hyperpolarize in response to light. This signal is directly transmitted, i.e., without sign inversion, by ionotropic glutamate receptors expressed on the dendrites of OFF bipolar cells (Euler et al., 2014) and sign inverted by metabotropic glutamate receptors expressed on the dendrites of ON bipolar cells (Masu et al., 1995). In case of Mi9, the functional interpretation of an inhibitory glutamatergic signal is less intuitive. Mi9 directly contacts the dendrites of T4 cells, the first direction-selective neurons in the ON pathway (Takemura et al., 2017). Given the OFF response of Mi9 cells (Figure 3D), T4 cells are expected to be inhibited in darkness via the Mi9-T4 synapse. A moving ON edge would inhibit Mi9 followed by a closure of chloride channels and, thus, an increased input resistance in postsynaptic T4 cells, resulting in an amplification of a subsequently delivered excitatory input signal. Computer simulations have shown that such a two-fold signal inversion can indeed form the biophysical basis of preferred direction enhancement underlying direction selectivity in T4 cells (Borst, 2018).

Taken together our results could demonstrate the functionality of the fast glutamate reporter iGluSnFR in glutamatergic neurons of the fruit fly *Drosophila melanogaster*. It allowed for a more faithful description of important elements of the motion vision pathway, in particular with respect to their temporal response properties.

Limitations of the Study

Since iGluSnFR is anchored to the outer side of the plasma membrane, it senses extracellular glutamate that is present in the synaptic cleft. In addition, the iGluSnFR signal is affected by spillover and diffusion to iGluSnFR molecules outside the cleft. Thus, the iGluSnFR signal should present an upper limit to the "real" time course, i.e., the one of glutamate in the synaptic cleft as seen by the postsynaptic receptors. For the same reason, one might record an iGluSnFR signal even if the indicator is expressed on a neuron that is not glutamatergic or does not receive glutamatergic input, but ramifies within the same volume where glutamate is being released from other cells.

METHODS

All methods can be found in the accompanying Transparent Methods supplemental file.

SUPPLEMENTAL INFORMATION

Supplemental Information includes Transparent Methods and two figures and can be found with this article online at https://doi.org/10.1016/j.isci.2018.08.019.

ACKNOWLEDGMENTS

We thank Aljoscha Leonhardt for careful proofreading of the manuscript. We would also like to acknowledge Hermann Aberle for sharing the VGlut antibody with us and Julia Kuhl for designing the graphical abstract. We thank Wolfgang Essbauer and Michael Sauter for fly husbandry. This work was supported by the Deutsche Forschungsgemeinschaft (SFB 870) and the Max Planck Society. F.G.R., M.S.D., S.F., and A.B. are members of the Graduate School of Systemic Neurosciences (GSN) Munich.

AUTHOR CONTRIBUTIONS

F.G.R., S.F., and A.B. conceived the study and designed the experiments. F.G.R. conducted and analyzed the imaging experiments for Mi9 and L1. S.F. performed and analyzed all stainings. J.H. performed and analyzed the LPi experiments. M.S.D. performed data analysis and model fitting of the receptive fields. F.G.R. wrote the manuscript with the help of all authors.

DECLARATION OF INTERESTS

The authors declare no competing interests.

Received: July 5, 2018
Revised: August 13, 2018
Accepted: August 23, 2018
Published: September 28, 2018

REFERENCES

Arenz, A., Drews, M.S., Richter, F.G., Ammer, G., and Borst, A. (2017). The temporal tuning of the *Drosophila* motion detectors is determined by the dynamics of their input elements. Curr. Biol. *27*, 929–944.

Barlow, H.B., and Levick, W.R. (1965). The mechanism of directionally selective units in rabbit's retina. J. Physiol. *178*, 477–504.

Bausenwein, B., Dittrich, A.P.M., and Fischbach, K.F. (1992). The optic lobe of *Drosophila melanogaster* - II. Sorting of retinotopic pathways in the medulla. Cell Tissue Res. *267*, 17–28.

Bausenwein, B., and Fischbach, K.F. (1992). Activity labeling patterns in the medulla of *Drosophila melanogaster* caused by motion stimuli. Cell Tissue Res. *270*, 25–35.

Behnia, R., Clark, D.A., Carter, A.G., Clandinin, T.R., and Desplan, C. (2014). Processing properties of ON and OFF pathways for *Drosophila* motion detection. Nature *512*, 427–430.

Bogdanik, L., Mohrmann, R., Ramaekers, A., Bockaert, J., Grau, Y., Broadie, K., and Parmentier, M.L. (2004). The *Drosophila* metabotropic glutamate receptor DmGluRA regulates activity-dependent synaptic facilitation and fine synaptic morphology. J. Neurosci. *24*, 9105–9116.

Borst, A. (2018). A biophysical mechanism for preferred direction enhancement in fly motion vision. PLoS Comput. Biol. *14* (6), e1006240.

Borst, A. (2014). In search of the holy grail of fly motion vision. Eur. J. Neurosci. *40*, 3285–3293.

Borst, A., and Abarbanel, H.D. (2007). Relating a calcium indicator signal to the unperturbed calcium concentration time-course. Theor. Biol. Med. Model. *4*, 7.

Cao, G., Platisa, J., Pieribone, V.A., Raccuglia, D., Kunst, M., and Nitabach, M.N. (2013). Genetically targeted optical electrophysiology in intact neural circuits. Cell *154*, 904–913.

Chen, T.-W., Wardill, T.J., Sun, Y., Pulver, S.R., Renninger, S.L., Baohan, A., Schreiter, E.R., Kerr, R.A., Orger, M.B., Jayaraman, V., et al. (2013). Ultrasensitive fluorescent proteins for imaging neuronal activity. Nature *499*, 295–300.

Chichilnisky, E.J. (2001). A simple white noise analysis of neuronal light responses. Network *12*, 199–213.

Clark, D.A., Bursztyn, L., Horowitz, M.A., Schnitzer, M.J., and Clandinin, T.R. (2011). Defining the computational structure of the motion detector in *Drosophila*. Neuron *70*, 1165–1177.

Conn, P.J., and Pin, J.-P. (1997). Pharmacology and function of metabotropic glutamate receptors. Annu. Rev. Pharmacol. Toxicol. *37*, 205–237.

Cruse, H. (1996). Neural Networks as Cybernetics Systems.

Cully, D.F., Paress, P.S., Liu, K.K., Schaeffer, J.M., and Arena, J.P. (1996). Identification of a *Drosophila melanogaster* glutamate-gated chloride channel sensitive to the antiparasitic agent avermectin. J. Biol. Chem. *271*, 20187–20191.

Daniels, R.W. (2004). Increased expression of the *Drosophila* vesicular glutamate transporter leads to excess glutamate release and a compensatory decrease in quantal content. J. Neurosci. *24*, 10466–10474.

Davis, F.P., Nern, A., Picard, S., Reiser, M.B., Rubin, G.M., Eddy, S.R., and Henry, G.L. (2018). A genetic, genomic, and computational resource for exploring neural circuit function. bioRxiv. https://doi.org/10.1101/385476.

Dayan, P., and Abbott, L.F. (2013). Theoretical neuroscience: computational and mathematical modeling of neural systems. J. Chem. Inf. Model. *53*, 1689–1699.

Di Maio, V. (2008). Regulation of information passing by synaptic transmission: a short review. Brain Res. *1225*, 26–38.

Eichner, H., Joesch, M., Schnell, B., Reiff, D.F., and Borst, A. (2011). Internal structure of the fly elementary motion detector. Neuron *70*, 1155–1164.

Euler, T., Haverkamp, S., Schubert, T., and Baden, T. (2014). Retinal bipolar cells: elementary building blocks of vision. Nat. Rev. Neurosci. *15*, 507–519.

French, A.S. (1976). Practical nonlinear system analysis by Wiener kernel estimation in the frequency domain. Biol. Cybern. *24*, 111–119.

Gruntman, E., Romani, S., and Reiser, M.B. (2018). Simple integration of fast excitation and offset, delayed inhibition computes directional selectivity in *Drosophila*. Nat. Neurosci. *21*, 250–257.

Haag, J., Arenz, A., Serbe, E., Gabbiani, F., and Borst, A. (2016). Complementary mechanisms create direction selectivity in the fly. Elife *5*, https://doi.org/10.7554/eLife.17421e.

Haag, J., Mishra, A., and Borst, A. (2017). A common directional tuning mechanism of *Drosophila* motion-sensing neurons in the ON and in the OFF pathway. Elife *6*, 1–15.

Hardie, R.C. (1989). A histamine-activated chloride channel involved in neurotransmission at a photoreceptor synapse. Nature *339*, 704–706.

Hardie, R.C., and Raghu, P. (2001). Visual transduction in *Drosophila*. Nature *413*, 186–193.

Hausen, K., Wolburg-Buchholz, K., and Ribi, W.A. (1980). The synaptic organization of visual interneurons in the lobula complex of flies - a light and electron microscopical study using silver-intensified cobalt-impregnations. Cell Tissue Res. *208*, 371–387.

Hopp, E., Borst, A., and Haag, J. (2014). Subcellular mapping of dendritic activity in optic flow processing neurons. J. Comp. Physiol. A Neuroethol. Sens. Neural Behav. Physiol. *200*, 359–370.

Jin, L., Han, Z., Platisa, J., Wooltorton, J.R.A., Cohen, L.B., and Pieribone, V.A. (2012). Single action potentials and subthreshold electrical events imaged in neurons with a fluorescent protein voltage probe. Neuron *75*, 779–785.

Joesch, M., Schnell, B., Raghu, S.V., Reiff, D.F., and Borst, A. (2010). ON and OFF pathways in *Drosophila* motion vision. Nature *468*, 300–304.

Joesch, M., Weber, F., Eichner, H., and Borst, A. (2013). Functional specialization of parallel motion detection circuits in the fly. J. Neurosci. *33*, 902–905.

Juusola, M., Dau, A., Zheng, L., and Rien, D. (2016). Electrophysiological method for recording intracellular voltage responses of *Drosophila* photoreceptors and interneurons to light stimuli in vivo. J. Vis. Exp. *112*, 1–16.

Kolodziejczyk, A., Sun, X., Meinertzhagen, I.A., and Nässel, D.R. (2008). Glutamate, GABA and acetylcholine signaling components in the lamina of the *Drosophila* visual system. PLoS One *3*, e2110.

Laughlin, S.B., Howard, J., and Blakeslee, B. (1987). Synaptic limitations to contrast coding in the retina of the blowfly *Calliphora*. Proc. R. Soc. Lond. B Biol. Sci. *231*, 437–467.

Leonhardt, A., Ammer, G., Meier, M., Serbe, E., Bahl, A., and Borst, A. (2016). Asymmetry of *Drosophila* ON and OFF motion detectors enhances real-world velocity estimation. Nat. Neurosci. *19*, 706–715.

Li, Y., Dharkar, P., Han, T.H., Serpe, M., Lee, C.H., and Mayer, M.L. (2016). Novel functional properties of *Drosophila* CNS glutamate receptors. Neuron *92*, 1036–1048.

Littleton, J.T., and Ganetzky, B. (2000). Ion channels and synaptic organization: analysis of the *Drosophila* genome. Neuron *26*, 35–43.

Liu, W.W., and Wilson, R.I. (2013). Glutamate is an inhibitory neurotransmitter in the *Drosophila* olfactory system. Proc. Natl. Acad. Sci. USA *110*, 10294–10299.

Mahr, A., and Aberle, H. (2006). The expression pattern of the *Drosophila* vesicular glutamate transporter: a marker protein for motoneurons and glutamatergic centers in the brain. Gene Expr. Patterns *6*, 299–309.

Maisak, M.S., Haag, J., Ammer, G., Serbe, E., Meier, M., Leonhardt, A., Schilling, T., Bahl, A., Rubin, G.M., Nern, A., et al. (2013). A directional tuning map of *Drosophila* elementary motion detectors. Nature *500*, 212–216.

Marvin, J.S., Borghuis, B.G., Tian, L., Cichon, J., Harnett, M.T., Akerboom, J., Gordus, A., Renninger, S.L., Chen, T.W., Bargmann, C.I., et al. (2013). An optimized fluorescent probe for visualizing glutamate neurotransmission. Nat. Methods *10*, 162–170.

Masu, M., Iwakabe, H., Tagawa, Y., Miyoshi, T., Yamashita, M., Fukuda, Y., Sasaki, H., Hiroi, K., Nakamura, Y., Shigemoto, R., et al. (1995). Specific deficit of the ON response in visual transmission by targeted disruption of the mGluR6 gene. Cell *80*, 757–765.

Mauss, A.S., Meier, M., Serbe, E., and Borst, A. (2014). Optogenetic and pharmacologic dissection of feedforward inhibition in *Drosophila* motion vision. J. Neurosci. *34*, 2254–2263.

Mauss, A.S., Pankova, K., Arenz, A., Nern, A., Rubin, G.M., and Borst, A. (2015). Neural circuit to integrate opposing motions in the visual field. Cell *162*, 351–362.

Meldrum, B.S. (2000). Glutamate as a neurotransmitter in the brain: review of physiology and pathology. J. Nutr. *130*, 1007S–1015S.

Mosbacher, J., Schoepfer, R., Monyer, H., Burnashev, N., Seeburg, P., and Ruppersberg, J. (1994). A molecular determinant for submillisecond desensitization in glutamate receptors. Science *266*, 1059–1062.

Raghu, S.V., and Borst, A. (2011). Candidate glutamatergic neurons in the visual system of *Drosophila*. PLoS One. https://doi.org/10.1371/journal.pone.0019472.

Ringach, D., and Shapley, R. (2004). Reverse correlation in neurophysiology. Cognit. Sci. *28*, 147–166.

Ringach, D.L. (2004). Mapping receptive fields in primary visual cortex. J. Physiol. *558*, 717–728.

Rister, J., Pauls, D., Schnell, B., Ting, C.Y., Lee, C.H., Sinakevitch, I., Morante, J., Strausfeld, N.J., Ito, K., and Heisenberg, M. (2007). Dissection of the peripheral motion channel in the visual system of *Drosophila melanogaster*. Neuron *56*, 155–170.

Schnell, B., Joesch, M., Forstner, F., Raghu, S.V., Otsuna, H., Ito, K., Borst, A., and Reiff, D.F. (2010). Processing of horizontal optic flow in three visual interneurons of the *Drosophila* brain. J. Neurophysiol. *103*, 1646–1657.

Scott, E.K., Raabe, T., and Luo, L. (2002). Structure of the vertical and horizontal system neurons of the lobula plate in *Drosophila*. J. Comp. Neurol. *454*, 470–481.

Shapley, R., and Lennie, P. (1985). Spatial frequency analysis in the visual system. Annu. Rev. Neurosci. *8*, 547–583.

Shinomiya, K., Karuppudurai, T., Lin, T.Y., Lu, Z., Lee, C.H., and Meinertzhagen, I.A. (2014). Candidate neural substrates for OFF edge motion detection in *Drosophila*. Curr. Biol. *24*, 1062–1070.

Silies, M., Gohl, D.M., Fisher, Y.E., Freifeld, L., Clark, D.A., and Clandinin, T.R. (2013). Modular use of peripheral input channels tunes motion-detecting circuitry. Neuron *79*, 111–127.

Srinivasan, M.V., Laughlin, S.B., and Dubs, A. (1982). Predictive coding: a fresh view of inhibition in the retina. Proc. R. Soc. Lond. B Biol. Sci. *216*, 1471–2954.

St-Pierre, F., Marshall, J.D., Yang, Y., Gong, Y., Schnitzer, M.J., and Lin, M.Z. (2014). High-fidelity optical reporting of neuronal electrical activity with an ultrafast fluorescent voltage sensor. Nat. Neurosci. *17*, 884–889.

Strother, J.A., Wu, S.T., Wong, A.M., Nern, A., Rogers, E.M., Le, J.Q., Rubin, G.M., and Reiser, M.B. (2017). The emergence of directional selectivity in the visual motion pathway of *Drosophila*. Neuron *94*, 168–182.

Takemura, S.Y., Nern, A., Chklovskii, D.B., Scheffer, L.K., Rubin, G.M., and Meinertzhagen, I.A. (2017). The comprehensive connectome of a neural substrate for 'ON' motion detection in *Drosophila*. Elife *6*, 1–16.

Takemura, S.Y., Karuppudurai, T., Ting, C.Y., Lu, Z., Lee, C.H., and Meinertzhagen, I.A. (2011). Cholinergic circuits integrate neighboring visual signals in a *Drosophila* motion detection pathway. Curr. Biol. *21*, 2077–2084.

Traynelis, S.F., Wollmuth, L.P., McBain, C.J., Menniti, F.S., Vance, K.M., Ogden, K.K., Hansen, K.B., Yuan, H., Myers, S.J., and Dingledine, R. (2010). Glutamate receptor ion channels: structure, regulation, and function. Pharmacol. Rev. *62*, 405–496.

Tsutsui, H., Jinno, Y., Tomita, A., Niino, Y., Yamada, Y., Mikoshiba, K., Miyawaki, A., and Okamura, Y. (2013). Improved detection of electrical activity with a voltage probe based on a voltage-sensing phosphatase. J. Physiol. *591*, 4427–4437.

Tuthill, J.C., Nern, A., Holtz, S.L., Rubin, G.M., and Reiser, M.B. (2013). Contributions of the 12 neuron classes in the fly lamina to motion vision. Neuron *79*, 128–140.

Von Hassenstein, B., and Reichardt, W. (1956). Systemtheoretische Analyse der Zeit-, Reihenfolgen-und Vorzeichenauswertung bei der Bewegungsperzeption des Rüsselkäfers Chlorophanus. Sect. B J. Chem. Sci. *11*, 513–524.

Wasserman, S.M., Aptekar, J.W., Lu, P., Nguyen, J., Wang, A.L., Keles, M.F., Grygoruk, A., Krantz, D.E., Larsen, C., and Frye, M.A. (2015). Olfactory neuromodulation of motion vision circuitry in *Drosophila*. Curr. Biol. *25*, 467–472.

Yang, H.H., St-Pierre, F., Sun, X., Ding, X., Lin, M.Z., and Clandinin, T.R. (2016). Subcellular imaging of voltage and calcium signals reveals neural processing in vivo. Cell *166*, 245–257.

Zucker, R.S. (1993). Calcium and transmitter release. J. Physiol. Paris *87*, 25–36.

ISCI, Volume *7*

Supplemental Information

Glutamate Signaling in the Fly Visual System

Florian G. Richter, Sandra Fendl, Jürgen Haag, Michael S. Drews, and Alexander Borst

Supplemental Information

Supplemental Figures

A

L1	GCaMP6f	iGluSnFR
τ_{LP}	350 ms	70 ms
τ_{HP}	1178 ms	407 ms
$FWHM_{cen}$	8.74	10.56
$FWHM_{sur}$	56.55	42.55
A_{rel}	19.33	20.51

B

Mi9	GCaMP6f	iGluSnFR
τ_{LP}	607 ms	75 ms
$FWHM_{cen}$	6.69	7.18
$FWHM_{sur}$	19.37	25.86
A_{rel}	2.81	3.56

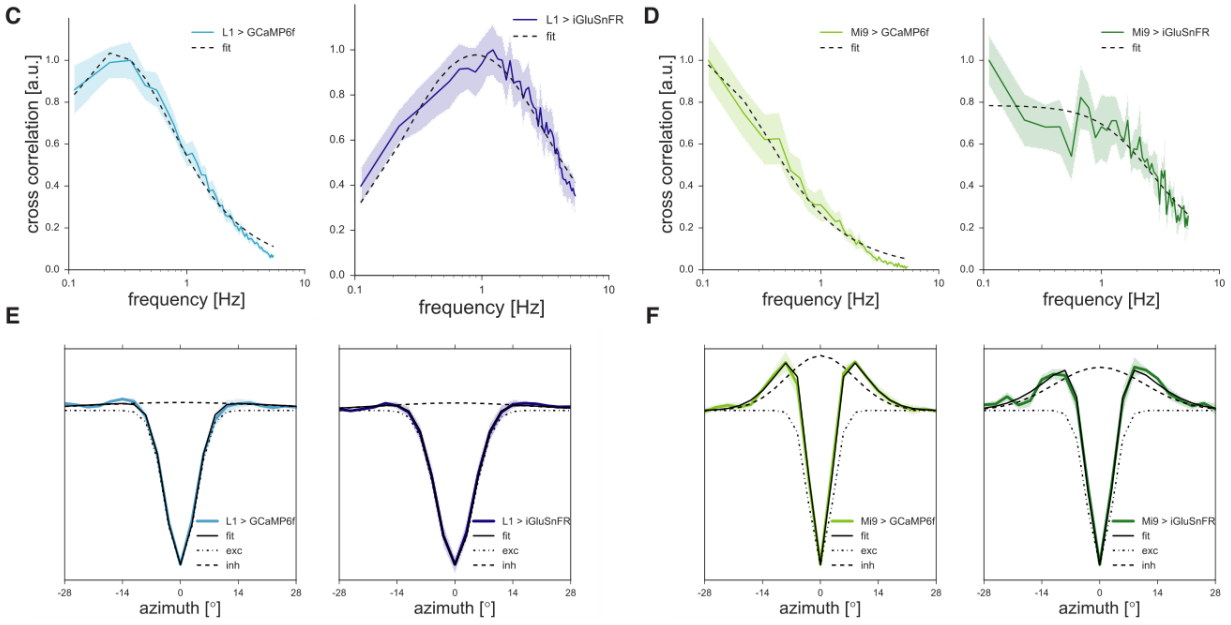

Figure S1. Model fits to L1 and Mi9 data, related to Fig 3
(A) Parameters to quantitatively describe the receptive field characteristics of L1 recorded either with GCaMP6f (left column) or iGluSnFR (right column). First two parameters describe temporal components of the receptive field, last three parameters describe those of the spatial component.
(B) Same as (A) only for Mi9. Description of highpass characteristics is missing, since Mi9 is best described by a pure low-pass.
(C) Impulse responses from Figure 3 D-E plotted in frequency space. Black dashed lines mark the fit of a 1st order band-pass filter (for time constants see table (A).
(D) Same as (C) only for Mi9. Black dashed lines mark the fit of a 1st order low-pass filter.
(E)+(F) Spatial receptive fields from Figure 3 D-E. Data are fitted with a Mexican hat function that captures both, the excitatory center as well as the inhibitory surround of these receptive fields. cen = center, sur = surround, LP = low-pass, HP = high-pass, A = amplitude, τ = time constant, FHWM = full width at half maximum.

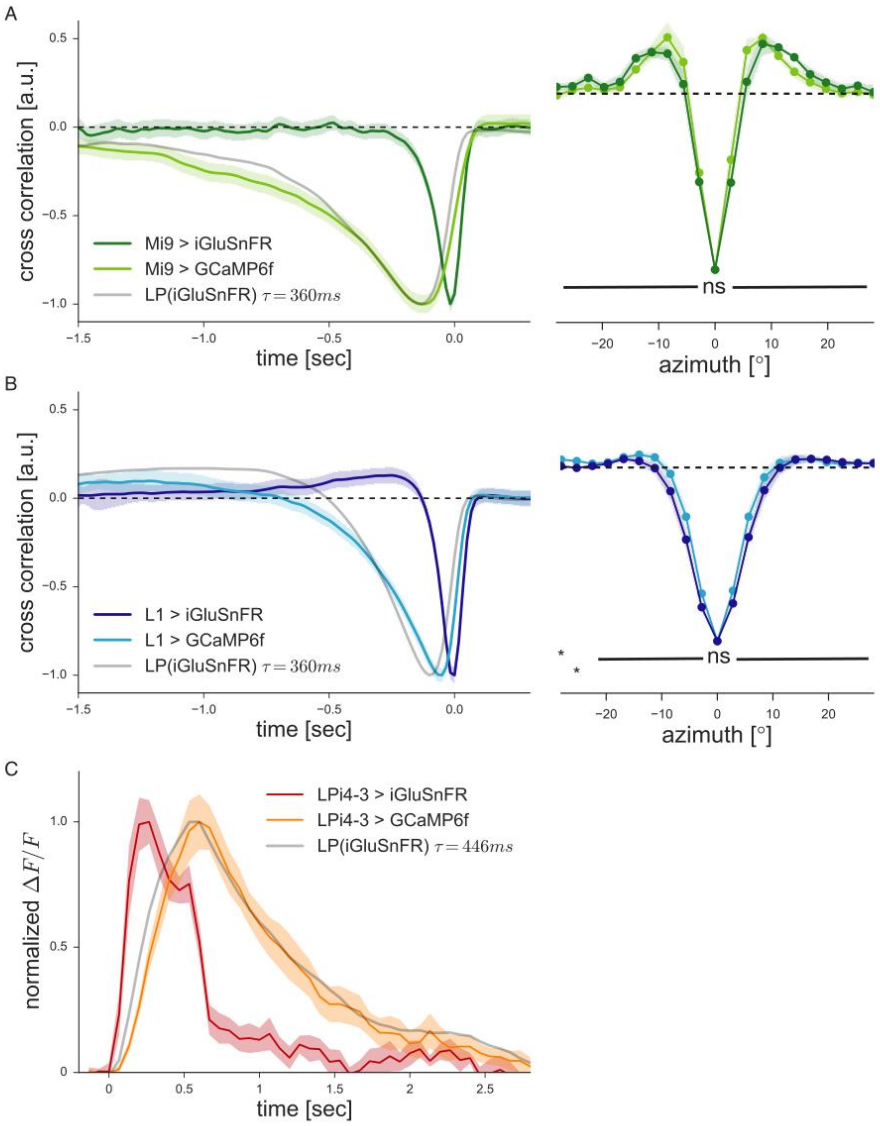

Figure S2. GCaMP data resembles low-pass filtered iGluSnFR data, related to Fig 3 and 4
(A) Low-pass filtering of the Mi9 impulse response measured with iGluSnFR with a time constant of 360 ms (grey) shows the best fit with the impulse response measured with GCaMP6f (left panel). Spatial receptive fields (right panel) are not significantly different from each other, when measured with the two different sensors.
(B) Same as (A) for L1
(C) Low-pass filtering of the LPi4-3 > iGluSnFR response to local flicker with a time constant of 446 ms (grey) shows the best fit to response measured with GCaMP6f (orange).

Transparent Methods

Flies/preparation

Flies were raised and kept on standard cornmeal-agar medium on a 12 hour light/12 hour dark cycle at 25°C and 60% humidity. For imaging experiments, the genetically-encoded calcium indicators GCaMP6f or the genetically encoded glutamate sensor iGluSnFR (Chen et al., 2013; Marvin et al., 2013) were expressed using the Gal4-UAS system in cell-type specific Gal4 fly lines, resulting in the following genotypes:

Genotypes:

L1>GC6f:	w+; R48A08-AD/UAS-GCaMP6f; R66A01-DBD/UAS-GCaMP6f
L1>iGluSnFR:	w+; R48A08-AD/+; R66A01-DBD/UAS-iGluSnFR (BL59611, AV184)
Mi9>GC6f:	w+; R48A07-AD/UAS-GCaMP6f; VT046779-DBD/UAS-GCaMP6f
Mi9>iGluSnFR:	w+; R48A07-AD/+; VT046779-DBD/UAS-iGluSnFR (BL59611, AV184)
LPi>GC6f:	w+; +/UAS-GCaMP6f; R38G02-Gal4/UAS-GCaMP6f
LPi>iGluSnFR:	w+; +; R38G02-Gal4/UAS-iGluSnFR (BL59611, AV184)

For immunohistochemical stainings in Figure 2:

L1>myr::GFP:	w-; R48A08-AD/UAS-myr::GFP; R66A01-DBD/+
Mi9>myr::GFP:	w-; R48A07-AD/ UAS-myr::GFP; VT046779-DBD/+
LPi4-3>myr::GFP:	w-; UAS-myr::GFP/+; R38G02-Gal4/+

The transgenic fly lines driving split-Gal4 expression in the lamina neuron L1 were generated and described in (Tuthill et al., 2013). Mi9 in (Strother et al., 2017) and the one of LPi's in (Mauss et al., 2015). For calcium and glutamate imaging experiments, flies were prepared as previously described (Maisak et al., 2013; Strother et al., 2017). Briefly, flies were anaesthetized on ice, fixed with their backs, legs and wings to a Plexiglas holder with the back of the head exposed to a recording chamber filled with fly external solution. The cuticle at the back of the head on one side was cut away with a fine hypodermic needle and removed together with muscles and air sacks covering the underlying optic lobe.

Data acquisition and analysis:

Data analysis was performed offline using custom-written routines in Matlab and Python 2.7 (with the SciPy and OpenCV-Python Libraries).

2-photon imaging:

Imaging was performed on custom-built 2-photon microscopes as previously described (Maisak et al., 2013) and controlled with the ScanImage software in Matlab (Pologruto et al., 2003). Acquisition rates were between 15 (for LPi experiments) and 23.67 Hz (for L1 and Mi9 experiments), image resolution between 64x64 and 128x32 pixels (for L1 and Mi9 experiments). Before starting the acquisition, we verified that the receptive fields of the cells were located on the stimulus arena by showing a search stimulus consisting of moving gratings.

Calcium imaging was performed as previously described in (Arenz et al., 2017). In brief: Images were automatically registered using horizontal and vertical translations to correct for the movement of the brain. Fluorescence changes (ΔF/F values) were then calculated using a standard baseline algorithm (Jia et al., 2011). Regions of interest (ROIs) were drawn on the average raw image by hand in the medulla layer M1 for L1 and in layer M10 for Mi9. For LPi neurons, ROIs were routinely chosen in the lobula plate, encompassing small regions with single to few axon terminals. Averaging the fluorescence change over this ROI in space resulted in a ΔF/F time course. Glutamate imaging was performed with the same settings as the calcium imaging experiments.

Visual stimulation for L1 and Mi9 experiments

The spatiotemporal response properties of the L1 and Mi9 columnar input elements were determined on a custom-built projector-based arena, as previously described in (Arenz et al., 2017). Stimuli were projected with 2 commercial micro-projectors (TI DLP Lightcrafter 3000) onto the back of an opaque cylindrical screen covering 180 ° in azimuth and 105 ° in elevation of the fly's visual field. The projectors refresh rate is 180 Hz (at 8 bit color depth). For all stimuli used here, we set the medium brightness to a 8-bit grayscale value of 50, which corresponds to a medium luminance of 55 ± 11 cd/m^2. Stimuli were rendered using a custom written software in Python 2.7.

Visual stimulation for LPi4-3 experiments with telescope

This technique has been previously described in (Haag et al., 2016). In brief: Antidromic illumination of the fly's head visualizes the hexagonal structure of the optical axes of the ommatidia (Franceschini, 1975; Schuling et al., 1989). Visual stimuli are generated on the AMOLED display (800x600 pixels, pixel size 15x15 mm, maximal luminance > 1500 cd/m^2; lambda = 530 nm; refresh rate 85 Hz) (SVGA050SG, Olightek). This allows to precisely position the stimuli onto single lamina cartriges. In order to prevent stimulus light from entering the photomultiplier of the two-photon micro-scope, light generated by the AMOLED display was filtered with a long-pass filter (514 LP, T: 529.4– 900 nm, AHF). The AMOLED display was controlled with MATLAB and the psychophysics toolbox (V3.0.11;(Brainard, 1997)).

White noise reverse-correlation

The analysis of spatial receptive fields was previously described in (Arenz et al., 2017). For the input elements, spatiotemporal receptive fields were calculated following standard reverse-correlation methods (Dayan and Abbott, 2013; French, 1976). First, the mean value was subtracted from the raw signals of single ROIs by using a low-pass filtered version of the signal (Gaussian filter with 120 seconds standard deviation) as a baseline for a ΔF/F-like representation of the signal.
The stimulus-response reverse correlation function was calculated as:

$$K(x,\tau) = \int_0^T dt\, S(x, t-\tau) \cdot R(t)$$

with S for the stimulus and R for the response of the neuron. The resulting spatiotemporal fields were normalized in z-score. Only receptive fields with peak amplitudes above 10 standard deviations from the mean were taken for further analysis (for Mi9-GCaMP6f the threshold

was lowered to 7). Cross-sections through the receptive fields along the space axis were fit with a Gaussian function to determine the position of the peak (Suppl. Fig. 1 E-F).

Gaussian noise stimulus

The same stimulus was used in (Arenz et al., 2017). In brief: The stimulus consisted of 64 vertical bars covering an angle of 180° in total. The intensity of each bar fluctuated randomly around a mean intensity of 50 on the 8-bit grayscale of the display. The intensities were drawn from a Gaussian distribution with a standard deviation of 25% contrast. In time, the stimulus was low-pass filtered with a Gaussian window with approximately 22ms standard deviation, which restricted the frequency content of the stimulus to frequencies below 10Hz. For Mi9-GCaMP6f imaging, similarly, the time window was 45ms long, covering frequencies until up to 5Hz.

Spatial receptive field

The analysis of spatial receptive fields was previously described in (Arenz et al., 2017). In brief: One-dimensional spatial receptive fields are cross-sections through the peak of the spatiotemporal receptive fields along the space axis and are averaged over the 12 samples (200ms) around the peak. For both L1 and Mi9 we found a small-field, antagonistic center-surround organization of the spatial receptive field using the vertical white noise stimulus.
The black dashed lines in Suppl. Fig 1 represents a Mexican hat function (Difference of Gaussian). Mathematically such a function can be described as follows:

$$RF_{1D}(\varphi) = e^{-\frac{1}{2}\frac{\varphi^2}{\sigma_{cen}{}^2}} - A_{rel} \cdot e^{-\frac{1}{2}\frac{\varphi^2}{\sigma_{sur}{}^2}}$$

with φ as azimuth, σ_{cen} and σ_{sur} as the standard deviations of center and surround, respectively, and $A_{rel} = A_{sur}/A_{cen}$ the relative strength of the surround in relation to the amplitude of the center Gaussian (which is normalized to 1).

Temporal receptive field

The analysis of temporal receptive fields was previously described in (Arenz et al., 2017). In brief: The time-reversed impulse responses shown in Figure 3 are cross-sections through the center of the spatiotemporal receptive fields along the time axis and are averaged over the three center pixels. For the determination of the time constants (tau), we sought to describe the response characteristic of each cell with a simplified model that catches the main properties. For that, we fitted simple 1st$_{st}$ order filters (e.g. 1st order low-pass for Mi9; 1st order bandpass for L1) to the impulse responses of all cells.
The model fit in Suppl. Fig 2 (grey lines) was performed by low-pass filtering the measured iGluSnFR response of each neuron type (L1, Mi9, LPi) with a 1st order low-pass filter and optimizing the time-constant such that the difference between the low-pass filtered signal and the measured calcium response of the neurons was minimal. The fitting procedure was implemented using standard least square algorithms (SciPy 0.19).

Immunohistochemistry

Fly brains were dissected in ice-cold 0.3% PBST and fixed in 4% PFA in 0.3% PBST for 25 min at room temperature. Subsequently, brains were washed 4-5 times in 0.3% PBST and blocked in 10% normal goat serum (NGS) in 0.3% PBST for 1 hour at room temperature. Primary antibodies used were mouse anti-bruchpilot brp (nc82, Developmental Studies

Hybridoma Bank, 1:20) and rabbit anti-VGlut (courtesy of H. Aberle, 1:500). Secondary antibodies used were: goat anti-mouse ATTO 647N (Rockland, 1:300) and goat anti-rabbit Alexa Fluor 568 (Life Technologies, 1:300). Myr::GFP-labeled cells were imaged natively without antibody staining. 5% NGS was added to all antibody solutions and both primary and secondary antibodies were incubated for at least 48 hours at 4°C.
Brains were mounted in Vectashield Antifade Mounting Medium (Vector Laboratories) and imaged on a Leica TCS SP8 confocal microscope.

Supplemental References

Brainard, D.H. (1997). The psychophysics toolbox. Spat. Vis. 10, 433–436.

Franceschini, N. (1975). Sampling of the visual environment by the compound eye of the fly: Fundamentals and applications. Photoreceptor Opt. 98–125.

Jia, H., Rochefort, N.L., Chen, X., Konnerth, A. (2011). In vivo two-photon imaging of sensory-evoked dendritic calcium signals in cortical neurons. Nat. Protoc. 6, 28–35.

Pologruto, T.A., Sabatini, B.L., Svoboda, K. (2003). ScanImage: Flexible software for operating laser scanning microscopes. Biomed. Eng. Online 2.

Schuling, F.H., Mastebroek, H.A.K., Bult, R., Lenting, B.P.M. (1989). Properties of elementary movement detectors in the fly *Calliphora erythrocephala*. J. Comp. Physiol. A 165, 179–192.

2.3 Manuscript 3: Conditional protein tagging methods reveal distinct subcellular distribution of ion channels in motion-sensing neurons

Abstract

Neurotransmitter receptors and ion channels shape the biophysical properties of neurons, from the sign of the response mediated by neurotransmitter receptors to the dynamics shaped by voltage-gated ion channels. Therefore, knowing the localizations and types of receptors and channels present in neurons is fundamental to our understanding of neural computation. Here, we developed two approaches to visualize the subcellular localization of specific proteins in *Drosophila*: The flippase-dependent expression of GFP-tagged receptor subunits in single neurons and 'FlpTag', a versatile new tool for the conditional labelling of endogenous proteins. Using these methods, we investigated the subcellular distribution of the receptors GluClα, Rdl, and Dα7 and the ion channels para and Ih in motion-sensing T4/T5 neurons of the *Drosophila* visual system. We discovered a strictly segregated subcellular distribution of these proteins and a sequential spatial arrangement of glutamate, acetylcholine, and GABA receptors along the dendrite that matched the previously reported EM-reconstructed synapse distributions.

Authors

Sandra Fendl*, Renee M. Vieira*, and Alexander Borst

* equal contribution

Contributions

S.F. conceived and designed the study; imaged all data shown and processed confocal images; wrote the manuscript and prepared the figures with the help of R.M.V. and A.B; R.M.V. conceived and designed the study; analyzed and quantified all imaged data; developed and created the UAS-lines and the FlpTag-construct and stocks with the help of S.F; A.B., Conceptualization, Resources, Supervision, Project administration, Writing - review and editing.

Conditional protein tagging methods reveal highly specific subcellular distribution of ion channels in motion-sensing neurons

Sandra Fendl[1,2†]*, Renee Marie Vieira[1†], Alexander Borst[1,2]

[1]Max Planck Institute of Neurobiology, Martinsried, Germany; [2]Graduate School of Systemic Neurosciences, LMU Munich, Martinsried, Germany

Abstract Neurotransmitter receptors and ion channels shape the biophysical properties of neurons, from the sign of the response mediated by neurotransmitter receptors to the dynamics shaped by voltage-gated ion channels. Therefore, knowing the localizations and types of receptors and channels present in neurons is fundamental to our understanding of neural computation. Here, we developed two approaches to visualize the subcellular localization of specific proteins in *Drosophila*: The flippase-dependent expression of GFP-tagged receptor subunits in single neurons and 'FlpTag', a versatile new tool for the conditional labelling of endogenous proteins. Using these methods, we investigated the subcellular distribution of the receptors GluClα, Rdl, and Dα7 and the ion channels para and Ih in motion-sensing T4/T5 neurons of the *Drosophila* visual system. We discovered a strictly segregated subcellular distribution of these proteins and a sequential spatial arrangement of glutamate, acetylcholine, and GABA receptors along the dendrite that matched the previously reported EM-reconstructed synapse distributions.

***For correspondence:** sfendl@neuro.mpg.de

[†]These authors contributed equally to this work

Competing interest: See page 22

Funding: See page 22

Received: 10 September 2020
Accepted: 14 October 2020
Published: 20 October 2020

Reviewing editor: Claude Desplan, New York University, United States

Introduction

How neural circuits implement certain computations in order to process sensory information is a central question in systems neuroscience. In the visual system of *Drosophila*, much progress has been made in this direction: numerous studies examined the response properties of different cell-types in the fly brain and electron microscopy studies revealed the neuronal wiring between them. However, one element crucial to our understanding is still missing; these are the neurotransmitter receptors used by cells at the postsynaptic site. This knowledge is essential since neurotransmitters and corresponding receptors define the sign and the time-course of a connection, that is whether a synapse is inhibitory or excitatory and whether the signal transduction is fast or slow. The same neurotransmitter can act on different receptors with widely differing effects for the postsynaptic neuron. Glutamate for instance is mainly excitatory, however, in invertebrates it can also have inhibitory effects when it acts on a glutamate-gated chloride channel, known as GluClα (***Cully et al., 1996***; ***Liu and Wilson, 2013***; ***Mauss et al., 2015***). Recently, it has also been shown that acetylcholine, usually excitatory, might also be inhibitory in *Drosophila*, if it binds to the muscarinic mAChR-A receptor (***Bielopolski et al., 2019***). Hence, knowledge inferring the type of transmitter receptor at a synapse is essential for our understanding of the way neural circuits process information.

Moreover, voltage-gated ion channels shape synaptic transmission and the integration of synaptic inputs by defining the membrane properties of every neural cell type. The voltage-gated calcium channel cacophony, for instance, mediates influx of calcium ions that drives synaptic vesicle fusion at presynaptic sites (***Kawasaki et al., 2004***; ***Fisher et al., 2017***). Voltage-gated sodium channels like paralytic (para) are important for the cell's excitability and the generation of sodium-dependent

action potentials. The voltage-gated channel Ih influences the integration and kinetics of excitatory postsynaptic potentials (**Magee, 1999**; **Littleton and Ganetzky, 2000**; **George et al., 2009**). However, only little is known about how these channels are distributed in neurons and how this shapes the neural response properties.

One of the most extensively studied neural circuits in *Drosophila* is the motion vision pathway in the optic lobe and the underlying computation for direction-selectivity. The optic lobe comprises four neuropils: lamina, medulla, lobula, and lobula plate (**Figure 1A**). As in the vertebrate retina, the fly optic lobe processes information in parallel ON and OFF pathways (**Joesch et al., 2010**; **Borst and Helmstaedter, 2015**). Along the visual processing chain, T4/T5 neurons are the first neurons that respond to visual motion in a direction selective way (**Maisak et al., 2013**; **Behnia et al., 2014**; **Fisher et al., 2015a**; **Arenz et al., 2017**; **Strother et al., 2017**). T4 dendrites reside in layer 10 of the medulla and compute the direction of moving bright edges (ON-pathway). T5 dendrites arborize in layer 1 of the lobula and compute the direction of moving dark edges (OFF-pathway) (**Maisak et al., 2013**). The four subtypes of T4/T5 neurons (a, b, c, d), project axon terminals to one of the four layers in the lobula plate, each responding only to movement in one of the four cardinal directions, their preferred direction (**Maisak et al., 2013**).

How do T4/T5 neurons become direction-selective? Both T4 and T5 dendrites span around eight columns collecting signals from several presynaptic input neurons, each of which samples information from visual space in a retinotopic manner (**Haag et al., 2016**; **Shinomiya et al., 2019**). The functional response properties of the presynaptic partners of T4/T5 have been described in great detail (**Behnia et al., 2014**; **Ammer et al., 2015**; **Fisher et al., 2015a**; **Fisher et al., 2015b**; **Serbe et al., 2016**; **Arenz et al., 2017**; **Strother et al., 2017**; **Strother et al., 2018**; **Drews et al., 2020**) along with their neurotransmitter phenotypes (**Takemura et al., 2017**; **Richter et al., 2018**; **Shinomiya et al., 2019**; **Davis et al., 2020**). T4 dendrites receive glutamatergic, GABAergic and cholinergic input, whereas T5 dendrites receive GABAergic and cholinergic input only. These input synapses are arranged in a specific spatial order along T4/T5 dendrites (s. **Figure 1C and D**; for overview **Takemura et al., 2017**; **Shinomiya et al., 2019**).

Which receptors receive this repertoire of different neurotransmitters at the level of T4/T5 dendrites? Recently, several RNA-sequencing studies described the gene expression pattern of nearly all cell-types in the optic lobe of the fruit fly including T4/T5 neurons (**Pankova and Borst, 2016**; **Konstantinides et al., 2018**; **Davis et al., 2020**; **Hörmann et al., 2020**). T4/T5 neurons were found to express numerous receptor subunits of different transmitter classes and voltage-gated ion channels at various expression strengths. However, RNA-sequencing studies do not unambiguously answer the above question for two reasons: mRNA and protein levels are regulated in complex ways via post-transcriptional, translational, and protein degradation mechanisms making it difficult to assign protein levels to RNA levels (**Vogel and Marcotte, 2012**). Secondly, standard RNA-sequencing techniques cannot provide spatial information about receptor localizations, hence, they are not sufficient to conclude which transmitter receptors receive which input signal. Both shortcomings could in principle be overcome by antibody staining since immunohistochemical techniques detect neurotransmitter receptors at the protein level and preserve spatial information. However, high-quality antibodies are not available for every protein of interest and may have variable affinity due to epitope recognition (**Fritschy, 2008**). Furthermore, labeling ion channels via antibodies and ascribing expression of a given channel to a cell-type in dense neuronal tissue remains challenging. The disadvantages of the above techniques highlight the need for new strategies for labeling neurotransmitter receptors in cell types of interest.

In this study, we employed existing and generated new genetic methods to label and visualize ion channels in *Drosophila*. For endogenous, cell-type-specific labeling of proteins, we developed a generalizable method called FlpTag which expresses a GFP-tag conditionally. Using these tools, we explored the subcellular distribution of the glutamate receptor subunit GluClα, the acetylcholine receptor subunit Dα7, and the GABA receptor subunit Rdl in motion-sensing T4/T5 neurons. We found these receptor subunits to be differentially localized between dendrites and axon terminals. Along the dendrites of individual T4/T5 cells, the receptor subunits GluClα, Rdl, and Dα7 reveal a distinct distribution profile that can be assigned to specific input neurons forming synapses in this area. Furthermore, we demonstrated the generalizability of the FlpTag approach by generating lines for the metabotropic GABA receptor subunit Gaba-b-r1 and the voltage-gated ion channels para

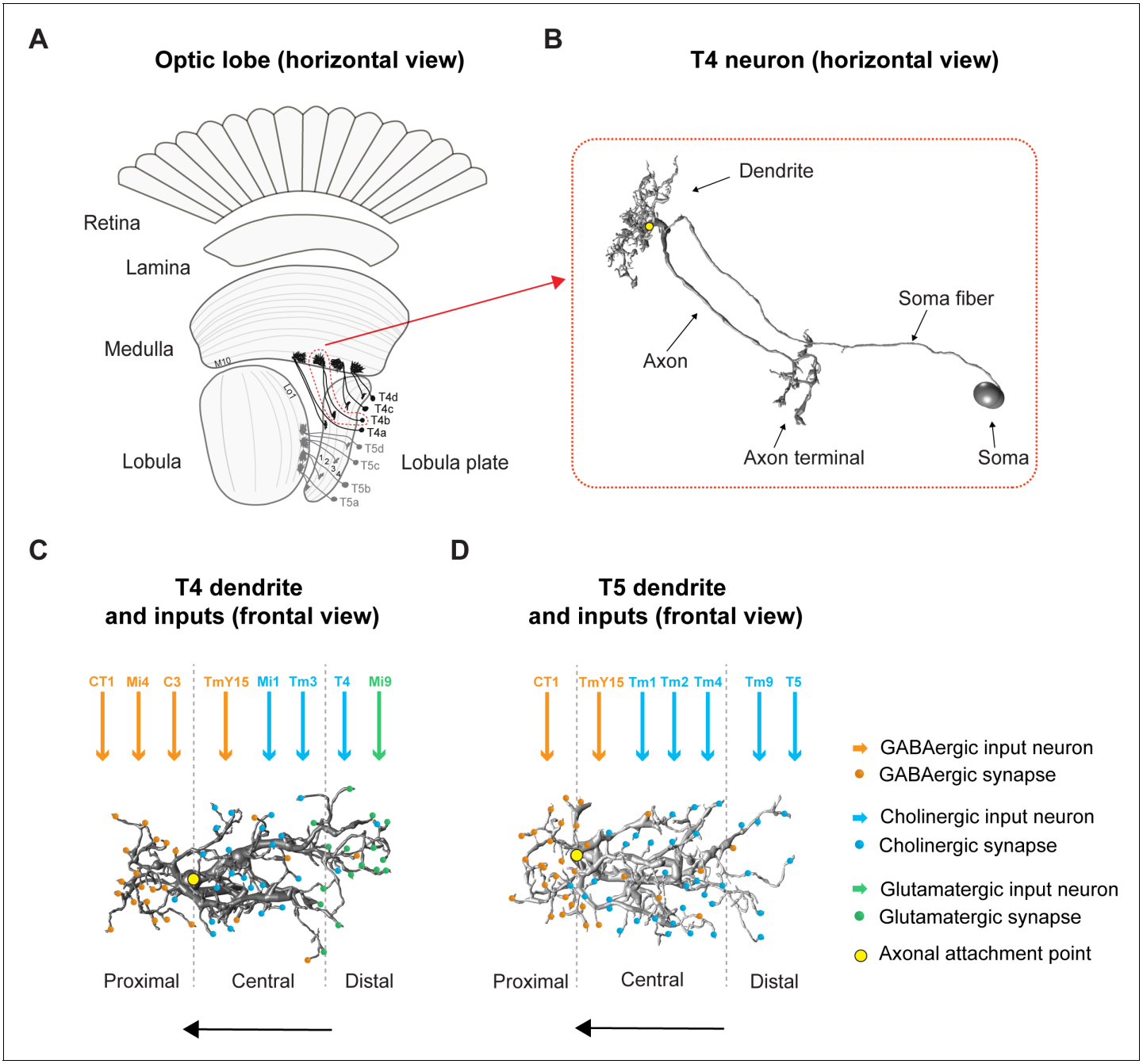

Figure 1. Overview of the fly optic lobe and anatomy of T4/T5 neurons with their presynaptic partners and distribution of input synapses. (**A**) Horizontal view of optic lobe with retina, lamina, medulla, lobula, and lobula plate. T4 dendrites (darker gray) reside in layer 10 of the medulla, T5 dendrites (lighter gray) in layer 1 of the lobula. T4/T5 axon terminals of all subtypes (**a, b, c, d**) project to the lobula plate in four layers. (**B**) Close-up, horizontal view of EM-reconstructed single T4 neuron with dendrite, axon, axon terminal, soma fiber and soma (image extracted from Seven medulla column connectome dataset, http://emdata.janelia.org/#/repo/medulla7column, #3b548, Janelia Research Campus). (**C**) Scheme of individual T4 dendrite and distribution of input synapses (frontal view). The dendrite depicted here is oriented pointing to the right side against its preferred direction from right to left (indicated by arrow). Input on proximal base of T4 dendrite: GABAergic CT1, Mi4 and C3. In the central area: GABAergic TmY15 and cholinergic Mi1 and Tm3. On the distal tips T4 receive input from cholinergic T4 from the same subtype and glutamatergic Mi9. Yellow circle labels first branching point of the dendritic arbor. Reproduced from ***Figure 4***, ***Shinomiya et al., 2019***, eLife, published under the Creative Commons Attribution 4.0 International Public License (CC BY 4.0; https://creativecommons.org/licenses/by/4.0/). (**D**) Scheme of individual T5 dendrite and distribution of input synapses (frontal view). The dendrite depicted here is oriented pointing to the right side against its preferred direction from right to left (indicated by arrow). The T5 dendrite receives GABAergic input from CT1 on the proximal base and from TmY15 in the central area. Cholinergic synapses are formed with Tm1, Tm2, and Tm4 in the central area and with Tm9 and T5 from the same subtype on the distal dendritic tips. Yellow circle labels first branching

Figure 1 continued on next page

Figure 1 continued

point of the dendritic arbor. Reproduced from ***Figure 4***, ***Shinomiya et al., 2019***, eLife, published under the Creative Commons Attribution 4.0 International Public License (CC BY 4.0; https://creativecommons.org/licenses/by/4.0/).

and Ih. The strategies described here can be applied to other cells as well as other proteins to reveal the full inventory and spatial distribution of the various ion channels within individual neurons.

Results

Subcellular localization of the inhibitory glutamate receptor GluClα in T4/T5 neurons

As suggested by the connectome (***Takemura et al., 2017***; ***Shinomiya et al., 2019***) and antibody staining against the vesicular glutamate transporter VGluT (***Richter et al., 2018***), T4 cells receive input on their dendrites from the glutamatergic medulla neuron Mi9. Since a multitude of glutamate receptors exist, both excitatory and inhibitory, we explored which glutamate receptor forms the synapse between the glutamatergic Mi9 input and T4 dendrites.

According to a RNA-sequencing study, GluClα is the most highly expressed glutamate receptor in T4 neurons (***Davis et al., 2020***). To investigate the distribution of this glutamate receptor in T4 and T5 neurons, we developed a transgenic fly line that allowed us to express a GFP-tagged GluClα in a cell-type specific way. We created a *UAS-GluClα::GFP* line bearing the cDNA of GluClα with a GFP-insertion (***Supplementary file 1***). This construct can be combined with any *Gal4*-line to study the receptor's expression and its subcellular localization. We combined the *UAS-GluClα::GFP* line with a membrane-bound *UAS-myr::tdTomato* and expressed both constructs under the control of a T4/T5-specific *Gal4*-driver line. We found GluClα in T4 dendrites of the medulla, where it is distributed in discrete puncta (***Figure 2A***; horizontal section, first two panels). A top view of the medulla of these flies reveals that these puncta are arranged in circular clusters, each corresponding to one column (***Figure 2A***, right panel). Since Mi9 is the only glutamatergic presynaptic partner of T4 cells in the medulla (***Takemura et al., 2017***; ***Richter et al., 2018***; ***Shinomiya et al., 2019***), this columnar arrangement likely reflects the columnar array of Mi9 cell inputs. Conversely, T5 dendrites are completely devoid of GluClα signal (***Figure 2A***, first two panels). This result is in agreement with T5 dendrites not receiving glutamatergic input (***Richter et al., 2018***). In addition to the medulla layer 10, GFP signal of GluClα::GFP is also visible in the axon terminals of T4/T5 in the lobula plate (***Figure 2A***, first two panels). However, both T4 and T5 cells send their axons into the lobula plate, therefore, this staining cannot be assigned to one of the cell types specifically. To differentiate between the two cell types, we used two different driver lines, one specific for either T4 or T5 cells. We confirmed the presence of GluClα in the dendritic layer of T4 cells (***Figure 2B***) and the lack thereof in the dendritic layer of T5 cells (***Figure 2C***). Interestingly, with these specific driver lines, both T4 and T5 neurons express the glutamate receptor in their axon terminals in the lobula plate (***Figure 2B*** and ***Figure 2C***). The presence of GluClα in the axon terminals of T5 neurons explains the high GluClα-mRNA levels in T5 (***Davis et al., 2020***) even though T5 dendrites are missing a glutamatergic presynaptic partner (***Takemura et al., 2017***; ***Richter et al., 2018***; ***Shinomiya et al., 2019***).

One caveat associated with overexpression-lines is a potential mis-localization of proteins. To control for this effect, we used a pan-neuronal *Gal4-line* to express the *UAS-GluClα::GFP* construct and compared this expression pattern to an existing MiMIC protein trap line with GFP insertion (MiMIC GFSTF) in the endogenous locus of GluClα (Mi02890) (***Nagarkar-Jaiswal et al., 2015a***). We observed broad expression of GluClα throughout all neuropils of the optic lobe in both genotypes (***Figure 2—figure supplement 1A and B***). We quantified the mean fluorescence intensity of manually drawn ROIs around the medulla and found both values to be similar for the pan-neuronal *UAS-GluClα::GFP* and the MiMIC line (***Figure 2—figure supplement 1D***). Furthermore, we expressed the *UAS-GluClα::GFP* line with a driver line for T1, a cell-type which lacks GluClα mRNA (***Davis et al., 2020***). Our *UAS*-line confirmed this result as we could not detect significant levels of GluClα::GFP protein in T1 (***Figure 2—figure supplement 1E***). Hence, overexpression of GFP-tagged GluClα, introduced as a transgene, leads to a subcellular localization pattern that seems to be identical to the endogenous GluClα protein.

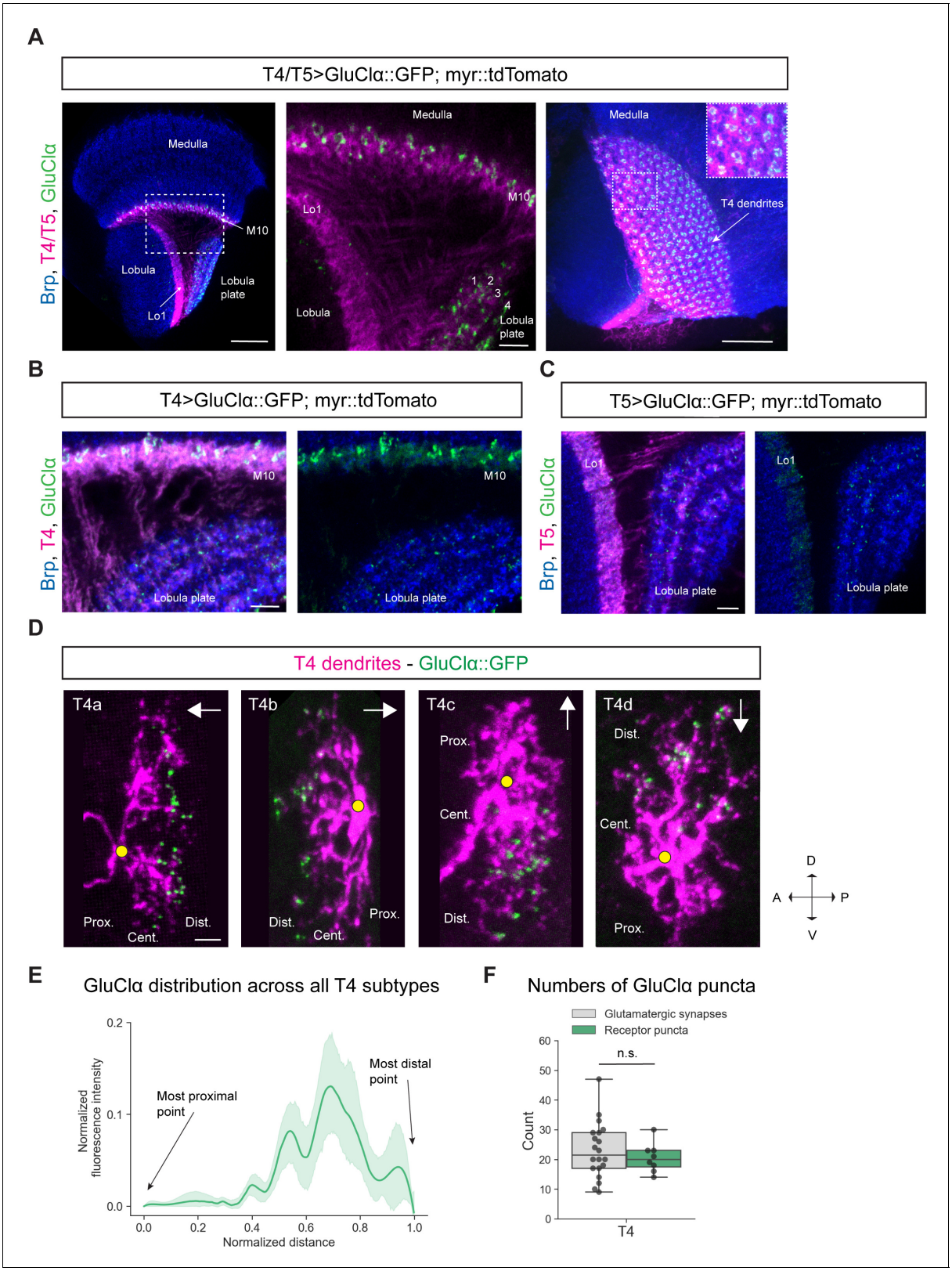

Figure 2. Subcellular localization of the inhibitory glutamate receptor GluClα in T4/T5 neurons. (**A**) Optic lobe with T4/T5 neurons labeled with myr::tdTomato and GluClα::GFP. Left panel: horizontal view on the optic lobe overview (scale bar: 20 µm). Central panel: close-up of medulla layer M10, lobula layer Lo1 and lobula plate layers 1–4 (scale bar: 5 µm). Right panel: Frontal view on medulla layer M10 with T4 dendrites (scale bar: 20 µm); inset: close-up of columnar GluClα::GFP structure in layer 10 of the medulla. (**B**) Close-up of T4 dendrites in layer 10 of the medulla and axon terminals in

Figure 2 continued on next page

Figure 2 continued

lobula plate labeled with myr::tdTomato and GluClα::GFP (scale bar: 5 μm). (**C**) Close-up of T5 dendrites in layer 1 of the lobula and axon terminals in lobula plate labeled with myr::tdTomato and GluClα::GFP (scale bar: 5 μm). (**D**) Individual T4 dendrites labeled with tdTomtato and GluClα::GFP; subtypes a-d pointing in their natural orientation in visual space coordinates (A = anterior, p=posterior, D = dorsal, V = ventral). White arrows indicate preferred directions for every subtype and the dendrites' proximal (Prox.), central (Cent.) and distal (Dist.) areas are labeled (scale bar: 2 μm). Yellow circle labels first branching point of the dendrite. (**E**) Quantification of GluClα distribution over the whole dendritic length (normalized distance) averaged across several T4 dendrites from all subtypes (n = 8). All dendrites were aligned pointing to the right with the most proximal point at 0.0 and the most distal point at 1.0. (**F**) Quantification of GluClα puncta averaged across several T4 dendrites from all subtypes (mean ± SD = 20.5, 4.98 [n = 8]) (same cells used in E) compared to number of glutamatergic input synapses from Mi9 (mean ± SD = 23.0, 9.34 [n = 20]) (EM numbers: personal communication, K. Shinomiya, May 2020). n.s., not significant p>0.05 (p=0.37, t-test).
The online version of this article includes the following source data and figure supplement(s) for figure 2:

Source data 1. Table with numbers of GluClα puncta quantified for T4 dendrites.
Figure supplement 1. Pan-neuronal GluClα levels and distribution in the optic lobe are comparable for MiMIC GFSTF, FlpTag and *UAS*-line.

Given that Mi9 is the only glutamatergic input neuron to T4 dendrites and GluClα is the corresponding glutamate receptor, we hypothesized that GluClα should localize on the individual T4 dendrite exclusively where Mi9 makes glutamatergic synapses with the latter. Therefore, we wanted to visualize the distribution of GluClα at the single-cell level along individual T4 dendrites. The dendrites of each T4/T5 subtype are oriented pointing against their preferred direction (***Takemura et al., 2017***; ***Shinomiya et al., 2019***). With respect to the point of axonal attachment to the dendrite, T4/T5 dendrites can be divided into a proximal, central and distal region (summarized in ***Figure 1B–D***). Electron microscopy studies have shown that Mi9 forms synaptic contacts with T4 on the distal tips of its dendrite (***Figure 1C***; ***Takemura et al., 2017***; ***Shinomiya et al., 2019***). Since T4/T5 dendrites are strongly intermingled in their respective layers, it is not possible to resolve receptor localizations at the single-cell level by labeling the whole population. We used a flippase-based mosaic approach (***Gordon and Scott, 2009***) to sparsely label single T4/T5 neurons with tdTomato together with the *UAS-GluClα::GFP* construct. By using a *FRT-Gal80-FRT* with an hs-FLP, both *UAS-myr::tdTomato* and *UAS-GluClα::GFP* expression are dependent on the same stochastic FLP-event. A heat-shock-activated flippase removes the FRT-flanked *Gal4-repressor Gal80*, which disinhibits Gal4, promoting transcription of both *UAS*-reporters simultaneously resulting in expression of membrane-bound tdTomato and GFP-tagged GluClα in only a few cells of interest. In individual T4 dendrites, we observed that GluClα was predominantly localized to the distal tips, which holds true for all four T4 subtypes (***Figure 2D***). We quantified the intensity distribution of the GluClα::GFP-signal over dendritic distance in individual T4 dendrites. To combine and average this distribution for all four subtypes, we rotated dendrites from each subtype such that the proximal side was on the left side of the image and the distal tips were pointing to the right. Averaged intensities across all subtypes confirmed our observations on individual cells, showing that GluClα is indeed localized toward the distal dendritic tips of T4 dendrites (***Figure 2E***). In addition, we quantified the numbers of GluClα puncta for all subtypes and compared them to the synapse numbers of glutamatergic Mi9 inputs onto T4 determined by the previous EM study (***Shinomiya et al., 2019***). The number of GluClα-puncta per T4 cell dendrite (mean: 20.5 puncta) matches closely the number of glutamatergic input synapses made by Mi9 onto one T4 cell (mean: 23 synaptic contacts; personal communication, K. Shinomiya, May 2020) (***Figure 2F***). This suggests that every GluClα-punctum resolved by confocal microscopy in individually labeled T4 dendrites represents one postsynaptic GluClα receptor cluster corresponding to one Mi9-T4 synapse.

In summary, GluClα localizes to the dendrites of T4 cells and to the axon terminals of both T4 and T5 cells. At the single-cell level, GluClα is distributed toward the distal tips of the dendrites in all T4 subtypes. Strikingly, the number of GluClα puncta closely matches the number of input synapses provided by Mi9, the only glutamatergic input neuron to T4 dendrites.

Rdl localizes to T4/T5 dendritic compartments receiving GABAergic input

Having identified glutamatergic synapses, we employed similar methods to visualize GABAergic synapses in T4/T5 neurons. T4 dendrites receive input from several GABAergic cell-types in the medulla: on the proximal base of the dendrite, these are the columnar cells Mi4, C3; the multicolumnar

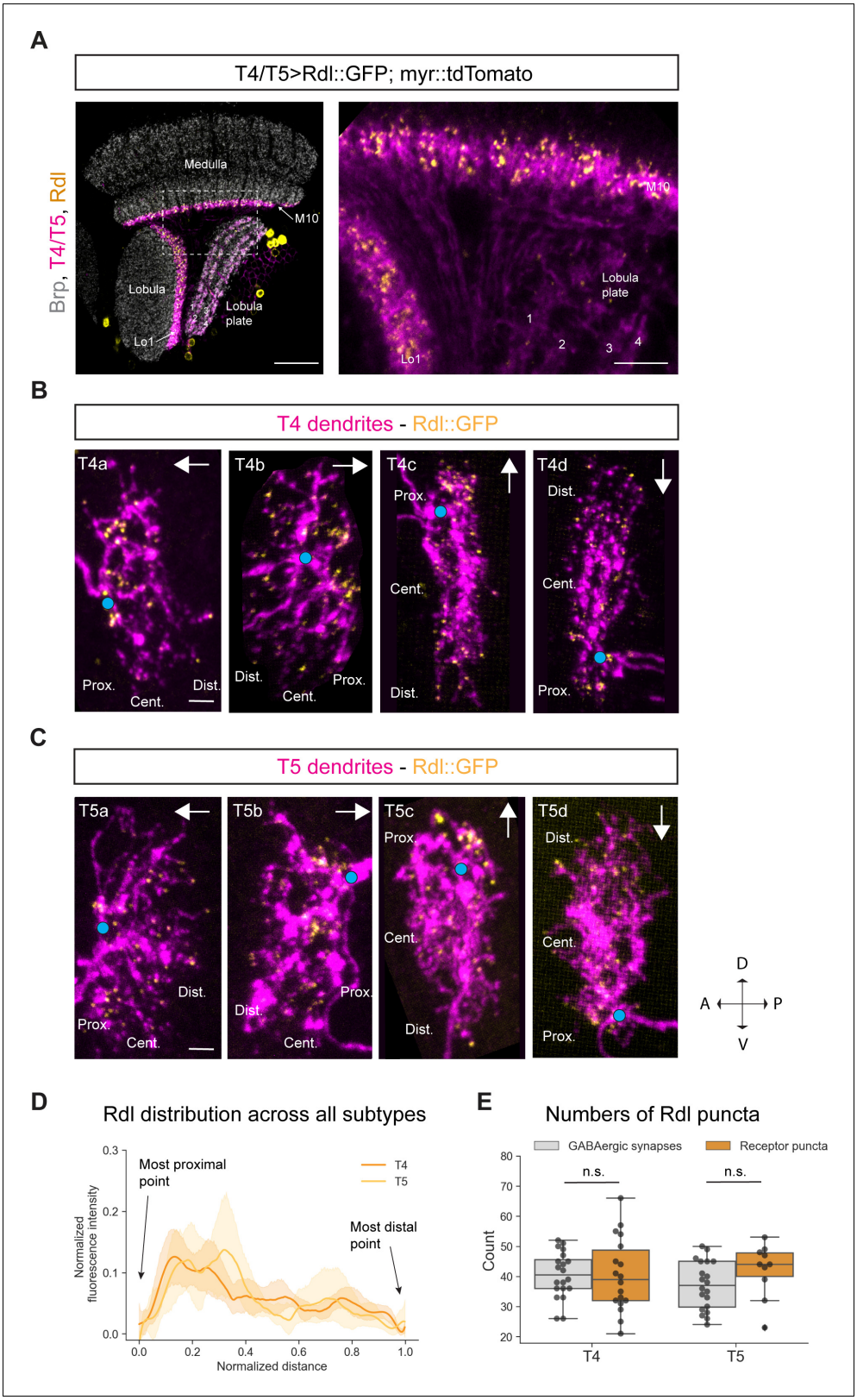

Figure 3. Subcellular localization of the GABA receptor Rdl in T4/T5 neurons. (**A**) Optic lobe with T4/T5 neurons labeled with myr::tdTomato and Rdl::GFP. Left panel: horizontal view on the optic lobe overview (scale bar: 20 µm). Right panel: close-up of medulla layer M10, lobula layer Lo1 and lobula plate layers 1–4 (scale bar: 5 µm). (**B**) Individual T4 dendrites labeled with tdTomtato and Rdl::GFP; subtypes a-d pointing in their natural orientation in visual space coordinates (A = anterior, p=posterior, D = dorsal, V = ventral). White arrows indicate preferred directions for every subtype and the

Figure 3 continued on next page

Figure 3 continued

dendrites' proximal (Prox.), central (Cent.) and distal (Dist.) areas are labeled (scale bar: 2 μm). Blue circle labels first branching point of the dendrite. (**C**) Individual T5 dendrites labeled with tdTomtato and Rdl::GFP; subtypes a-d pointing in their natural orientation in visual space coordinates (A = anterior, p=posterior, D = dorsal, V = ventral). White arrows indicate preferred directions for every subtype and the dendrites' proximal (Prox.), central (Cent.) and distal (Dist.) areas are labeled (scale bar: 2 μm). Blue circle labels first branching point of the dendrite. (**D**) Quantification of Rdl distribution over the whole dendritic length (normalized distance) averaged across several T4 (n = 18) and T5 dendrites (n = 10) from all subtypes. All dendrites were aligned pointing to the right with the most proximal point at 0.0 and the most distal point at 1.0. (**E**) Quantification of Rdl puncta averaged across several T4 (mean ± SD = 40.4, 12.17 [n = 18]) and T5 dendrites (mean ± SD = 42.2, 8.88 [n = 10]) (same cells used in D) from all subtypes compared to number of GABAergic input synapses from T4 (mean ± SD = 40.5, 7.67 [n = 20]) and T5 (mean ± SD = 37.0, 8.05 [n = 20]) (EM numbers: personal communication, K. Shinomiya, May 2020). n.s., not significant p>0.05 (p=0.99 and p=0.13 respectively, t-test).
The online version of this article includes the following source data and figure supplement(s) for figure 3:

Source data 1. Table with numbers of Rdl puncta quantified for T4/T5 dendrites.
Figure supplement 1. Rdl is not detectable in the lamina neuron L1.

amacrine cell CT1 in the middle and distal part of the dendrite as well as TmY15 (***Figure 1C***). In contrast, T5 dendrites receive GABAergic input from only two cell-types: CT1 on the proximal base and TmY15 again throughout the central and distal area of the dendrite (***Figure 1D***). In total, T4 and T5 dendrites receive roughly the same number of GABAergic input synapses (***Takemura et al., 2017***; ***Shinomiya et al., 2019***). Three ionotropic GABA receptor subunits are described in the *Drosophila* genome: Rdl, Lcch3, and Grd (***Liu et al., 2007***). We focused on the GABA receptor subunit Rdl, since RNA-sequencing studies had identified Rdl as the most highly expressed ionotropic GABA receptor subunit in T4 and T5 neurons (***Pankova and Borst, 2016***; ***Davis et al., 2020***). Five Rdl subunits can form a homomeric chloride channel which leads to hyperpolarization upon GABA-binding, thus representing a receptor (***Ffrench-Constant et al., 1993***). Previous studies had created and used a UAS-Rdl::HA line to investigate the distribution of this GABA receptor subunit in *Drosophila* motoneurons and LPTCs (***Sánchez-Soriano et al., 2005***; ***Raghu et al., 2007***; ***Kuehn and Duch, 2013***). In our hands, the anti-HA staining of this line was too weak for conclusive results (data not shown), hence, we created a *UAS-Rdl::GFP* line, consisting of the coding sequence of Rdl and a GFP-tag (***Supplementary file 2***). Combining this line with a T4/T5 specific *Gal4*-line and a membrane-bound tdTomato revealed Rdl expression in both T4/T5 dendrites, but not in the axon terminals (***Figure 3A***). Taken together, both T4 and T5 neurons receive GABAergic inhibition via Rdl receptors on their dendrites.

In a control experiment, we tested for potential overexpression artifacts of the *UAS-Rdl::GFP* line. According to RNA-sequencing, Rdl is not expressed in the lamina monopolar neuron L1 (***Davis et al., 2020***). When we overexpressed *UAS-Rdl::GFP* by means of a *L1-Gal4* driver line, Rdl signal is not detectable in L1 dendrites (***Figure 3—figure supplement 1***). The Rdl::GFP protein was only visible in the cell bodies, presumably due to impaired protein translocation. This suggests that overexpressed Rdl only localizes to endogenous GABA synapses that are composed of the Rdl subunit. Hence, this line can be used to study the subcellular localization of Rdl in any given cell of interest.

Next, we looked at the distribution of the GABA receptor Rdl on individual T4 and T5 dendrites. Using the sparse labeling technique described above, we examined the Rdl::GFP distribution in individual T4/T5 dendrites. We found Rdl on the proximal base and in the central area of both T4 and T5 dendrites across all four subtypes (***Figure 3B*** and ***Figure 3C***). On the proximal base most of the Rdl-signal was arranged in strong discrete clusters, whereas sparse puncta localized to the central area and toward the distal tips. The strong Rdl-signal on the proximal base of the dendrite likely corresponds to the high number of GABAergic inputs provided by the following inputs: CT1, Mi4 and C3 for T4 (32.2 synapses) and CT1 for T5 (30.3 synapses) (personal communication, K. Shinomiya, May 2020). The sparsely distributed Rdl-puncta in the center and tips likely correspond to TmY15 inputs for both T4 and T5 dendrites. This distribution is recapitulated in the intensity quantification across all T4/T5 subtypes, with high Rdl intensity on the proximal side and lower signal in the central and distal area (***Figure 3D***). We quantified the numbers of Rdl receptor clusters in T4 and T5 dendrites and compared them to the sum of all GABAergic input synapses (Mi4, C3, CT1, TmY15 for T4 and CT1, TmY15 for T5) to T4/T5 mapped by EM studies. We found similar numbers of roughly 40 receptor clusters for both T4 and T5 which match the sum of all GABAergic input synapses to T4

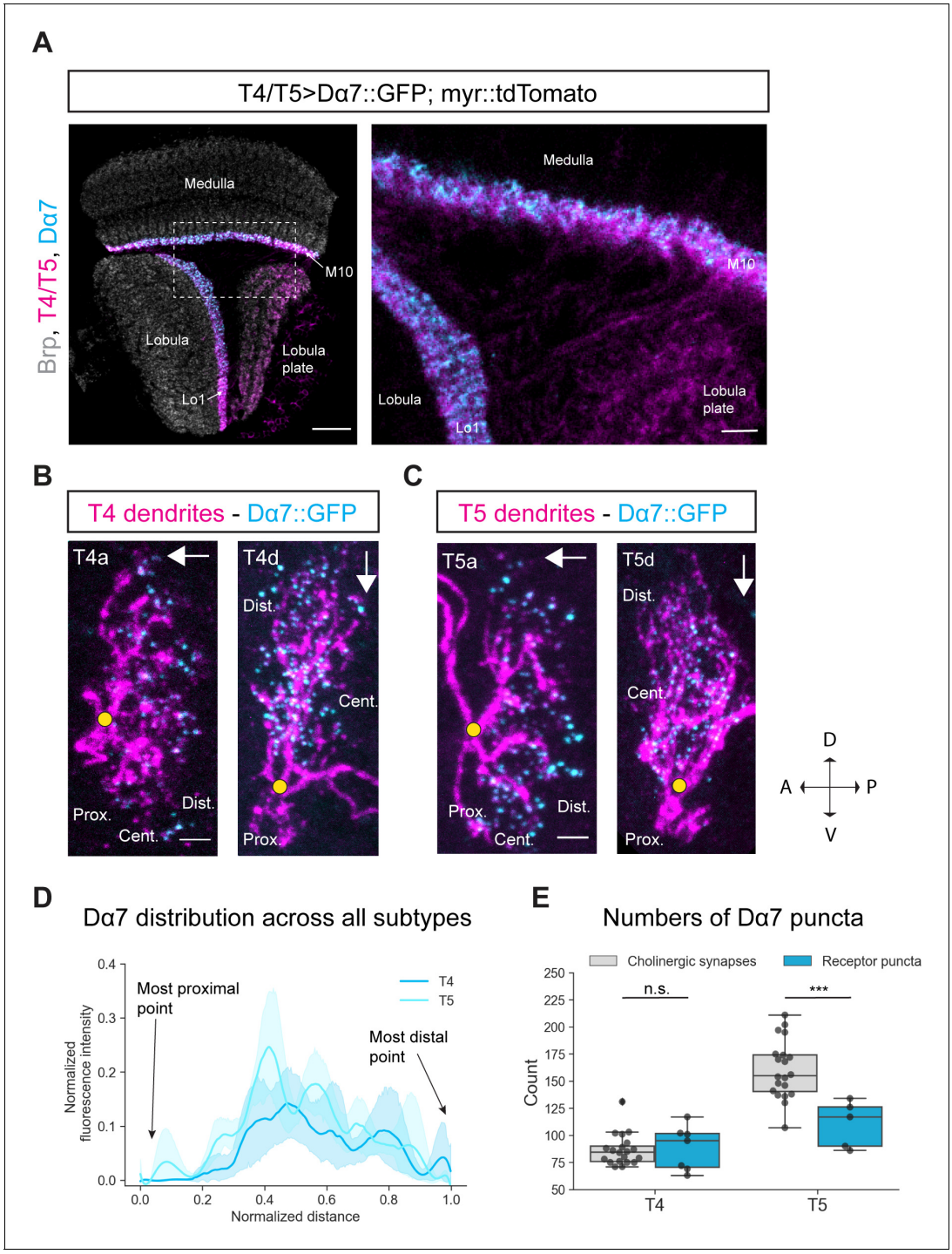

Figure 4. Subcellular localization of the ACh receptor subunit Dα7 in T4/T5 neurons. (**A**) Optic lobe with T4/T5 neurons labeled with myr::tdTomato and Dα7::GFP. Left panel: horizontal view on the optic lobe overview (scale bar: 20 µm). Right panel: close-up of medulla layer M10, lobula layer Lo1 and lobula plate layers 1–4 (scale bar: 5 µm). (**B**) Individual T4 dendrites labeled with tdTomtato and Dα7::GFP; subtypes a and d pointing in their natural orientation in visual space coordinates (A = anterior, p=posterior, D = dorsal, V = ventral). White arrows indicate preferred directions for every subtype and the dendrites' proximal (Prox.), central (Cent.) and distal (Dist.) areas are labeled (scale bar: 2 µm). Yellow circle labels first branching point of the dendrite. (**C**) Individual T5 dendrites labeled with tdTomtato and Dα7::GFP; subtypes a and d pointing in their natural orientation in visual space coordinates (A = anterior, p=posterior, D = dorsal, V = ventral). White arrows indicate preferred directions for every subtype and the dendrites' proximal (Prox.), central (Cent.) and distal (Dist.) areas are labeled (scale bar: 2 µm). Yellow circle labels first branching point of the dendrite. (**D**) Quantification of Dα7 distribution over the whole dendritic length (normalized distance) averaged across several T4 (n = 6) and T5 dendrites (n = 5) from all subtypes. All dendrites were aligned pointing to the right with the most proximal point at 0.0 and the most distal point at 1.0. (**E**) Quantification

Figure 4 continued on next page

Figure 4 continued

of Dα7 puncta averaged across several T4 (mean ± SD = 92.67, 18.67 [n = 6]) and T5 dendrites (mean ± SD = 110.6, 21.53 [n = 5]) (same cells like in D) from all subtypes compared to number of cholinergic input synapses for T4 (mean ± SD = 86.45, 14.37 [n = 20]) and T5 (mean ± SD = 160.50, 26.93 [n = 20]) (EM numbers: personal communication, K. Shinomiya, May 2020). n.s., not significant, p>0.05; ***p<0.001 (p=0.46 and p=2.1e-4 respectively, t-test).

The online version of this article includes the following source data and figure supplement(s) for figure 4:

Source data 1. Table with numbers of Dα7 puncta quantified for T4/T5 dendrites.

Figure supplement 1. Pan-neuronal Dα7 levels and distribution in the optic lobe as seen with *UAS-Dα7::GFP* line, Dα7 antibody staining and *Dα7-Trojan-Gal4* line.

(mean: 40.45) and T5 (mean: 37) (***Figure 3E***) (EM numbers: personal communication, K. Shinomiya, May 2020). Taken together, Rdl receptor subunits localize to the proximal base, and to a lesser extent, in the central area of the dendritic arbor of T4 and T5 neurons, reflecting their GABAergic inputs revealed by EM (***Shinomiya et al., 2019***).

Dα7 localizes to T4/T5 dendritic compartments receiving cholinergic input

According to connectome data, T4 dendrites receive most of their input synapses from cholinergic Mi1 and Tm3 cells at the center of their dendrite (***Takemura et al., 2017***; ***Shinomiya et al., 2019***). Furthermore, T4 neurons of the same subtype form synapses with each other at the distal tips of their dendrites (***Figure 1C***). As T4 neurons are cholinergic (***Mauss et al., 2014***; ***Davis et al., 2020***), these T4-T4 synapses are thought to be cholinergic as well. With the exception of GABAergic CT1, T5 dendrites receive cholinergic input from Tm1, Tm2, and Tm4 in the central area of the dendrite. Tm9 and T5 provide cholinergic input mainly towards the distal tips of the dendrite (***Figure 1D***; ***Takemura et al., 2017***; ***Shinomiya et al., 2019***). T5 dendrites receive almost twice as many cholinergic inputs as T4; 160 and 87 synapses, respectively (***Shinomiya et al., 2019***). We used an existing GFP-tagged *UAS-Dα7::GFP* line to explore the subcellular distribution of these cholinergic synapses (***Raghu et al., 2009***). Dα7 is one of 10 different nicotinic ACh receptor subunits (Dα1-Dα7 and Dß1-Dß3) found in the *Drosophila* genome. All these subunits can form heteromeric receptors consisting of two or three subunits. In addition, Dα5, Dα6, and Dα7 can also form homomeric ACh receptors (***Lansdell and Millar, 2004***; ***Lansdell et al., 2012***). According to RNA-sequencing data, both T4 and T5 neurons express almost every ACh receptor subunit, except for Dα6 and Dß3 (***Davis et al., 2020***). Expression of *UAS-Dα7::GFP* with a *T4/T5-Gal4* line, revealed the distribution of Dα7 to both T4 and T5 dendrites while their axon terminals remained devoid (***Figure 4A***).

As previously conducted, we tested for potential overexpression artifacts of the *UAS-Dα7::GFP* line. We expressed Dα7::GFP in all neurons and compared the expression pattern to two controls: first, an antibody staining against Dα7, and second, a MiMIC Trojan-*Gal4* (TG4) line for Dα7 combined with *UAS-Dα7::GFP* (***Figure 4—figure supplement 1A–C***; ***Fayyazuddin et al., 2006***; ***Diao et al., 2015***; Lee et al.; 2018). The Trojan-*Gal4* (TG4) line has a *Gal4* insertion in the Dα7 gene, which drives expression of *Gal4* only under endogenous transcriptional control of Dα7. Combining this line with the reporter lines *UAS-myr::tdTomato* and *UAS-Dα7::GFP* should label all Dα7-expressing cells with tdTomato, and only within those cells, the Dα7 receptor subunits with GFP. In the pan-neuronal overexpression of *UAS-Dα7::GFP*, the ACh receptor subunit is broadly expressed throughout all neuropils with specific strong Dα7 signal in medulla layer 10 where T4 dendrites reside and lobula layer 1 where T5 dendrites reside (***Figure 4—figure supplement 1A***). However, in both the antibody- and the TG4-experiment, there is only weak Dα7 signal in M10 and Lo1 detectable (***Figure 4—figure supplement 1B and C***). Thus, under UAS-driven overexpression, the levels of Dα7 are increased compared to endogenous Dα7 levels in M10 and Lo1.

To assess whether the subcellular distribution of Dα7 is qualitatively altered by overexpression, we characterized the distribution of Dα7 in a cell type that does not express this receptor subunit endogenously. Transcriptomic data revealed that Dα7 is not expressed in Mi1 (***Davis et al., 2020***). However, Mi1 receives cholinergic input from L3 and L5 and expresses several different ACh receptor subunits (***Takemura et al., 2017***; ***Shinomiya et al., 2019***; ***Davis et al., 2020***). We tested the *UAS-Dα7::GFP* line in Mi1 to explore the qualitative overexpression-effects of this line. When *UAS-*

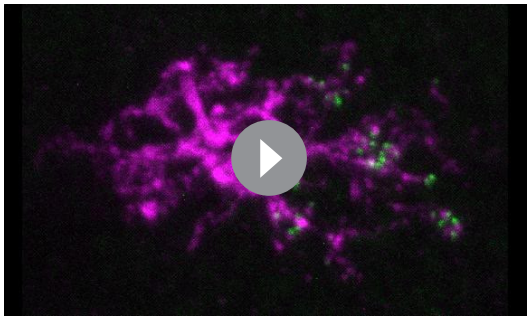

Video 1. 3D-image of a T4 dendrite (subtype d) (magenta) with GluClα::GFP (green).
https://elifesciences.org/articles/62953#video1

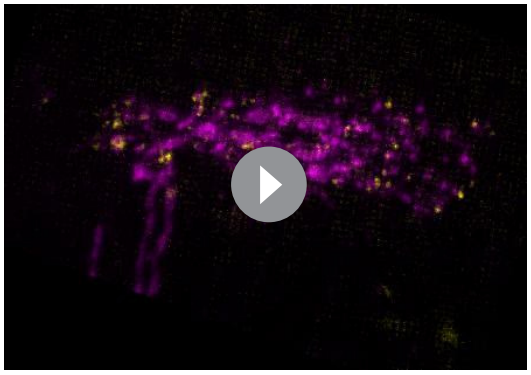

Video 2. 3D-image of a T4 dendrite (subtype d) (magenta) with Rdl::GFP (yellow).
https://elifesciences.org/articles/62953#video2

Dα7::GFP was overexpressed in Mi1, Dα7 localized to layers 1 and 5 of the medulla, where the dendrites of Mi1 neurons arborize and receive cholinergic input from L3 and L5 (***Takemura et al., 2017***; ***Figure 4—figure supplement 1D***). This suggests that overexpressed Dα7::GFP localizes to cholinergic synapses and becomes part of an ACh-receptor, even if this subtype is not endogenously expressed in this neuron. If this scenario is true, the *UAS-Dα7::GFP* line does not report real endogenous subunit compositions with Dα7, but in general it can still be used as a marker for postsynaptic cholinergic sites.

To test this hypothesis, we performed sparse labeling of individual T4/T5 dendrites with the earlier described Gal80-hs-flippase method to explore the subcellular distribution of Dα7 along T4/T5 dendrites. Dα7 was distributed along the central area and distal tips of both T4 and T5 dendrites whereas the proximal base of the dendrite was completely devoid of Dα7 signal (***Figure 4B and C***). In the quantification, it becomes clear that for all subtypes the Dα7-intensity is strongest in the central area and slightly reduced toward the distal tips (***Figure 4D***). Taken together, these results demonstrate that with the *UAS-Dα7::GFP* line, Dα7 localizes to the areas where T4/T5 dendrites receive cholinergic input and not to the proximal base which receives only GABAergic synapses. We quantified the number of Dα7-puncta and compared it to the number of cholinergic synaptic contacts from T4/T5 inputs. For T4 dendrites the numbers of Dα7 puncta quantified (mean: 88.4) matched the numbers of cholinergic input synapses mapped by EM reconstruction (mean: 86.9; personal communication, K. Shinomiya, May 2020) (***Figure 4E***). This strongly suggests that Dα7 localizes only to cholinergic synapses. However, for T5 dendrites the Dα7 puncta exhibited 60 synapses less on average when compared to the mean of the summed cholinergic EM input synapse (***Figure 4E***). The levels of Dα7 along the dendrite are similar for T4 and T5 (***Figure 4D***), even though T5 receive more cholinergic inputs on their distal tips than T4 (***Shinomiya et al., 2019***). The main cholinergic input to T5 in the distal area is Tm9, which makes approximately 60 synapses with T5 dendrites. These 60 synapses could potentially be formed via different cholinergic receptors other than Dα7, for instance muscarinic ACh receptors (***Davis et al., 2020***).

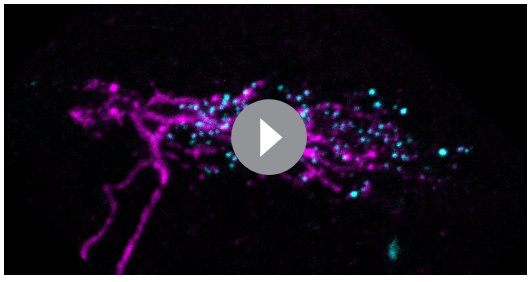

Video 3. 3D-image of a T4 dendrite (subtype d) (magenta) with Dα7::GFP (cyan).
https://elifesciences.org/articles/62953#video3

In summary, the *UAS-Dα7::GFP* line cannot be used to define the exact composition of ACh receptor subunits of cholinergic synapses, but labels (nicotinic) ACh receptors in general. It, nevertheless, can be used as a marker for postsynaptic ACh receptors. Using this approach, we found that the central and distal areas of both T4 and T5 dendrites possess cholinergic receptors. The proximal base of the dendrites, as well as axon terminals are devoid of cholinergic input.

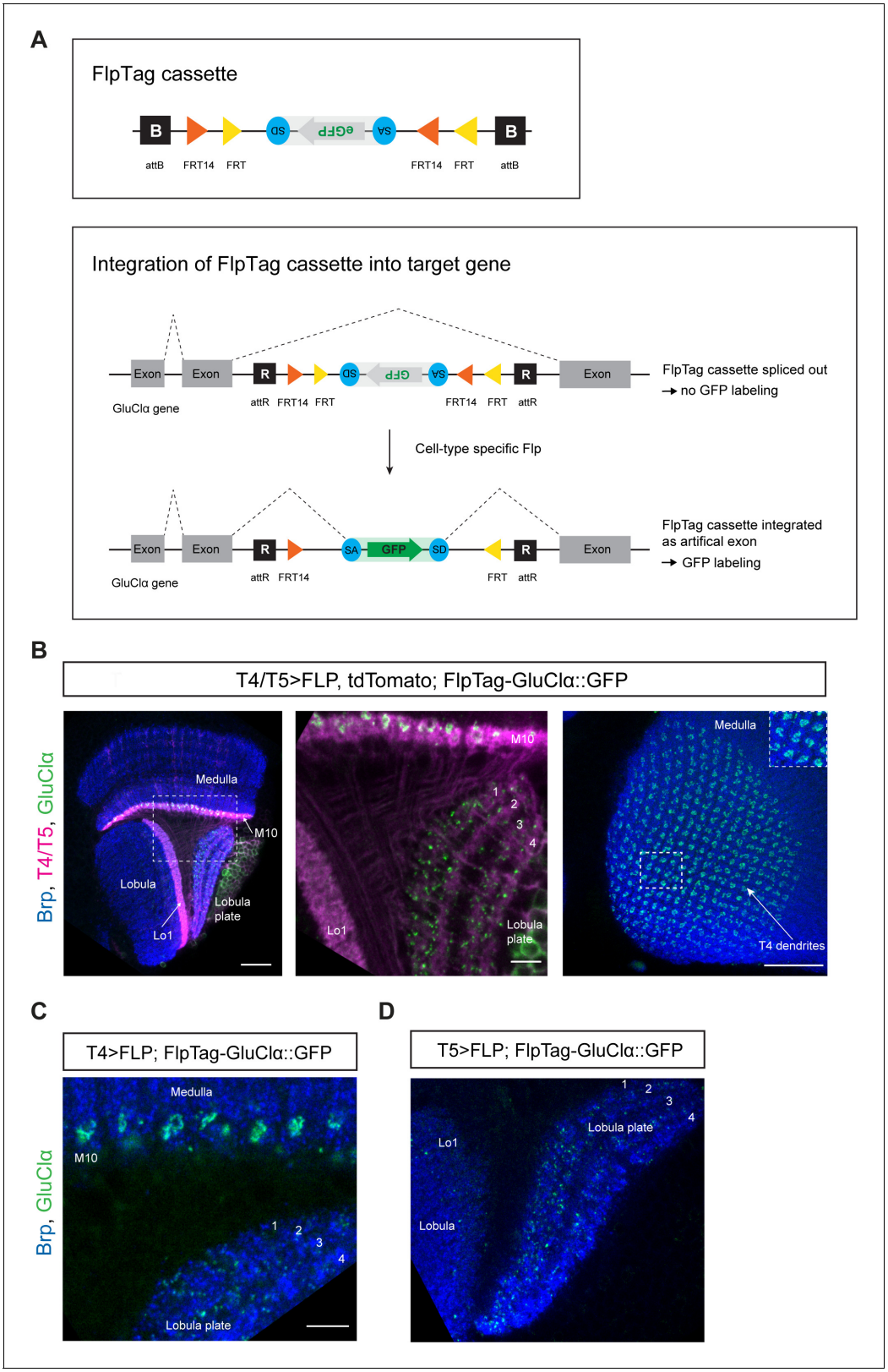

Figure 5. FlpTag, a new tool for cell-type-specific, endogenous labeling as shown with GluClα. (**A**) Scheme of FlpTag cassette (first panel) and integration of FlpTag cassette into target gene (second panel). The FlpTag cassette consists of attB-sites, specific FRT sites which form a FLEx-switch, a splice acceptor, GFP and a splice donor. After ΦC31-dependent integration of the FlpTag cassette into a coding intron of the GluClα target gene, two lines with opposite orientations of the cassette can be obtained. In the initial line with the cassette and GFP in opposite orientation with respect to the

Figure 5 continued on next page

Figure 5 continued

gene (shown here), the cassette is spliced out together with the intron and no GFP-labeling occurs. After cell-type-specific Flp expression, the FlpTag cassette is flipped, stably integrated as an artificial exon and GluClα is labeled with GFP. (**B**) Optic lobe with T4/T5 neurons labeled with myr::tdTomato and FlpTag-GluClα::GFP. Left panel: horizontal view on the optic lobe overview (scale bar: 20 μm). Central panel: close-up of medulla layer M10, lobula layer Lo1 and Lobula plate layers 1–4 (scale bar: 5 μm). Right panel: Frontal view on medulla layer M10 with T4 dendrites (scale bar: 20 μm); inset: close-up of columnar GluClα::GFP structure in layer 10 of the medulla. (**C**) Close-up of FlpTag-GluClα::GFP driven with a *T4-Gal4*-line; shown are layer 10 of the medulla where T4 dendrites reside and lobula plate layers 1–4 where T4 project their axon terminals to (scale bar: 5 μm). (**D**) Close-up of FlpTag-GluClα::GFP driven with a *T5-Gal4*-line; shown are layer 10 of the medulla where T4 dendrites reside and lobula plate layers 1–4 where T4 project their axon terminals to (scale bar: 5 μm).

FlpTag - a new tool for cell-type-specific, endogenous protein labeling

Additionally, we sought to observe the spatial distribution of endogenous receptors using a cell-type specific approach. We designed FlpTag, a new conditional, endogenous protein labeling strategy inspired by recently published flippase-dependent methods (***Fisher et al., 2017***; ***Nagarkar-Jaiswal et al., 2017***; ***Williams et al., 2019***).

The FlpTag cassette is a protein trap cassette consisting of a central GFP tag placed between a splice acceptor (SA) and splice donor (SD), flanked by specific Frt sites forming a FLEX-switch for stable inversion (***Figure 5A***, upper panel) (***Schnütgen et al., 2003***; ***Xue et al., 2014***). The FlpTag cassette is integrated into an intronic coding region of interest by recombinase mediate cassette exchange (RMCE) in vivo. We used the existing intronic MiMIC gene trap with attP landing sites to facilitate ΦC31-dependent exchange of the MiMIC insertion with our FlpTag cassette, consisting of ΦC31 integrase attB sites on either end (***Venken et al., 2011***; ***Nagarkar-Jaiswal et al., 2015b***). After ΦC31-dependent knock-in, two independent lines can be isolated. One in which the GFP is in the 5' to 3' direction; the same orientation as the gene. In this configuration FlpTag acts as a protein trap, revealing the protein's expression pattern. In the alternate orientation the FlpTag cassette is in the 3' to 5' direction; oppositely oriented to the gene. For the FlpTag approach, we used the oppositely oriented line in which the coding intron with the FlpTag cassette is naturally cut out during mRNA splicing and no labeling takes place. Only upon UAS-Gal4 driven, cell-type-specific expression of the Flp recombinase, the cassette is flipped in the same orientation as the gene. Due to the presence of flanking SA and SD, the GFP cassette is then spliced into the mature mRNA which is translated, labeling the protein with GFP (***Figure 5A***, lower panel).

FlpTag line for GluClα

In a first proof-of-principle experiment, we generated a FlpTag line for the glutamate receptor subunit GluClα. The FlpTag cassette was inserted in the MiMIC insertion site MI02890, in the coding intron between the last two exons of the GluClα gene. For comparison of the various GluClα-tagged lines, we examined the expression patterns generated by pan-neuronal FlpTag-GluClα::GFP, MiMIC GFSTS GluClα, and pan-neuronal *UAS-GluClα::GFP*. The expression patterns were similar for all three lines (***Figure 2—figure supplement 1***). We combined the GluClα-FlpTag line with *UAS-FLPD.1* and a T4/T5-specific driver-line. The distribution pattern of GluClα seen here is virtually identical to the *UAS-GluClα::GFP* genotype: GluClα is localized to T4 dendrites, the T5 dendrite area is devoid of GluClα signal, and T4/T5 axon terminals in the lobula plate co-localize with GluClα (***Figure 5B***, compare with ***Figure 2A***). Expression of flippase and FlpTag-GluClα in T4 neurons only further demonstrates the localization of the glutamate receptor to T4 dendrites and axon terminals, as seen before with the *UAS-GluClα::GFP* line (***Figure 5C***, compare with ***Figure 2B***). Specific expression of flippase and FlpTag-GluClα in T5 neurons revealed that the receptor localizes specifically to the axon terminals in all T5 subtypes, as visualized by the presence of GluClα puncta in all layers of the lobula plate (***Figure 5D***, compare with ***Figure 2C***).

Taken together, we generated a new *UAS*-line and developed a new tool for studying the localization of GluClα in a cell-type-specific manner. Both the *UAS-GluClα::GFP* line and the FlpTag-line led to similar results when compared to the pan-neuronal and T4/T5-specific experiments. These tools can be used interchangeably to study the subcellular localization of GluClα in any given cell of interest.

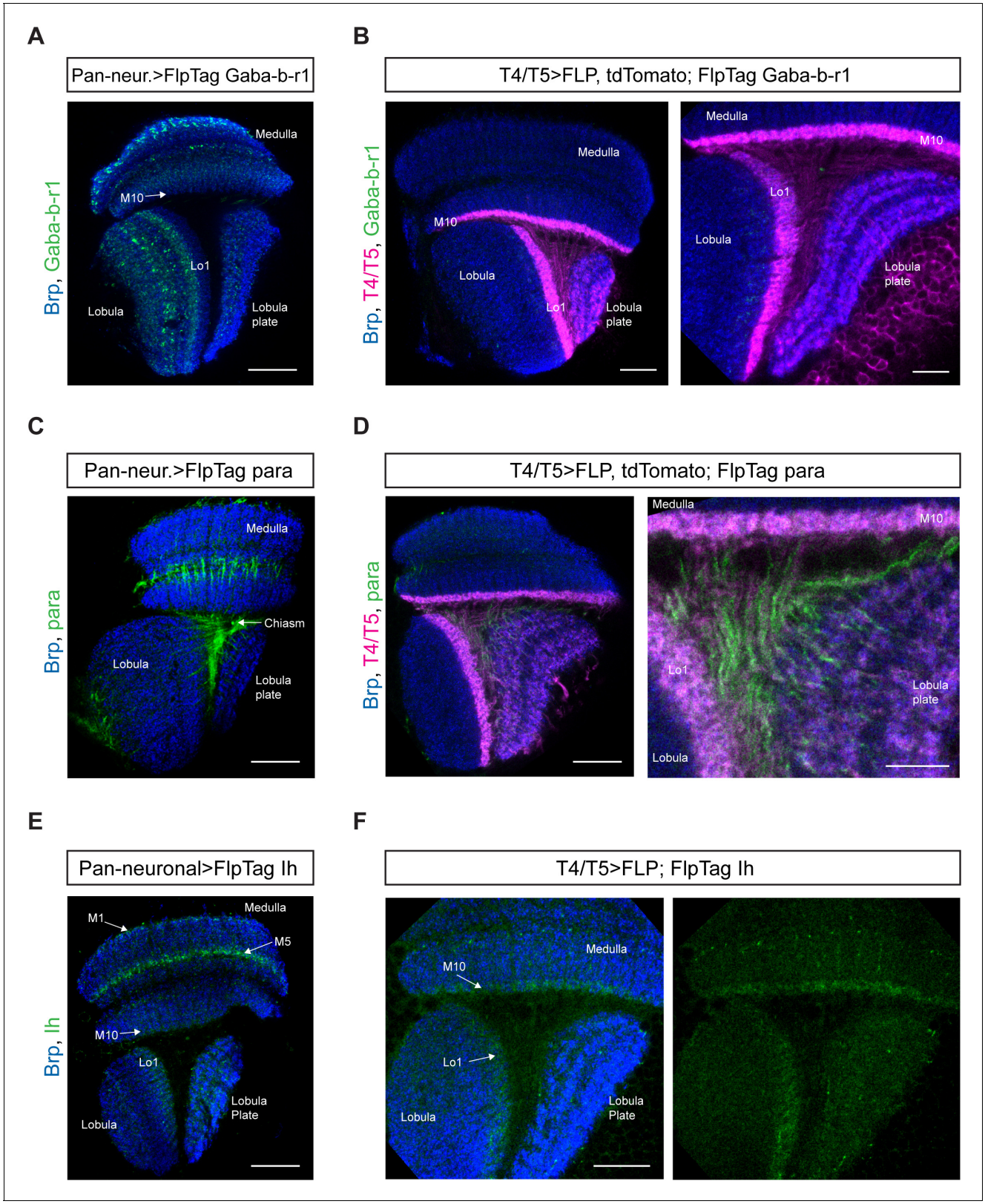

Figure 6. FlpTag lines for Gaba-b-r1, para and Ih. Optic lobes with pan-neuronal expression of FlpTag Gaba-b-r1 (**A**), FlpTag para (**C**), and FlpTag Ih (**E**). (**B**) Expression of FlpTag Gaba-b-r1 in T4/T5 neurons labeled with myr::tdTomato. Left panel: horizontal view on the optic lobe overview (scale bar: 20 μm). Right panel: close-up of medulla layer M10, lobula layer Lo1 and Lobula plate layers 1–4 (scale bar: 10 μm). (**D**) Expression of FlpTag para in T4/T5 neurons labeled with myr::tdTomato. Left panel: horizontal view on the optic lobe overview (scale bar: 20 μm). Right panel: close-up of medulla layer

Figure 6 continued on next page

Figure 6 continued

M10, lobula layer Lo1 and Lobula plate layers 1–4 (scale bar: 10 μm). (**F**) Expression of FlpTag Ih in T4/T5 neurons. Horizontal view on the optic lobe with medulla layer M10, lobula layer Lo1 and Lobula plate layers 1–4 (scale bar: 12 μm). Left panel: Background staining anti-brp in blue and. Right panel: Ih::GFP signal only.

FlpTag lines for Gaba-b-r1, para and Ih

The FlpTag approach is generalizable and can be applied to any of the >2800 fly lines available with MiMIC attP insertions in coding introns (***Nagarkar-Jaiswal et al., 2015b***). To demonstrate the universal applicability of our FlpTag strategy, we set out to generate more FlpTag lines with the aforementioned approach of integrating the FlpTag cassette into existing MiMIC landing sites in coding introns. In keeping with our interest in neurotransmitter receptors we explored another GABA receptor subunit, the metabotropic channel Gaba-b-r1. Additionally, we examined other proteins that shape the biophysical response properties of neurons, such as the voltage-gated ion channels para and Ih.

The metabotropic GABA receptor subunit Gaba-b-r1 is the most highly expressed GABA receptor subunit in T4/T5 neurons after Rdl (***Pankova and Borst, 2016***; ***Davis et al., 2020***). Gaba-b-r1 is one out of three G-protein-coupled GABA receptor subunits described in *Drosophila* and has been shown to be involved in sleep and appetitive long-term memory (***Mezler et al., 2001***; ***Kim et al., 2017***; ***Pavlowsky et al., 2018***). We inserted the FlpTag cassette in the MiMIC site between the first and second exon (MI01930) of the Gaba-b-r1 locus via RMCE. Again, two lines with two different orientations of the FlpTag cassette were obtained. The line with the cassette in the same orientation as the gene was used to observe the pan-neuronal distribution of the endogenous GABA receptor subunit. Gaba-b-r1 is expressed throughout all neuropils with strongest signal in the outer distal layers of the medulla and the medial part of the lobula (***Figure 6A***). Upon cell-type specific, FLP-dependent inversion of the FlpTag cassette in T4/T5 neurons, we could not observe any Gaba-b-r1::GFP signal in T4/T5 dendrites or axons (***Figure 6B***). Although RNAseq studies detected Gaba-b-r1 mRNA in T4/T5 neurons (***Pankova and Borst, 2016***; ***Davis et al., 2020***), we could not confirm this result at the protein level.

Paralytic (para) is the only voltage-gated sodium channel described in *Drosophila* and highly expressed in T4/T5 neurons (***Pankova and Borst, 2016***). It is required for the generation of sodium-dependent action potentials. We created the FlpTag para line by inserting the FlpTag cassette into the MiMIC landing site between the first and second exon (MI08578), thereby covering all of its 60 isoforms. Surprisingly, the pan-neuronal expression pattern is rather sparse with some bundles labeled in the medulla across the serpentine layer and axonal fibers in the chiasm between medulla, lobula and lobula plate (***Figure 6C***). In the T4/T5 specific FlpTag genotype, para is strongly expressed in the axonal fibers connecting dendrites and axon terminals in T4/T5 neurons (***Figure 6D***).

Ih is a voltage-gated, hyperpolarization-activated ion channel which is highly expressed in T4/T5 neurons (***Chen and Wang, 2012***; ***Hu et al., 2015***; ***Pankova and Borst, 2016***). To generate the corresponding FlpTag line, the FlpTag cassette was inserted in the MiMIC site MI12136 housed by the coding intron between the first and second exons of the Ih gene locus. In the pan-neuronal FlpTag line, Ih is expressed most strongly in two layers of the distal medulla (M1 and M5), as well as in the lobula plate and in Lo1 of the lobula (***Figure 6E***). In the T4/T5-specific FlpTag genotype, Ih is localized to the T4 and T5 dendrite area in medulla layer 10 and lobula plate layer 1 (***Figure 6F***).

Taken together, we generated four working FlpTag lines which uncovered the differential subcellular distribution of the neurotransmitter receptor subunits GluClα and Gaba-b-r1 and the voltage-gated ion channels para and Ih. We demonstrated that the FlpTag approach is generalizable and can be expanded to many genes with MiMIC insertion sites.

Discussion

Neurotransmitter receptors are essential neuronal elements that define the sign and temporal dynamics of synaptic connections. For our understanding of complex neural circuits, it is indispensable to examine which transmitter receptor types are used by the participating neurons and to which compartment they localize. Here, we developed FlpTag, a generalizable method for endogenous,

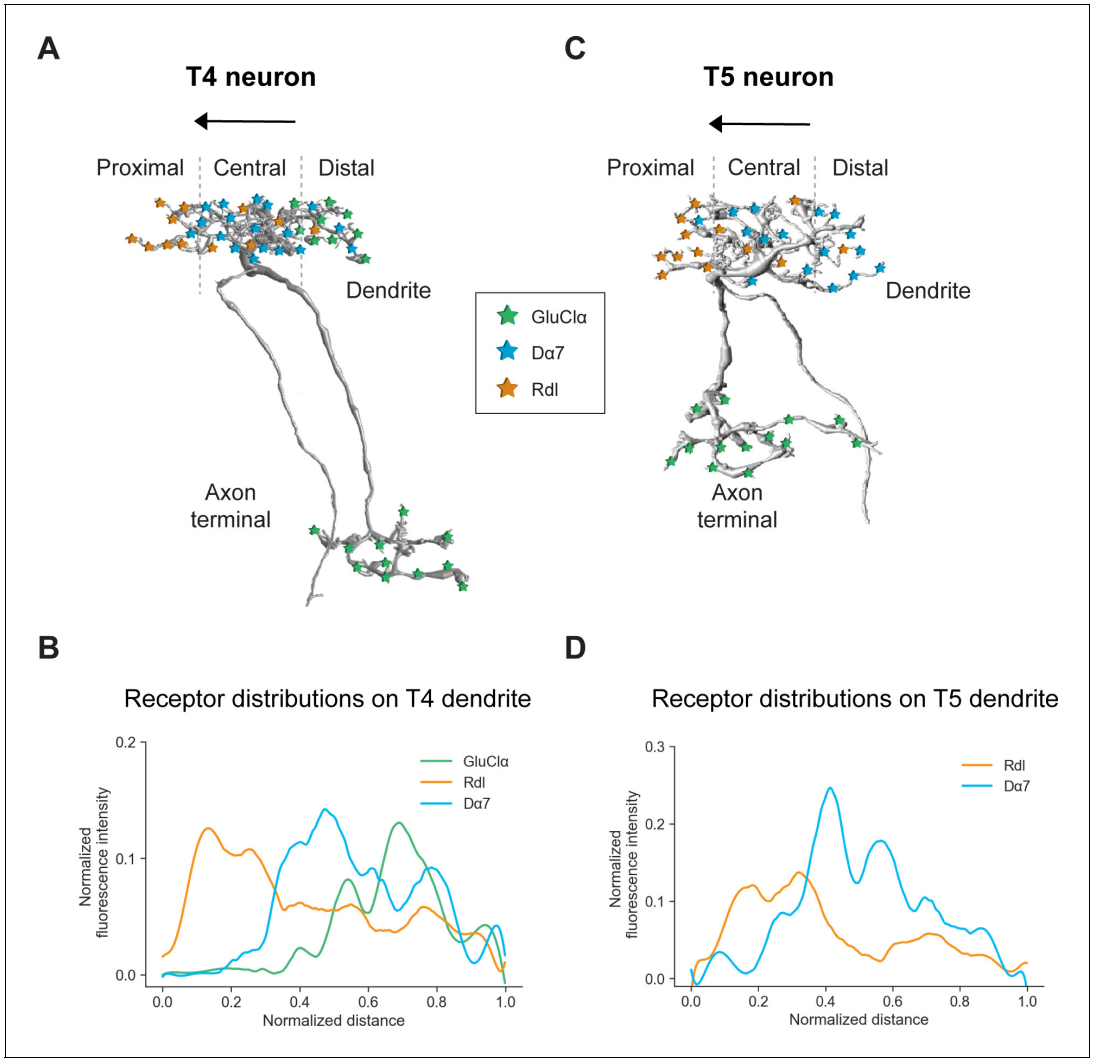

Figure 7. Summary of the receptor distributions of GluClα, Rdl and Dα7 in T4 and T5 neurons. (**A**) Scheme of EM-reconstructed T4 neuron with distribution of receptors on dendrite and axon terminal (image extracted from Seven medulla column connectome dataset, http://emdata.janelia.org/#/repo/medulla7column, #3b548, Janelia Research Campus). (**B**) Quantification of GluClα (green), Rdl (orange) and Dα7 (blue) distribution over the whole dendritic length (distance) averaged across several T4 from all subtypes (combined data from ***Figures 2E***, ***4D*** and ***5D***). All dendrites were aligned pointing to the right with the most proximal point at 0.0 and the most distal point at 1.0. (**C**) Scheme of EM-reconstructed T5 neuron with distribution of receptors on dendrite and axon terminal (image extracted from Seven medulla column connectome dataset, http://emdata.janelia.org/#/repo/medulla7column, #3b548, Janelia Research Campus). (**D**) Rdl (orange) and Dα7 (blue) distribution over the whole dendritic length (normalized distance) averaged across several T5 from all subtypes (combined data from ***Figures 2E***, ***4D*** and ***5D***). All dendrites were aligned pointing to the right with the most proximal point at 0.0 and the most distal point at 1.0.

cell-type-specific labeling of proteins. Alongside several GFP-tagged UAS-lines, we used our newly developed FlpTag lines to explore the distribution of receptor subunits GluClα, Rdl, Dα7, Gaba-b-r1 and voltage-gated ion channels para and Ih in motion-sensing T4/T5 neurons of the visual system of *Drosophila*. We found that these ion channels are localized to either the dendrite, the axonal fiber or the axon terminal (summarized in ***Figure 7A and C***). Even at the level of individual dendrites, GluClα, Rdl and Dα7 were differentially distributed precisely matching the locations where T4 and T5 neurons sample signals from their glutamatergic, cholinergic, or GABAergic input neurons, respectively (summarized in ***Figure 7***).

Protein tagging methods: endogenous tags and UAS-lines

Working with *Drosophila* as model organism bears some unrivaled advantages when it comes to genetic tools. The MiMIC and FlyFos libraries, for instance, are large-scale approaches of enormous

value for the fly community as they provide GFP-tagged protein lines for thousands of *Drosophila* genes including several neurotransmitter receptors and voltage-gated ion channels (**Venken et al., 2011**; **Nagarkar-Jaiswal et al., 2015a**; **Sarov et al., 2016**). Recently, Kondo et al. expanded these existing libraries with T2A-Gal4 insertions in 75 neurotransmitter receptor genes that can also be exchanged by the fluorescent protein tag Venus (**Kondo et al., 2020**). While all these approaches tag genes at their endogenous locus, none of them are conditional, for example they cannot be applied in a cell-type-specific manner. Hence, ascribing the expression of the pan-neuronally tagged proteins to cell-types of interest are challenging in dense neuronal tissue.

To overcome these difficulties, we used two conditional strategies for the investigation of membrane protein localizations in our cell types of interest, T4 and T5 neurons. First, we developed GFP-tagged *UAS*-lines for GluClα and Rdl and tested an existing *UAS-Dα7::GFP* line. As stated above, aberrant localization of overexpressed proteins can occur, however, this is not always the case. Overexpression of *UAS-GluClα::GFP* shows a similar receptor localization pattern as both MiMIC and FlpTag endogenous lines (**Figure 2—figure supplement 1**), thus, validating the use of *UAS-GluClα::GFP* for studying receptor distribution. Additionally, previous studies reported that the *UAS-Dα7::GFP* line showed proper localization of the acetylcholine receptor to endogenous synapses when compared to antibody stainings or endogenous bruchpilot (Brp) puncta (**Kuehn and Duch, 2013**; **Mosca and Luo, 2014**). Here, we confirmed this finding and further showed that Dα7::GFP presumably localizes only to cholinergic synapses. Overexpressing Dα7::GFP in a medulla neuron that is devoid of endogenous Dα7 demonstrated that Dα7::GFP localized to apparent cholinergic synapses. Hence, the *UAS-Dα7::GFP* line can be used to study the distribution of cholinergic synapses, but not the exact composition of cholinergic receptor subunits. A recent study showed that quantitatively the levels of the postsynaptic density protein PSD95 change when overexpressed, but qualitatively the localization is not altered (**Willems et al., 2020**). Altogether, this suggests that tagged overexpression lines can be used for studying protein localizations, but they have to be controlled carefully and drawn conclusions might be different for every line.

The FlpTag method is generalizable and can be expanded to many genes

Ideally, a tool for protein tagging should be both endogenous and conditional. This can be achieved by introducing an FRT-flanked STOP cassette upstream of the gene of interest which was engineered with an epitope tag or fluorescent protein. Only upon cell-type specific expression of Flp, the tagged protein will be expressed in a cell-type specific manner. This genetic strategy was utilized by two independent studies to label the presynaptic protein Brp, the histamine channel ort and the vesicular acetylcholine transporter VAChT (**Chen et al., 2014**; **Pankova and Borst, 2017**). Recently, a new approach based on the split-GFP system was utilized for endogenous, conditional labeling of proteins in two independent studies (**Kondo et al., 2020**; **Luo et al., 2020**). However, all these aforementioned approaches are not readily generalizable and easily applicable to any gene of interest.

Table 1.

	Gene	MiMIC insertion (coding intron)	MiMIC GFSTF existing	MiMIC GFSTF working	Chromosome	Phase	FlpTag working	Localization in T4/T5 neurons
1	GluClα	MI02890, MI14426	MI02890	Yes	III	2	Yes, MI02890	T4: dendrites + terminals; T5: terminals
2	Rdl	MI02620, MI02957	MI02620	No	III	0	No, MI02620	From UAS line: dendrites
3	Dα7	MI12545	This study (MI12545)	No	X	1	No	From UAS line: dendrites
4	Gaba-b-r1	MI01930, MI05755	MI01930	Yes	II	0	Yes, MI01930	No
5	para	MI08578	This study (MI08578)	Yes	X	0	Yes, MI08578	T4/T5 axonal fibers
6	Ih	MI03196, MI12136	This study (MI12136)	Yes	II	2	Yes, MI12136	T4/T5 dendrites

The FlpTag strategy presented here overcomes these caveats by allowing for endogenous, conditional tagging of proteins and by offering a generalizable toolbox for targeting many genes of interest. Similar to the conditional knock-out tools FlpStop and FlipFlop (**Fisher et al., 2017**; **Nagarkar-Jaiswal et al., 2017**), FlpTag utilizes a FLEx switch to conditionally control expression of a reporter gene, in our case GFP. Likewise, FlpTag also easily integrates using the readily available intronic MiMIC insertions. Here, we attempted to generate FlpTag lines for six genes, GluClα, Rdl, Dα7, Gaba-b-r1, para and Ih (overview of lines in **Table 1**). Four out of these six lines yielded conditional GFP-tagged protein lines (GluClα, Gaba-b-r1, para, Ih). We injected the FlpTag cassette in MI02620 for Rdl and MI12545 for Dα7, but could not observe any GFP expression across the brain (data not shown). The MiMiC insertion sites used for Rdl and Dα7 seem to be in a suboptimal location for tagging the protein.

Expansion of the FlpTag toolbox

As of now, there are MiMIC insertions in coding introns for more than 2800 genes available, which covers approximately 24% of neuronal genes (**Venken et al., 2011**; **Nagarkar-Jaiswal et al., 2015a**; **Fisher et al., 2017**). Additionally, the attP insertion sites generated in the study by Kondo et al. provide possible landing sites for the FlpTag cassette for 75 neurotransmitter receptor genes (**Kondo et al., 2020**). Transmembrane proteins such as neurotransmitter receptors form complex 3D structures making fluorescent tagging especially difficult. Neither the MiMIC insertion sites, nor the target sites of the Kondo study at the C-terminus of several transmitter receptor genes, ensure a working GFP-tagged protein line. For genes of interest lacking a suitable MiMIC insertion site we generated a homology directed repair (HDR) cassette which utilizes CRISPR/Cas9-mediated gene editing to integrate the FlpTag cassette in any desired gene locus (**Supplementary file 6–8**; **Gratz et al., 2014**; **Fisher et al., 2017**). The plasmid consists of the FlpTag cassette flanked by multiple cloning sites for the insertion of homology arms (HA). Through HDR the FlpTag cassette can be knocked-in into any desired locus. Taken together, the FlpTag cassette is a generalizable tool that can be integrated in any available attP-site in genes of interest (**Venken et al., 2011**; **Nagarkar-Jaiswal et al., 2015a**; **Kondo et al., 2020**) or inserted by CRISPR-HDR into genes lacking attP landing sites. This allows for the investigation of the endogenous spatial distributions of proteins, as well as the correct temporal dynamics of protein expression.

Further, the FlyFos project demonstrated that most fly lines with an extra copy of GFP-tagged protein-coding genes worked normally and GFP-tagged proteins could be imaged in living fly embryos and pupae (**Sarov et al., 2016**). In principle, live-imaging of the GFP-tagged lines we created could be performed during different developmental stages of the fruit fly. In general, the tools generated here can be used as specific postsynaptic markers, visualizing glutamatergic, GABAergic, and cholinergic synapses with standard confocal light microscopy. This extends the existing toolbox of *Drosophila* postsynaptic markers (**Sánchez-Soriano et al., 2005**; **Raghu et al., 2009**; **Andlauer et al., 2014**; **Chen et al., 2014**; **Petzoldt et al., 2014**; **Kondo et al., 2020**; **Luo et al., 2020**) for studying the localization and development of various types of synapses.

Functional relevance of transmitter receptors and voltage-gated channels for *Drosophila* motion-sensitive neurons

T4/T5 neurons combine spatiotemporal input from their presynaptic partners, leading to selective responses to one of the four cardinal directions. Numerous studies investigated the mechanisms underlying direction-selective responses in T4/T5 neurons, yet the computation is still not fully understood. At an algorithmic level, a three-arm detector model is sufficient to describe how direction-selective responses in T4/T5 neurons arise (**Arenz et al., 2017**; **Haag et al., 2017**). This model relies on the comparison of signals originating from three neighboring points in space via a delay-and-compare mechanism. The central arm provides fast excitation to the neuron. While one flanking arm amplifies the central signal for stimuli moving along the preferred direction, the other inhibits the central signal for stimuli moving along the null direction of the neuron. Exploring the neurotransmitter receptors and their distribution on T4/T5 dendrites allows us to define the sign as well as the temporal dynamics of some of the input synapses to T4/T5.

According to the algorithmic model, we expect an excitatory, amplifying input signal on the distal side of T4/T5 dendrites. Here, we found that T4 cells receive an inhibitory, glutamatergic input from

Mi9 via GluClα, which, at first sight, seems to contradict our expectation. However, since Mi9 has an OFF-center receptive field (**Arenz et al., 2017**; **Richter et al., 2018**; **Drews et al., 2020**), this glutamatergic synapse will invert the polarity from Mi9-OFF to T4-ON. Theoretically, in darkness, Mi9 inhibits T4 via glutamate and GluClα, and this inhibition is released upon an ON-edge moving into its receptive field. The concomitant closure of chloride channels and subsequent increased input resistance in T4 cells results in an amplification of a subsequent excitatory input signal from Mi1 and Tm3. As shown by a recent modeling study, this biophysical mechanism can indeed account for preferred direction enhancement in T4 cells (**Borst, 2018**). Some studies failed to detect preferred direction enhancement in T4/T5 neurons and they proposed that the enhanced signal in PD seen in GCaMP recordings could be a result from a non-linear calcium-to-voltage transformation (**Gruntman et al., 2018**; **Gruntman et al., 2019**; **Wienecke et al., 2018**). If this was really the case, the role of Mi9 and GluClα must be reconsidered and future functional experiments will shed light onto this topic.

Nevertheless, Strother et al. showed that the RNAi- knock-down of GluClα in T4/T5 neurons leads to enhanced turning responses on the ball set-up for faster speeds of repeating ON and OFF edges (**Strother et al., 2017**). Although this observation cannot answer the question about preferred direction enhancement in T4 cells, it indicates that both T4 and T5 receive inhibitory input and that removal of such create enhanced turning responses at the behavioral level. In line with these observations, we also found the glutamate receptor GluClα in T4/T5 axon terminals. A possible functional role of these inhibitory receptors in the axon terminals could be a cross-inhibition of T4/T5 cells with opposite preferred directions via lobula plate intrinsic neurons (LPis). Glutamatergic LPi neurons are known to receive a cholinergic, excitatory signal from T4/T5 neurons within one layer and to inhibit lobula plate tangential cells, the downstream postsynaptic partners of T4/T5 neurons, via GluClα in the adjacent oppositely tuned layer. This mechanism induces a motion opponent response in lobula plate tangential cells and increases their flow-field selectivity (**Mauss et al., 2015**). In addition, LPi neurons could also inhibit T4/T5 neurons presynaptically at their axon terminals via GluClα in order to further sharpen the flow-field selectivity of lobula plate tangential cells. Taken together, exploring the subcellular distribution of GluClα in T4/T5 neurons highlights its differential functional roles in different parts of these cell types.

Secondly, the Dα7 signal in the center of T4/T5 dendrites discovered here, corresponds to ionotropic, cholinergic input from Mi1 and Tm3 for T4, and Tm1, Tm2 and Tm4 for T5. These signals correspond to the central, fast, excitatory arm of the motion detector model. As T4 and T5 express a variety of different ACh receptor subunits (**Davis et al., 2020**), the exact subunit composition and underlying biophysics of every cholinergic synapse on T4/T5 dendrites still awaits further investigations.

Third, inhibition via GABA plays an essential role in creating direction-selective responses in both T4 and T5 neurons (**Fisher et al., 2015a**; **Arenz et al., 2017**; **Strother et al., 2017**; **Gruntman et al., 2018**) by providing null direction suppression. Computer simulations showed that direction selectivity decreases in T4/T5 motion detector models without this inhibitory input on the null side of the dendrite (**Arenz et al., 2017**; **Borst, 2018**; **Strother et al., 2017**). Here, we show that T4 and T5 neurons possess the inhibitory GABA receptor subunit Rdl mainly on the proximal base on the null side of their dendrites, providing the synaptic basis for null direction suppression. We did not detect the metabotropic GABA receptor subunit Gaba-b-r1 in T4/T5 neurons using the newly generated FlpTag Gaba-b-r1 line. Finally, all of the receptor subunits GluClα, Rdl and Dα7 investigated here are ionotropic, fast receptors, which presumably do not add a temporal delay at the synaptic level. In the detector model described above, the two outer arms provide a slow and sustained signal, and such properties are already intrinsic properties of these input neurons (**Arenz et al., 2017**; **Serbe et al., 2016**). However, we cannot exclude that slow, metabotropic receptor subunits for acetylcholine or GABA (e.g. Gaba-br2) which are also present in T4/T5 and could induce additional delays at the synaptic level (**Takemura et al., 2011**; **Davis et al., 2020**).

Furthermore, we investigated the subcellular distribution of the voltage-gated ion channels para and Ih in T4/T5 neurons. We found para, a voltage-gated sodium channel, to be distributed along the axonal fibers of both T4 and T5 neurons. As para is important for the generation of sodium-dependent action potentials, it will be interesting for future functional studies to investigate, if T4/T5 really fire action potentials and how this shapes their direction-selective response. Further, we detected Ih, a voltage-gated ion channel permeable for several types of ions, in T4/T5 dendrites

using the FlpTag strategy. Ih channels are activated at negative potentials below −50 mV and as they are permeable to sodium and potassium ions, they can cause a depolarization of the cell after hyperpolarization (**Magee, 1999**; **Littleton and Ganetzky, 2000**; **George et al., 2009**). Loss-of-function studies will unravel the functional role of the Ih channel for direction-selective responses in T4/T5 neurons.

Outlook

Since the ability to combine synaptic inputs from different neurotransmitters at different spatial sites is common to all neurons, the approaches described here represent an important future perspective for other circuits. Our tools can be used to study the ion channels GluClα, Rdl, Dα7, Gaba-b-r1, para and Ih in any given *Drosophila* cell-type and circuit. Furthermore, the FlpTag tool box can be used to target many genes of interest and thereby foster molecular questions across fields.

The techniques described here can be transferred to other model organisms as well, to study the distribution of different transmitter receptors. For instance, in the mouse retina - similar to motion-sensing T4/T5 neurons in the fruit fly - so-called On-Off direction-selective ganglion cells receive asymmetric inhibitory GABAergic inputs from presynaptic starburst amacrine cells during null-direction motion. A previous study investigated the spatial distribution of GABA receptors of these direction-selective ganglion cells using super-resolution imaging and antibody staining (**Sigal et al., 2015**). Additionally, starburst amacrine cells also release ACh onto ganglion cells which contributes to the direction-selective responses of ganglion cells. Thus, mapping the distribution of ACh receptors on direction-selective ganglion cells will be the next important step to further investigate cholinergic transmission in this network (**Sethuramanujam et al., 2020**).

Overall, we demonstrated the importance of exploring the distributions of neurotransmitter receptors and ion channels for systems neuroscience. The distinct distributions in T4/T5 neurons discovered here and the resulting functional consequences expand our knowledge of the molecular basis of motion vision. Although powerful, recent RNAseq studies lacked information about spatial distributions of transmitter receptors which can change the whole logic of wiring patterns and underlying synaptic signs. Future studies can use this knowledge to target these receptors and directly probe their role in functional experiments or incorporate the gained insights into model simulations. However, this study is only highlighting some examples of important neural circuit components: expanding the approaches described here to other transmitter receptors and ion channels, as well as gap junction proteins will reveal the full inventory and the spatial distributions of these decisive determinants of neural function within an individual neuron.

Materials and methods

Fly strains

Flies were raised at 25˚C and 60% humidity on standard cornmeal agar medium at 12 hr light/dark cycle. The following driver lines were used: *R42F06-Gal4* to label T4/T5 neurons, *R57C10-Gal4* for addressing all neurons, *SS03734-splitGal4* to address L1, *R19F01-AD; R71D01-DBD* to address Mi1, *10–50* Gal4 to label T1, and *Dα7-TG4* (BL#77828). The *T4-splitGal4* line was generated by combining the hemidriver lines *VT16255-AD* (BL#75205) and *VT12314-DBD* (unpublished, T. Schilling); the *T5-splitGal4* line was generated by combining the hemidriver lines *VT13975-AD* and *R42F06-DBD* (unpublished, T. Schilling). The following *UAS*-reporter lines were used for labeling cell-types and drive flippase-expression: *UAS-myr::tdTomato* (BL#32222), and *UAS-FLP1.D* (BL#4539). For labeling individual T4/T5 neurons stochastically together with the receptor lines, we combined *UAS-myr::tdTomato; UAS-GluClα::GFP/UAS-Rdl::GFP/UAS-Dα7::GFP* with *hs-FLP; FRT-Gal80-FRT; R42F06-Gal4* and heat-shocked pupae (P1-P3) for 5–8 min at 37˚C in a water bath.

Generation of new genetic *UAS*-lines

The coding sequencing (CDS) of *GluClα* isoform K was acquired from flybase.org and along with the sequence of *GFP* flanked by 4xGGS linker was synthesized by Eurofins Genomics and inserted into pEX-A258 backbone between NotI and XbaI restriction sites. Using restriction digestion with NotI and XbaI the *GluClα* fragment was cloned into *pJFRC7-20XUAS-IVS-mCD8::GFP* (**Pfeiffer et al., 2010**) vector. Similarly, the CDS of *Rdl* isoform F was acquired from flybase.org and with the

sequence of *GFP* flanked by 4xGGS linker was synthesized as three DNA fragments by Invitrogen GeneArt Gene Synthesis. Each fragment carried a complementary overlapping section of 25–35 bps on both ends. *pJFRC7-20XUAS-IVS-mCD8::GFP* (**Pfeiffer et al., 2010**) vector was digested with NotI and XbaI restriction enzymes and all three DNA fragments were inserted using NEBuilder HiFi DNA Assembly. Embryo injections were performed by BestGene Inc (Chino Hills, CA, USA).

For the generation of the FlpTag constructs, the pFlip-Flop-P0 plasmid (**Nagarkar-Jaiswal et al., 2017**) ordered from *Drosophila* Genomics Resource Center (NIH Grant 2P40OD010949) was digested with BsmFI and EcoRI leaving the plasmid backbone with FRT, FRT14 and attB sites. Six DNA fragments were synthesized by Invitrogen GeneArt Gene Synthesis. Three fragments contained a predicted splice donor site (one for each phase) and half of an inverted 4xGGS-GFP. The other three contained half of an inverted GFP-4xGGS followed by a slice acceptor (SA) site (one for each phase). All fragments had complementary overlapping sections of 25–35 bps which was used to insert phase-paired fragments into the digested pFlip-Flop plasmid using NEBuilder HiFi DNA Assembly. Embryo injections were performed by BestGene Inc (Chino Hills, CA, USA), including PCR-verifications and balancing.

S2 Schneider cell culture

We used *Drosophila* S2R+ Schneider cells in culture *Drosophila* Genomics Resource Center, stock #150 for testing the newly generated *UAS*-receptor::GFP constructs before embryo injections. S2R+ cells were cultured in Schneider's *Drosophila* medium (Thermo Fisher Scientific) supplemented with 10% fetal bovine serum (Thermo Fisher Scientific) and penicillin/streptomycin (Cytiva). *UAS*-constructs were tested by transfecting 250 ng of *UAS*-plasmid and 250 ng of *actin5C-Gal4* plasmid (gift from T. Kornberg) in 24-well plates using the FuGENE HD Kit (Promega). Two days later, we checked for GFP-expression in transfected S2 cells with a fluorescence binocular microscope.

Immunohistochemistry

Fly brains were dissected in cold 0.3% PBST and fixed in 4% PFA in 0.3% PBST for 25 min at room temperature. Subsequently, brains were washed four to five times in 0.3% PBST and blocked in 10% normal goat serum (NGS) in 0.3% PBST for 1 hr at room temperature. Primary antibodies used were mouse anti-Bruchpilot Brp (nc82, Developmental Studies Hybridoma Bank, 1:20, RRID:AB_2314867), rabbit anti-dsRed (Takara Bio, 1:300, RRID:AB_10013483), and rat anti-Dα7 (gift from H. Bellen, 1:2000). Secondary antibodies used were: goat anti-mouse ATTO 647N (Rockland, 1:300, RRID:AB_2614870), goat anti-rabbit Alexa Fluor 568 (Thermo Fisher Scientific, 1:300, RRID:AB_10563601), and goat anti-rat Alexa Fluor 647 (Thermo Fisher Scientific, 1:300, RRID:AB_141778). GFP-labeled receptors were imaged natively without antibody staining. 5% NGS was added to all antibody solutions and both primary and secondary antibodies were incubated for at least 48 hr at 4˚C. Brains were mounted in Vectashield Antifade Mounting Medium (Vector Laboratories) and imaged on a Leica TCS SP8 confocal microscope equipped with 488-, 561-, and 633 nm lasers, using a 63X glycerol objective.

Quantifications of receptor distributions and number of puncta

For intensity quantification, confocal stacks were processed in ImageJ using maximum intensity projection. These images were then analyzed in python using the Skimage and Numpy packages. For each image, florescence was normalized to the maximum intensity within an image. Additionally, images were cropped to include the entire dendritic cross section and aligned pointing to the right with the most proximal point to the left and the most distal point to the right. These images were normalized to the maximum cropped image length.

For quantification of number of receptor puncta, confocal stacks were taken from the entire cross-section of the dendrite as above. Puncta were counted in ImageJ software using the 3D object counter plugin of Fiji (**Bolte and Cordelières, 2006**).

Statistical analysis

Statistical significance was tested with a Student t-test when comparing two groups. A p-value below 0.05 was considered significant. In the case of pan-neuronal quantification where multiple groups were compared, statistical significance was tested using one-way ANOVA. In all figures, *

was used to indicate a p-value<0.05, ** for p<0.01, and *** for p<0.001. Statistical analysis and graphs were generated in Python 3.4 using SciPy and Seaborn packages respectively. Figures were generated in Adobe Illustrator CC.

Acknowledgements

We are grateful to T Schilling for unpublished driver lines, the Bloomington *Drosophila* Stock Center for fly lines and the *Drosophila* Genomics Resource Center (supported by NIH grant 2P40OD010949) for S2 cells; T Kornberg (UCSF) for the *actin-Gal4* plasmid for S2 cell culture and H Bellen for the Dα7-antibody. We thank W Essbauer for technical assistance with molecular work and R Kutlesa and I Ribeiro for help with the S2 cell culture; T Schilling and J Pujol-Marti for discussions and support throughout all stages of this project; I Ribeiro, A Mauss, L Groschner, G Ammer, J Malis, A Harbauer and A Barker for carefully reading the manuscript; M Drews and N Pirogova for helping with programming.

Additional information

Competing interests

Alexander Borst: Reviewing editor, *eLife*. The other authors declare that no competing interests exist.

Funding

Funder	Author
Max-Planck-Gesellschaft	Sandra Fendl Renee Marie Vieira Alexander Borst

The funders had no role in study design, data collection and interpretation, or the decision to submit the work for publication.

Author contributions

Sandra Fendl, Conceptualization, Formal analysis, Validation, Investigation, Visualization, Methodology, Writing - original draft, Project administration, Writing - review and editing, S.F. conceived and designed the study; imaged all data shown and processed confocal images; wrote the manuscript and prepared the figures with the help of R.M.V. and A.B; Renee Marie Vieira, Conceptualization, Software, Formal analysis, Visualization, Methodology, Writing - review and editing, R.M.V. conceived and designed the study; analyzed and quantified all imaged data; developed and created the UAS-lines and the FlpTag-construct and stocks with the help of S.F; Alexander Borst, Conceptualization, Resources, Supervision, Project administration, Writing - review and editing

Author ORCIDs

Sandra Fendl https://orcid.org/0000-0001-6442-2542
Renee Marie Vieira https://orcid.org/0000-0001-8520-7382

Decision letter and Author response

Decision letter https://doi.org/10.7554/eLife.62953.sa1
Author response https://doi.org/10.7554/eLife.62953.sa2

Additional files

Supplementary files

- Supplementary file 1. Plasmid map of the full sequence of pJFRC7-20xUAS-GluClα-GFP.
- Supplementary file 2. Plasmid map of the full sequence of pJFRC7-20xUAS-Rdl-GFP.
- Supplementary file 3. Plasmid map of the full sequence of pUC57-FlpTag-GFP-ph0.

- Supplementary file 4. Plasmid map of the full sequence of pUC57-FlpTag-GFP-ph1.
- Supplementary file 5. Plasmid map of the full sequence of pUC57-FlpTag-GFP-ph2.
- Supplementary file 6. Plasmid map of the full sequence of pHD-FlpTag-DsRed-HDR-ph0.
- Supplementary file 7. Plasmid map of the full sequence of pHD-FlpTag-DsRed-HDR–ph1.
- Supplementary file 8. Plasmid map of the full sequence of pHD-FlpTag-DsRed-HDR-ph2.
- Transparent reporting form

Data availability

All data generated or analysed during this study are included in the manuscript and supporting files. Source data files have been provided for Figures 2, 3 and 4. Previously Published Datasets: Seven medulla column connectome: Kazunori Shinomiya, 2019, http://emdata.janelia.org/#/repo/medulla7-column, #3b548.

The following previously published dataset was used:

Author(s)	Year	Dataset title	Dataset URL	Database and Identifier
Shinomiya K	2019	Seven medulla column connectome	http://emdata.janelia.org/#/repo/medulla7column	3b548, http://emdata.janelia.org/#/repo/medulla7column

References

Ammer G, Leonhardt A, Bahl A, Dickson BJ, Borst A. 2015. Functional specialization of neural input elements to the *Drosophila* ON Motion Detector. *Current Biology* **25**:2247–2253. DOI: https://doi.org/10.1016/j.cub.2015.07.014, PMID: 26234212

Andlauer TFM, Scholz-Kornehl S, Tian R, Kirchner M, Babikir HA, Depner H, Loll B, Quentin C, Gupta VK, Holt MG, Dipt S, Cressy M, Wahl MC, Fiala A, Selbach M, Schwärzel M, Sigrist SJ. 2014. Drep-2 is a novel synaptic protein important for learning and memory. *eLife* **3**:e03895. DOI: https://doi.org/10.7554/eLife.03895

Arenz A, Drews MS, Richter FG, Ammer G, Borst A. 2017. The temporal tuning of the *Drosophila* Motion Detectors Is Determined by the Dynamics of Their Input Elements. *Current Biology* **27**:929–944. DOI: https://doi.org/10.1016/j.cub.2017.01.051, PMID: 28343964

Behnia R, Clark DA, Carter AG, Clandinin TR, Desplan C. 2014. Processing properties of ON and OFF pathways for *Drosophila* motion detection. *Nature* **512**:427–430. DOI: https://doi.org/10.1038/nature13427, PMID: 25043016

Bielopolski N, Amin H, Apostolopoulou AA, Rozenfeld E, Lerner H, Huetteroth W, Lin AC, Parnas M. 2019. Inhibitory muscarinic acetylcholine receptors enhance aversive olfactory learning in adult *Drosophila*. *eLife* **8**:e48264. DOI: https://doi.org/10.7554/eLife.48264, PMID: 31215865

Bolte S, Cordelières FP. 2006. A guided tour into subcellular colocalization analysis in light microscopy. *Journal of Microscopy* **224**:213–232. DOI: https://doi.org/10.1111/j.1365-2818.2006.01706.x, PMID: 17210054

Borst A. 2018. A biophysical mechanism for preferred direction enhancement in fly motion vision. *PLOS Computational Biology* **14**:e1006240. DOI: https://doi.org/10.1371/journal.pcbi.1006240, PMID: 29897917

Borst A, Helmstaedter M. 2015. Common circuit design in fly and mammalian motion vision. *Nature Neuroscience* **18**:1067–1076. DOI: https://doi.org/10.1038/nn.4050, PMID: 26120965

Chen Y, Akin O, Nern A, Tsui CY, Pecot MY, Zipursky SL. 2014. Cell-type-specific labeling of synapses in vivo through synaptic tagging with recombination. *Neuron* **81**:280–293. DOI: https://doi.org/10.1016/j.neuron.2013.12.021, PMID: 24462095

Chen Z, Wang Z. 2012. SCIENCE CHINA functional study of hyperpolarization activated channel (Ih) in *Drosophila* behavior. *Science China. Life Sciences* **55**:2–7. DOI: https://doi.org/10.1007/s11427-012-4270-6, PMID: 22314484

Colangelo C, Shichkova P, Keller D, Markram H, Ramaswamy S. 2019. Cellular, synaptic and network effects of acetylcholine in the neocortex. *Frontiers in Neural Circuits* **13**:24. DOI: https://doi.org/10.3389/fncir.2019.00024, PMID: 31031601

Cully DF, Paress PS, Liu KK, Schaeffer JM, Arena JP. 1996. Identification of a *Drosophila melanogaster* glutamate-gated chloride channel sensitive to the antiparasitic agent avermectin. *Journal of Biological Chemistry* **271**:20187–20191. DOI: https://doi.org/10.1074/jbc.271.33.20187, PMID: 8702744

Davis FP, Nern A, Picard S, Reiser MB, Rubin GM, Eddy SR, Henry GL. 2020. A genetic, genomic, and computational resource for exploring neural circuit function. *eLife* **9**:e50901. DOI: https://doi.org/10.7554/eLife.50901, PMID: 31939737

Diao F, Ironfield H, Luan H, Diao F, Shropshire WC, Ewer J, Marr E, Potter CJ, Landgraf M, White BH. 2015. Plug-and-play genetic access to *Drosophila* cell types using exchangeable exon cassettes. *Cell Reports* **10**:1410–1421. DOI: https://doi.org/10.1016/j.celrep.2015.01.059, PMID: 25732830

Dobosiewicz M, Liu Q, Bargmann CI. 2019. Reliability of an interneuron response depends on an integrated sensory state. *eLife* **8**:e50566. DOI: https://doi.org/10.7554/eLife.50566, PMID: 31718773

Drews MS, Leonhardt A, Pirogova N, Richter FG, Schuetzenberger A, Braun L, Serbe E, Borst A. 2020. Dynamic signal compression for robust motion vision in flies. *Current Biology* **30**:209–221. DOI: https://doi.org/10.1016/j.cub.2019.10.035, PMID: 31928873

Fayyazuddin A, Zaheer MA, Hiesinger PR, Bellen HJ. 2006. The nicotinic acetylcholine receptor Dalpha7 is required for an escape behavior in *Drosophila*. *PLOS Biology* **4**:e63. DOI: https://doi.org/10.1371/journal.pbio.0040063, PMID: 16494528

Ffrench-Constant RH, Rocheleau TA, Steichen JC, Chalmers AE. 1993. A point mutation in a *Drosophila* GABA receptor confers insecticide resistance. *Nature* **363**:449–451. DOI: https://doi.org/10.1038/363449a0, PMID: 8389005

Fisher YE, Leong JC, Sporar K, Ketkar MD, Gohl DM, Clandinin TR, Silies M. 2015a. A class of visual neurons with Wide-Field properties is required for local motion detection. *Current Biology* **25**:3178–3189. DOI: https://doi.org/10.1016/j.cub.2015.11.018, PMID: 26670999

Fisher YE, Silies M, Clandinin TR. 2015b. Orientation selectivity sharpens motion detection in *Drosophila*. *Neuron* **88**:390–402. DOI: https://doi.org/10.1016/j.neuron.2015.09.033, PMID: 26456048

Fisher YE, Yang HH, Isaacman-Beck J, Xie M, Gohl DM, Clandinin TR. 2017. FlpStop, a tool for conditional gene control in *Drosophila*. *eLife* **6**:e22279. DOI: https://doi.org/10.7554/eLife.22279, PMID: 28211790

Fritschy JM. 2008. Is my antibody-staining specific? how to deal with pitfalls of immunohistochemistry. *European Journal of Neuroscience* **28**:2365–2370. DOI: https://doi.org/10.1111/j.1460-9568.2008.06552.x, PMID: 19087167

George MS, Abbott LF, Siegelbaum SA. 2009. HCN hyperpolarization-activated cation channels inhibit EPSPs by interactions with M-type K+ channels. *Nature Neuroscience* **12**:577–584. DOI: https://doi.org/10.1038/nn.2307

Gordon MD, Scott K. 2009. Motor control in a *Drosophila* taste circuit. *Neuron* **61**:373–384. DOI: https://doi.org/10.1016/j.neuron.2008.12.033, PMID: 19217375

Gratz SJ, Ukken FP, Rubinstein CD, Thiede G, Donohue LK, Cummings AM, O'Connor-Giles KM. 2014. Highly specific and efficient CRISPR/Cas9-catalyzed homology-directed repair in *Drosophila*. *Genetics* **196**:961–971. DOI: https://doi.org/10.1534/genetics.113.160713, PMID: 24478335

Gruntman E, Romani S, Reiser MB. 2018. Simple integration of fast excitation and offset, delayed inhibition computes directional selectivity in *Drosophila*. *Nature Neuroscience* **21**:250–257. DOI: https://doi.org/10.1038/s41593-017-0046-4, PMID: 29311742

Gruntman E, Romani S, Reiser MB. 2019. The computation of directional selectivity in the *Drosophila* OFF motion pathway. *eLife* **8**:e50706. DOI: https://doi.org/10.7554/eLife.50706, PMID: 31825313

Haag J, Arenz A, Serbe E, Gabbiani F, Borst A. 2016. Complementary mechanisms create direction selectivity in the fly. *eLife* **5**:e17421. DOI: https://doi.org/10.7554/eLife.17421, PMID: 27502554

Haag J, Mishra A, Borst A. 2017. A common directional tuning mechanism of *Drosophila* motion-sensing neurons in the ON and in the OFF pathway. *eLife* **6**:e29044. DOI: https://doi.org/10.7554/eLife.29044, PMID: 28829040

Hörmann N, Schilling T, Ali AH, Serbe E, Mayer C, Borst A, Pujol-Martí J. 2020. A combinatorial code of transcription factors specifies subtypes of visual motion-sensing neurons in *Drosophila*. *Development* **147**:dev186296. DOI: https://doi.org/10.1242/dev.186296, PMID: 32238425

Hu W, Wang T, Wang X, Han J. 2015. Ih channels control feedback regulation from amacrine cells to photoreceptors. *PLOS Biology* **13**:e1002115. DOI: https://doi.org/10.1371/journal.pbio.1002115, PMID: 25831426

Joesch M, Schnell B, Raghu SV, Reiff DF, Borst A. 2010. ON and OFF pathways in *Drosophila* motion vision. *Nature* **468**:300–304. DOI: https://doi.org/10.1038/nature09545, PMID: 21068841

Kawasaki F, Zou B, Xu X, Ordway RW. 2004. Active zone localization of presynaptic calcium channels encoded by the cacophony locus of *Drosophila*. *Journal of Neuroscience* **24**:282–285. DOI: https://doi.org/10.1523/JNEUROSCI.3553-03.2004, PMID: 14715960

Kim M, Jang D, Yoo E, Oh Y, Sonn JY, Lee J, Ki Y, Son HJ, Hwang O, Lee C, Lim C, Choe J. 2017. Rogdi defines GABAergic control of a Wake-promoting dopaminergic pathway to sustain sleep in *Drosophila*. *Scientific Reports* **7**:1–14. DOI: https://doi.org/10.1038/s41598-017-11941-3

Kondo S, Takahashi T, Yamagata N, Imanishi Y, Katow H, Hiramatsu S, Lynn K, Abe A, Kumaraswamy A, Tanimoto H. 2020. Neurochemical organization of the *Drosophila* brain visualized by endogenously tagged neurotransmitter receptors. *Cell Reports* **30**:284–297. DOI: https://doi.org/10.1016/j.celrep.2019.12.018

Konstantinides N, Kapuralin K, Fadil C, Barboza L, Satija R, Desplan C. 2018. Phenotypic convergence: distinct transcription factors regulate common terminal features. *Cell* **174**:622–635. DOI: https://doi.org/10.1016/j.cell.2018.05.021, PMID: 29909983

Kuehn C, Duch C. 2013. Putative excitatory and putative inhibitory inputs are localised in different dendritic domains in a *Drosophila* flight motoneuron. *European Journal of Neuroscience* **37**:860–875. DOI: https://doi.org/10.1111/ejn.12104, PMID: 23279094

Lansdell SJ, Collins T, Goodchild J, Millar NS. 2012. The *Drosophila* nicotinic acetylcholine receptor subunits dα5 and dα7 form functional homomeric and heteromeric ion channels. *BMC Neuroscience* **13**:73. DOI: https://doi.org/10.1186/1471-2202-13-73, PMID: 22727315

Lansdell SJ, Millar NS. 2004. Molecular characterization of Dalpha6 and Dalpha7 nicotinic acetylcholine receptor subunits from *Drosophila*: formation of a high-affinity alpha-bungarotoxin binding site revealed by expression of subunit chimeras. *Journal of Neurochemistry* **90**:479–489. DOI: https://doi.org/10.1111/j.1471-4159.2004.02499.x, PMID: 15228604

Littleton JT, Ganetzky B. 2000. Ion channels and synaptic organization: analysis of the *Drosophila* genome. *Neuron* **26**:35–43. DOI: https://doi.org/10.1016/s0896-6273(00)81135-6, PMID: 10798390

Liu X, Krause WC, Davis RL. 2007. GABAA receptor RDL *inhibits Drosophila* olfactory associative learning. *Neuron* **56**:1090–1102. DOI: https://doi.org/10.1016/j.neuron.2007.10.036, PMID: 18093529

Liu WW, Wilson RI. 2013. Glutamate is an inhibitory neurotransmitter in the *Drosophila* olfactory system. *PNAS* **110**:10294–10299. DOI: https://doi.org/10.1073/pnas.1220560110, PMID: 23729809

Luo J, Ting CY, Li Y, McQueen P, Lin TY, Hsu CP, Lee CH. 2020. Antagonistic regulation by insulin-like peptide and activin ensures the elaboration of appropriate dendritic field sizes of amacrine neurons. *eLife* **9**:e50568. DOI: https://doi.org/10.7554/eLife.50568, PMID: 32175842

Magee JC. 1999. Dendritic Ih normalizes temporal summation in hippocampal CA1 neurons. *Nature Neuroscience* **2**:508–514. DOI: https://doi.org/10.1038/9158, PMID: 10448214

Maisak MS, Haag J, Ammer G, Serbe E, Meier M, Leonhardt A, Schilling T, Bahl A, Rubin GM, Nern A, Dickson BJ, Reiff DF, Hopp E, Borst A. 2013. A directional tuning map of *Drosophila*. *Nature* **500**:212–216. DOI: https://doi.org/10.1038/nature12320

Mauss AS, Meier M, Serbe E, Borst A. 2014. Optogenetic and pharmacologic dissection of feedforward inhibition in *Drosophila* motion vision. *Journal of Neuroscience* **34**:2254–2263. DOI: https://doi.org/10.1523/JNEUROSCI.3938-13.2014, PMID: 24501364

Mauss AS, Pankova K, Arenz A, Nern A, Rubin GM, Borst A. 2015. Neural circuit to integrate opposing motions in the visual field. *Cell* **162**:351–362. DOI: https://doi.org/10.1016/j.cell.2015.06.035, PMID: 26186189

Megías M, Emri Z, Freund TF, Gulyás AI. 2001. Total number and distribution of inhibitory and excitatory synapses on hippocampal CA1 pyramidal cells. *Neuroscience* **102**:527–540 . DOI: https://doi.org/10.1016/S0306-4522(00)00496-6

Mezler M, Müller T, Raming K. 2001. Cloning and functional expression of GABA(B) receptors from *Drosophila*. *The European Journal of Neuroscience* **13**:477–486. DOI: https://doi.org/10.1046/j.1460-9568.2001.01410.x, PMID: 11168554

Mosca TJ, Luo L. 2014. Synaptic organization of the *Drosophila* antennal lobe and its regulation by the teneurins. *eLife* **3**:e03726. DOI: https://doi.org/10.7554/eLife.03726, PMID: 25310239

Nagarkar-Jaiswal S, DeLuca SZ, Lee P-T, Lin W-W, Pan H, Zuo Z, Lv J, Spradling AC, Bellen HJ. 2015a. A genetic toolkit for tagging intronic MiMIC containing genes. *eLife* **4**:e08469. DOI: https://doi.org/10.7554/eLife.08469

Nagarkar-Jaiswal S, Lee P-T, Campbell ME, Chen K, Anguiano-Zarate S, Cantu Gutierrez M, Busby T, Lin W-W, He Y, Schulze KL, Booth BW, Evans-Holm M, Venken KJT, Levis RW, Spradling AC, Hoskins RA, Bellen HJ. 2015b. A library of MiMICs allows tagging of genes and reversible, spatial and temporal knockdown of proteins in *Drosophila*. *eLife* **4**:e05338. DOI: https://doi.org/10.7554/eLife.05338

Nagarkar-Jaiswal S, Manivannan SN, Zuo Z, Bellen HJ. 2017. A cell cycle-independent, conditional gene inactivation strategy for differentially tagging wild-type and mutant cells. *eLife* **6**:e26420. DOI: https://doi.org/10.7554/eLife.26420, PMID: 28561736

Pankova K, Borst A. 2016. RNA-Seq transcriptome analysis of Direction-Selective T4/T5 neurons in *Drosophila*. *PLOS ONE* **11**:e0163986. DOI: https://doi.org/10.1371/journal.pone.0163986, PMID: 27684367

Pankova K, Borst A. 2017. Transgenic line for the identification of cholinergic release sites in *Drosophila melanogaster*. *The Journal of Experimental Biology* **220**:1405–1410. DOI: https://doi.org/10.1242/jeb.149369, PMID: 28167805

Pavlowsky A, Schor J, Plaçais PY, Preat T. 2018. A GABAergic feedback shapes dopaminergic input on the *Drosophila* Mushroom Body to Promote Appetitive Long-Term Memory. *Current Biology* **28**:1783–1793. DOI: https://doi.org/10.1016/j.cub.2018.04.040, PMID: 29779874

Petzoldt AG, Lee YH, Khorramshahi O, Reynolds E, Plested AJ, Herzel H, Sigrist SJ. 2014. Gating characteristics control glutamate receptor distribution and trafficking in vivo. *Current Biology* **24**:2059–2065. DOI: https://doi.org/10.1016/j.cub.2014.07.051, PMID: 25131677

Pfeiffer BD, Ngo TT, Hibbard KL, Murphy C, Jenett A, Truman JW, Rubin GM. 2010. Refinement of tools for targeted gene expression in *Drosophila*. *Genetics* **186**:735–755. DOI: https://doi.org/10.1534/genetics.110.119917, PMID: 20697123

Raghu SV, Joesch M, Borst A, Reiff DF. 2007. Synaptic organization of lobula plate tangential cells in *Drosophila*: gamma-aminobutyric acid receptors and chemical release sites. *The Journal of Comparative Neurology* **502**:598–610. DOI: https://doi.org/10.1002/cne.21319, PMID: 17394161

Raghu SV, Joesch M, Sigrist SJ, Borst A, Reiff DF. 2009. Synaptic organization of lobula plate tangential cells in *Drosophila:* dalpha7 cholinergic receptors. *Journal of Neurogenetics* **23**:200–209. DOI: https://doi.org/10.1080/01677060802471684, PMID: 19306209

Richter FG, Fendl S, Haag J, Drews MS, Borst A. 2018. Glutamate signaling in the fly visual system. *iScience* **7**:85–95. DOI: https://doi.org/10.1016/j.isci.2018.08.019, PMID: 30267688

Sánchez-Soriano N, Bottenberg W, Fiala A, Haessler U, Kerassoviti A, Knust E, Löhr R, Prokop A. 2005. Are dendrites in *Drosophila* homologous to vertebrate dendrites? *Developmental Biology* **288**:126–138. DOI: https://doi.org/10.1016/j.ydbio.2005.09.026, PMID: 16223476

Sarov M, Barz C, Jambor H, Hein MY, Schmied C, Suchold D, Stender B, Janosch S, K J VV, Krishnan RT, Krishnamoorthy A, Ferreira IR, Ejsmont RK, Finkl K, Hasse S, Kämpfer P, Plewka N, Vinis E, Schloissnig S, Knust E, et al. 2016. A genome-wide resource for the analysis of protein localisation in *Drosophila*. *eLife* **5**:e12068. DOI: https://doi.org/10.7554/eLife.12068, PMID: 26896675

Schnütgen F, Doerflinger N, Calléja C, Wendling O, Chambon P, Ghyselinck NB. 2003. A directional strategy for monitoring Cre-mediated recombination at the cellular level in the mouse. *Nature Biotechnology* **21**:562–565. DOI: https://doi.org/10.1038/nbt811, PMID: 12665802

Serbe E, Meier M, Leonhardt A, Borst A. 2016. Comprehensive characterization of the major presynaptic elements to the *Drosophila* OFF Motion Detector. *Neuron* **89**:829–841. DOI: https://doi.org/10.1016/j.neuron.2016.01.006, PMID: 26853306

Sethuramanujam S, Matsumoto A, McIntosh JM, Jing M, Li Y, Berson D, Yonehara K, Awatramani GB. 2020. Rapid 'multi-directed' cholinergic transmission at central synapses. *bioRxiv*. DOI: https://doi.org/10.1101/2020.04.18.048330

Shinomiya K, Huang G, Lu Z, Parag T, Xu CS, Aniceto R, Ansari N, Cheatham N, Lauchie S, Neace E, Ogundeyi O, Ordish C, Peel D, Shinomiya A, Smith C, Takemura S, Talebi I, Rivlin PK, Nern A, Scheffer LK, et al. 2019. Comparisons between the ON- and OFF-edge motion pathways in the *Drosophila* brain. *eLife* **8**:e40025. DOI: https://doi.org/10.7554/eLife.40025, PMID: 30624205

Sigal YM, Speer CM, Babcock HP, Zhuang X. 2015. Mapping synaptic input fields of neurons with Super-Resolution imaging. *Cell* **163**:493–505. DOI: https://doi.org/10.1016/j.cell.2015.08.033, PMID: 26435106

Strother JA, Wu S-T, Wong AM, Nern A, Rogers EM, Le JQ, Rubin GM, Reiser MB. 2017. The emergence of directional selectivity in the visual motion pathway of *Drosophila*. *Neuron* **94**:168–182. DOI: https://doi.org/10.1016/j.neuron.2017.03.010

Strother JA, Wu ST, Rogers EM, Eliason JLM, Wong AM, Nern A, Reiser MB. 2018. Behavioral state modulates the ON visual motion pathway of *Drosophila*. *PNAS* **115**:E102–E111. DOI: https://doi.org/10.1073/pnas.1703090115, PMID: 29255026

Takemura SY, Karuppudurai T, Ting CY, Lu Z, Lee CH, Meinertzhagen IA. 2011. Cholinergic circuits integrate neighboring visual signals in a *Drosophila* motion detection pathway. *Current Biology : CB* **21**:2077–2084. DOI: https://doi.org/10.1016/j.cub.2011.10.053, PMID: 22137471

Takemura SY, Nern A, Chklovskii DB, Scheffer LK, Rubin GM, Meinertzhagen IA. 2017. The comprehensive connectome of a neural substrate for 'ON' motion detection in *Drosophila*. *eLife* **6**:e24394. DOI: https://doi.org/10.7554/eLife.24394, PMID: 28432786

Venken KJT, Schulze KL, Haelterman NA, Pan H, He Y, Evans-Holm M, Carlson JW, Levis RW, Spradling AC, Hoskins RA, Bellen HJ. 2011. MiMIC: a highly versatile transposon insertion resource for engineering *Drosophila melanogaster* genes. *Nature Methods* **8**:737–743 . DOI: https://doi.org/10.1038/nmeth.1662

Vogel C, Marcotte EM. 2012. Insights into the regulation of protein abundance from proteomic and transcriptomic analyses. *Nature Reviews Genetics* **13**:227–232 . DOI: https://doi.org/10.1038/nrg3185

Wienecke CFR, Leong JCS, Clandinin TR. 2018. Linear summation underlies direction selectivity in *Drosophila*. *Neuron* **99**:680–688. DOI: https://doi.org/10.1016/j.neuron.2018.07.005, PMID: 30057202

Willems J, de Jong APH, Scheefhals N, Mertens E, Catsburg LAE, Poorthuis RB, de Winter F, Verhaagen J, Meye FJ, MacGillavry HD. 2020. ORANGE: a CRISPR/Cas9-based genome editing toolbox for epitope tagging of endogenous proteins in neurons. *PLOS Biology* **18**:e3000665. DOI: https://doi.org/10.1371/journal.pbio.3000665, PMID: 32275651

Williams JL, Shearin HK, Stowers RS. 2019. Conditional synaptic vesicle markers for *Drosophila* . *G3: Genes, Genomes, Genetics* **9**:737–748. DOI: https://doi.org/10.1534/g3.118.200975

Xue M, Atallah BV, Scanziani M. 2014. Equalizing excitation-inhibition ratios across visual cortical neurons. *Nature* **511**:596–600. DOI: https://doi.org/10.1038/nature13321, PMID: 25043046

3. DISCUSSION

Neurotransmitters and their corresponding receptors are the substrate of neural communication. As neurons are discrete individual units, they need to form synaptic contacts to allow for information flow in neural circuits. Today, the neuroscientific community has unraveled the wiring diagram of many circuits in the fly brain. However, it is still largely unknown which neurotransmitters certain neural types use or which receptors are localized on the postsynaptic partner neuron. I set out to develop tools to discover neurotransmitter receptors on motion-sensitive T4/T5 neurons. First, we described the glutamatergic phenotype and response properties of three cell types in the motion vision circuit of *Drosophila*. We used the genetically encoded glutamate sensor iGluSnFR to monitor glutamate release and found that these responses are significantly faster than Ca^{2+}-signals, the proxy of neural activity usually recorded with genetically encoded Ca^{2+} sensors (GCaMP). Next, realizing that methods for studying subcellular receptor distributions are limited, we designed and generated new conditional tools for this purpose. UAS-driven GFP-tagged receptor lines and a new genetic strategy called FlpTag allowed us to investigate the distribution of several transmitter receptor subunits in T4/T5 neurons. We found an asymmetric distribution of glutamate, GABA and ACh receptor subunits on individual T4/T5 dendrites, as well as some voltage-gated ion channels that localized to the dendrite or the axonal fibers only.

3.1 Methods for investigating neurotransmitters and their receptors

The genetic toolkit of *Drosophila* is constantly expanding, allowing researchers to answer questions that have been unimaginable in the past. On the technical side, light microscopy-based techniques are pushed more and more beyond earlier proposed resolution limits. Taken together, genetic and technical developments have allowed researchers to unravel protein localizations at the tissue and subcellular level across many different species. However, there are still drawbacks and limitations of the existing methods that need to be overcome in order to see the big picture.

3.1.1 Defining the transmitter phenotype

Defining the neurotransmitter used by a cell type of interest can be done by a multitude of tools that exist for this question. Antibodies, gene specific Gal4-lines

or RNAseq data usually allow for a clear assignment of transmitter type. For instance, antibodies against vesicular transporters or synthesizing enzymes of neurotransmitters label the somata or terminals of cell types of interest and can be detected under the confocal microscope. The neurotransmitter types used by the input cells to T4 neurons were determined by antibody-labeling of their somata against the enzymes VGlut, GAD1 and ChAT (Takemura et al., 2017). These transmitter phenotypes were confirmed later at the mRNA level (Davis et al., 2020). The same study also determined the neurotransmitter types of the T5 input cells via RNAseq (Davis et al., 2020). In a study contained in this thesis, we applied antibody staining against VGlut to confirm the glutamatergic phenotype of L1, Mi9 and LPi neurons, the only glutamatergic neurons in the motion vision pathway described so far (**Manuscript 2**- Richter et al., 2018). Enhancer Gal4-lines, specific for genes coding for vesicular transporters or synthesizing enzymes of one type of neurotransmitter, combined with UAS-membrane-tagged-fluorophores label the whole cell that produce that transmitter (Raghu & Borst, 2011; Kondo et al., 2020). Another approach is a genetic strategy which labels the transporter or synthesizing enzyme at the protein level, e.g. the vesicular ACh transporter VAChT for cholinergic neurons (Pankova & Borst, 2017). From RNAseq data one can obtain the mRNA levels of a synthesizing enzyme or vesicular transporter gene of interest to eventually conclude which neurotransmitter the cell type is using (Pankova & Borst, 2016; Davis et al., 2020). A new approach used a deep learning classifier to predict the neurotransmitter from an *Drosophila* EM data set with 87% accuracy on average (Eckstein et al., 2020). Inferring the neurotransmitter phenotypes directly from the connectomic EM data set is a promising future direction as it circumvents additional tedious light microscopy approaches.

3.1.2 Defining receptor expression

RNAseq is the gold standard of transcriptomic analysis nowadays. mRNA levels are used as a readout of gene expression resulting in the respective protein levels. Recently, several RNAseq studies have been performed in flies including the transcriptome of T4/T5 neurons (Pankova & Borst, 2016; Davis et al., 2020; Hoermann et al., 2020). They all found certain types of GABA, ACh and glutamate receptors highly expressed, while others were only expressed at moderate levels (Fig. 15). However, it is hard to determine whether these different expression levels represent quantitative differences at the corresponding protein level. A paired transcriptome/ proteome analysis at 14 timepoints during *Drosophila* embryogenesis revealed a moderate mRNA-protein correlation of $p = 0.54$ (Becker et al., 2018).

While former studies name post-transcriptional mechanisms as a possible mechanism for this discrepancy (Greenbaum et al., 2003; Vogel & Marcotte, 2012), this study could explain protein time-courses by describing protein translation and degradation. Hence, mRNA levels derived from RNAseq experiments have to be treated carefully as they do not always correspond one to one to the protein levels, due to post-transcriptional, translational and protein degradation mechanisms (Vogel & Marcotte, 2012).

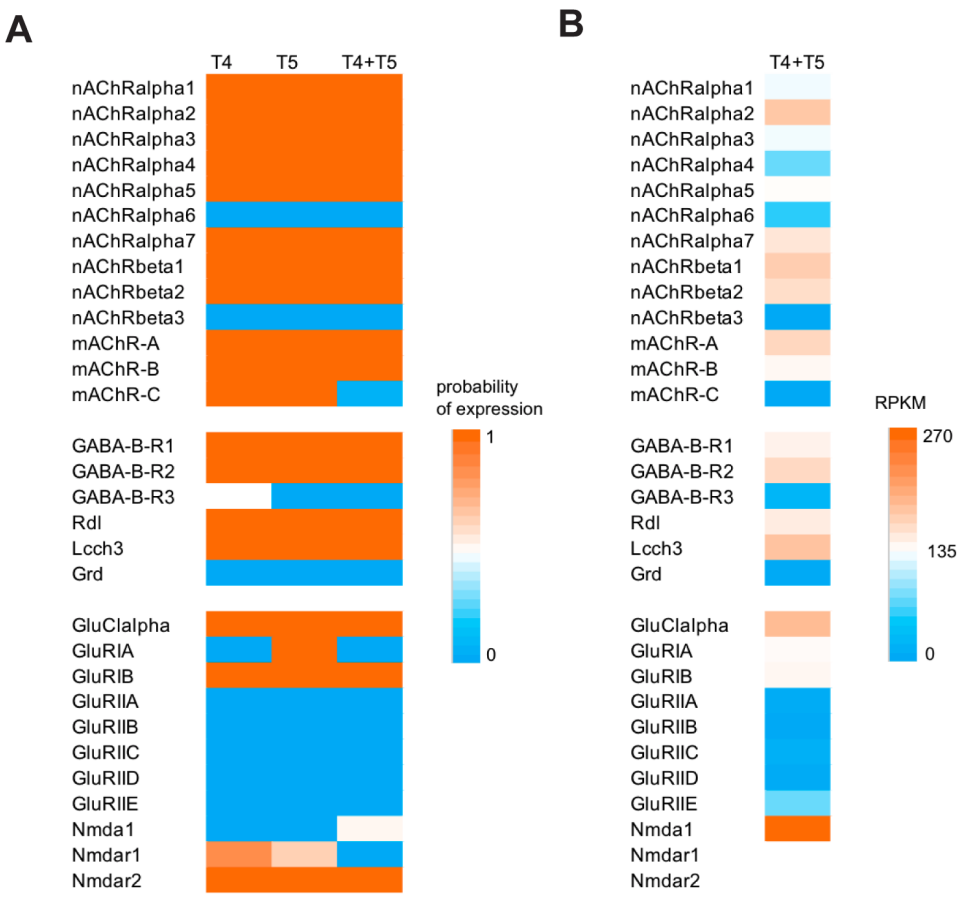

Figure 15. Expression of neurotransmitter receptors in T4/T5 neurons.
A) Gene expression levels of receptors for ACh, GABA and glutamate plotted as probability of expression using a color scale with the minimum at 0 (blue, not expressed) and the maximum at 1 (orange, expressed), adapted from Davis et al., 2020. **B)** Gene expression levels of same genes plotted as mean RPKM values using a color scale with the minimum at 0 (blue) and maximum at 270 (orange); adapted from Pankova & Borst, 2016.

3.1.3 Receptor localization

Endogenous labeling

One drawback of RNAseq approaches is the lack of spatial information which is essential when it comes to neurotransmitter receptors. As described in one of our studies, it had been known already from RNAseq studies that GluClα is expressed

in T4 and T5 neurons (**Manuscript 3**- Richter et al., 2018; Pankova & Borst, 2016; Davis et al., 2020). However, only the investigation at the protein level revealed that GluClα is localized to dendrites and axon terminals in T4 and merely in the axon terminals in T5. These differential sites of inhibition play different roles in T4 and T5 neurons, respectively. In T4 dendrites release of inhibition via GluClα is meant to account for PD enhancement, whereas to date the function of the presynaptic inhibition in T4/T5 terminals is not known.

Integrating a tag such as GFP or small epitopes (HA, V5, FLAG) in the endogenous locus of the gene of interest is a reliable method for studying the localization of this protein within its cellular environment. Large-scale approaches such as the MiMIC or the FlyFos library generated thousands of endogenously GFP-tagged fly lines readily available for researchers (Venken et al., 2011; Nagarkar-Jaiswal et al., 2015; Sarov et al., 2016). However, not all existing MiMIC GFSTF lines show a detectable GFP-signal due to several reasons (discussed below in paragraph 'Challenges of making tagged receptor lines'). A recent study targeted 75 neurotransmitter receptor genes with a T2A-Gal4 cassette that can be exchanged for a fluorescent tag such as Venus (Kondo et al., 2020). The disadvantage of these strategies is that they label the protein in every cell. Hence, ascribing the localization of the pan-neuronally tagged protein to a specific cell type or even a subcellular structure can be challenging in dense neuronal tissue. Often, conventional confocal microscopy lacks the required resolution to prove co-localization of the protein and the membrane of a cell.

Theoretically, this problem can be overcome with super-resolution microscopy techniques such as STED (Stimulated Emission Depletion) or STORM (Stochastic Optical Reconstruction Microscopy). The STED microscope uses two laser beams; one for excitation and the second one- the so-called STED beam- for donut-shaped depletion around the excitation site (Klar et al., 2000). Thereby, its resolution is improved compared to conventional confocal microscopy with the Abbe diffraction limit of around 250 nm (Abbe, 1873). STORM microscopy is based on high-accuracy localization of photo-switchable fluorophores which is able to create high resolution images with an axial imaging resolution of 20 nm (Rust et al., 2006). Sigal et al. demonstrated the feasibility of combining immunohistochemical staining with STORM super-resolution microscopy to map receptor subunit-specific GABAergic inputs on direction-selective ganglion cells in the mouse retina (Sigal et al., 2015). In **Manuscript 1** presented in this thesis, we demonstrated the improved resolution

of dendritic neurites in *Drosophila* brain slices obtained with STED microscopy (Fendl et al., 2017). Combining super-resolution STED microscopy with endogenously tagged receptors from the MiMIC or FlyFos line collection and labeled neurons could in theory enable co-localization studies. However, due to light scattering STED microcopy is restricted to the surface of specimens, making it difficult to analyze neurons deep in the fly brain with adequately high resolution. In light of this fact, we developed a protocol for STED imaging in thin *Drosophila* brain slices which should enable high-resolution imaging throughout the brain (Fendl et al., 2017). Nevertheless, this technique comes with a new caveat: depending on the slicing angle and the location of the neurons of interest in the tissue, labeled neurons might be cut in separate slices and reconstituting individual neurons from vibratome slices without informational loss is not possible. Taken together, we were not able to obtain reliable receptor co-localization data from the combination of pan-neuronal receptor labeling and STED super-resolution imaging.

Cell-type-specific (conditional) labeling

The simplest way to visualize the localization of a receptor in a given neuro is by expressing the tagged protein conditionally only in the cell type of interest via the UAS-Gal4 system. Several studies have employed UAS-lines with the coding sequence of a receptor and a small epitope or fluorophore tag. For instance, the UAS-lines for the nicotinic receptor subunit Dα7 and the GABA receptor subunit Rdl have been used to study their distribution in lobula plate tangential cells (Raghu et al., 2007; 2009) or motor neurons in the fly (Kuehn & Duch, 2013). However, it is thought that overexpression of proteins can lead to mistargeting and false localization. Previous studies reported that the *UAS-Dα7::GFP* line showed proper localization of the acetylcholine receptor to endogenous synapses when compared to antibody stainings or endogenous bruchpilot (Brp) puncta (Kuehn & Duch, 2013; Mosca & Luo, 2014). Another study showed that when the postsynaptic density protein PSD95 is overexpressed, the quantitative levels change, but qualitatively the localization is not altered (Willems et al., 2020). In our hands, the *UAS-Dα7::GFP* line seemed to localize only to cholinergic synapses, though it was not clear if these ACh receptors were really composed of the Dα7 subunit (**Manuscript 3**- Fendl et al., 2020). However, we generated a *UAS-GluClα::GFP* line which showed the same distribution patterns as the endogenously tagged control lines. Taken together, it is difficult to draw a general conclusion about UAS overexpression lines and their possible mistargeting effects. Every line requires careful controls, and the outcome might be different in every case.

Cell-type-specific (conditional) and endogenous labeling

The best method for receptor labeling would combine both endogenous and conditional labeling to make sure that the protein localization is trustworthy and can be resolved in the cell type of interest. To date, this endeavor has only been achieved in a few studies which I would like to discuss in the following paragraphs.

The STaR method (**S**ynaptic **Ta**gging with **R**ecombination) allows for cell-type-specific tagging via a FRT-flanked STOP cassette followed by a small epitope tag that is introduced in an extra BAC-copy of the gene of interest (Chen et al., 2014) (Fig. 8A). Although the inclusion of a T2A-LexA in combination with a UAS-tdTomato allowed for co-labeling of the gene-expressing cells in the case of Brp, this was not possible for the histamine channel ort. Since the T2A-LexA can disrupt the expression of the tagged gene, this method lacks a universal strategy for single cell labeling of receptor-expressing neurons. Furthermore, the STaR strategy is not truly endogenous as it introduces an additional copy of the engineered gene in a different genomic locus via artificial bacterial chromosomes instead of targeting the endogenous gene locus. It is also not easily generalizable, as it does not provide an easily cloneable plasmid or cassette which can be applied to any gene of interest. Nowadays, this approach could be extended and CIRSPR-Cas9 methods could enable faster and more flexible gene editing.

The split-GFP method used in Kondo et al. and Luo et al. to apply cell type-specific fluorescent labeling of target proteins are both inspired by the GRASP method which was originally developed to label synaptic contact sites (Feinberg et al., 2008; Kondo et al., 2020; Luo et al., 2020) (Fig. 8C and 8D). Both techniques rely on the expression of one GFP half in the gene of interest and do not require additional flippase expression. The study from Luo et al. additionally combined their method with FRT-STOP-FRT line which allows for single-cell labeling of the receptor-expressing neurons. The limitation of both methods is that they do not provide a generalizable toolkit or cassette that can be applied to further genes of interest. Moreover, the Kondo et al., study tagged neurotransmitter receptor genes only on the C-terminus which bears potential complications as discussed in the next chapter.

The FlpTag method that we designed complements the existing tools for protein tagging (**Manuscript 3**- Fendl et al., 2020). The strongest advantage of the FlpTag method is that it is generalizable and can be applied to any gene of interest via

insertion of the FlpTag cassette into MiMIC sites or via CRISPR/Cas9 mediated integration. The other existing methods focused mainly on their genes of interest and failed to provide a general plasmid or cassette that can be easily used for genome editing. The drawback of the FlpTag method is that to date it cannot be used in combination with sparse labeling of single neurons.

Overall, the methods that became available in the past few years offer many possibilities for cell-type-specific, endogenous protein tagging. None of the methods is perfect and fulfills all requirements, though, together they complement each other and enable various applications.

3.1.4 Challenges of generating tagged receptor lines

Independent of the exact strategy, it is challenging to generate a tagged protein line. Proteins such as ligand-gated ion channels form complex 3D structures, and already small changes in the amino acid sequence can lead to transformational changes of the protein. Hence, introducing tags in for instance a neurotransmitter receptor subunit, may cause conformational changes of the receptor which in turn can lead to dis-functional receptors, degraded proteins, or tags that are not detectable.

Usually, the common approach is to tag the protein at the N- or C-terminus to prevent interference with the 3D structure. Lately, one study also used this approach to tag 75 neurotransmitter receptors on the C-terminus neglecting the complex conformational structure of each individual receptor protein (Kondo et al., 2020). Another study tested the effects of N-terminal and C-terminal GFP-tagging on the subcellular localization of 16 different proteins in HEK293T cells and found that all C-terminal tagged proteins localized correctly, in contrast to less than half of the N-terminal tagged proteins (Palmer & Freeman, 2004). The N-terminus of proteins is important for protein folding after transition from the ribosome to the cytoplasm. It is possible that the GFP on the N-terminus is, thus, disrupting protein folding and proper translocation. Although tagging proteins at the C-terminus seems to be more promising it still has certain limitations. Depending on the 3D structure the C-terminal end can be folded into the inner side of the protein masking its fluorescence.

These difficulties can also be showcased by our attempts to generate a *UAS-GluClα::GFP* line: In our first trial, we placed the GFP-tag on the C-terminus which resulted in no detectable GluClα::GFP signal. Subsequently, we checked the 3D

structure of the protein GluClα (composed of five GluClα-subunits) and found the C-terminus hidden in the transmembrane domain resulting in a 'hidden' GFP. In our second attempt, we took advantage of the working MiMIC GFSTF GluClα line and placed the GFP in the same locus as the MiMIC insertion, in between the last two exons which resemble an intracellular loop of the GluClα channel. This new GFP-attachment site resulted in a functioning *UAS-GluClα::GFP* line.

In conclusion, there is no general recipe for generating functioning protein tagging lines. It is commendable to investigate the crystal structure, or if not available, use protein structure prediction softwares when deciding where to place the tag. In any case, it is difficult to predict the exact confirmation of the tagged protein and how trafficking and localization will be affected. Hence, every generated line needs to be tested and controlled carefully.

3.2 Receptors and voltage-gated ion channels in T4/T5 and their relevance for motion detection

A growing body of data is expanding our understanding of motion detection in flies. While the circuit mechanisms have been probed mainly with classical methods such as electrophysiological recordings, Ca^{2+}-imaging and behavioral paradigms (Maisak et al., 2013; Serbe et al., 2016; Arenz et al., 2017; Strother et al., 2017, 2018; Drews et al., 2020), new approaches are now pushing towards a deeper molecular understanding (Pankova & Borst, 2016; Davis et al., 2020; Hoermann et al., 2020). The first step for unraveling the molecular basis of motion detection is defining neurotransmitter types of the inputs and the corresponding transmitter receptors in T4/T5 neurons. Since T4/T5 neurons receive input from several neurotransmitter classes, a rather complex picture is expected at the level of receptors on their dendrites. First and foremost, neurotransmitter receptors are important neural circuit elements since they define the sign of a synaptic connection. Ionotropic receptors are ligand-gated ion channels for sodium, chloride, calcium or potassium, hence, the conductance change they elicit is either excitatory or inhibitory. Furthermore, transmitter receptors influence the temporal dynamics of synaptic transmission by either fast ionotropic actions or rather slow metabotropic mechanisms via second messenger cascades.

What is the relevance of the discovered receptors and their distribution on the T4/T5 dendrites? What can we learn and how is this information improving our

understanding of the motion detection computation? The most recent model for motion detection is the three-arm detector model described earlier in the introduction. In order to find the neural correlates of the algorithmic model the following questions need to be answered (visualized in Fig. 16):

1) Which cell type corresponds to which arm of the detector?
2) How and where is the delay mechanism implemented?
3) What is the cellular representation of the required non-linearities?

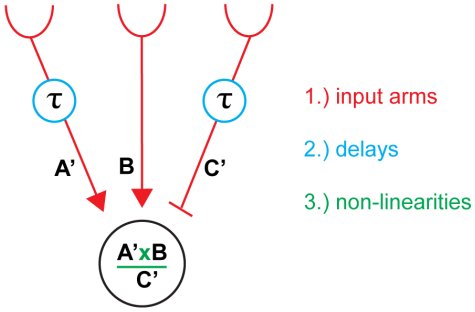

Figure 16. The three-arm detector model with its key elements.
Three spatially offset input arms (A', B, C) provide input to the motion detector; Two of the three input arms (A' and C') are delayed in time compared to the third arm (B). These three arms are integrated in a non-linear way by means of a multiplication and a division: A'xB/C'. Adapted from Arenz et al., 2017.

3.2.1 The sign of the input arms

The classical way of **linking the arms** of the algorithmic detector model with the different input cell types is by measuring their functional response properties. Several studies described the polarity, the temporal dynamics and the spatial receptive fields of the input neurons to T4 and T5. For instance, the four main T5 inputs in the OFF-pathway, Tm1, Tm2, Tm4 and Tm9, could be divided into three groups according to their Ca^{2+}-responses to moving edges: fast, transient Tm2 and Tm4, intermediate Tm1 and tonic, slow Tm9 (Serbe et al., 2016). Recently, the response properties of all major inputs to T4 and T5 have been characterized, and different combinations of cell arrangements on the three-arm model were tested in an unbiased simulation (Arenz et al., 2017). EM studies also revealed the anatomical arrangement of input synapses on T4/T5 dendrites, providing another resource for probing the theoretical model (Takemura et al., 2017; Shinomiya et al., 2019). By combining anatomical and physiological data, several studies found combinations of cells that led to highly direction-selective detector responses in the simulations (Serbe et al., 2016; Arenz et al., 2017). However, the **sign** of the synaptic connections has mostly been inferred from neurotransmitter phenotypes of the different input

neurons, although this is not a definite determinant. Depending on the receptor forming the synapse, all main neurotransmitters can in principle be inhibitory or excitatory. The most prominent example for this ambiguity is the glutamate-gated chloride channel GluClα which is an inhibitory glutamate receptor only present in invertebrates (Liu & Wilson, 2013; Mauss et al., 2015). Two recent studies demonstrated the inhibitory action of ACh via the two metabotropic ACh receptors mAChR-A and mAChR-B (Bielopolski et al., 2019; Qin et al., 2019).

In **Manuscript 3**, we started investigating the repertoire of receptors and their distribution on T4/T5 dendrites to obtain information about the input signs (summarized in Fig. 17; Fendl et al., 2020). As already speculated, the glutamatergic synapse between Mi9 and T4 is formed by the inhibitory receptor GluClα. The sign of the Mi9 input is therefore negative. However, since Mi9 responds to OFF-stimuli, this negative sign is inverted and T4 experiences a release of inhibition upon ON-stimuli. The input sign of the cholinergic Mi1 and Tm3 is positive, as they form the synapse with T4 via the excitatory ACh receptor Dα7. Pure inhibitory input to T4 is provided by GABAergic Mi4, C3 and CT1 via the Rdl receptor. In the case of T5, most of the cholinergic inputs Tm1, Tm2, Tm4 and Tm9 make synaptic contacts via the excitatory ACh receptor Dα7. However, we quantified less Dα7 puncta than cholinergic input synapses on T5 dendrites, indicating that some cholinergic synapses might be formed over different ACh receptor subunits. In the future, protein labeling strategies like FlpTag will allow the investigation of further ionotropic and metabotropic ACh receptor subunits on T5 dendrites. CT1, the only GABAergic input to T5 provides the negative input sign as it makes synaptic contacts via the GABA receptor subunit Rdl.

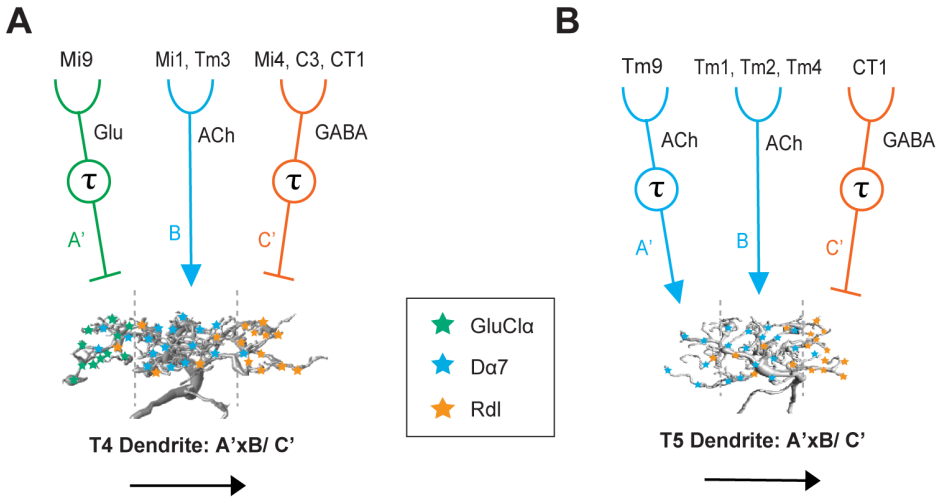

Figure 17. T4 and T5 dendrites, their input cells, corresponding receptors, and how they map onto the algorithmic three-arm detector model.

Receptor distributions of GluClα, Dα7, and Rdl on T4 **(A)** and T5 dendrites **(B)** indicated by green, blue, and orange stars. The input neurons in corresponding colors (green= glutamatergic, blue= cholinergic, orange= GABAergic) are assigned to the arms of the three-arm detector model. Images adapted from Fendl et al., 2020.

Although the three-arm detector model seems to hold true in many experimental and theoretical tests, there are several studies that failed to detect PD enhancement in the electrophysiological responses of T4/T5 neurons (Gruntman et al., 2018; 2019). A possible explanation is that the enhancement seen in the calcium traces results purely from a nonlinear voltage-to-calcium transformation (Wienecke et al., 2018). If this is the case, the role of Mi9 and the biophysical implications of GluClα need to be reconsidered.

Unexpectedly, we also found GluClα in the axon terminals of T4/T5 neurons. This finding showcases the necessity of investigations at the protein level when describing the neurotransmitter receptor repertoire of a specific neural cell type. RNAseq studies had shown already that GluClα is expressed in both T4 and T5 neurons (Pankova & Borst, 2016; Davis et al., 2020). While this result made sense for T4 neurons, as they receive glutamatergic input by Mi9 on their dendrites, it was puzzling why T5 possess glutamate receptors without any glutamatergic input on their dendrites (Richter et al., 2018; Shinomiya et al., 2019). T5-specific expression of GFP-tagged GluClα demonstrated the localization of this glutamate receptor to axon terminals in the lobula plate (**Manuscript 3**- Fendl et al., 2020). In T4, on the other hand, GluClα localized to both dendrites and axon terminals. What is the functional role of these inhibitory glutamate receptors in T4/T5 terminals? Possibly, glutamatergic LPi neurons could cross-inhibit T4/T5 cells with opposite preferred directions via GluClα. This presynaptic inhibition at the level of T4/T5 axon terminals could in turn further sharpen the flow field selectivity of lobula plate tangential neurons, the downstream postsynaptic partners of T4/T5 neurons (Mauss et al., 2015).

3.2.2 Delayed inputs

Another prerequisite of the three-arm model, as well as of its predecessors the Hassenstein-Reichardt-detector and the Barlow- Levick-detector, is a **delayed response** for some of the inputs compared to the others. This delay can be implemented by cell-intrinsic mechanisms at the level of presynaptic inputs, which have been already described in several studies (Ammer et al., 2015; Serbe et al., 2016; Arenz et al., 2017). Another way of employing temporal delays are

postsynaptic mechanisms on T4/T5 dendrites. In theory, metabotropic receptors can introduce temporal delays via second-messenger cascades which are slower compared to fast-acting ionotropic receptors. (Reiner & Levitz, 2018). For T5 dendrites, some cholinergic input arms could be delayed via muscarinic ACh receptors as discussed previously (Shinomiya et al., 2014). According to recent RNAseq studies (Pankova & Borst, 2016; Davis et al., 2020), both T4 and T5 neurons express metabotropic receptors for ACh and GABA which await further investigations. Although a number of simulations already perform well with the delayed signals as measured for some input neurons (Serbe et al., 2016; Arenz et al., 2017; Drews et al., 2020), it cannot be ruled out that postsynaptic metabotropic receptors introduce an additional delay.

3.2.3 Non-linearities

Lastly, it is not fully understood how the non-linearities proposed in the three-arm detector are implemented in T4 and T5 cells. The model involves an excitatory non-linearity in the form of PD enhancement and an inhibitory non-linearity in the form of ND suppression. When stimulated with apparent motion in the preferred direction, T4/T5 cells respond with an increased response compared to the sum of the flicker response of two adjacent ommatidia as seen with Ca^{2+}-imaging (Haag et al., 2016, 2017). Hence, they show a non-linear, enhanced response for preferred direction (PD enhancement). At the algorithmic level, the three-arm detector model implements PD enhancement as a multiplication.

The biophysical mechanism of PD enhancement in the ON pathway could be as follows (Borst, 2018): T4 receives input from inhibitory glutamatergic Mi9 (OFF-center) via GluClα on the preferred side of the dendrite, followed by cholinergic, excitatory input (ON-center) in the central dendritic area. When an ON edge is moving along the preferred direction of the T4 cell, Mi9's inhibitory input is suppressed which releases T4 from inhibition. This leads to an increase of the input resistance of T4, amplifying its response to the subsequent excitatory input signal in the center. This enhancement can take place even in a passive T4 dendrite without voltage-gated ion channels. Additionally, voltage-gated ion channels can also lead to a non-linear integration of input signals (Koch, 1999; McCormick, 1991). Another possibility is that PD enhancement is a result of the non-linear voltage-to-calcium transformation seen with Ca^{2}-imaging using GCaMP but not in electrophysiological recordings (Gruntman et al., 2018, 2019; Wienecke et al., 2018). Strother et al., demonstrated that RNAi-mediated knockdown of GluClα in T4/T5 causes enhanced

turning responses on the ball set-up under certain stimulus conditions (Strother et al., 2017). This indicates that both T4 and T5 neurons receive inhibitory input and blocking this inhibition leads to an enhanced turning response, probably, due to the enhanced activity of T4/T5. However, this behavioral paradigm did not probe the effects of GluClα-loss on PD enhancement in T4 neurons. It is more likely that the observed enhanced turning response is caused by the lack of inhibition via GluClα on the axon terminals of T4/T5 neurons.

In T5 neurons, the neural implementation of PD ehancement is less clear. On the distal side of its dendrite, T5 mainly receives input from cholinergic Tm9 which also shows low-pass characteristics (Arenz et al., 2017; Shinomiya et al., 2019). The distribution of the excitatory ACh receptor Dα7 on T5 dendrites throughout the central and distal areas indicates that most of the cholinergic inputs (Tm1, Tm2, Tm4, and Tm9) form synaptic contacts via this ACh receptor (**Manuscript 3**- Fendl et al., 2020). However, we quantified less Dα7 puncta than cholinergic input synapses on T5 dendrites, indicating that some cholinergic synapses might be formed over different ACh receptor subunits. Before the GABAergic input CT1 to T5 was discovered (Shinomiya et al., 2019), it was speculated that the inhibitory input expected from the Barlow-Levick model could be provided via muscarinic ACh receptor. Potentially, such muscarinic cholinergic receptors could lead to calcium release, causing the activation of a high-conductance calcium-dependent potassium channel, which eventually leads to membrane hyperpolarization in T5 cells (Shinomiya et al., 2014). For instance, it would be possible for Tm9 to form synapses via inhibitory metabotropic ACh receptors. Furthermore, Tm9 could connect to T4 via metabotropic ACh receptors that act via slower second messenger cascades.

The non-linearity for ND suppression is implemented as a divisive inhibition on the null side of the three-arm detector similarly to the Barlow-Levick detector. The divisive inhibition, also called 'shunting inhibition' is, mathematically speaking, suppressing the excitatory input by division rather than linear subtraction (Carandini & Heeger, 1994). This is the case when the inhibitory conductance is bigger than the leak conductance of the cell. Such a strong, shunting inhibition could be implemented via the GABA receptor Rdl on the null side of both T4 and T5 neurons, as described in one manuscript included in this thesis (**Manuscript 3**- Fendl et al., 2020). $GABA_A$ receptors can mediate shunting inhibition since their activation shunts the depolarization caused by concurrent excitatory input (Alvarez-Leefmans et al., 2009). In the case of T4, the GABAergic inputs Mi4, C3 and CT1 form

inhibitory synapses via Rdl on the proximal side of the dendrite. T5 dendrites only receive GABAergic input from CT1 via Rdl on the base of the dendrite.

3.2.4 Voltage-gated ion channels

While neurotransmitter receptors, first and foremost, define the sign of the synaptic input to a neuron, voltage-gated ion channels shape the amplitude and dynamics of the response. There are several voltage-gated ion channels expressed in T4/T5 neurons (Pankova & Borst, 2016; Davis et al., 2020). However, only little was known about their distribution or function in these neurons. Using our newly developed FlpTag approach, we investigated the subcellular localization of Ih and para in T4/T5 neurons (**Manuscript 3**- Fendl et al., 2020).

Ih channels or HCN (hyperpolarization-activated cyclic nucleotide–gated) channels are activated at hyperpolarized potentials around -50mV at which they gate Na+ and K+, causing a depolarization of the cell. In vertebrates, HCN channels are encoded by four genes (*HCN1*, *HCN2*, *HCN3*, and *HCN4*) which are expressed in neurons, as well as in heart cells. In *Drosophila*, there is only one gene described, which is named *Ih* after the so-called I_h current running through HCN channels. However, in bees and fruit flies, the gene has been shown to undergo alternative splicing, resulting in multiple Ih splice variants (Gisselmann, et al., 2004; Gisselmann et al., 2005). Ih channels cover a wide range of functional roles, from regulating glutamate release at presynaptic sites in *Drosophila* (Hu et al., 2015; Hegle et al., 2017), to shaping the postsynaptic potential kinetics and integration in cortical neurons in the mouse brain (Magee, 1999; Tsay et al., 2007; George et al., 2009). Furthermore, the Ih current is necessary to maintain dopamine patterns important for sleep consolidation in the fly brain (Gonzalo-Gomez et al., 2012).

In **Manuscript 3**, we found expression of Ih in both T4 and T5 dendrites (Fendl et al., 2020). Ih channels are known to cause rebound-excitation after hyperpolarization in the retina (Van Hook & Berson, 2010). In T4 dendrites, Ih channels could be the biophysical substrate of PD enhancement by providing rebound-excitation. Upon stimulation with a moving bright edge, T4 is released from glutamatergic inhibition by Mi9 via GluClα. Ih channels which are activated by hyperpolarization could potentially be activated and cause a rebound-excitation after the hyperpolarization. This rebound excitation could cause a non-linear enhanced depolarization of T4 which is excited even more once the stimulus reaches the central area of the dendrite with excitatory input from Mi1 and Tm3. The problem with this hypothesis is that

the rebound-excitation via Ih channels would also take place upon hyperpolarization for stimuli moving in the null direction. Future loss-of-function experiments using RNAi or other knock-out methods will examine the role of Ih channels for direction selectivity in T4 neurons.

para is the only voltage-gated sodium channel gene described in *Drosophila* and it is highly expressed in T4/T5 neurons (Pankova & Borst, 2016; Davis et al., 2020). In general, para is involved in the sodium-dependent generation of action potentials (Loughney et al., 1989). In **Manuscript 3**, we used FlpTag to investigate the subcellular localization of para in T4/T5 neurons and we found it localized to the axonal fibers connecting dendrites and axon terminals (**Manuscript 3**- Fendl et al., 2020). Further loss-of-function studies should focus on the following questions: Do T4/T5 indeed fire action potentials? If so, is para required for the generation of action potentials? How does this affect direction-selectivity in T4/T5 neurons?

Taken together, the findings about GluClα, Dα7 and Rdl on T4/T5 dendrites support some of the theoretical expectations of the algorithmic three-arm detector model. To some extent we could answer open questions about the sign, the delay and the non-linearities of the input arms. However, as suggested by RNAseq studies T4/T5 neurons express many more transmitter receptors and voltage-gated ion channels that shape their biophysical response properties. Future experiments should investigate the whole set of expressed channels and subsequently test their role in loss-of-function experiments to understand the whole underlying molecular complexity of motion vision.

3.3 Receptors and neurotransmitters in the mammalian retina

In the mouse retina, different cell types use various neurotransmitters to communicate. Glutamate, acetylcholine and GABA are essential to the vertical signaling pathway of the retina. The most abundant transmitter is glutamate, from the first synapse of photoreceptors, onto bipolar cells, to the last layer of direction-selective ganglion cells (DSGCs) projecting to the LGN in the thalamus. In this chapter I would like to discuss similarities and differences of the mammalian retina and the fly optic lobe in terms of neurotransmitters and receptors used in their respective motion detection circuits.

3.3.1 Comparison of the ON and OFF pathways in the mouse retina and the fly optic lobe

Motion vision circuits across species are split into an ON and an OFF pathway which detect light increments or decrements, respectively (Borst & Helmstaedter, 2015). This specification allows for more efficient encoding of visual stimuli (Gjorgjieva et al., 2014). ON/ OFF dichotomy was described in both the mouse retina and the fly optic lobe; however, they differ in their underlying cellular and synaptic mechanisms.

In the mouse retina, photoreceptors hyperpolarize in response to light and release glutamate onto their postsynaptic partners, the bipolar cells, in the dark. There are ON- and OFF-responsive bipolar cells and the split occurs at the synaptic level between photoreceptors and bipolar cells. ON bipolar cells express the metabotropic inhibitory glutamate receptor mGluR6 which leads to a sign inversion and the creation of the ON channel (Masu et al., 1995). On the other hand, OFF bipolar cells express ionotropic AMPA receptors which cause a depolarization upon glutamate-binding (Euler et al., 2014). There are fast and slow bipolar cells, similar to the medulla and transmedulla neurons in the fly optic lobe which also come as ON or OFF cells with different temporal dynamics (Euler et al., 2014).

In the fly, the split into ON- and OFF-pathway occurs at the level of the lamina cells, an additional layer of cell types that have no equivalent in the mouse retina. *Drosophila* photoreceptors depolarize in response to light and release histamine which in turn acts on inhibitory histamine-gated chloride channels in the lamina neurons (Hardie, 1989). Lamina neurons L2-L5 are cholinergic and convey the photoreceptor signal onto the next layer of medulla and transmedulla neurons. L1 is the main input to the ON channel, whereas L2 is the main input to the OFF channel (Joesch et al., 2010). To create an ON channel, glutamatergic L1 neurons are thought to inhibit postsynaptic Mi1 and Tm3 neurons via the glutamate-gated chloride channel GluClα, implementing a sign inversion. Hence, in response to light photoreceptors depolarize which inhibits L1 neurons and this in turn disinhibits Mi1 and Tm3 neurons, leading to ON-responses. Recently, it was shown that this sign inversion in the ON pathway is a multi-synaptic process that indeed involves both GluClα and Rdl receptors (Molina-Obando et al., 2019). Interestingly, both in the mouse and the fly visual system, glutamatergic, inhibitory signaling is responsible for the sign inversion in the ON pathway. While in the mouse retina, the mGluR6

receptor causes the required inhibition, the fly uses the GluClα channel which is unique to invertebrates.

In the mouse, this split into ON- and OFF-pathway happens directly at the level of the synapse between photoreceptors and bipolar cells, which can be compared to the fly medulla and transmedulla neurons. The direction-selective T4/T5 cells in the fly are comparable to the starburst amacrine cells (SACs) in the mammalian retina and the lobula plate tangential cells in the fly resemble the direction-selective ganglion cells (summarized comparison of the fly and mouse motion detection circuits in Fig. 18).

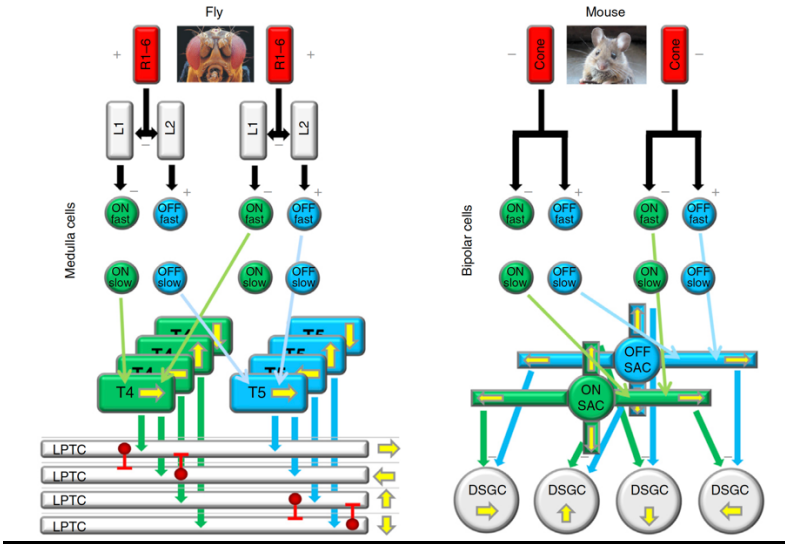

Figure 18. Motion detection circuits of the fly and mouse.
Fly and mouse use two different ways of splitting the photoreceptor signal into ON and OFF pathways: The photoreceptors in the fly connect via sign-inverting synapses to lamina monopolar cells L1 and L2, the entry to the ON and OFF pathway, respectively. The mouse retina lacks this additional layer of lamina cells and splits the signal directly via two types of glutamate receptors onto ON and OFF bipolar cells. The first stage of direction-selective cells are the T4 (ON) and T5 (OFF) neurons in the fly optic lobe and the ON and OFF SACs in the mouse retina. Direction-selective information from the two pathways is integrated in lobula plate tangential cells (LPTCs) in the fly and in ON-OFF direction-selective ganglion cells (DSGCs) in the mouse. Image taken with permission from Borst & Helmstaedter, 2015.

3.3.2 Neurotransmitters and receptors in the mammalian retina involved in motion-detection

The first direction-selective neurons described in the mammalian retina are the ON-OFF direction-selective retinal ganglion cells, which were discovered in the rabbit eye (Barlow et al., 1964; Barlow & Levick, 1965). Similar to the elementary motion detectors in the fly (T4/T5 neurons), they come in four subtypes each responding to motion in one of the four cardinal directions (Oyster & Barlow, 1967; Elstrott et al.,

2008). The inhibitory input of GABAergic starburst amacrine cells (SACs) is necessary for direction-selective responses in retinal ganglion cells as shown by pharmacology and ablation experiments (Famiglietti, 1983; Yoshida et al., 2001). Interestingly, starburst amacrine cells are already direction-selective themselves in a centrifugal fashion, e.g. for stimuli from the soma to the dendritic tips (Euler et al., 2002). It was later shown that starburst amacrine cells and direction-selective ganglion cells are wired in an asymmetric way such that individual dendrites of starburst amacrine cells connect strongly to ganglion cells with opposite directional preference (Briggman et al., 2011) (Fig. 19B). The synaptic basis of the inhibitory action of starburst amacrine cells is the GABA receptor $GABA_AR$ α2 as shown by knock-out experiments, in which direction-selective responses in On-Off retinal ganglion cells are reduced (Auferkorte et al., 2012). In line with this observation, a super-resolution microscopy study mapped the distribution of $GABA_AR$ α2 receptors on individual dendrites of On-Off ganglion cells (Sigal et al., 2015) (Fig. 19C).

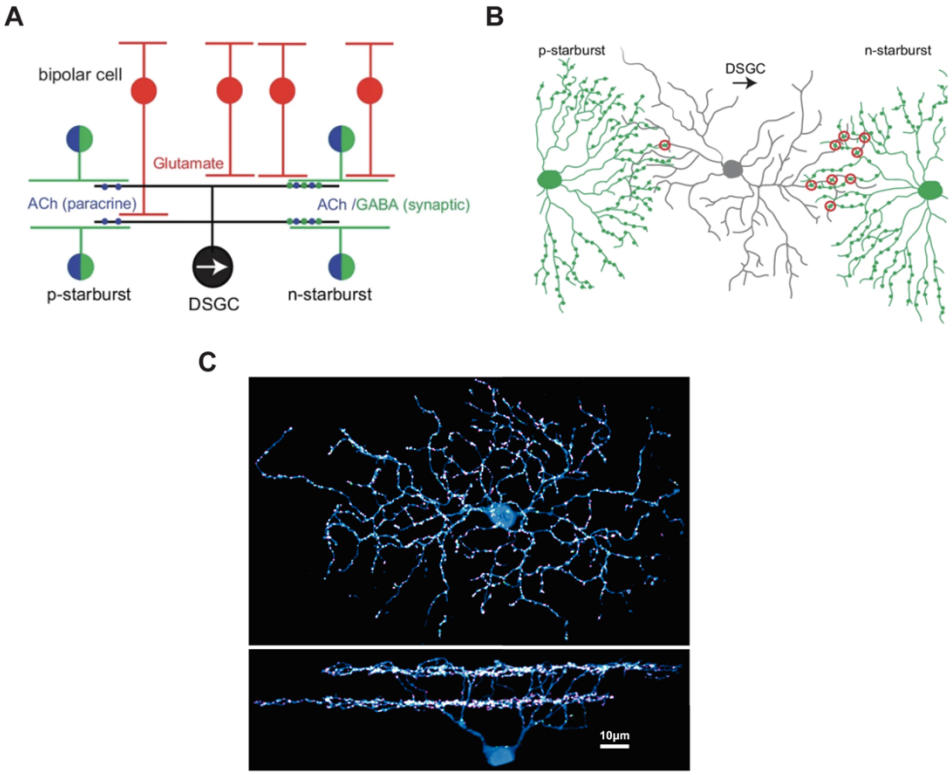

Figure 19. Synaptic wiring in motion detecting circuits in the mouse retina.
A) Schematic illustration of the direction-selective circuit impinging on ON-OFF direction-selective ganglion cells (DSGCs) (horizontal view). DSGCs receive glutamatergic inputs from ON and OFF bipolar cells and from cholinergic/GABAergic starburst amacrine cells (SACs). Preferred side SACs (p-starburst) provide mainly paracrine, excitatory, cholinergic ACh input, whereas null side SACs (n-SACs) provide cholinergic excitation and GABAergic inhibition. **B)** Asymmetric wiring between starbursts and DSGCs (top view). 'Wrap-around' synaptic connections (circles in red) are mainly made by n-starbursts mediating 'null'

inhibition. **C)** Top view (top) and side view (bottom) of the STORM microscopy reconstructed ON-OFF DSGCs (blue) with synaptic gephyrin (green) and postsynaptic (magenta) clusters. Images in A and B taken with permission from Hanson et al., 2019. Imag in C taken with permission from Sigal et al., 2015.

Altogether, the field has mainly focused on the question of how starburst amacrine cells and retinal ganglion cells become direction-selective. Bipolar cells provide glutamatergic excitatory input to both cell types and there are several hypothesis and lines of evidence about how they shape the direction-selective responses of both postsynaptic partners (Fig. 19A). It was shown that starburst amacrine cells which respond preferentially to stimuli moving from the soma to the dendritic tips, receive input from different types of bipolar cells, including cells with fast and slow temporal dynamics (Baden et al., 2013). Additionally, these different types of bipolar cells show a 'space-time wiring specificity' with starburst amacrine cells: slower bipolar cells predominantly form synapses with the starburst amacrine cells on the proximal part of the dendrite, whereas faster bipolar cells wire with the distal area of the starburst amacrine dendrite. Potentially, this constitutes the basis of the centrifugal preferred direction of the amacrine cells (Kim et al., 2014).

When it comes to retinal ganglion cells, the picture is getting more complicated. Originally, it was thought that non-direction-selective excitatory input from glutamatergic bipolar cells and direction-selective inhibitory input from starburst amacrine cells are globally integrated in direction-selective ganglion cells leading to spiking responses in the soma. Recently, several lines of evidence suggest a different model. First, it was shown that the glutamatergic bipolar cell signal acts on silent NMDA synapses on starburst amacrine cells which affects the direction-selective ganglion cells' response in a modulatory fashion (Sethuramanujam et al., 2017). Hence, cholinergic input from starburst amacrine cells is the primary source of excitation to ganglion cells, except under extremely high contrasts (Sethuramanujam et al., 2016). This is also supported by the observation that the starburst amacrine network alone, without bipolar cell input, can generate direction-selective responses in On-Off retinal ganglion cells (Sethuramanujam et al., 2016). Furthermore, a recent study demonstrated that some cholinergic transmission of starburst amacrine cells is non-synaptic, but still retains the ability to generate rapid miniature currents in direction-selective ganglion cells. Acetylcholine released from starburst amacrine cells is locally tuned for direction, thus leading to a local integration model of direction selectivity with fine-tuned balance of excitation and inhibition (Sethuramanujam et al., 2020). This compartmentalized non-linear dendritic

integration is more efficient since it requires less overall inhibition and it provides a higher resolution readout of direction-selective information. In this respect, it will be very interesting to map cholinergic receptors on retinal ganglion cells as there should be more receptors than cholinergic synapses in the volumetric transmission scenario. In addition, it is possible that there are other GABA and ACh receptors present on direction-selective ganglion cells (Sigal et al., 2015).

Taken together, it becomes obvious that underlying neurotransmitters and receptors are of great interest for the direction-selective circuit in the mammalian retina. While research in the field of retina motion vision is moving more towards the subcellular level of direction-selectivity, the questions arising are similar to those in the field of fly motion vision: which receptors are present on the dendrites of direction-selective neurons and how do they shape the functional responses? For instance, in the case of cholinergic volume transmission of starburst amacrine cells onto direction-selective ganglion cells, researchers are just beginning to unravel the complexity of different neurotransmitters and their corresponding receptors (Sethuramanujam et al., 2020).

3.4 Conclusion and outlook

Investigating the subcellular localization and distribution of neurotransmitter receptors across different neural compartments is the first step towards understanding their functional roles. It also lays the logical foundation for any subsequent loss-of-function experiments. In my thesis, I developed tools to investigate the distribution of GluClα, Rdl and Dα7 in T4/T5 neurons. Depending on their localization on T4/T5 dendrites or terminals I discussed their potential roles for the computation of motion detection.

As a next step, the various ideas about the function of these receptors can be probed in loss-of-function experiments. The receptor subunits can be depleted with RNAi-mediated knockdown or FlpStop knock-outs (Dietzl et al., 2007; Perkins et al., 2015; Fisher et al., 2017) and the functional consequences can be monitored directly at the level of T4/T5 neurons by Ca^{2+}-imaging with GCaMP or by electrophysiological recordings. In theory, it is expected that the response of T4/T5 neurons is less direction-selective when receptors important for PD enhancement or ND suppression are depleted. For instance, a knock-down of GluClα in T4 neurons should abolish PD enhancement and decrease its direction-selectivity. However, it

is not clear to which extent this effect is related to the depletion of dendritic or axonal GluClα. The functional relevance of dendritic vs. axonal GluClα receptors in T4/T5 could be uncovered by blocking their corresponding presynaptic partners, e.g. Mi9 neurons for T4 dendrites and, presumably, LPi neurons for T4 and T5 axon terminals. A clearer picture should arise with depletion of the GABA-receptor Rdl which is only localized to T4/T5 dendrites and presumably responsible for ND suppression. In this case, Rdl-knockdown is expected to diminish ND suppression and to cause an even stronger decrease of direction-selectivity in T4/T5 neurons (Borst, 2018). Additionally, the effects of the receptor knock-downs can be examined in behavioral essays such as the optomotor response which relies on T4/T5 neurons (Bahl et al., 2013).

The receptors and channels that we investigated are only the starting point, and there are many more receptors and voltage-gated ion channels which are yet to be discovered. According to RNAseq data, there are several ionotropic acetylcholine and GABA receptors expressed in T4/T5 neurons. With our newly developed methods it is possible to investigate the exact subunit compositions that are used across the different synaptic sites. Furthermore, there are a few metabotropic ACh and GABA receptor subunits that could play an important role for the temporal dynamic range on the postsynaptic side. In addition, voltage-gated ion channels are crucial components that shape the response properties of neurons.

Altogether, the findings about neurotransmitter receptors and voltage-gated ion channels are important steps towards the understanding of T4/T5 neurons' functioning at the molecular level. With most of the information about circuit elements, response properties, neurotransmitter phenotypes and wiring patterns at hand, the field of motion vision research is moving deeper into the biophysical intricacies of neural computation. Neural circuits are more than the sum of their participating neurons and too often the different neural cell types are treated like black boxes. It is only if we consider the different neurotransmitter types, receptors and ion channels with their various functional implications, that we can understand neural circuits as a whole. I believe that this is the future direction for systems neuroscience, not only for fruit fly research, but in general in our endeavor to understand the brain.

4. REFERENCES

Abbe, E. (1873). Beiträge zur Theorie des Mikroskops und der mikroskopischen Wahrnehmung: I. Die Konstruktion von Mikroskopen auf Grund der Theorie. *Archiv Für Mikroskopische Anatomie*, *9*(1), 413–418.

Alekseyenko, O. V., Chan, Y. B., Li, R., & Kravitz, E. A. (2013). Single dopaminergic neurons that modulate aggression in *Drosophila*. *Proceedings of the National Academy of Sciences of the United States of America*, *110*(15), 6151–6156.

Alekseyenko, O. V., Lee, C., & Kravitz, E. A. (2010). Targeted manipulation of serotonergic neurotransmission affects the escalation of aggression in adult male *Drosophila melanogaster*. *PLoS ONE*, *5*(5).

Ammer, G., Leonhardt, A., Bahl, A., Dickson, B. J., & Borst, A. (2015). Functional specialization of neural input elements to the *Drosophila* on motion detector. *Current Biology*, *25*(17), 2247–2253.

Arenz, A., Drews, M. S., Richter, F. G., Ammer, G., & Borst, A. (2017). The temporal tuning of the *Drosophila* motion detectors Is determined by the dynamics of their input elements. *Current Biology*, *27*(7), 929–944.

Aso, Y., & Rubin, G. M. (2016). Dopaminergic neurons write and update memories with cell-type-specific rules. *eLife* 5.

Auferkorte, O. N., Baden, T., Kaushalya, S. K., Zabouri, N., Rudolph, U., Haverkamp, S., & Euler, T. (2012). GABAA receptors containing the α2 subunit are critical for direction-selective inhibition in the retina. *PLoS ONE*, *7*(4), e35109.

Baden, T., Berens, P., Bethge, M., & Euler, T. (2013). Spikes in mammalian bipolar cells support temporal layering of the inner retina. *Current Biology*, *23*(1), 48–52.

Bahl, A., Ammer, G., Schilling, T., & Borst, A. (2013). Object tracking in motion-blind flies. *Nature Neuroscience*, *16*(6), 730–738.

Baines, R. A., Uhler, J. P., Thompson, A., Sweeney, S. T., & Bate, M. (2001). Altered electrical properties in *Drosophila* neurons developing without synaptic transmission. *Journal of Neuroscience*, *21*(5), 1523–1531.

Barlow, H. B., Hill, R. M., & Levick, W. R. (1964). Retinal ganglion cells responding selectively to direction and speed of image motion in the rabbit. *The Journal of Physiology*, *173*(3), 377–407.

Barlow, H. B., & Levick, W. R. (1965). The mechanism of directionally selective units in rabbit's retina. *The Journal of Physiology*, *178*(3), 477–504.

Becker, K., Bluhm, A., Casas-Vila, N., Dinges, N., Dejung, M., Sayols, S., Kreutz, C., Roignant, J. Y., Butter, F., & Legewie, S. (2018). Quantifying post-transcriptional regulation in the development of *Drosophila melanogaster*. *Nature Communications*, *9*(1), 1–14.

Becnel, J., Johnson, O., Luo, J., Nässel, D. R., & Nichols, C. D. (2011). The serotonin 5-HT7Dro receptor is expressed in the brain of *Drosophila*, and is essential for normal courtship and mating. *PLoS ONE*, *6*(6), e20800.

Behnia, R., Clark, D. A., Carter, A. G., Clandinin, T. R., & Desplan, C. (2014).

Processing properties of on and off pathways for *Drosophila* motion detection. *Nature*, *512*(7515), 427–430.

Berry, J. A., Cervantes-Sandoval, I., Chakraborty, M., & Davis, R. L. (2015). Sleep facilitates memory by blocking dopamine neuron-mediated forgetting. *Cell*, *161*(7), 1656–1667.

Bielopolski, N., Amin, H., Apostolopoulou, A. A., Rozenfeld, E., Lerner, H., Huetteroth, W., Lin, A. C., & Parnas, M. (2019). Inhibitory muscarinic acetylcholine receptors enhance aversive olfactory learning in adult *Drosophila*. *eLife*, 8.

Blenau, W., & Thamm, M. (2011). Distribution of serotonin (5-HT) and its receptors in the insect brain with focus on the mushroom bodies. Lessons from *Drosophila melanogaster* and *Apis mellifera*. *Arthropod Structure and Development* (Vol. 40, Issue 5, pp. 381–394).

Bogdanik, L., Mohrmann, R., Ramaekers, A., Bockaert, J., Grau, Y., Broadie, K., & Parmentier, M. L. (2004). The *Drosophila* metabotropic glutamate receptor DmGluRA regulates activity-dependent synaptic facilitation and fine synaptic morphology. *Journal of Neuroscience*, *24*(41), 9105–9116.

Borghuis, B. G., Marvin, J. S., Looger, L. L., & Demb, J. B. (2013). Two-photon imaging of nonlinear glutamate release dynamics at bipolar cell synapses in the mouse retina. *Journal of Neuroscience*, *33*(27), 10972–10985.

Borst, A. (2018). A biophysical mechanism for preferred direction enhancement in fly motion vision. *PLOS Computational Biology*, *14*(6), e1006240.

Borst, A., & Helmstaedter, M. (2015). Common circuit design in fly and mammalian motion vision. *Nature Neuroscience*, Vol. 18, Issue 8, pp. 1067–1076.

Brand, A. H., & Perrimon, N. (1993). Targeted gene expression as a means of altering cell fates and generating dominant phenotypes. *Development*, *118*(2), 401–415.

Brembs, B., Christiansen, F., Pflüger, H. J., & Duch, C. (2007). Flight initiation and maintenance deficits in flies with genetically altered biogenic amine levels. *Journal of Neuroscience*, *27*(41), 11122–11131.

Briggman, K. L., Helmstaedter, M., & Denk, W. (2011). Wiring specificity in the direction-selectivity circuit of the retina. *Nature*, *471*(7337), 183–190.

Brody, T., & Cravchik, A. (2000). *Drosophila melanogaster* G protein-coupled receptors. *Journal of Cell Biology*, *150*(2), F83–F88.

Carandini, M., & Heeger, D. J. (1994). Summation and division by neurons in primate visual cortex. *Science*, *264*(5163), 1333–1336.

Cascio, M. (2004). Structure and function of the glycine receptor and related nicotinicoid receptors. *Journal of Biological Chemistry*, Vol. 279, Issue 19, pp. 19383–19386.

Catterall, W. A. (1998). Structure and function of neuronal Ca2+ channels and their role in neurotransmitter release. *Cell Calcium*, Vol. 24, Issues 5–6, pp. 307–323.

Chen, T. W., Wardill, T. J., Sun, Y., Pulver, S. R., Renninger, S. L., Baohan, A., Schreiter, E. R., Kerr, R. A., Orger, M. B., Jayaraman, V., Looger, L. L., Svoboda, K., & Kim, D. S. (2013). Ultrasensitive fluorescent proteins for imaging neuronal activity. *Nature*, *499*(7458), 295–300.

Chen, Y., Akin, O., Nern, A., Tsui, C. Y. K., Pecot, M. Y., & Zipursky, S. L. (2014). Cell-type-specific labeling of synapses in vivo through synaptic tagging with

recombination. *Neuron*, *81*(2), 280–293.

Coons, A. H., Creech, H. J., & Jones, R. N. (1941). Immunological properties of an antibody containing a fluorescent group. *Experimental Biology and Medicine*, *47*(2), 200–202.

Dana, H., Sun, Y., Mohar, B., Hulse, B. K., Kerlin, A. M., Hasseman, J. P., Tsegaye, G., Tsang, A., Wong, A., Patel, R., Macklin, J. J., Chen, Y., Konnerth, A., Jayaraman, V., Looger, L. L., Schreiter, E. R., Svoboda, K., & Kim, D. S. (2019). High-performance calcium sensors for imaging activity in neuronal populations and microcompartments. *Nature Methods*, *16*(7), 649–657.

Daniels, R. W., Collins, C. A., Gelfand, M. V., Dant, J., Brooks, E. S., Krantz, D. E., & DiAntonio, A. (2004). Increased expression of the *Drosophila* vesicular glutamate transporter leads to excess glutamate release and a compensatory decrease in quantal content. *Journal of Neuroscience*, *24*(46), 10466–10474.

Daniels, R. W., Gelfand, M. V., Collins, C. A., & DiAntonio, A. (2008). Visualizing glutamatergic cell bodies and synapses in *Drosophila* larval and adult CNS. *Journal of Comparative Neurology*, *508*(1), 131–152.

Das, A., Chiang, A., Davla, S., Priya, R., Reichert, H., VijayRaghavan, K., & Rodrigues, V. (2011a). Identification and analysis of a glutamatergic local interneuron lineage in the adult *Drosophila* olfactory system. *Neural Systems & Circuits*, *1*(1), 4.

Das, S., Sadanandappa, M. K., Dervan, A., Larkin, A., Lee, J. A., Sudhakaran, I. P., Priya, R., Heidari, R., Holohan, E. E., Pimentel, A., Gandhi, A., Ito, K., Sanyal, S., Wang, J. W., Rodrigues, V., & Ramaswamia, M. (2011b). Plasticity of local GABAergic interneurons drives olfactory habituation. *Proceedings of the National Academy of Sciences of the United States of America*, *108*(36), E646–E654.

Davie, K., Janssens, J., Koldere, D., De Waegeneer, M., Pech, U., Kreft, Ł., Aibar, S., Makhzami, S., Christiaens, V., Bravo González-Blas, C., Poovathingal, S., Hulselmans, G., Spanier, K. I., Moerman, T., Vanspauwen, B., Geurs, S., Voet, T., Lammertyn, J., Thienpont, B., … Aerts, S. (2018). A single-cell transcriptome atlas of the aging *Drosophila* brain. *Cell*, *174*(4), 982-998.e20.

Davis, F. P., Nern, A., Picard, S., Reiser, M. B., Rubin, G. M., Eddy, S. R., & Henry, G. L. (2020). A genetic, genomic, and computational resource for exploring neural circuit function. *eLife*, *9*.

Davis, R. L. (2004). Olfactory learning. *Neuron*, Vol. 44, Issue 1, pp. 31–48.

Deng, B., Li, Q., Liu, X., Cao, Y., Li, B., Qian, Y., Xu, R., Mao, R., Zhou, E., Zhang, W., Huang, J., & Rao, Y. (2019). Chemoconnectomics: mapping chemical transmission in *Drosophila*. *Neuron*, *101*(5), 876-893.e4.

Diao, F., Ironfield, H., Luan, H., Diao, F., Shropshire, W. C., Ewer, J., Marr, E., Potter, C. J., Landgraf, M., & White, B. H. (2015). Plug-and-play genetic access to *Drosophila* cell types using exchangeable exon cassettes. *Cell Reports*, *10*(8), 1410–1421.

Dietzl, G., Chen, D., Schnorrer, F., Su, K. C., Barinova, Y., Fellner, M., Gasser, B., Kinsey, K., Oppel, S., Scheiblauer, S., Couto, A., Marra, V., Keleman, K., & Dickson, B. J. (2007). A genome-wide transgenic RNAi library for conditional gene inactivation in *Drosophila*. *Nature*, *448*(7150), 151–156.

Drews, M. S., Leonhardt, A., Pirogova, N., Richter, F. G., Schuetzenberger, A., Braun, L., Serbe, E., & Borst, A. (2020). Dynamic signal compression for

robust motion vision in flies. *Current Biology*, *30*(2), 209-221.e8.

Dvorak, D. R., Bishop, L. G., & Eckert, H. E. (1975). On the identification of movement detectors in the fly optic lobe. *Journal of Comparative Physiology*, *100*(1), 5–23.

Ecker, J. R., Geschwind, D. H., Kriegstein, A. R., Ngai, J., Osten, P., Polioudakis, D., Regev, A., Sestan, N., Wickersham, I. R., & Zeng, H. (2017). The BRAIN initiative cell census consortium: lessons learned toward generating a comprehensive brain cell atlas. *Neuron*, Vol. 96, Issue 3, pp. 542–557).

Eckstein, N., Bates, A. S., Du, M., Hartenstein, V., Jefferis, G. S. X. E., & Funke, J. (2020). Neurotransmitter classification from electron microscopy images at synaptic sites in *Drosophila*. *bioRxiv*, 2020.06.12.148775.

El-Kholy, S., Stephano, F., Li, Y., Bhandari, A., Fink, C., & Roeder, T. (2015). Expression analysis of octopamine and tyramine receptors in *Drosophila*. *Cell and Tissue Research*, *361*(3), 669–684.

Elstrott, J., Anishchenko, A., Greschner, M., Sher, A., Litke, A. M., Chichilnisky, E. J., & Feller, M. B. (2008). Direction selectivity in the retina is established independent of visual experience and cholinergic retinal waves. *Neuron*, *58*(4), 499–506.

Emrich, S. J., Barbazuk, W. B., Li, L., & Schnable, P. S. (2007). Gene discovery and annotation using LCM-454 transcriptome sequencing. *Genome Research*, *17*(1), 69–73.

Euler, T., Detwiler, P. B., & Denk, W. (2002). Directionally selective calcium signals in dendrites of starburst amacrine cells. *Nature*, *418*(6900), 845–852.

Euler, T., Haverkamp, S., Schubert, T., & Baden, T. (2014). Retinal bipolar cells: Elementary building blocks of vision. *Nature Reviews Neuroscience*, Vol. 15, Issue 8, pp. 507–519.

Famiglietti, E. V. (1983). "Starburst" amacrine cells and cholinergic neurons: mirror-symmetric ON and OFF amacrine cells of rabbit retina. *Brain Research*, *261*(1), 138–144.

Fayyazuddin, A., Zaheer, M. A., Hiesinger, P. R., & Bellen, H. J. (2006). The nicotinic acetylcholine receptor Dα7 is required for an escape behavior in *Drosophila*. *PLoS Biology*, *4*(3), e63.

Featherstone, D. E., Rushton, E. M., Hilderbrand-Chae, M., Phillips, A. M., Jackson, F. R., & Broadie, K. (2000). Presynaptic glutamic acid decarboxylase is required for induction of the postsynaptic receptor field at a glutamatergic synapse. *Neuron*, *27*(1), 71–84.

Fei, H., Chow, D. M., Chen, A., Romero-Calderón, R., Ong, W. S., Ackerson, L. C., Maidment, N. T., Simpson, J. H., Frye, M. A., & Krantz, D. E. (2010). Mutation of the *Drosophila* vesicular GABA transporter disrupts visual figure detection. *Journal of Experimental Biology*, *213*(10), 1717–1730.

Feinberg, E. H., VanHoven, M. K., Bendesky, A., Wang, G., Fetter, R. D., Shen, K., & Bargmann, C. I. (2008). GFP reconstitution across synaptic partners (GRASP) defines cell contacts and synapses in living nervous systems. *Neuron*, *57*(3), 353–363.

Fendl, S., Pujol-Martí, J., Ryan, J., Borst, A., & Kasper, R. (2017). STED imaging in *Drosophila* brain slices. *Methods in Molecular Biology (Clifton, N.J.)*, *1563*, 143–150.

Fendl, S., Vieira, R. M., & Borst, A. (2020). Conditional protein tagging methods

reveal highly specific subcellular distribution of ion channels in motion-sensing neurons. *eLife*, *9*.

Ffrench-Constant, R. H., Mortlock, D. P., Shaffer, C. D., MacIntyre, R. J., & Roush, R. T. (1991b). Molecular cloning and transformation of cyclodiene resistance in *Drosophila*: An invertebrate γ-aminobutyric acid subtype A receptor locus. *Proceedings of the National Academy of Sciences of the United States of America*, *88*(16), 7209–7213.

Ffrench-Constant, R. H., & Rocheleau, T. (1992). *Drosophila* cyclodiene Resistance gene shows conserved genomic organization with vertebrate gamma-aminobutyric acid receptors. *Journal of Neurochemistry*, *59*(4), 1562–1565.

Ffrench-Constant, R. H., & Roush, R. T. (1991a). Gene mapping and cross-resistance in cyclodiene insecticide-resistant *Drosophila melanogaster* (Mg.). *Genetical Research*, *57*(1), 17–21.

Ffrench-Constant, Richard H., Rocheleau, T. A., Steichen, J. C., & Chalmers, A. E. (1993). A point mutation in a *Drosophila* GABA receptor confers insecticide resistance. *Nature*, *363*(6428), 449–451.

Fisher, Y. E., Leong, J. C. S., Sporar, K., Ketkar, M. D., Gohl, D. M., Clandinin, T. R., & Silies, M. (2015a). A class of visual neurons with wide-field properties is required for local motion detection. *Current Biology*, *25*(24), 3178–3189.

Fisher, Y. E., Silies, M., & Clandinin, T. R. (2015b). Orientation selectivity sharpens motion detection in *Drosophila*. *Neuron*, *88*(2), 390–402.

Fisher, Y. E., Yang, H. H., Isaacman-Beck, J., Xie, M., Gohl, D. M., & Clandinin, T. R. (2017). FlpStop, a tool for conditional gene control in *Drosophila*. *eLife*, *6*.

Franke, K., Berens, P., Schubert, T., Bethge, M., Euler, T., & Baden, T. (2017). Inhibition decorrelates visual feature representations in the inner retina. *Nature*, *542*(7642), 439–444.

Fritschy, J.-M. (2008). Is my antibody-staining specific? How to deal with pitfalls of immunohistochemistry. *European Journal of Neuroscience*, *28*(12), 2365–2370.

Frolov, R. V., Bagati, A., Casino, B., & Singh, S. (2012). Potassium channels in *Drosophila*: Historical breakthroughs, significance, and perspectives. In *Journal of Neurogenetics,* Vol. 26, Issues 3–4, pp. 275–290.

Gengs, C., Leung, H. T., Skingsley, D. R., Iovchev, M. I., Yin, Z., Semenov, E. P., Burg, M. G., Hardie, R. C., & Pak, W. L. (2002). The target of *Drosophila* photoreceptor synaptic transmission is a histamine-gated chloride channel encoded by ort (hclA). *Journal of Biological Chemistry*, *277*(44), 42113–42120.

George, M. S., Abbott, L. F., & Siegelbaum, S. A. (2009). HCN hyperpolarization-activated cation channels inhibit EPSPs by interactions with M-type K+ channels. *Nature Neuroscience*, *12*(5), 577–584.

Gisselmann, G., Pusch, H., Hovemann, B. T., & Hatt, H. (2002). Two cDNAS coding for histamine-gated ion channels in *D. melanogaster*. *Nature Neuroscience*, *5*(1), 11–12. https://doi.org/10.1038/nn787

Gisselmann, Günter, Gamerschlag, B., Sonnenfeld, R., Marx, T., Neuhaus, E. M., Wetzel, C. H., & Hatt, H. (2005). Variants of the *Drosophila melanogaster* Ih-channel are generated by different splicing. *Insect Biochemistry and Molecular Biology*, *35*(5), 505–514.

Gisselmann, Günter, Plonka, J., Pusch, H., & Hatt, H. (2004). *Drosophila melanogaster* GRD and LCCH3 subunits form heteromultimeric GABA-gated cation channels. *British Journal of Pharmacology*, *142*(3), 409–413.

Gisselmann, Günter, Wetzel, C. H., Warnstedt, M., & Hatt, H. (2004). Functional characterization of Ih-channel splice variants from *Apis mellifera*. *FEBS Letters*, *575*(1–3), 99–104.

Gjorgjieva, J., Sompolinsky, H., & Meister, M. (2014). Benefits of pathway splitting in sensory coding. *Journal of Neuroscience*, *34*(36), 12127–12144.

Gonzalo-Gomez, A., Turiegano, E., León, Y., Molina, I., Torroja, L., & Canal, I. (2012). Ih current is necessary to maintain normal Dopamine fluctuations and sleep consolidation in *Drosophila*. *PLoS ONE*, *7*(5), e36477.

Greenbaum, D., Colangelo, C., Williams, K., & Gerstein, M. (2003). Comparing protein abundance and mRNA expression levels on a genomic scale. *Genome Biology*, Vol. 4, Issue 9, p. 117.

Greenspan, R. J. (1980). Mutations of choline acetyltransferase and associated neural defects. *Journal of Comparative Physiology*, *137*(1), 83–92.

Gruntman, E., Romani, S., & Reiser, M. B. (2018). Simple integration of fast excitation and offset, delayed inhibition computes directional selectivity in *Drosophila*. *Nature Neuroscience*, *21*(2), 250–257.

Gruntman, E., Romani, S., & Reiser, M. B. (2019). The computation of directional selectivity in the *Drosophila* off motion pathway. *eLife*, *8*.

Gschweng, K. M. M., Sampson, M. M., Hardcastle, B. J., Sizemore, T. R., Dacks, A. M., Frye, M. A., & Krantz, D. E. (2019). Serotonergic modulation of a visual microcircuit in *Drosophila melanogaster*. *bioRxiv*, 619759.

Haag, J., Arenz, A., Serbe, E., Gabbiani, F., & Borst, A. (2016). Complementary mechanisms create direction selectivity in the fly. *eLife*, *5*.

Haag, J., Mishra, A., & Borst, A. (2017). A common directional tuning mechanism of *Drosophila* motion-sensing neurons in the ON and in the OFF pathway. *eLife*, *6*, 1–15.

Hamada, F. N., Rosenzweig, M., Kang, K., Pulver, S. R., Ghezzi, A., Jegla, T. J., & Garrity, P. A. (2008). An internal thermal sensor controlling temperature preference in *Drosophila*. *Nature*, *454*(7201), 217–220.

Hamasaka, Y., Rieger, D., Parmentier, M.-L., Grau, Y., Helfrich-Förster, C., & Nässel, D. R. (2007). Glutamate and its metabotropic receptor in *Drosophila* clock neuron circuits. *The Journal of Comparative Neurology*, *505*(1), 32–45.

Hamasaka, Y., Wegener, C., & Nässel, D. R. (2005). GABA modulates *Drosophila* circadian clock neurons via GABAB receptors and decreases in calcium. *Journal of Neurobiology*, *65*(3), 225–240.

Hardie, R. C. (1989). A histamine-activated chloride channel involved in neurotransmission at a photoreceptor synapse. *Nature*, *339*(6227), 704–706.

Harrison, J. B., Chen, H. H., Sattelle, E., Barker, P. J., Huskisson, N. S., Rauh, J. J., Bai, D., & Sattelle, D. B. (1996). Immunocytochemical mapping of a C-terminus anti-peptide antibody to the GABA receptor subunit, RDL in the nervous system of *Drosophila melanogaster*. *Cell and Tissue Research*, *284*(2), 269–278.

Hearn, M. G., Ren, Y., McBride, E. W., Reveillaud, I., Beinborn, M., & Kopin, A. S. (2002). A *Drosophila* dopamine 2-like receptor: Molecular characterization and identification of multiple alternatively spliced variants. *Proceedings of the*

National Academy of Sciences of the United States of America, *99*(22), 14554–14559.

Hegle, A. P., Frank, C. A., Berndt, A., Klose, M., Allan, D. W., & Accili, E. A. (2017). The Ih channel gene promotes synaptic transmission and coordinated movement in *Drosophila melanogaster*. *Frontiers in Molecular Neuroscience*, *10*, 41.

Heidenreich, M., & Zhang, F. (2016). Applications of CRISPR-Cas systems in neuroscience. *Nature Reviews Neuroscience*, Vol. 17, Issue 1, pp. 36–44.

Heisenberg, M., & Buchner, E. (1977). The role of retinula cell types in visual behavior of *Drosophila melanogaster*. *Journal of Comparative Physiology*, *117*(2), 127–162.

Hodgkin, A. L., & Huxley, A. F. (1939). Action potentials recorded from inside a nerve fibre. *Nature*, Vol. 144, Issue 3651, pp. 710–711.

Hodgkin, A. L., & Huxley, A. F. (1945). Resting and action potentials in single nerve fibres. *The Journal of Physiology*, *104*(2), 176–195.

Hodgkin, A. L., & Huxley, A. F. (1952). Propagation of electrical signals along giant nerve fibers. *Proceedings of the Royal Society of London. Series B, Containing Papers of a Biological Character. Royal Society (Great Britain)*, *140*(899), 177–183.

Hoermann, N., Schilling, T., Haji Ali, A., Serbe, E., Mayer, C., Borst, A., & Pujol-Martí, J. (2020). A combinatorial code of transcription factors specifies subtypes of visual motion-sensing neurons in *Drosophila* . *Development*, dev.186296.

Hosie, A. M., Aronstein, K., Sattelle, D. B., & Ffrench-Constant, R. H. (1997). Molecular biology of insect neuronal GABA receptors. *Trends in Neuroscience,* Vol. 20, Issue 12, pp. 578–583.

Hosie, A. M., & Sattelle, D. B. (1996). Agonist pharmacology of two *Drosophila* GABA receptor splice variants. *British Journal of Pharmacology*, *119*(8), 1577–1585.

Hu, W., Wang, T., Wang, X., & Han, J. (2015). Ih channels control feedback regulation from amacrine cells to photoreceptors. *PLOS Biology*, *13*(4), e1002115.

Hubel, D. H., & Wiesel, T. N. (1959). Receptive fields of single neurones in the cat's striate cortex. *The Journal of Physiology*, *148*(3), 574–591.

Iniguez, J., Schutte, S. S., & O'Dowd, D. K. (2013). Ca_v 3-type α1T calcium channels mediate transient calcium currents that regulate repetitive firing in *Drosophila* antennal lobe PNs. *Journal of Neurophysiology*, *110*(7), 1490–1496.

Ishimoto, H., Wang, Z., Rao, Y., Wu, C. F., & Kitamoto, T. (2013). A novel role for ecdysone in *Drosophila* conditioned behavior: Linking GPCR-mediated non-canonical steroid action to cAMP signaling in the adult brain. *PLoS Genetics*, *9*(10).

Jackson, F. R., Newby, L. M., & Kulkarni, S. J. (1990). *Drosophila* GABAergic systems: Sequence and expression of glutamic acid decarboxylase. *Journal of Neurochemistry*, *54*(3), 1068–1078.

Jenett, A., Rubin, G. M., Ngo, T. T. B., Shepherd, D., Murphy, C., Dionne, H., Pfeiffer, B. D., Cavallaro, A., Hall, D., Jeter, J., Iyer, N., Fetter, D., Hausenfluck, J. H., Peng, H., Trautman, E. T., Svirskas, R. R., Myers, E. W.,

Iwinski, Z. R., Aso, Y., … Zugates, C. T. (2012). A GAL4-driver line Resource for *Drosophila* neurobiology. *Cell Reports*, *2*(4), 991–1001.

Jing, M., Zhang, P., Wang, G., Feng, J., Mesik, L., Zeng, J., Jiang, H., Wang, S., Looby, J. C., Guagliardo, N. A., Langma, L. W., Lu, J., Zuo, Y., Talmage, D. A., Role, L. W., Barrett, P. Q., Zhang, L. I., Luo, M., Song, Y., … Li, Y. (2018). A genetically encoded fluorescent acetylcholine indicator for in vitro and in vivo studies. *Nature Biotechnology*, *36*(8).

Joesch, M., Schnell, B., Raghu, S. V., Reiff, D. F., & Borst, A. (2010). ON and OFF pathways in *Drosophila* motion vision. *Nature*, *468*(7321), 300–304.

Jung, S. N., Borst, A., & Haag, J. (2011). Flight activity alters velocity tuning of fly motion-sensitive neurons. *Journal of Neuroscience*, *31*(25), 9231–9237.

Kamb, A., Iverson, L. E., & Tanouye, M. A. (1987). Molecular characterization of Shaker, a *Drosophila* gene that encodes a potassium channel. *Cell*, *50*(3), 405–413.

Kaneko, T., Macara, A. M., Li, R., Hu, Y., Iwasaki, K., Dunnings, Z., Firestone, E., Horvatic, S., Guntur, A., Shafer, O. T., Yang, C. H., Zhou, J., & Ye, B. (2017). Serotonergic modulation enables pathway-specific plasticity in a developing sensory circuit in *Drosophila*. *Neuron*, *95*(3), 623-638.e4.

Kasture, A. S., Hummel, T., Sucic, S., & Freissmuth, M. (2018). Big lessons from tiny flies: *Drosophila melanogaster* as a model to explore dysfunction of dopaminergic and serotonergic neurotransmitter systems. *International Journal of Molecular Sciences,* Vol. 19, Issue 6.

Ki, Y., & Lim, C. (2019). Sleep-promoting effects of threonine link amino acid metabolism in *Drosophila* neuron to GABAergic control of sleep drive. *eLife*, *8*.

Kim, J. S., Greene, M. J., Zlateski, A., Lee, K., Richardson, M., Turaga, S. C., Purcaro, M., Balkam, M., Robinson, A., Behabadi, B. F., Campos, M., Denk, W., & Seung, H. S. (2014). Space-time wiring specificity supports direction selectivity in the retina. *Nature*, *509*(7500), 331–336.

Kimmerling, R. J., Lee Szeto, G., Li, J. W., Genshaft, A. S., Kazer, S. W., Payer, K. R., De Riba Borrajo, J., Blainey, P. C., Irvine, D. J., Shalek, A. K., & Manalis, S. R. (2016). A microfluidic platform enabling single-cell RNA-seq of multigenerational lineages. *Nature Communications*, *7*(1), 1–7.

Kitamoto, T. (2001). Conditional modification of behavior in *Drosophila* by targeted expression of a temperature-sensitiveshibire allele in defined neurons. *Journal of Neurobiology*, *47*(2), 81–92.

Kitamoto, T., Wang, W., & Salvaterra, P. M. (1998). Structure and organization of the *Drosophila* cholinergic locus. *Journal of Biological Chemistry*, *273*(5), 2706–2713.

Klapoetke, N. C., Murata, Y., Kim, S. S., Pulver, S. R., Birdsey-Benson, A., Cho, Y. K., Morimoto, T. K., Chuong, A. S., Carpenter, E. J., Tian, Z., Wang, J., Xie, Y., Yan, Z., Zhang, Y., Chow, B. Y., Surek, B., Melkonian, M., Jayaraman, V., Constantine-Paton, M., … Boyden, E. S. (2014). Independent optical excitation of distinct neural populations. *Nature Methods*, *11*(3), 338–346.

Klar, T. A., Jakobs, S., Dyba, M., Egner, A., & Hell, S. W. (2000). Fluorescence microscopy with diffraction resolution barrier broken by stimulated emission. *Proceedings of the National Academy of Sciences of the United States of America*, *97*(15), 8206–8210.

Koch, C. (1999). Biophysics of Computation: Information Processing in Single Neurons. *Oxford University Press*. SBN-10 : 0195181999.

Kolodziejczyk, A., Sun, X., Meinertzhagen, I. A., & Nässel, D. R. (2008). Glutamate, GABA and acetylcholine signaling components in the lamina of the *Drosophila* visual system. *PLoS ONE*, *3*(5).

Kondo, S., Takahashi, T., Yamagata, N., Imanishi, Y., Katow, H., Hiramatsu, S., Lynn, K., Abe, A., Kumaraswamy, A., & Tanimoto, H. (2020). Neurochemical organization of the *Drosophila* brain visualized by endogenously tagged neurotransmitter receptors. *Cell Reports*, *30*(1), 284-297.e5.

Konstantinides, N., Fadil, C., Barboza, L., Satija, R., Desplan, C., & Kapuralin, K. (2018). Phenotypic convergence: Distinct transcription factors regulate common terminal features. *Cell*, *174*(3), 622-635.e13.

Kuehn, C., & Duch, C. (2013). Putative excitatory and putative inhibitory inputs are localised in different dendritic domains in a *Drosophila* flight motoneuron. *European Journal of Neuroscience*, *37*(6), 860–875.

Kurmangaliyev, Y. Z., Yoo, J., Locascio, S. A., & Lawrence Zipursky, S. (2019). Modular transcriptional programs separately define axon and dendrite connectivity. *eLife*, *8*.

Lansdell, S. J., Collins, T., Goodchild, J., & Millar, N. S. (2012). The *Drosophila* nicotinic acetylcholine receptor subunits Dα5 and Dα7 form functional homomeric and heteromeric ion channels. *BMC Neuroscience*, *13*(1), 73.

Lansdell, S. J., & Millar, N. S. (2004). Molecular characterization of Dα6 and Dα7 nicotinic acetylcholine receptor subunits from *Drosophila*: Formation of a high-affinity α-bungarotoxin binding site revealed by expression of subunit chimeras. *Journal of Neurochemistry*, *90*(2), 479–489.

Lee, P. T., Zirin, J., Kanca, O., Lin, W. W., Schulze, K. L., Li-Kroeger, D., Tao, R., Devereaux, C., Hu, Y., Chung, V., Fang, Y., He, Y., Pan, H., Ge, M., Zuo, Z., Housden, B. E., Mohr, S. E., Yamamoto, S., Levis, R. W., … Bellen, H. J. (2018). A gene-specific T2A-GAL4 library for *Drosophila*. *eLife*, *7*.

Leong, J. C. S., Esch, J. J., Poole, B., Ganguli, S., & Clandinin, T. R. (2016). Direction selectivity in *Drosophila* emerges from preferred-direction enhancement and null-direction suppression. *Journal of Neuroscience*, *36*(31), 8078–8092.

Lettvin, J. Y., Maturana, H. R., Maturana, H. R., Mcculloch, W. S., & Pitts, W. H. (1959). What the frog's eye tells the frog's brain. *Proceedings of the IRE*, *47*(11), 1940–1951.

Lima, S. Q., & Miesenböck, G. (2005). Remote control of behavior through genetically targeted photostimulation of neurons. *Cell*, *121*(1), 141–152.

Lin, J. Y., Knutsen, P. M., Muller, A., Kleinfeld, D., & Tsien, R. Y. (2013). ReaChR: A red-shifted variant of channelrhodopsin enables deep transcranial optogenetic excitation. *Nature Neuroscience*, *16*(10), 1499–1508.

Liu, W. W., & Wilson, R. I. (2013). Glutamate is an inhibitory neurotransmitter in the *Drosophila* olfactory system. *Proceedings of the National Academy of Sciences*, *110*(25), 10294–10299.

Liu, X., Krause, W. C., & Davis, R. L. (2007). GABAA Receptor RDL Inhibits *Drosophila* Olfactory Associative Learning. *Neuron*, *56*(6), 1090–1102.

Long, X., Colonell, J., Wong, A. M., Singer, R. H., & Lionnet, T. (2017). Quantitative mRNA imaging throughout the entire *Drosophila* brain. *Nature*

Methods, *14*(7), 703–706.

Longden, K. D., & Krapp, H. G. (2010). Octopaminergic modulation of temporal frequency coding in an identified optic flow-processing interneuron. *Frontiers in Systems Neuroscience*, *4*, 153.

Loughney, K., Kreber, R., & Ganetzky, B. (1989). Molecular analysis of the para locus, a sodium channel gene in *Drosophila*. *Cell*, *58*(6), 1143–1154.

Luo, J., Becnel, J., Nichols, C. D., & Nässel, D. R. (2012). Insulin-producing cells in the brain of adult *Drosophila* are regulated by the serotonin 5-HT 1A receptor. *Cellular and Molecular Life Sciences*, *69*(3), 471–484.

Luo, J., Ting, C. Y., Li, Y., McQueen, P., Lin, T. Y., Hsu, C. P., & Lee, C. H. (2020). Antagonistic regulation by insulin-like peptide and activin ensures the elaboration of appropriate dendritic field sizes of amacrine neurons. *eLife*, *9*.

Ma, Y., Creanga, A., Lum, L., & Beachy, P. A. (2006). Prevalence of off-target effects in *Drosophila* RNA interference screens. *Nature*, *443*(7109), 359–363.

Magee, J. C. (1999). Dendritic I(h) normalizes temporal summation in hippocampal CA1 neurons. *Nature Neuroscience*, *2*(6), 508–514.

Mahr, A., & Aberle, H. (2006). The expression pattern of the *Drosophila* vesicular glutamate transporter: A marker protein for motoneurons and glutamatergic centers in the brain. *Gene Expression Patterns*, *6*(3), 299–309.

Maisak, M. S., Haag, J., Ammer, G., Serbe, E., Meier, M., Leonhardt, A., Schilling, T., Bahl, A., Rubin, G. M., Nern, A., Dickson, B. J., Reiff, D. F., Hopp, E., & Borst, A. (2013). A directional tuning map of *Drosophila*. *Nature*, *500*, 212–216.

Majeed, ZR., Abdeljaber, E., Soveland, R., Cornwell, K., Bankemper, Koch, F., & Cooper, RL. (2016). Modulatory Action by the Serotonergic System: Behavior and Neurophysiology in *Drosophila Melanogaster*. *Neural Plasticity*, *2016*.

Marvin, J. S., Borghuis, B. G., Tian, L., Cichon, J., Harnett, M. T., Akerboom, J., Gordus, A., Renninger, S. L., Chen, T. W., Bargmann, C. I., Orger, M. B., Schreiter, E. R., Demb, J. B., Gan, W. B., Hires, S. A., & Looger, L. L. (2013). An optimized fluorescent probe for visualizing glutamate neurotransmission. *Nature Methods*, *10*(2), 162–170.

Marvin, J. S., Shimoda, Y., Magloire, V., Leite, M., Kawashima, T., Jensen, T. P., Kolb, I., Knott, E. L., Novak, O., Podgorski, K., Leidenheimer, N. J., Rusakov, D. A., Ahrens, M. B., Kullmann, D. M., & Looger, L. L. (2019). A genetically encoded fluorescent sensor for in vivo imaging of GABA. *Nature Methods*, *16*(8), 763–770.

Masu, M., Iwakabe, H., Tagawa, Y., Miyoshi, T., Yamashita, M., Fukuda, Y., Sasaki, H., Hiroi, K., Nakamura, Y., Shigemoto, R., Takada, M., Nakamura, K., Nakao, K., Katsuki, M., & Nakanishi, S. (1995). Specific deficit of the ON response in visual transmission by targeted disruption of the mGIuR6 gene. *Cell*, *80*(5), 757–765.

Mauss, A. S., Meier, M., Serbe, E., & Borst, A. (2014). Optogenetic and pharmacologic dissection of feedforward inhibition in *Drosophila* motion vision. *Journal of Neuroscience*, *34*(6), 2254–2263.

Mauss, Alex S., & Borst, A. (2020). Optic flow-based course control in insects. *Current Opinion in Neurobiology*, Vol. 60, pp. 21–27.

Mauss, Alex S., Busch, C., & Borst, A. (2017). Optogenetic neuronal silencing in *Drosophila* during visual processing. *Scientific Reports*, *7*(1).

Mauss, Alex S., Pankova, K., Arenz, A., Nern, A., Rubin, G. M., & Borst, A. (2015). Neural circuit to integrate opposing motions in the visual field. *Cell*, *162*(2), 351–362.

McCormick, D. A. (1991). Functional properties of a slowly inactivating potassium current in guinea pig dorsal lateral geniculate relay neurons. *Journal of Neurophysiology*, *66*(4), 1176–1189.

Meier, M., Serbe, E., Maisak, M. S., Haag, J., Dickson, B. J., & Borst, A. (2014). Neural circuit components of the *Drosophila* off motion vision pathway. *Current Biology*, *24*(4), 385–392.

Meissner, G. W., Aljoschanern, Singer, R. H., Wong, A. M., Malkesman, O., & Long, X. (2019). Mapping neurotransmitter identity in the whole-mount *Drosophila* brain using multiplex high-throughput fluorescence in situ hybridization. *Genetics*, *211*(2), 473–482.

Mezler, M., Müller, T., & Raming, K. (2001). Cloning and functional expression of $GABA_B$ receptors from *Drosophila*. *European Journal of Neuroscience*, *13*(3), 477–486.

Millar, N. S., Baylis, H. A., Reaper, C., Bunting, R., Mason, W. T., & Sattelle, D. B. (1995). Functional expression of a cloned *Drosophila* muscarinic acetylcholine receptor in a stable *Drosophila* cell line. *Journal of Experimental Biology*, *198*(9).

Mirzoyan, Z., Sollazzo, M., Allocca, M., Valenza, A. M., Grifoni, D., & Bellosta, P. (2019). *Drosophila melanogaster*: A model organism to study cancer. *Frontiers in Genetics,* Vol. 10, p. 51.

Molina-Obando, S., Vargas-Fique, J. F., Henning, M., Gür, B., Schlad, T. M., Akhtar, J., Berger, T. K., & Silies, M. (2019). On selectivity in the *Drosophila* visual system is a multisynaptic process involving both glutamatergic and GABAergic inhibition. *eLife*, *8*.

Morgan, T. H., & Cattell, E. (1912). Data for the study of sex-linked inheritance in *Drosophila*. *Journal of Experimental Zoology*, *13*(1), 79–101.

Mosca, T. J., & Luo, L. (2014). Synaptic organization of the *Drosophila* antennal lobe and its regulation by the Teneurins. *eLife*, *3*, e03726.

Nagarkar-Jaiswal, S., Lee, P. T., Campbell, M. E., Chen, K., Anguiano-Zarate, S., Gutierrez, M. C., Busby, T., Lin, W. W., He, Y., Schulze, K. L., Booth, B. W., Evans-Holm, M., Venken, K. J. T., Levis, R. W., Spradling, A. C., Hoskins, R. A., & Bellen, H. J. (2015). A library of MiMICs allows tagging of genes and reversible, spatial and temporal knockdown of proteins in *Drosophila*. *eLife*, *2015*(4).

Nagel, G., Szellas, T., Huhn, W., Kateriya, S., Adeishvili, N., Berthold, P., Ollig, D., Hegemann, P., & Bamberg, E. (2003). Channelrhodopsin-2, a directly light-gated cation-selective membrane channel. *Proceedings of the National Academy of Sciences of the United States of America*, *100*, 13940–13945.

Nakai, J., Ohkura, M., & Imoto, K. (2001). A high signal-to-noise Ca2+ probe composed of a single green fluorescent protein. *Nature Biotechnology*, *19*(2), 137–141.

Nern, A., Pfeiffer, B. D., & Rubin, G. M. (2015). Optimized tools for multicolor stochastic labeling reveal diverse stereotyped cell arrangements in the fly visual system. *Proceedings of the National Academy of Sciences of the United States of America*, *112*(22), E2967–E2976.

Nitz, D. A., Van Swinderen, B., Tononi, G., & Greenspan, R. J. (2002). Electrophysiological correlates of rest and activity in *Drosophila melanogaster*. *Current Biology*, *12*(22), 1934–1940.

Olsen, S. R., & Wilson, R. I. (2008). Lateral presynaptic inhibition mediates gain control in an olfactory circuit. *Nature*, *452*(7190), 956–960. https://doi.org/10.1038/nature06864

Oyster, C. W., & Barlow, H. B. (1967). Direction-selective units in rabbit retina: Distribution of preferred directions. *Science*, *155*(3764), 841–842.

Palmer, E., & Freeman, T. (2004). Investigation into the use of C-and N-terminal GFP fusion proteins for subcellular localization studies using reverse transfection microarrays. *Comparative and Functional Genomics Comp Funct Genom*, *5*, 342–353.

Pankova, K., & Borst, A. (2016). RNA-Seq transcriptome analysis of direction-selective T4/T5 neurons in *Drosophila*. *PLOS ONE*, *11*(9), e0163986.

Pankova, K., & Borst, A. (2017). Transgenic line for the identification of cholinergic release sites in *Drosophila melanogaster*. *The Journal of Experimental Biology*, *220*(Pt 8), 1405–1410.

Patriarchi, T., Cho, J. R., Merten, K., Howe, M. W., Marley, A., Xiong, W. H., Folk, R. W., Broussard, G. J., Liang, R., Jang, M. J., Zhong, H., Dombeck, D., von Zastrow, M., Nimmerjahn, A., Gradinaru, V., Williams, J. T., & Tian, L. (2018). Ultrafast neuronal imaging of dopamine dynamics with designed genetically encoded sensors. *Science*, *360*(6396).

Perkins, L. A., Holderbaum, L., Tao, R., Hu, Y., Sopko, R., McCall, K., Yang-Zhou, D., Flockhart, I., Binari, R., Shim, H. S., Miller, A., Housden, A., Foos, M., Randkelv, S., Kelley, C., Namgyal, P., Villalta, C., Liu, L. P., Jiang, X., … Perrimon, N. (2015). The transgenic RNAi project at Harvard medical school: Resources and validation. *Genetics*, *201*(3), 843–852.

Pfeiffer, B. D., Jenett, A., Hammonds, A. S., Ngo, T. T. B., Misra, S., Murphy, C., Scully, A., Carlson, J. W., Wan, K. H., Laverty, T. R., Mungall, C., Svirskas, R., Kadonaga, J. T., Doe, C. Q., Eisen, M. B., Celniker, S. E., & Rubin, G. M. (2008). Tools for neuroanatomy and neurogenetics in *Drosophila*. *Proceedings of the National Academy of Sciences of the United States of America*, *105*(28), 9715–9720.

Pfeiffer, B. D., Ngo, T. T. B., Hibbard, K. L., Murphy, C., Jenett, A., Truman, J. W., & Rubin, G. M. (2010). Refinement of tools for targeted gene expression in *Drosophila*. *Genetics*, *186*(2), 735–755.

Philip M. Borden, et al. (2020). A fast genetically encoded fluorescent sensor for faithful. *biorxiv*, 2020.02.07.939504.

Piggott, B. J., Peters, C. J., He, Y., Huang, X., Younger, S., Jan, L. Y., & Jan, Y. N. (2019). Paralytic, the *Drosophila* voltage-gated sodium channel, regulates proliferation of neural progenitors. *Genes & Development*, *33*(23–24), 1739–1750.

Port, F., Chen, H. M., Lee, T., & Bullock, S. L. (2014). Optimized CRISPR/Cas tools for efficient germline and somatic genome engineering in *Drosophila*. *Proceedings of the National Academy of Sciences of the United States of America*, *111*(29), E2967–E2976.

Port, F., Strein, C., Stricker, M., Rauscher, B., Heigwer, F., Zhou, J., Beyersdörffer, C., Frei, J., Hess, A., Kern, K., Lange, L., Langner, N., Malamud, R., Pavlović,

B., Rädecke, K., Schmitt, L., Voos, L., Valentini, E., & Boutros, M. (2020). A large-scale resource for tissue-specific CRISPR mutagenesis in *Drosophila*. *eLife*, *9*.

Porter, J. R., Telford, W. G., & Batchelor, E. (2017). Single-cell gene expression profiling using FACS and qPCR with internal standards. *Journal of Visualized Experiments*, *2017*(120).

Purves, D., Augustine, G. J., Fitzpatrick, D., Katz, L. C., LaMantia, A.-S., McNamara, J. O., & Williams, S. M. (2001). Electrical Synapses. https://www.ncbi.nlm.nih.gov/books/NBK11164/

Qin, B., Humberg, T. H., Kim, A., Kim, H. S., Short, J., Diao, F., White, B. H., Sprecher, S. G., & Yuan, Q. (2019). Muscarinic acetylcholine receptor signaling generates OFF selectivity in a simple visual circuit. *Nature Communications*, *10*(1), 1–16.

Raghu, S. V., & Borst, A. (2011). Candidate glutamatergic neurons in the visual system of *Drosophila*. *PLoS ONE*, *6*(5), 1–11.

Raghu, S. V., Joesch, M., Borst, A., & Reiff, D. F. (2007). Synaptic organization of lobula plate tangential cells in *Drosophila* : γ-Aminobutyric acid receptors and chemical release sites. *The Journal of Comparative Neurology*, *502*(4), 598–610.

Raghu, S. V., Joesch, M., Sigrist, S. J., Borst, A., & Reiff, D. F. (2009). Synaptic organization of lobula plate tangential cells in *Drosophila*: Dα7 cholinergic receptors. *Journal of Neurogenetics*, *23*(1–2), 200–209.

Ranson, D. C., Ayoub, S. S., Corcoran, O., & Casalotti, S. O. (2020). Pharmacological targeting of the GABAB receptor alters *Drosophila*'s behavioural responses to alcohol. *Addiction Biology*, *25*(2).

Reiner, A., & Levitz, J. (2018). Glutamatergic Signaling in the central nervous system: Ionotropic and metabotropic receptors in concert. *Neuron*, Vol. 98, Issue 6, pp. 1080–1098.

Ren, G. R., Folke, J., Hauser, F., Li, S., & Grimmelikhuijzen, C. J. P. (2015). The A- and B-type muscarinic acetylcholine receptors from *Drosophila melanogaster* couple to different second messenger pathways. *Biochemical and Biophysical Research Communications*, *462*(4), 358–364.

Richter, F. G., Fendl, S., Haag, J., Drews, M. S., & Borst, A. (2018). Glutamate signaling in the fly visual system. *iScience*, *7*, 85–95.

Riemensperger, T., Isabel, G., Coulom, H., Neuser, K., Seugnet, L., Kume, K., Iché-Torres, M., Cassar, M., Strauss, R., Preat, T., Hirsh, J., & Birman, S. (2011). Behavioral consequences of dopamine deficiency in the *Drosophila* central nervous system. *Proceedings of the National Academy of Sciences of the United States of America*, *108*(2), 834–839.

Rister, J., Pauls, D., Schnell, B., Ting, C. Y., Lee, C. H., Sinakevitch, I., Morante, J., Strausfeld, N. J., Ito, K., & Heisenberg, M. (2007). Dissection of the peripheral motion channel in the visual system of *Drosophila melanogaster*. *Neuron*, *56*(1), 155–170.

Rodriques, S. G., Stickels, R. R., Goeva, A., Martin, C. A., Murray, E., Vanderburg, C. R., Welch, J., Chen, L. M., Chen, F., & Macosko, E. Z. (2019). Slide-seq: A scalable technology for measuring genome-wide expression at high spatial resolution. *Science*, *363*(6434), 1463–1467.

Rosenbaum, D. M., Rasmussen, S. G. F., & Kobilka, B. K. (2009). The structure and

function of G-protein-coupled receptors. *Nature*, Vol. 459, Issue 7245, pp. 356–363.

Rust, M. J., Bates, M., & Zhuang, X. (2006). Sub-diffraction-limit imaging by stochastic optical reconstruction microscopy (STORM). *Nature Methods*, *3*(10), 793–795.

Salvaterra, P. M., & McCaman, R. E. (1985). Choline acetyltransferase and acetylcholine levels in *Drosophila melanogaster*: A study using two temperature-sensitive mutants. *Journal of Neuroscience*, *5*(4), 903–910.

Sánchez-Soriano, N., Bottenberg, W., Fiala, A., Haessler, U., Kerassoviti, A., Knust, E., Löhr, R., & Prokop, A. (2005). Are dendrites in *Drosophila* homologous to vertebrate dendrites? *Developmental Biology*, *288*(1), 126–138.

Sarov, M., Barz, C., Jambor, H., Hein, M. Y., Schmied, C., Suchold, D., Stender, B., Janosch, S., Vikas, V. K., Krishnan, R., Krishnamoorthy, A., Ferreira, I. R., Ejsmont, R. K., Finkl, K., Hasse, S., Kä mpfer, P., Plewka, N., Vinis, E., Schloissnig, S., … Schnorrer, F. (2016). A genome-wide resource for the analysis of protein localisation in *Drosophila*. *eLife*, 5.

Scheunemann, L., Plaçais, P. Y., Dromard, Y., Schwärzel, M., & Preat, T. (2018). Dunce phosphodiesterase acts as a checkpoint for *Drosophila* long-term memory in a pair of serotonergic neurons. *Neuron*, *98*(2), 350-365.e5.

Schilling, T., & Borst, A. (2015). Local motion detectors are required for the computation of expansion flow-fields. *Biology Open*, *4*(9), 1105–1108.

Schnell, B., Raghu, S. V., Nern, A., & Borst, A. (2012). Columnar cells necessary for motion responses of wide-field visual interneurons in *Drosophila*. *Journal of Comparative Physiology A: Neuroethology, Sensory, Neural, and Behavioral Physiology*, *198*(5), 389–395.

Schwaerzel, M., Monastirioti, M., Scholz, H., Friggi-Grelin, F., Birman, S., & Heisenberg, M. (2003). Dopamine and octopamine differentiate between aversive and appetitive olfactory memories in *Drosophila*. *Journal of Neuroscience*, *23*(33), 10495–10502.

Schwiening, C. J. (2012). A brief historical perspective: Hodgkin and Huxley. *Journal of Physiology*, Vol. 590, Issue 11, pp. 2571–2575.

Serbe, E., Meier, M., Leonhardt, A., & Borst, A. (2016). Comprehensive characterization of the major presynaptic elements to the *Drosophila* OFF motion detector. *Neuron*, *89*(4), 829–841.

Sethuramanujam, S., Matsumoto, A., McIntosh, J. M., Jing, M., Li, Y., Berson, D., Yonehara, K., & Awatramani, G. B. (2020). Rapid 'multi-directed' cholinergic transmission at central synapses. *bioRxiv*, 2020.04.18.048330.

Sethuramanujam, S., McLaughlin, A. J., deRosenroll, G., Hoggarth, A., Schwab, D. J., & Awatramani, G. B. (2016). A central role for mixed acetylcholine/GABA transmission in direction coding in the retina. *Neuron*, *90*(6), 1243–1256.

Sethuramanujam, S., Yao, X., deRosenroll, G., Briggman, K. L., Field, G. D., & Awatramani, G. B. (2017). "Silent" NMDA synapses enhance motion sensitivity in a mature retinal circuit. *Neuron*, *96*(5), 1099-1111.e3.

Shapiro, R. A., Wakimoto, B. T., Subers, E. M., & Nathanson, N. M. (1989). Characterization and functional expression in mammalian cells of genomic and cDNA clones encoding a *Drosophila* muscarinic acetylcholine receptor. *Proceedings of the National Academy of Sciences of the United States of America*, *86*(22), 9039–9043.

Shinomiya, K., Huang, G., Lu, Z., Parag, T., Xu, C. S., Aniceto, R., Ansari, N., Cheatham, N., Lauchie, S., Neace, E., Ogundeyi, O., Ordish, C., Peel, D., Shinomiya, A., Smith, C., Takemura, S., Talebi, I., Rivlin, P. K., Nern, A., … Meinertzhagen, I. A. (2019). Comparisons between the ON- and OFF-edge motion pathways in the *Drosophila* brain. *eLife*, *8*.

Shinomiya, K., Lu, Z., Meinertzhagen, I. A., Karuppudurai, T., Lin, T.-Y., & Lee, C.-H. (2014). Candidate neural substrates for off-edge motion detection in *Drosophila*. *Current Biology*, *24*(10), 1062–1070.

Sigal, Y. M., Speer, C. M., Babcock, H. P., & Zhuang, X. (2015). Mapping synaptic input fields of neurons with super-resolution imaging. *Cell*, *163*(2), 493–505.

Silies, M., Gohl, D. M., Fisher, Y. E., Freifeld, L., Clark, D. A., & Clandinin, T. R. (2013). Modular use of peripheral input channels tunes motion-detecting circuitry. *Neuron*, *79*(1), 111–127.

Sitaraman, D., Zars, M., LaFerriere, H., Chen, Y. C., Sable-Smith, A., Kitamoto, T., Rottinghaus, G. E., & Zars, T. (2008). Serotonin is necessary for place memory in *Drosophila*. *Proceedings of the National Academy of Sciences of the United States of America*, *105*(14), 5579–5584.

Sombati, S., & Hoyle, G. (1984). Generation of specific behaviors in a locust by local release into neuropil of the natural neuromodulator octopamine. *Journal of Neurobiology*, *15*(6), 481–506.

Sprang, S. R., Chen, Z., & Du, X. (2007). Structural basis of effector regulation and signal termination in heterotrimeric Gα proteins. *Advances in Protein Chemistry,* Vol. 74, pp. 1–65.

Ståhl, P. L., Salmén, F., Vickovic, S., Lundmark, A., Navarro, J. F., Magnusson, J., Giacomello, S., Asp, M., Westholm, J. O., Huss, M., Mollbrink, A., Linnarsson, S., Codeluppi, S., Borg, Å., Pontén, F., Costea, P. I., Sahlén, P., Mulder, J., Bergmann, O., … Frisén, J. (2016). Visualization and analysis of gene expression in tissue sections by spatial transcriptomics. *Science*, Vol. 353, Issue 6294, pp. 78–82.

Stevens, N. M. (1905). A study of the germ cells of *Aphis rosæ* and *Aphis ænotheræ*. *Journal of Experimental Zoology*, *2*(3), 313–333.

Stevens, N. M. (1908). A study of the germ cells of certain diptera, with reference to the heterochromosomes and the phenomena of synapsis. *Journal of Experimental Zoology*, *5*(3), 359–374.

Strother, J. A., Nern, A., & Reiser, M. B. (2014). Direct observation of ON and OFF pathways in the *Drosophila* visual system. *Current Biology*, *24*(9), 976–983.

Strother, J. A., Rogers, E. M., Wu, S.-T., Reiser, M. B., Nern, A., Rubin, G. M., Le, J. Q., & Wong, A. M. (2017). The emergence of directional selectivity in the visual motion pathway of *Drosophila*. *Neuron*, *94*(1), 168-182.e10.

Strother, J. A., Wu, S.-T., Rogers, E. M., Eliason, J. L. M., Wong, A. M., Nern, A., & Reiser, M. B. (2018). Behavioral state modulates the ON visual motion pathway of *Drosophila* . *Proceedings of the National Academy of Sciences*, *115*(1), E102–E111.

Suver, M. P., Mamiya, A., & Dickinson, M. H. (2012). Octopamine neurons mediate flight-induced modulation of visual processing in *Drosophila*. *Current Biology*, *22*(24), 2294–2302.

Suzuki, Y., Schenk, J. E., Tan, H., & Gaudry, Q. (2020). A population of interneurons signals changes in the basal concentration of serotonin and

mediates gain control in the *Drosophila* antennal lobe. *Current Biology*, *30*(6), 1110-1118.e4.

Sweeney, S. T., Broadie, K., Keane, J., Niemann, H., & O'Kane, C. J. (1995). Targeted expression of tetanus toxin light chain in *Drosophila* specifically eliminates synaptic transmission and causes behavioral defects. *Neuron*, *14*(2), 341–351.

Takemura, S. Y., Bharioke, A., Lu, Z., Nern, A., Vitaladevuni, S., Rivlin, P. K., Katz, W. T., Olbris, D. J., Plaza, S. M., Winston, P., Zhao, T., Horne, J. A., Fetter, R. D., Takemura, S., Blazek, K., Chang, L. A., Ogundeyi, O., Saunders, M. A., Shapiro, V., … Chklovskii, D. B. (2013). A visual motion detection circuit suggested by *Drosophila* connectomics. *Nature*, *500*(7461), 175–181.

Takemura, S. Y., Karuppudurai, T., Ting, C. Y., Lu, Z., Lee, C. H., & Meinertzhagen, I. A. (2011). Cholinergic circuits integrate neighboring visual signals in a *Drosophila* motion detection pathway. *Current Biology*, *21*(24), 2077–2084.

Takemura, S. ya, Nern, A., Chklovskii, D. B., Scheffer, L. K., Rubin, G. M., & Meinertzhagen, I. A. (2017). The comprehensive connectome of a neural substrate for 'ON' motion detection in *Drosophila*. *eLife*, *6*.

Tomita, J., Ueno, T., Mitsuyoshi, M., Kume, S., & Kume, K. (2015). The NMDA receptor promotes sleep in the fruit fly, *Drosophila melanogaster*. *PLOS ONE*, *10*(5), e0128101.

Tsay, D., Dudman, J. T., & Siegelbaum, S. A. (2007). HCN1 channels constrain synaptically evoked Ca2+ spikes in distal dendrites of CA1 pyramidal neurons. *Neuron*, *56*(6), 1076–1089.

Ugur, B., Chen, K., & Bellen, H. J. (2016). *Drosophila* tools and assays for the study of human diseases. *DMM Disease Models and Mechanisms*, Vol. 9, Issue 3, pp. 235–244.

Van Hook, M. J., & Berson, D. M. (2010). Hyperpolarization-activated current (Ih) in ganglion-cell photoreceptors. *PLoS ONE*, *5*(12), e15344.

Venken, K. J. T., Schulze, K. L., Haelterman, N. A., Pan, H., He, Y., Evans-Holm, M., Carlson, J. W., Levis, R. W., Spradling, A. C., Hoskins, R. A., & Bellen, H. J. (2011). MiMIC: A highly versatile transposon insertion resource for engineering *Drosophila melanogaster* genes. *Nature Methods*, *8*(9), 737–747.

Vogel, C., & Marcotte, E. M. (2012). Insights into the regulation of protein abundance from proteomic and transcriptomic analyses. *Nature Reviews Genetics*, *13*(4), 227–232.

Von Hassenstein, B., & Reichardt, W. (1956). Systemtheoretische Analyse der Zeit, Reihenfolgen-und Vorzeichenauswertung bei der Bewegungsperzeption des Rüsselkäfers *Chlorophanus*. *Zeitschrift fur Naturforschung - Section B Journal of Chemical Science,* Vol. 11, Issues 9–10, pp. 513–524.

Waddell, S. (2013). Reinforcement signalling in *Drosophila*; dopamine does it all after all. *Current Opinion in Neurobiology*, Vol. 23, Issue 3, pp. 324–329.

Warmke, J. W., Reenan, R. A. G., Wang, P., Qian, S., Arena, J. P., Wang, J., Wunderler, D., Liu, K., Kaczorowski, G. J., Van Der Ploeg, L. H. T., Ganetzky, B., & Cohen, C. J. (1997). Functional expression of *Drosophila* para sodium channels modulation by the membrane protein tipE and toxin pharmacology. *Journal of General Physiology*, *110*(2), 119–133.

Weber, A. P. M. (2015). Discovering new biology through sequencing of RNA.

Plant Physiology, *169*(3), 1524–1531.

Weber, A. P. M., Weber, K. L., Carr, K., Wilkerson, C., & Ohlrogge, J. B. (2007). Sampling the arabidopsis transcriptome with massively parallel pyrosequencing. *Plant Physiology*, *144*(1), 32–42.

Wienecke, C. F. R., Leong, J. C. S., & Clandinin, T. R. (2018). Linear summation underlies direction selectivity in *Drosophila*. *Neuron*, *99*(4), 680-688.e4.

Willems, J., de Jong, A. P. H., Scheefhals, N., Mertens, E., Catsburg, L. A. E., Poorthuis, R. B., de Winter, F., Verhaagen, J., Meye, F. J., & MacGillavry, H. D. (2020). ORANGE: A CRISPR/Cas9-based genome editing toolbox for epitope tagging of endogenous proteins in neurons. *PLOS Biology*, *18*(4), e3000665.

Wu, C. L., Xia, S., Fu, T. F., Wang, H., Chen, Y. H., Leong, D., Chiang, A. S., & Tully, T. (2007). Specific requirement of NMDA receptors for long-term memory consolidation in *Drosophila* ellipsoid body. *Nature Neuroscience*, *10*(12), 1578–1586.

Xia, R.-Y., Li, M.-Q., Wu, Y.-S., Qi, Y.-X., Ye, G.-Y., & Huang, J. (2016). A new family of insect muscarinic acetylcholine receptors. *Insect Molecular Biology*, *25*(4), 362–369.

Xia, S., Miyashita, T., Fu, T. F., Lin, W. Y., Wu, C. L., Pyzocha, L., Lin, I. R., Saitoe, M., Tully, T., & Chiang, A. S. (2005). NMDA receptors mediate olfactory learning and memory in *Drosophila*. *Current Biology*, *15*(7), 603–615.

Yamagata, N., Ichinose, T., Aso, Y., Plaçais, P. Y., Friedrich, A. B., Sima, R. J., Preat, T., Rubin, G. M., & Tanimoto, H. (2015). Distinct dopamine neurons mediate reward signals for short- and long-term memories. *Proceedings of the National Academy of Sciences of the United States of America*, *112*(2), 578–583.

Yamaguchi, S., Desplan, C., & Heisenberg, M. (2010). Contribution of photoreceptor subtypes to spectral wavelength preference in *Drosophila*. *Proceedings of the National Academy of Sciences of the United States of America*, *107*(12), 5634–5639.

Yamaguchi, S., Wolf, R., Desplan, C., & Heisenberg, M. (2008). Motion vision is independent of color in *Drosophila*. *Proceedings of the National Academy of Sciences of the United States of America*, *105*(12), 4910–4915.

Yang, H. H. H., St-Pierre, F., Sun, X., Ding, X., Lin, M. Z. Z., & Clandinin, T. R. R. (2016). Subcellular imaging of voltage and calcium signals reveals neural processing in vivo. *Cell*, *166*(1), 245–257.

Yoshida, K., Watanabe, D., Ishikane, H., Tachibana, M., Pastan, I., & Nakanishi, S. (2001). A key role of starburst amacrine cells in originating retinal directional selectivity and optokinetic eye movement. *Neuron*, *30*(3), 771–780.

Yuan, Q., Joiner, W. J., & Sehgal, A. (2006). A sleep-rromoting role for the *Drosophila* serotonin receptor 1A. *Current Biology*, *16*(11), 1051–1062.

Yuan, Q., Lin, F., Zheng, X., & Sehgal, A. (2005). Serotonin modulates circadian entrainment in *Drosophila*. *Neuron*, *47*(1), 115–127.

Zeleny C. (1922) The effect of selection for eye facet number in the white bar-eye race of *Drosophila melanogaster*. Genetics 7(1):1–115.

Zhang, H. G., Lee, H. J., Rocheleau, T., Ffrench-Constant, R. H., & Jackson, M. B. (1995). Subunit composition determines picrotoxin and bicuculline sensitivity of *Drosophila* gamma-aminobutyric acid receptors. *Molecular Pharmacology*,

48(5).

Zheng, Y., Hirschberg, B., Yuan, J., Wang, A. P., Hunt, D. C., Ludmerer, S. W., Schmatz, D. M., & Cully, D. F. (2002). Identification of two novel *Drosophila melanogaster* histamine-gated chloride channel subunits expressed in the eye. *Journal of Biological Chemistry*, *277*(3), 2000–2005.

Zhou, C., Rao, Y., & Rao, Y. (2008). A subset of octopaminergic neurons are important for *Drosophila* aggression. *Nature Neuroscience*, *11*(9), 1059–1067.

5. APPENDIX

5.1 Acknowledgements

First and foremost, I would like to thank Axel for being the best boss one can ask for. Despite being a renowned scientist and director of the MPI of Neurobiology, you always remained down to earth and approachable for everybody. You never gave up on me, even in the darkest times of my projects. Thank you for your trust and support.

Above all, I want to thank all members of the Borst lab for amazing years, countless parties, retreats, conferences, happy hours, barbecues, graduation days, and dances… it was a blast! Furthermore, I am grateful to many people who supported me on my PhD journey: My TAC committee members, Frank Schnorrer, Rüdiger Klein and Jesus Pujol-Marti for their advice and new creative ideas. Jesus for being my unofficial supervisor, especially in the initial phase of my PhD when I did not really know what I was doing. You were always there for me and asking a quick question often ended in hour-long conversations about science and other topics in your office. Thank you for taking me under your wing and teaching me about the beauty of developmental neurobiology. Tabea for being a loyal colleague and friend, both at work and in private. We always had a great time together at conferences in Copenhagen, Berlin, Heidelberg, and Krakow. Renee for being an incredible HiWi, master student, PhD student and colleague. Only with your help was I able to finish my projects and together we made the wildest genetic dreams come true. As you always say, "Team work makes the dream work"! Georg for fun times in P5, many discussions about science and failed experiments, and for proofreading several manuscripts including this thesis. Ines for help with genetic and molecular questions, for proofreading my paper, and for guidance in general. Flo for our collaboration in the initial phase of the PDE project, our GluSnFR paper and for your patience with all GluCl-related experiments. Anna for our shared time as PhD representatives, joint gardening projects, and your scientific precision. Nadya for proofreading my thesis and for bringing joy to the lab. Michi for teaching me about mathematical models and for good times with drinks and music. Lukas for teaching me about channels and especially GluCl physiology, and for improving our eLife paper with your entertaining comments. All the girls from the lab- Tabea, Ines, Renee, Nadya, Aicha, Maria, Amalia, Birte- for numerous comforting Ladies Nights and for the inclusive atmosphere in the lab. Wolfgang for help with countless clonings. Robert Kasper, together with Joel Ryan and Andreas Thomae, for introducing me to the super-resolution microscopy world.

Finally, I would like to thank my parents and my brother for their unconditional support and belief in me and everything I do. Most importantly, I want to thank Jonatan for supporting me through bad times and being part of my happiness in good times.